THE ROLE OF ADIPOSE TISSUE IMMUNE CELLS IN IMMUNE RESPONSES

By

ALISTAIR JAMES MCINTOSH

A thesis submitted to The University of Birmingham

For the degree of DOCTOR OF PHILOSOPHY

Institute of Immunology and Immunotherapy

College of Medical and Dental Sciences

University of Birmingham

September 2017

Abstract

There is growing evidence that immune cells within adipose tissues can drive the formation of ectopic lymphoid structures, known as Fat Associated Lymphoid Clusters (FALC). FALC support B cell antibody production in response to infection and inflammation. This investigation explores the immune cell composition and role of different adipose tissues both in steady state and during immune responses in mice. Firstly, a detailed analysis of the immune cell composition of different adipose tissues was performed. To investigate the function and migratory properties of these tissue-resident cells, cytokine and chemokine receptor expression was then assessed. How immune cells responded to infection in surrounding tissues was examined using an intestinal helminth infection with the parasite *Heligmosomoides polygyrus.* A comparison of the immune cell composition and FALC number was performed in adipose tissue of infected and uninfected animals.

The results established a detailed description of the immune compartment within murine adipose tissues, including regulatory T cells, invariant natural killer T cells and group 2 Innate Lymphoid Cells (ILC2s). Significant differences were observed in composition, surface protein expression and cytokine production of group 2 ILCs between adipose tissues and secondary lymphoid tissues, indicating that adipose tissue specific signals can direct ILC2 responses within these tissues. Finally, increases were observed in ILC2 and FALC numbers in the mesenteries of WT mice following parasite infection. As ILC2s are crucial for the clearance of this helminth in mice, and FALCs have been shown to support immune responses within adipose tissues, this indicates immune cells within adipose tissues may contribute to immune responses in the local tissue environment.

Acknowledgements

First of all, I would like to thank my supervisors Dr. Jorge Caamano and Dr. David Withers for their guidance and help throughout the four years of my PhD, sharing their knowledge both in and outside the lab.

I would also like to express my gratitude to Dr. Sara Cruz Migoni, who was always there for me when I needed advice or assistance. Additionally, Claire Dempsey, Emma Dutton and Rhys Jones deserve a special mention for the moral support they have given me which has been instrumental in helping me during some of the more challenging aspects of my PhD. Thanks also to all other members of the 4th floor IBR for providing both advice and reagents.

Special thanks go to my fiancée, Jessica Hawes, for her enduring support and motivation throughout the PhD. Lastly, the constant encouragement provided by my parents and sister was of paramount importance during the entirety of my PhD study so a huge ‘thank you’ to them all.

TABLE OF CONTENTS

TABLE OF FIGURES

TABLE OF TABLES

LIST OF ABBREVIATIONS

-/-	Deficient
A. alternata	*Alternaria alternata*
AAM	Alternatively activated macrophage
AP(s)	Adipocyte progenitor(s)
APC	Allophycocyanin
APCs	Antigen presenting cells
AT(s)	Adipose tissue(s)
ATP	Adenosine triphosphate
BAFF	B cell activating factor
BALT	Bronchus-associated lymphoid tissue
BAT	Brown adipose tissue
BrdU	5-bromo-2-deoxyuridine
BSA	Bovine serum albumin
CCL	CC chemokine ligand
CCR	CC chemokine receptor
CCRL2	CC chemokine receptor-like 2
CD	Cluster of differentiation
CHILP	Common helper ILC precursor
CLP	Common lymphoid progenitor
COPD	Chronic obstructive pulmonary disease
CRTH2	Chemokine receptor homologous molecule expressed on Th2 lymphocytes
CXCL	C-X-C chemokine ligand
CXCR	C-X-C chemokine receptor
CysLTR1	Cysteinyl leukotriene receptor 1
DC	Dendritic cell
E	Embryonic day
EDTA	Ethylenediaminetetraacetic acid
ELISA	Enzyme-linked immunosorbent assay
FA	Fatty acids
FALC	Fat associated lymphoid clusters
FDC	Follicular dendritic cell
FGF21	Fibroblast growth factor 21
FITC	Fluorescein isothiocyanate
FOXO1	Forkhead box protein O1
FRC	Fibroblastic reticular cell
GALT	Gut Associated Lymphoid Tissue
GATA-3	GATA transcription factor family member 3
GFI1	Growth factor independent 1
GFP	Green fluorescent protein
GLP-1	Glucagon-like peptide 1
H.polygyrus	*Heligmosomoides polygyrus*
HCMV	Human cytomegalovirus
HEV	High endothelial venules

HFD	High fat diet
ICAM-1	Intercellular adhesion molecule 1
ICOS	Inducible T cell costimulator
ICOSL	ICOS ligand
ID2	Inhibitor of DNA binding 2
IKKβ	Inhibitor of nuclear factor κ-B kinase subunit β
IFN-γ	Interferon γ
IgA	Immunoglobulin A
IgG	Immunoglobulin G
IL-	Interleukin
IL1RAP	Interleukin 1 receptor accessory protein
IL1RL1/ST2	Interleukin 1 receptor-like 1
IL-2Rα	Interleukin 2 receptor α
IL-4Rα	Interleukin 4 receptor α
IL-7Rα	Interleukin 7 receptor α
ILC	Innate lymphoid cell
ILC1	Group 1 innate lymphoid cell
ILC2	Group 2 innate lymphoid cell
ILCP	ILC precursor
ILN	Inguinal lymph node
iNKT	Invariant natural killer T cell
JNK	c-Jun N-terminal kinase
KLRG1	Killer cell lectin-like receptor subfamily G member 1
L.sigmodontis	*Litomosoides sigmodontis*
Lin	Lineage exclusion channel
LN(s)	Lymph node(s)
LTC4	Leukotriene C 4
LTD4	Leukotriene D 4
LTi	Lymphoid tissue inducer cell
LTi-like cell	Lymphoid tissue inducer-like cell
LTo	Lymphoid tissue organiser cell
$LT\alpha_1\beta_2$	Lymphotoxin $\alpha_1\beta_2$
LTβR	Lymphotoxin β receptor
MAdCAM-1	Mucosal vascular addressin cell adhesion molecule 1
MALT	Mucosal-associated lymphoid tissue
MAPK	Mitogen-activated protein kinase
MFI	Median Fluorescence Intensity
Metrnl	Meteorin-like 1
MHC II	Major histocompatibility complex class two
MLN	Mesenteric lymph node
MS	Milky spots
MyD88	Myeloid differentiation primary response protein 88
N.brasiliensis	*Nippostrongylus brasiliensis*
NCR	Natural cytotoxicity receptor
NFIL3	Nuclear factor interleukin 3 regulated

NFκB	Nuclear factor κ B
NK	Natural killer cell
PAMPs	Pattern associated molecular patterns
PBS	Phosphate buffered saline
PDGFRα	Platelet-derived growth factor receptor α
PE	Phycoerythrin
PGD2	Prostaglandin D 2
PLZF	Promyelocytic leukaemia zinc finger protein
PMA	Phorbol 12-myristate 13-acetate
Podoplanin	Gp38
PPARγ	Peroxisome proliferator-activated receptor γ
PPARδ	Peroxisome proliferator-activated receptor δ
PRDM16	PR domain containing 16 protein
Pref-1	Preadipocyte factor 1
PUFA	Polyunsaturated fatty acids
RA	Retinoic acid
RANK/RANKL	Receptor activator of nuclear factor κ B /ligand
RPMI	Roswell Park Memorial Institute medium
SCAT	Subcutaneous adipose tissue
SCID	Severe combined immunodeficiency
SI	Small intestine
SILP	Small intestine lamina propria
SLT(s)	Secondary lymphoid tissue(s)
STAT6	Signal transducer and activator of transcription 6
SVF	Stromal vascular fraction
T-bet	T box transcription factor T-bet
TCR	T cell receptor
Th	T helper
TH	Tyrosine hydroxylase
TNF	Tumour necrosis factor
TNFRSF	Tumour necrosis factor receptor superfamily
TNFSF	Tumour necrosis factor superfamily
TOX	Thymocyte selection-associated high mobility group box protein
Treg	Regulatory T cell
TSLP	Thymic stromal lymphopoietin
UCP1	Uncoupling protein 1
VAT	Visceral adipose tissue
VCAM-1	Vascular cell adhesion molecule 1
WAT	White adipose tissue
WHO	World health organisation
WT	Wild type
α-gal-cer	α-galactosidase
α-LP	α-lymphoid progenitor
γc/IL-2Rγ	Common gamma chain/ interleukin 2 receptor γ

1. INTRODUCTION

1.1. THE IMMUNE SYSTEM

The primary role of the immune system is to protect against harmful pathogens. There is evidence of some form of immune system in most organisms, with increasing complexity of the immune system concomitant with increasing complexity of organisms throughout evolution, illustrating the importance of protection against pathogens in the survival of organisms (Boehm *et al.*, 2012). Another key feature of the immune system is the recognition of 'self' and 'non-self' in order to prevent autoimmunity, where an immune response against a host's own cells occurs (Janeway, 2005).

The immune system can be broadly split into two categories; non-specific (innate) and specific (adaptive) immunity. The innate immune system responds to conserved molecules found on the surface of pathogens. This allows cells from the innate immune system, including macrophages, eosinophils and neutrophils, to respond to different types of pathogen in a non-specific manner (Thaiss *et al.*, 2016). As these cells can respond directly, a much faster immune response is mounted, which acts to limit pathogen mediated damage to the host. As the innate system is more basic, it is evolutionarily conserved, thus examples of innate immunity can be found in more primitive multicellular organisms, such as fungi (Boehm *et al.*, 2012). Despite this, some pathogens have developed mechanisms to bypass detection or destruction by the innate immune system. The function, therefore, of the adaptive immune system is to produce a more specific response to pathogens, by recognition of molecules unique to individual pathogens, known as antigens. This process is more complex, and is therefore only found in more evolutionarily advanced vertebrates. The

adaptive immune system is also slower-acting than the innate immune system, taking many days in humans before a fully functioning response is generated (Janeway, 2005). Therefore, the fast-responding innate immune system acts initially to limit pathogen colonisation and damage to the host, and also to activate cells of the adaptive immune system. Cells of the adaptive immune system can then mount an antigen-specific response through T-cells and B-cells to produce specific antibodies and cytokines to stimulate immune cells specific to the response (Janeway, 2005). Another feature of adaptive immune responses is the ability to generate memory cells, which facilitate a faster immune response if the same pathogen is encountered again, giving long-lasting protection against specific pathogens (Janeway, 2005). The requirement for this specificity is evident in humans born with genetic mutations that result in a malfunction of a variety of the components of the adaptive immune system, collectively termed Severe Combined Immunodeficiency (SCID), which is fatal in early childhood if not treated with gene therapy or haematopoietic stem cell transplant (Vely *et al.*, 2016). This demonstrates that innate immune responses alone are insufficient for complete survival against the wide array of pathogens humans encounter in everyday life. As outlined above, one final feature of the adaptive immune system is to prevent autoimmunity. During the development of T and B cells in mammals, mechanisms exist to delete or inhibit self-reactive lymphocytes, a process which is referred to as central tolerance (Sandel and Monroe, 1999, Halverson *et al.*, 2004, Reddy, 2017). However, despite these mechanisms auto-reactivity can still arise. Therefore, a subset of T cells acts to regulate auto-reactivity, referred to as regulatory T cells (Tregs). Tregs can inhibit auto-reactive cells through a variety of mechanisms including by production of Interleukin 10

(IL-10) and by direct cell: cell contacts (Rubtsov *et al.*, 2008, Shevach, 2009, Qureshi *et al.*, 2011).

Whilst cells from the innate immune system include macrophages, Natural Killer (NK) cells, dendritic cells (DCs), eosinophils, neutrophils and basophils, adaptive immunity is mediated through different subsets of T and B cells. A newly identified group of cells named Innate Lymphoid Cells (ILCs) show rapid responses to pathogens following infection, consistent with many other cells of the innate immune system, but also show surprising similarity in protein expression to T-cell subsets (Spits *et al.*, 2013, Artis and Spits, 2015). Due to this dual-characteristic, ILCs have been described as 'bridging the gap between innate and adaptive immunity (Pishdadian *et al.*, 2012). As such, these cells have been the focus of many recent studies.

1.2. INNATE LYMPHOID CELLS (ILCs)

Over the past decade there have been many reports describing an array of cell subsets which are analogous to classical T helper (Th) subsets, Th1, Th2 and Th17, based on cytokine expression (Moro *et al.*, 2010, Neill *et al.*, 2010, Koyasu and Moro, 2013). However, these cells lacked lineage markers classically associated with T cells and also lacked antigen specific receptors, indicating that they were members of the innate immune system. As research in the field developed, it was clear different research groups began referring to the same cell subset by different names (c.f. nuocytes (Neill *et al.*, 2010), natural helper cells (Koyasu and Moro, 2013) and innate helper 2 cells (Price *et al.*, 2010)), leading to confusion in the field. In order to boost further advances in this research area, a uniform nomenclature was proposed (Spits *et al.*, 2013). This led to ILCs being categorised into three subsets based on their functional characteristics and transcription factor expression. ILCs were also

categorised into helper and cytotoxic ILCs (Spits *et al.*, 2013, Artis and Spits, 2015). Herein, the focus is on the features of helper ILCs and consequently cytotoxic ILCs (NK cells) are not discussed. This is illustrated in Figure 1.1A. Both Group 1 ILCs (ILC1s) and Th1 cells express the transcription factor T-box expressed in T cells (T-bet), produce interferon γ (IFN-γ) and are required for clearance of intracellular parasites in mammals, primarily bacteria (Klose *et al.*, 2014).

Group 2 ILCs (ILC2s) and Th2 cells both rely on the transcription factor GATA-3 for the production of the type 2 cytokines IL-5 and IL-13 (Hoyler *et al.*, 2012). ILC2s, unlike Th2 cells, also produce IL-4. Together these cytokines function to provide immunity to multicellular parasites in mammals, such as helminths (Voehringer *et al.*, 2006, Price *et al.*, 2010, Pelly *et al.*, 2016), and promote tissue repair following damage (Monticelli *et al.*, 2011). As discussed later in chapter 1.3, ILC2s are also crucial in maintenance of metabolic homeostasis through both direct and indirect mechanisms (Hams *et al.*, 2013, Molofsky *et al.*, 2013, Qiu *et al.*, 2014, Rao *et al.*, 2014, Brestoff *et al.*, 2015, Lee *et al.*, 2015a). However, these type-2 cytokines produced by ILC2s can also contribute to adverse immune responses including asthma and atopic dermatitis (Salimi *et al.*, 2013).

Finally, ILCs expressing the transcription factor RAR-related orphan receptor gamma t (RORγt), collectively termed Group 3 ILCs, can be subdivided into Lymphoid Tissue Inducer (LTi)-like cells and Natural Cytotoxicity Receptor^{+}ILC3 (NCR^{+}ILC3s), based on their expression of cytokines. LTi-like cells are the adult equivalent of LTi cells, which are responsible for the formation of Secondary Lymphoid Tissues (SLTs) during embryogenesis. In adult mice these cells still appear to be endowed with the ability of lymphoid tissue formation (lymphogenesis),

although in the context of adults this is more associated with repair of lymphoid tissues following infection or inflammation (Scandella *et al.*, 2008). Furthermore, research suggests that LTi-like cells are also important in the maintenance of Cluster of Differentiation 4^+ ($CD4^+$) memory T cells (Withers *et al.*, 2012). In contrast, ILC3s are involved in immunity against extracellular bacteria and are also key mediators of irritable bowel disease (Takayama *et al.*, 2010).

The transcription factors of ILCs, T-bet, GATA-3 and RORγt are not only important for categorising these cells, but are also crucial for the diverse functional roles described above. This is predominantly due to the fact that these proteins are direct transcriptional regulators of cytokine production. For example, GATA-3 directly regulates type-two cytokine expression, including IL-5 and IL-13, and mice lacking this protein had defective ILC2 formation, but showed no change in ILC3 differentiation (Hoyler *et al.*, 2012). Thus, it seems that these transcriptional factors represent some of the signals required for the formation of mature ILC subsets. Further details on the currently established signals in ILC formation are discussed in chapter 1.2.1 below.

The grouping of ILC subsets gives the impression that they exist as static cellular populations. This appears not to be the case, as there is a growing evidence of ILC plasticity in both mice and humans, which arises when environmental signals drive expression of different ILC subset-defining transcription factors (Vonarbourg *et al.*, 2010, Di Santo, 2014, Bernink *et al.*, 2015, Serafini *et al.*, 2015, Bal *et al.*, 2016, Lim *et al.*, 2016, Ohne *et al.*, 2016, Silver *et al.*, 2016, Lim *et al.*, 2017). This is summarised in Figure 1.1B**.** Bernink *et al.* observed the reversible upregulation of RORγt by human ILC1s following exposure to IL-23 and IL-1β (Bernink *et al.*, 2015).

These ILC1s lost the expression of IFN-γ, whilst acquiring the ability to produce IL-22 and, consistent with this process being driven by RORγt expression, IL-22 production was enhanced when retinoic acid (RA) was added to the culture conditions and inhibited in the presence of a RORγt inhibitor. The spontaneous conversion of ILC1 to ILC3 was also demonstrated *in vivo* by injection of ILC1s labelled with a tracker dye. The reverse transition has also been noted by Vonarbourg *et al.,* who demonstrated that LTi-like cells in the intestine were able to first upregulate NCR to become NCR^{+}ILC3 before losing RORγt and IL-22 expression and acquiring T-bet and IFN-γ expression (Vonarbourg *et al.*, 2010). This conversion was driven by expression of IL-12 and IL-15. In addition, the authors showed that these 'ex-ILC3' contributed to the onset and maintenance of inflammatory bowel disease. Plasticity of human ILC2s has also been reported by a number of groups in association with severe chronic obstructive pulmonary disease (COPD), viral infections and Crohn's disease (Bal *et al.*, 2016, Lim *et al.*, 2016, Ohne *et al.*, 2016, Silver *et al.*, 2016). In response to IL-12, ILC2s downregulated GATA-3 expression and upregulated T-bet and IFN-γ. This process was reversible following IL-4 expression (Silver *et al.*, 2016). Finally, conversion of ILC2s to IL-17 producing ILC3s has been demonstrated in response to *Candida albicans* and Notch signalling (Huang *et al.*, 2015, Zhang *et al.*, 2017). Both of these signals drove the expression of RORγt in these cells.

Research on ILC subsets has covered a broad spectrum of areas ranging from development and tissue residency, to studying their role in various disease settings. The results of these studies are summarised in chapters 1.2.1-1.2.4 below.

Figure 1.1: ILC subsets and plasticity

A) ILC subsets are grouped based on their expression of transcription factor and cytokines (Spits *et al.*, 2013, Artis and Spits, 2015). Whilst all ILC subsets appear to play a beneficial physiological role, they have also been implicated in driving the development and progression of a number of diseases in humans (Takayama *et al.*, 2010, Chang *et al.*, 2011, Bernink *et al.*, 2013, Klose and Artis, 2016, Saunders *et al.*, 2016, Maazi *et al.*, 2017). Illustration based on figure by Artis and Spits (Artis and Spits, 2015).

B) Despite ILCs being grouped into functional subsets, there is growing evidence of functional plasticity in all three subsets of ILCs (Vonarbourg *et al.*, 2010, Di Santo, 2014, Klose *et al.*, 2014, Bernink *et al.*, 2015, Serafini *et al.*, 2015, Bal *et al.*, 2016, Lim *et al.*, 2016, Ohne *et al.*, 2016, Silver *et al.*, 2016, Lim *et al.*, 2017). The signals which drive changes in transcription factor (in red) expression, and thus are responsible for the functional plasticity, are outlined.

A

	Group 1 ILCs	Group 2 ILCs	Group 3 ILCs	
	ILC1	ILC2	LTi	NCR+ ILC3
Transcription factors:	T-bet	GATA-3	RORγt	RORγt
Cytokines/proteins produced:	IFN-γ, TNF-α	IL-4, IL-5, IL-13, amphiregulin, catecholamines,	IL-17A, IL-22, GM-CSF	IL-22, GM-CSF
Physiological role(s):	Immunity against intracellular bacteria	Immunity against parasites, Metabolic homeostasis, Tissue repair	Lymphoid tissue generation and maintenance, T-cell homeostasis	Immunity to bacteria, Intestinal homeostasis
Pathogenic role(s):	Crohn's Disease	Asthma, Atopic dermatitis	Crohn's disease	Psoriasis

B

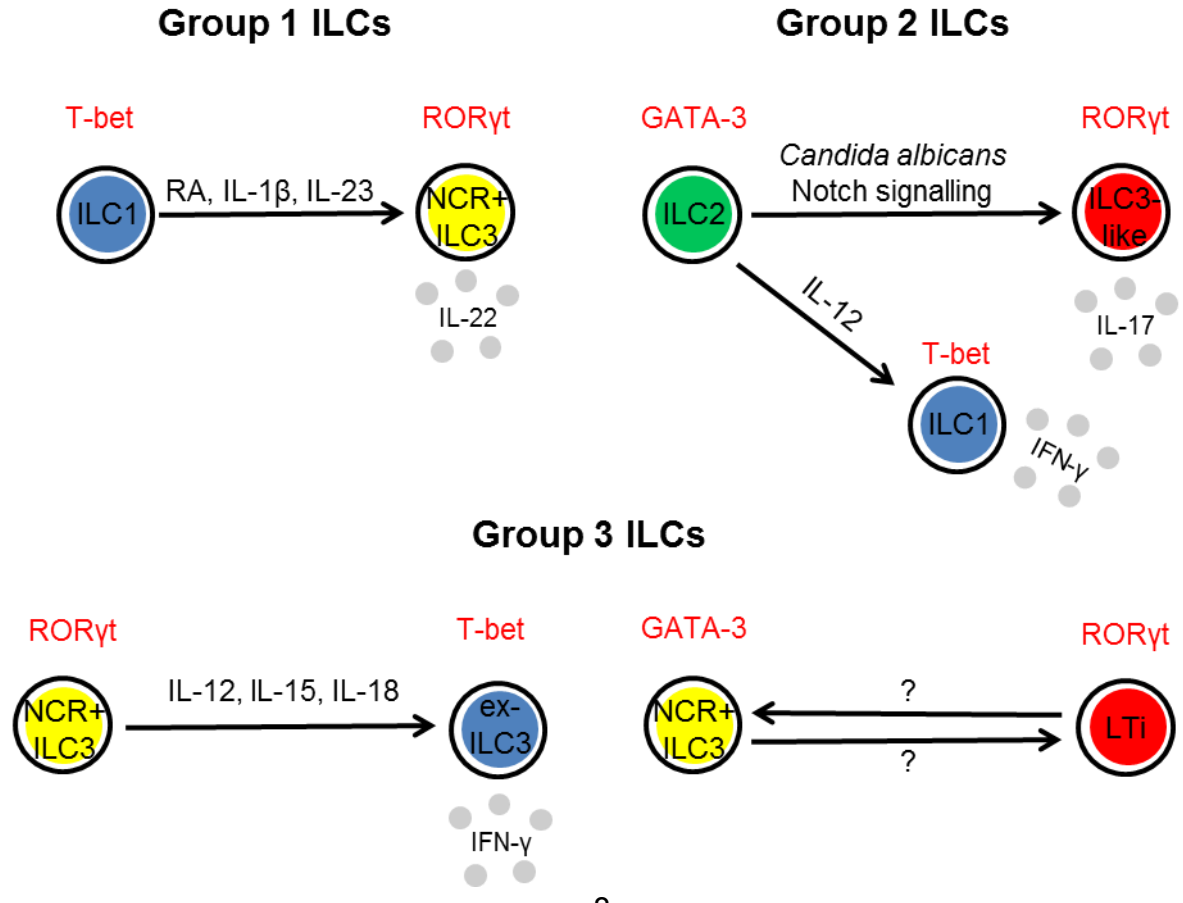

1.2.1. Development of ILCs

Consistent with their functional analogy with Th cells, ILCs develop in the bone marrow from the same initial multipotent stem cell population as Th cells, the common lymphoid progenitor (CLP) (Eberl *et al.*, 2004, Boos *et al.*, 2007, Takatori *et al.*, 2009, Possot *et al.*, 2011, Cherrier *et al.*, 2012, Spooner *et al.*, 2013, Constantinides *et al.*, 2014, Yu *et al.*, 2014, Juelke and Romagnani, 2016). CLP are formed from multipotent haematopoietic stem cells following expression of the transcription factor E2A and growth factor independent 1 (GFI1), among others (Yokota *et al.*, 1999, Boos *et al.*, 2007, Cherrier *et al.*, 2012). This maturation to CLP results in a more restricted number of different cell fate potentials, namely cells can only mature to lymphocyte populations from CLP, and not cells of erythroid, megakaryocytoid and myeloid lineages. These progenitor populations continue to mature with decreasing cell fates potential until mature ILC subsets are formed. This is summarised in Figure 1.2.

Both NK cells and helper ILCs appear to share a progenitor population which has lost the potential to form other lymphocyte populations, called the α-lymphoid progenitor population (α-LP) (Yu *et al.*, 2014, Serafini *et al.*, 2015). The differentiation of CLP to α-LP appears to rely on the transcription factor Inhibitor of DNA binding 2 (ID2), as demonstrated by defective ILC formation in *Id2*$^{-/-}$ animals (Moro *et al.*, 2010), and α-LP are marked by expression of the C-X-C chemokine receptor 6 (CXCR6) and also nuclear factor IL-3 induced (NFIL3) (Vonarbourg *et al.*, 2010, Possot *et al.*, 2011). It is thought that IL-7 receptor signalling may induce NFIL3 expression, leading to the expression of ID2 and thymocyte selection-associated high mobility group box protein (TOX) by α-LP (Yokota *et al.*, 1999, Cherrier *et al.*, 2012, Yu *et al.*, 2014,

Serafini *et al.*, 2015). α-LP can subsequently mature to common helper ILC precursors (CHILP), which lose the ability to potentiate NK cell formation but retain the ability to differentiate into all helper ILC subsets (Satoh-Takayama *et al.*, 2010). Interestingly, this process appears to rely on GATA-3, as mice deficient in this protein lacked mature ILC subsets in the bone marrow and fetal liver (Klose *et al.*, 2014, Serafini *et al.*, 2015). Notch signalling can then drive differentiation of CHILP to a precursor population expressing the transcription factor promyelocytic leukaemia zinc finger protein (PLZF), known as ILC precursor (ILCP), which can give rise to ILC1, ILC2 and NCR ILC3s, but not LTi, indicating that a separate progenitor population for this ILC subset (Possot *et al.*, 2011, Constantinides *et al.*, 2014). Thus, the environmental signals CHILP receive determine the relative development of ILC subsets.

Finally, as introduced in chapter 1.2, differentiation of mature ILC subsets from ILCP is predominantly defined by the expression of the canonical ILC transcription factors T-bet, GATA-3 and RORγt. However, the signals which induce these transcription factors are currently not fully elucidated (Eberl *et al.*, 2004, Luci *et al.*, 2009, Hoyler *et al.*, 2012). Of note, whilst CHILP and ILCP express low levels of GATA-3, for the formation of mature ILC2s, cells must undergo further upregulation of GATA-3 which leads to the expression of ST2. Therefore, GATA-3 upregulation, by some currently unknown mechanism, drives differentiation to an ILC2 restricted lineage (Hoyler *et al.*, 2012). In line with this, research found that the transcription factor GFI1, which directly controls GATA-3 expression, was required for maturation of ILCP to ILC2P and mature ILC2s (Spooner *et al.*, 2013). IL-15 expression is thought to drive

maturation of ILCP to an ILC1 restricted progenitor, although the source of this IL-15 is unknown (Klose *et al.*, 2014).

Whilst the signals which control ILCs maturation during embryogenesis have been reasonably well-established, it is not clear whether these signals are required for post-natal maintenance of tissue-resident ILCs. Data from Possot *et al.* suggests that acquisition of defining transcription factors by ILC progenitors to form mature ILCs occurs in peripheral tissues, as RORγt^{-} CLP-like cells with the potential to give rise to ILC3 *in vitro* were isolated from both adult spleen and Small Intestine Lamina Propria (SILP), although from this data it is unclear at what stage of maturation the progenitor populations seed these tissues (Possot *et al.*, 2011). Studies using parabiosis revealed little net migration of ILCs from adipose tissues (ATs), lung, small intestine (SI) and liver, even after a year of parabiosis or following infection (Gasteiger *et al.*, 2015, Moro *et al.*, 2016, O'Sullivan *et al.*, 2016, Boulenouar *et al.*, 2017). These findings would therefore support the conclusions of Possot *et al.,* whereby peripheral tissues are seeded by progenitor populations during embryogenesis and these maintain mature ILC populations in these tissues and that mature ILCs are strictly tissue resident (Possot *et al.*, 2011, Gasteiger *et al.*, 2015, Moro *et al.*, 2016, O'Sullivan *et al.*, 2016, Boulenouar *et al.*, 2017). Further evidence of this in humans came from a study by Vély *et al*., who showed that ILCs were not replenished following haematopoietic stem cell transfer in SCID individuals lacking ILCs at birth, due to mutations in the *IL2RG* or *JAK3* genes (Vely *et al.*, 2016). Overall this indicates that mature, tissue-resident populations are maintained by precursor cells within the same tissue, which are seeded during ontogeny. The signals involved in the homeostatic maintenance of ILCs populations are explored below.

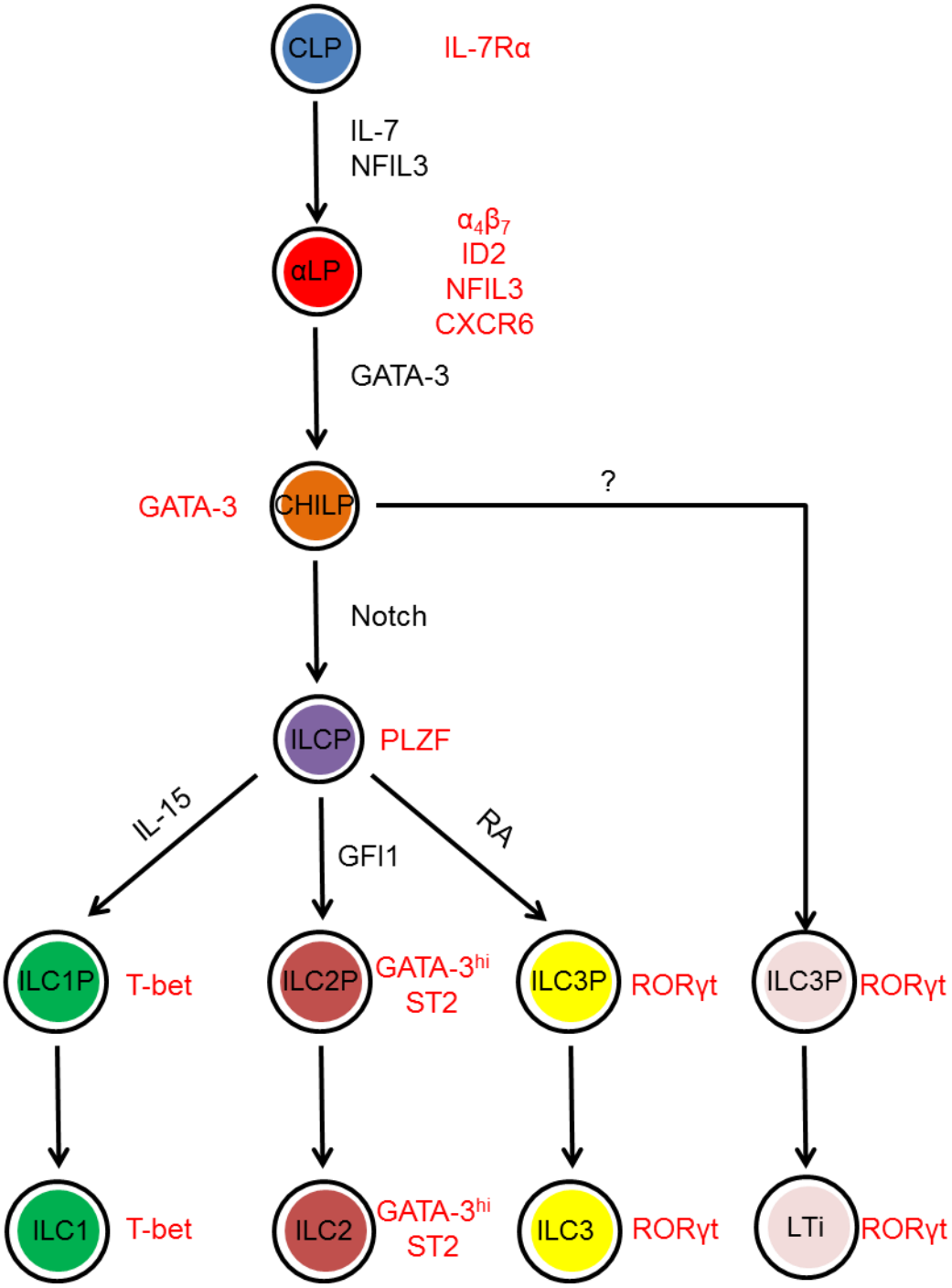

Figure 1.2: ILC development

Schematic based on illustrations by Serafini, Vosshenrich and Di Santo (Serafini *et al.*, 2015). Signals which drive differentiation are in black, whilst subset-defining protein expression is highlighted in red. ILCs develop from a multipotent CLP. IL-7 signalling results in NFIL3 expression and downstream activation of ID2. Subsequent activation of GATA-3 and Notch signalling results in maturation of CHILP and PLZF-expressing ILCP. Whilst IL-15 expression drives ILC1 specification from ILC1P, GFI drives differentiation to ILC2P. Signals driving ILC3 and LTi maturation are less well established, but appear to involve RA.

1.2.2. Signals in ILC homeostasis

Despite differing transcriptional programmes and protein expression, the signals which are required for homeostatic maintenance are conserved amongst the different ILC subsets. Crucially, all ILCs are absent in mice deficient in IL-2Rγ, also referred to as the common gamma chain (γ_c). This feature has been exploited to develop animal models to investigate the role of ILCs in the absence of adaptive immunity; by comparing *RAG2*$^{-/-}$, which lack T cells and B cells, and *RAG2*$^{-/-}$*IL2RG*$^{-/-}$ animals it is possible to infer the relative contribution of ILCs in an immune response (Moro *et al.*, 2010, Hoyler *et al.*, 2012, Spits *et al.*, 2013, Moro *et al.*, 2016). IL-2Rγ forms part of the receptor complexes required for signalling of the cytokines IL-2, IL-4, IL-7, IL-9 and IL-15, indicating that some, if not all, of these factors are required for maintenance of ILCs (Spits *et al.*, 2013, Xu and Di Santo, 2013). The contribution of some of these cytokines to ILC homeostasis is discussed below.

As discussed in chapter 1.2.1, IL-7 receptor signalling is required for the development of ILCs from CLPs (Serafini *et al.*, 2015). In addition, mature ILCs (but not NK cells) require IL-7 for survival and homeostasis (Moro *et al.*, 2010, Hoyler *et al.*, 2012, Huang and Luther, 2012, Vonarbourg and Diefenbach, 2012, Spits *et al.*, 2013). A recent paper by Martin *et al.* demonstrated that IL-7 is produced by stromal cells and suggests a mechanism by which proliferation of lymphocyte populations is controlled by a constitutive pool of IL-7 in LNs during homeostasis and thus the turnover of these cells is limited by the amount of IL-7 in the environment (Martin *et al.*, 2017). Furthermore, by a number of methods including depletion of ILCs, the authors demonstrate that ILCs, especially ILC3 which express high levels of IL-7Rα, outcompete T cells in consumption of this IL-7 pool on a per cell basis. This was due

in part to the increased expression of the transcription factor forkhead box protein 1 (FOXO1), in the T cells which mediates IL-7Rα downregulation in response to IL-7 stimulation. However, this investigation focused only on lymphoid tissues and did not address whether the same mechanism exists in non-lymphoid tissues.

Another well-established protein responsible for homeostatic maintenance of ILCs is the transcription factor ID2. As outlined in chapter 1.2.1, ID2 is required early in the development of ILC progenitor subsets from CLPs to αLP (Yokota *et al.*, 1999, Boos *et al.*, 2007, Hoyler *et al.*, 2012). Before ILC subsets had been recognised, it was discovered that *ID2*$^{-/-}$ animals also lack peripheral lymph nodes (LNs), which require LTi cells for their formation, providing further evidence for the requirement of ID2 in the development of ILCs (Yokota *et al.*, 1999).

A final signal which is important for the maintenance of mature ILCs is IL-2. Mice lacking IL-2, or its receptor IL-2Rα, show similar numbers of ILCs, but reduced cytokine responses (Moro *et al.*, 2010, Dumoutier *et al.*, 2011, Spits *et al.*, 2013, Oliphant *et al.*, 2014, Roediger *et al.*, 2015). IL-2 has been shown to induce proliferation in ILC2s and ILC3s and is produced predominantly by T-cells, which demonstrates the part of the crucial crosstalk between ILCs and T cells (Roediger *et al.*, 2013, Gasteiger *et al.*, 2015, Roediger *et al.*, 2015). Taken together this data may suggest that, although not fully required for homeostatic turnover of ILCs, IL-2 may be important in stimulating proliferation of ILCs following infection or inflammation. Further signals which are known to stimulate effector responses in ILCs by inducing cytokine production are discussed below.

1.2.3. Signals in activation of ILCs

Whilst the signals for the maintenance of mature ILCs are shared between ILC subsets, the signals required for activation (cytokine production) differ drastically amongst the ILC subsets (Xu and Di Santo, 2013). Herein, the focus is on the signals for activation of ILC2, the reasons for which will become clear later in this report.

The first established activators of ILC2 cytokine production were IL-25, IL-33 and Thymic Stromal Lymphopoietin (TSLP). These are cytokines produced by stromal cells, especially epithelial cells, upon damage or invasion of pathogens (Bianchi, 2007). These cytokines therefore act as some of earliest signals during an immune response and are referred to as alarmins.

The action of IL-33 on ILC2s is best established of the alarmins (Mjosberg *et al.*, 2011, Barlow *et al.*, 2013, Molofsky *et al.*, 2015b, Han *et al.*, 2017). IL-33 is a member of the IL-1 family of cytokines and can be found as a stable intranuclear protein within epithelial cells, which is released upon cellular damage or upon pathogen entry, stimulating recruitment and activation of other cells (Molofsky *et al.*, 2015a).

The receptor for IL-33, ST2, is expressed by Th2, Tregs and mast cells (Kakkar and Lee, 2008, Vasanthakumar *et al.*, 2015). ST2 is also found on the surface of ILC2s (Lohning *et al.*, 1998, Spooner *et al.*, 2013). IL-33 binding of ST2 and IL-1 receptor accessory protein (IL1RAP) results in activation of the adaptor protein myeloid differentiation primary response gene 88 (MyD88) (Schmitz *et al.*, 2005, Griesenauer and Paczesny, 2017). This in turn activates downstream signalling pathways including the mitogen activated protein kinase (MAPK) and nuclear factor kappa-

light-chain-enhancer of activated B cells (NF-κB) pathways (Schmitz *et al.*, 2005). Of note, one of the downstream targets of ST2 signalling is GATA-3, which is likely to be the mechanism by which ST2 induces type-two cytokine production on both Th2 cells and ILC2s. Furthermore, GATA-3 can bind the promoter region of ST2, resulting in increased ST2 expression and thus a positive feedback loop is formed through ST2 signalling. IL-33 also induces proliferation of ILC2s, and ILC2s are found in reduced numbers in tissues of *IL1RL1*$^{-/-}$ mice (Califano *et al.*, 2015, Molofsky *et al.*, 2015b). Of the alarmins discussed above, IL-33 is the most potent in inducing *ex vivo* type-two cytokine expression, and is the only alarmin to induce IL-4 expression by ILC2s in culture (Molofsky *et al.*, 2015b). Consistent with this induction of type-two cytokines *in vitro*, IL-33 also contributes to ILC2 function *in vivo* including clearance of helminth infection and driving allergen-induced lung inflammation (Neill *et al.*, 2010, Barlow *et al.*, 2013, Pelly *et al.*, 2016, Han *et al.*, 2017).

IL-25, also known as IL-17E, is structurally similar to IL-17 and signals through IL-17RB (Lee *et al.*, 2001). IL-25, like IL-33, induces production of IL-5 and IL-13 by ILC2s and Th2 both *in vitro* and *in vivo,* but can only stimulate IL-4 production by the latter cells *in vitro* (Fort *et al.*, 2001, Barlow *et al.*, 2013, Califano *et al.*, 2015, Moro *et al.*, 2016, Han *et al.*, 2017). Again, like IL-33, IL-25 receptor signalling through IL-17RB leads to activation of NFκB signalling. IL-25 has also been shown to contribute to *in vivo* ILC2 function (Neill *et al.*, 2010). Research by Huang *et al* identified a population of KLRG1^{-} ILC2s in the lung which, upon activation with IL-25 but not IL-33, expressed KLRG1 and contributed to allergen-induced lung inflammation (Huang *et al.*, 2015). Finally, there is growing evidence for a ‘memory’ population of ILC2s, which survives following a primary response and its cytokine

production is augmented upon reactivation (Halim *et al.*, 2016, Martinez-Gonzalez *et al.*, 2016, Martinez-Gonzalez *et al.*, 2017). These memory ILC2s were demonstrated to express higher levels of IL-17RB than non-antigen experienced ILC2s (Martinez-Gonzalez *et al.*, 2016). However, unlike conventional memory lymphocytes, these memory cells respond in a non-antigen specific manner, hence this enhanced cytokine production may be against an entirely different antigen than the primary response. Thus, it remains controversial whether these cells can be described as memory cells (Martinez-Gonzalez *et al.*, 2017). As this study focused exclusively on lung ILC2s, it is important that further research is undertaken into whether this feature exists in other tissues.

TSLP is an alarmin which was initially discovered in the thymus of mice, but it also appears to be more widely expressed by epithelial cells of other tissues as well, including skin and lung (Takai, 2012). TSLP has also been shown to stimulate type-two cytokine production by ILC2 *ex vivo,* although to a lesser extent than IL-33 (Soumelis *et al.*, 2002, Ying *et al.*, 2005, Ying *et al.*, 2008, Hanabuchi *et al.*, 2010, Han *et al.*, 2017). Consistent with this, TSLP levels are increased in the lungs of asthmatic patients and correlates with severity of the disease. TSLP and IL-25 both appear to synergise with IL-33 to increase ILC2 type-two cytokine production *in vitro*, although this effect has not been tested *in vivo* (Han *et al.*, 2017).

In addition to cytokines, recent evidence indicates ILC2s can also respond to eicosanoid derivatives, including prostaglandins and cysteinyl leukotrienes (Barnig *et al.*, 2013, Doherty *et al.*, 2013, Qiu *et al.*, 2014, Xue *et al.*, 2014, Lee *et al.*, 2015a, Wojno *et al.*, 2015, Lund *et al.*, 2017).

A recent paper by Xue *et al.* investigated the effect of prostaglandin D_2 (PGD_2) on human ILC2 effector function (Xue *et al.*, 2014). PGD_2 induced *ex vivo* type-two cytokine production by human peripheral blood ILC2s, an effect which synergised with IL-33 or IL-25 treatment. Blocking of one of the PGD_2 receptors, chemokine receptor homologous molecule expressed on Th2 lymphocytes (CRTH2), abrogated these effects, indicating that this effect was mediated through this receptor. *Ex vivo,* PGD_2 also had a chemotactic effect on cultured ILC2s. This effect was also confirmed in the lungs of mice, although no antibody currently exists to detect CRTH2 protein in mice, therefore it is unknown whether this effect is mediated by CRTH2 (Wojno *et al.*, 2015). Interestingly, in the former study, PGD_2 treatment, but not IL-25 or IL-33, induced production of other pro-inflammatory cytokines including IL-3, IL-8 and IL-21 (Xue *et al.*, 2014). Consistent with this, pulmonary inflammation following helminth infection in mice was shown to be partially CRTH2-dependent (Wojno *et al.*, 2015). Further investigation is required to determine whether this inflammation was due to production of these pro-inflammatory cytokines, or due to the classical type two cytokine signature of ILC2s, as these cytokines have also been shown to drive allergen or IL-33-induced lung inflammation (Ying *et al.*, 2005, Ying *et al.*, 2008, Molofsky *et al.*, 2015a, Martinez-Gonzalez *et al.*, 2016).

The final signals known to induce ILC2 cytokine production is the cysteinyl leukotrienes leukotriene C_4 (LTC_4) and leukotriene D_4 (LTD_4) (Doherty *et al.*, 2013, Lund *et al.*, 2017). Like the alarmins discussed previously, LTD_4 has been shown to induce production of IL-5 and IL-13 by mouse ILC2s *ex vivo*, with similar potency to IL-33 (Doherty *et al.*, 2013). However, unlike the alarmins, LTD_4 treatment also stimulated a significant production of IL-4 by isolated ILC2s.

Lund *et al*. also explored the effect of LTC_4 on ILC2 function (Lund *et al.*, 2017). As with LTD_4, LTC_4 also induced IL-5 and IL-13 production in freshly isolated mouse ILC2s. Additionally, LTC_4 treatment *in vivo* induced lung inflammation, and this effect synergised with IL-33 co-treatment. This effect was mediated by the receptor for both LTC_4 and LTD_4, cysteinyl leukotriene receptor 1 (CysLTR1), indicating a shared mechanism by which cysteinyl leukotrienes may exert their effects on ILC2s function.

Consistent with the role of ILC2-derived cytokine production in the beigeing of fat (see chapter 1.3.4), eicosanoids, which include cysteinyl leukotrienes, were found to contribute to cold-induced beigeing of AT (Qiu *et al.*, 2014, Brestoff *et al.*, 2015, Lee *et al.*, 2015a). As eicosanoids are generated from polyunsaturated fatty acids (PUFA), this pathway may represent an underappreciated mechanism by which the metabolic status of the tissues (concentration of PUFA) can be detected by the immune system and manipulated to improve metabolic homeostasis by inducing beigeing of AT, but additional research is required to confirm this.

1.2.4. ILC2 tissue distribution

Presence of ILC subsets have been reported in peripheral and mucosal LN, spleen, bone marrow and liver in mice and in the peripheral blood of humans (Price *et al.*, 2010, Mackley *et al.*, 2015). However, ILC subsets appear to be particularly enriched at barrier surfaces, including mucosal sites such as the lung and SILP, and also in the skin of both humans and mice (Price *et al.*, 2010, Salimi *et al.*, 2013, Mashiko *et al.*, 2017). Another tissue that appears to be enriched for ILCs, especially ILC2s, are ATs (Molofsky *et al.*, 2013, Molofsky *et al.*, 2015a, Molofsky *et al.*, 2015b, Moro *et al.*, 2015, Uhm and Saltiel, 2015, Moro *et al.*, 2016). Furthermore, lymphoid clusters which are found in varying numbers in different ATs, termed Fat Associated

Lymphoid Clusters (FALC), appear to also be enriched in ILC2s (Moro *et al.*, 2010, Benezech *et al.*, 2015, Jackson-Jones *et al.*, 2016). Interestingly, Moro *et al.* noted an enrichment of ILC2s in the mesenteries, which has a greater number of FALC than the other ATs examined in the study, suggesting that the FALC were the predominant source of ILC2s within this tissue. However, other groups have noted high numbers of ILC2s in tissues with low numbers of FALC, such as the perigonadal fat (Benezech *et al.*, 2015). The structure of both lymphoid tissues and ATs are discussed in chapters 1.3 and 1.4.

1.3. STRUCTURE AND FUNCTION OF ADIPOSE TISSUES

ATs are evolutionarily conserved, as demonstrated by their presence in both vertebrates and invertebrates, and they play a diverse range of functions ranging from thermal insulation to endocrine function, depending on the type of AT (Azeez *et al.*, 2014). The main constituents of ATs are stromal cells, called adipocytes, which are key to the variety of functions described above. ATs can be broadly classified as white adipose tissue (WAT), brown adipose tissue (BAT) or beige adipose tissue, based largely on their composition and function, as outlined below.

1.3.1. WAT structure and function

WAT is the predominant form of AT found in both humans and mice (Bjorndal *et al.*, 2011, Chusyd *et al.*, 2016). WAT can be further characterised by its anatomical location; visceral adipose tissue (VAT) is localised around internal organs, whilst subcutaneous adipose tissue (SCAT) is found under the epidermal and dermal layers of the skin. In both locations the WAT acts as an insulating layer in addition to being the primary site of lipid metabolism. During states of caloric excess lipids are stored

as triglyceride droplets within adipocytes, and when energy stores are low these lipids can be catabolised to free fatty acids (FFA), which can be used as a cellular energy source (Young and Zechner, 2013). In addition to these functions, WAT is categorised as an endocrine organ as it can release hormones, such as Leptin and Adiponectin, which both control energy metabolism. Release of these hormones can be stimulated by a range of stimuli including cellular and neural signalling (Zeng *et al.*, 2015). Adipocytes from WAT can also secrete many different cytokines and chemokines including TNF and IL-6 (Coppack, 2007). Through both the metabolism of lipids and the endocrine function of adipocytes, WAT plays a crucial role in coordinating both local and systemic metabolic homeostasis.

In humans, the main VAT depots are the omental, mesenteric, retroperitoneal, gonadal and pericardial depots (Bjorndal *et al.*, 2011, Chusyd *et al.*, 2016). In contrast, SCAT is located in the gluteofemoral and intramuscular regions.

According to the World Health Organisation (WHO), rates of obesity have doubled worldwide since 1980 and ~3.5 million deaths a year are attributable to obesity (WHO, 2015). There is a strong correlation between the anatomical distribution of adiposity and metabolic dysfunction, more specifically high intra-abdominal adiposity has a strong correlation with metabolic dysregulation (Koster *et al.*, 2010). Moreover, obesity appears to be predominantly associated with excess VAT adiposity, not SCAT (Bjorndal *et al.*, 2011, Lee *et al.*, 2013, Strissel *et al.*, 2014). As a result of these findings, significant research into understanding the mechanisms underlying metabolic disease, and potential therapeutic interventions are being performed both in humans and in mouse models.

Like humans, mouse WAT can be sub-divided into VAT and SCAT. However, the distribution of fat depots in mice is different to humans. As discussed by Chusyd *et al.*, the VAT depot that is most similar between humans and mice is the mesenteric depot (Chusyd *et al.*, 2016). Despite this, the majority of studies performed in mice have focused on the perigonadal depot, referred to as epididymal fat in males and periovarian fat in females (Chusyd *et al.*, 2016). In this study both the mesenteric and epididymal fat (henceforth referred to as gonadal fat) depots are investigated in a variety of contexts.

1.3.2. Features of WAT adipocytes

As described above, one of the functions of WAT is to maintain both local and systemic homeostasis (Ouchi *et al.*, 2011, Kang *et al.*, 2016, Man *et al.*, 2017). The main constituents of WAT are adipocytes, which are crucial in this role of controlling the metabolic status. Mature adipocytes are generated from a multipotent progenitor population which expresses preadipocyte factor 1 (Pref-1), platelet derived growth factor receptor α (PDGFRα), and lymphotoxin beta receptor (LTβR) (Benezech *et al.*, 2012). In a study by Bénézech *et al.,* these cells are referred to as adipocyte progenitors (APs) and were isolated from both foetal and adult AT (Benezech *et al.*, 2012). These APs spontaneously develop into mature adipocytes in culture (adipogenesis). However, further investigation revealed that stimulation of the non-canonical LTβR pathway, which involves RelB, blocked this adipogenesis and instead resulted in differentiation of AP cells into lymphoid stromal cells. The presence of these multipotent cells within adult AT indicates the ability to remodel both SLT and AT postnatally in response to unknown stimuli.

As outlined above in chapter 1.3.1, one of the functions of WAT adipocytes is the storage of lipid. In situations of extreme calorie excess, such as in obesity, adipocytes become hypertrophic and hyperplasic due to an overabundance of lipid stored within these cells (Pradhan *et al.*, 2001, Hotamisligil, 2006, Kang *et al.*, 2016, Czech, 2017, Man *et al.*, 2017). This results in the release of both TNF and IL-6 from adipocytes (Pradhan *et al.*, 2001, Hotamisligil, 2006, Kang *et al.*, 2016). Release of these pro-inflammatory cytokines has a wide ranging impact on the metabolic status of WAT, which is discussed in chapter 1.3.5.

1.3.3. Structure and function of BAT

In contrast to WAT, which is anatomically distributed throughout both humans and mice, BAT depots are less numerous (Bjorndal *et al.*, 2011, Chusyd *et al.*, 2016). In adult humans only two BAT depots exist around the shoulder blades and collarbone, whilst in mice only one depot exists in a similar area (Saito *et al.*, 2009, Virtanen *et al.*, 2009, Chusyd *et al.*, 2016). Interestingly in infant humans a greater distribution of BAT is seen, which decreases with age (Lidell *et al.*, 2014).

Unlike WAT, which functions as energy storage, BAT instead uses energy to generate heat, referred to as thermogenesis. This is achieved predominantly through the expression of the protein uncoupling protein 1 (UCP1) (Qiu *et al.*, 2014, Rao *et al.*, 2014, Brestoff *et al.*, 2015, Lee *et al.*, 2015a, Lynch *et al.*, 2016). The human body uses energy in the form of Adenosine Triphosphate (ATP), which is produced via a variety of metabolic pathways, including oxidative phosphorylation in the mitochondria. During this process a proton gradient is generated across the mitochondrial membrane, which is then used by the enzyme ATP synthase to produce ATP. UCP1 prevents this process by increasing the permeability of the inner

mitochondrial membrane to reduce the proton electrochemical gradient (Rao *et al.*, 2014). The net result is generation of heat, at the expense of ATP production. One stimulus which induces UCP1 expression is cold exposure (Himms-Hagen, 1990, Razzoli *et al.*, 2016). Due to this, BAT is found in large quantities in hibernating mammals and this is also why infants, who are less able to maintain their body temperature, have a greater volume of BAT than adults (Virtanen *et al.*, 2009, Lidell *et al.*, 2014).

Another contrast between WAT and BAT is the mechanisms by which their function is controlled. As discussed in chapters 1.3.2 and 1.3.5, WAT function is controlled by cytokines and other proteins. In contrast, BAT is highly enriched in neurons, which deliver signals from the sympathetic nervous system to this tissue via the neurotransmitter norepinephrine (noradrenalin). Although the expression of UCP1 is constitutive in BAT (Brestoff *et al.*, 2015)**,** norepinephrine production induces upregulation of thermogenic activity in BAT. One stimulus which induces norepinephrine release and UCP1 upregulation is exposure to a cold environment. In contrast, the neurotransmitter serotonin inhibits UCP-1 upregulation and is increased in obesity (Crane *et al.*, 2015).

These strong contrasts in structure and function between WAT and BAT are also reflected in the stromal vascular fraction (SVF). Both the immune cell composition and the predominance of AP differed between BAT and WAT (Prunet-Marcassus *et al.*, 2006). Furthermore, the adipocyte precursor population within BAT showed a reduced plasticity compared with WAT. This is consistent with studies which have shown that BAT and WAT form from different stem cell populations during

embryogenesis (Xue *et al.*, 2007, Seale *et al.*, 2008, Petrovic *et al.*, 2010, Sharp *et al.*, 2012, Wu *et al.*, 2012).

1.3.4. Beige adipose tissue

Recent research indicates that adipocytes within WAT can acquire UCP1 expression in response to a variety of stimuli including environmental temperature, acquiring the thermogenic properties of BAT (Lim *et al.*, 2012, Qiu *et al.*, 2014, Rao *et al.*, 2014, Brestoff *et al.*, 2015, Lee *et al.*, 2015a, Lynch *et al.*, 2016). Studies investigating the development of these responses have confirmed that this process occurs specifically in WAT and is distinct from the processes which form adipocytes in BAT (Xue *et al.*, 2007, Seale *et al.*, 2008, Petrovic *et al.*, 2010, Sharp *et al.*, 2012, Wu *et al.*, 2012, Shinoda *et al.*, 2015). As a result, this process has been referred to as 'beigeing' of fat. Due to the clearly apparent therapeutic opportunity to manipulate this process to counteract obesity, and thus metabolic dysregulation, there has been a surge in research to understand the underlying mechanisms by which beigeing occurs (Lidell *et al.*, 2014, Qiu *et al.*, 2014, Rao *et al.*, 2014, Brestoff *et al.*, 2015, Lee *et al.*, 2015a, Lynch *et al.*, 2016).

A number of groups initially indicated the presence of BAT-like depots in adults humans, which had increased glucose uptake following cold-exposure (Qiu *et al.*, 2014, Rao *et al.*, 2014, Lee *et al.*, 2015a). This led both Rao *et al.* and Qiu *et al.* to further investigate the mechanisms by which this phenomenon occurred (Qiu *et al.*, 2014, Rao *et al.*, 2014). The finding of these studies, and others, are summarised in Figure 1.3.

Qiu *et al.* demonstrated that, following exposure to cold, eosinophils and AAM migrate into SCAT where they induce UCP1 expression through production of type two cytokines IL-4 and IL-13 (Qiu *et al.*, 2014). Further work by this group demonstrated eosinophils to be the predominant producer of IL-4 and IL-13 (Lee *et al.*, 2015a). These cytokines signal through the IL4Rα on AAM leading to the release of catecholamines. Lee *et al.* also noted the expression of IL-4Rα on the surface of AP cells and demonstrated that both type two cytokines and catecholamines led to the proliferation and differentiation of AP cells, which acquired the expression of UCP1 (Lee *et al.*, 2015a). However, research by Fischer *et al.* disputes this catecholamine production by AAMs, as when Tyrosine Hydroxylase, which is required for catecholamine production, was deleted from haematopoietic cells, no net differences were observed in beigeing of adipocytes or in energy expenditure (Fischer *et al.*, 2017). Research by Rao *et al.* built upon the proposed model above, demonstrating that upon cold exposure, the expression of the protein Meteorin-like (Metrnl) was induced within AT, although the cellular source of Metrnl within AT was not investigated (Rao *et al.*, 2014). The authors also established that Metrnl expression stimulated type-two cytokine production by eosinophils. Finally, both Brestoff *et al.* and Lee *et al.* show evidence for ILC2s contributing to beigeing of WAT by both the production of type-two cytokines (Lee *et al.*, 2015a) and methionine-encephalin ((met-encephalin),(Brestoff *et al.*, 2015)) acting directly on APs (Figure 1.3).

In addition to the ILC2, eosinophil and macrophage circuit, Lynch *et al.* demonstrated that invariant natural killer T cells (iNKT) cells can also induce UCP1 expression in WAT adipocytes (Lynch *et al.*, 2016). Activation of iNKT with either

α-Galactosylceramide (α-gal-cer) or glucagon-like peptide 1 (GLP-1) receptor agonists led to the production of fibroblast growth factor 21 (FGF21), which induced UCP1 expression in WAT adipocytes. This resulted in a reduction in mass of both inguinal and epididymal fat pads in mice and also resulted in improved metabolic parameters including fasting glucose levels.

Thus, in summary, ILC2, eosinophils, iNKTs and AAM along with Metrnl, met-encephalin, catecholamines, FGF21 and type 2 cytokines contributed to beigeing of WAT ((Figure 1.3), (Qiu *et al.*, 2014, Rao *et al.*, 2014, Brestoff *et al.*, 2015, Lee *et al.*, 2015a, Lynch *et al.*, 2016)). This pathway is of particular relevance as exogenous induction of WAT beigeing resulted in improved metabolic parameters including increased oxygen consumption, energy expenditure and insulin sensitivity and reduced fat mass in mice (Rao *et al.*, 2014, Brestoff *et al.*, 2015, Lynch *et al.*, 2016). The coregulatory protein PR domain containing 16 (PRDM16) appears to also appears control the thermogenic potential of WAT, but not BAT, adipocytes and is upstream of UCP1 expression (Cohen *et al.*, 2014). In accordance with this, when mice lacking the protein PR domain containing 16 (PRDM16) were fed a HFD, they presented with increased weight gain and insulin resistance compared to WT animals (Cohen *et al.*, 2014). Taken together these results indicate that targeting this pathway may be a novel therapeutic strategy in the treatment of obesity and metabolic disorder (Lidell *et al.*, 2014, Xue *et al.*, 2015, Lynch *et al.*, 2016).

Figure 1.3: Beigeing of WAT

Illustration of signals driving UCP1 expression in WAT adipocytes based on work by Lynch *et al.*, Rao *et al.*, Qiu *et al.,* Lee *et al.* and Brestoff *et al.*(Qiu *et al.*, 2014, Rao *et al.*, 2014, Brestoff *et al.*, 2015, Lee *et al.*, 2015a, Lynch *et al.*, 2016). IL-33 stimulates production of type two cytokines by ILC2s. IL-5 drives proliferation and activation of eosinophils, resulting in IL-4 and IL-13 expression. These cytokines can act both directly on AP and on macrophages, resulting in conversion of the latter cells to AAM and stimulating the production of catecholamines through expression of tyrosine hydroxylase (TH). Catecholamines produced by AAM and ILC2s and met-enk also by ILC2s result in differentiation of AP to mature UCP1-expressing adipocytes. iNKT cells can also drive UCP1 expression in adipocytes through the production of FGF21. Finally, a feedback loop exists, whereby adipocyte production of metrnl drives activation of eosinophils.

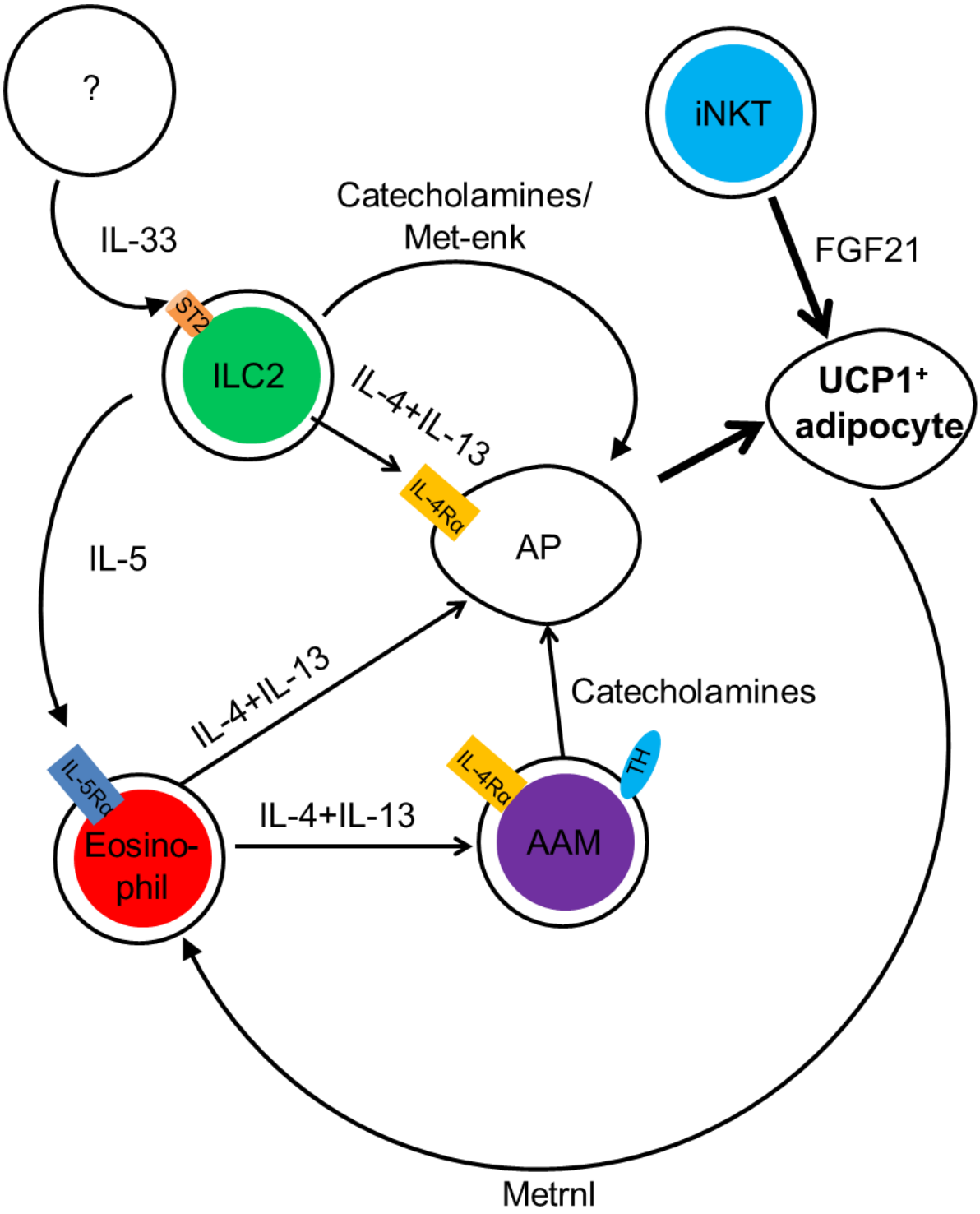
?
iNKT
IL-33
Catecholamines/
Met-enk
FGF21
ST2
ILC2
IL-4+IL-13
UCP1+
adipocyte
IL-4Rα
AP
IL-5
IL-4+IL-13
Catecholamines
IL-5Rα
IL-4Rα
TH
Eosino-
phil
IL-4+IL-13
AAM
Metrnl

1.3.5. Immunometabolism

As reviewed by Man, Kutyavin and Chawla, the crosstalk between adipocytes, other stromal cells and immune cells within WAT are crucial not only for maintaining tissue metabolic homeostasis, but also have an impact on systemic metabolism (Man *et al.*, 2017). Conversely the metabolic status of a tissue also has an effect on immune cells function, as certain metabolic checkpoints exist in immune cell activation and must be overcome for full function (Venken *et al.*, 2014, Xu *et al.*, 2017)**.** Moreover, activation of immune cells by a variety of mechanisms, including ligation of co-stimulatory/co-inhibitory receptors and activation of pathogen-associated molecular patterns (PAMPs), results in changes in cellular metabolism (Fox *et al.*, 2005, Pearce and Pearce, 2013, O'Neill and Pearce, 2016). This has led to the field of immunometabolism research.

As outlined in chapter 1.3.2, during obesity adipocytes become stressed, leading to the release of pro-inflammatory mediators (Kang *et al.*, 2016, Shan *et al.*, 2017). There is growing evidence that both TNF and IL-6 release by adipocytes lead to an influx in pro-inflammatory cells (Hotamisligil *et al.*, 1993, Weisberg *et al.*, 2003, Hotamisligil, 2006, Lumeng *et al.*, 2007, Wu *et al.*, 2007, Kintscher *et al.*, 2008, Nishimura *et al.*, 2009, McLaughlin *et al.*, 2014, Cho *et al.*, 2016). These pro-inflammatory pathways listed above increase signalling through a variety of ‘physiological stress’ pathways, one of which is the Jun N-terminal kinase (JNK) pathway, and leads to decreased insulin signalling (Hotamisligil, 2010). This ultimately leads to insulin resistance and a variety of other diseases due to metabolic dysfunction (Hotamisligil *et al.*, 1993, Hotamisligil, 2006, Ouchi *et al.*, 2011). However, there is also evidence that anti-inflammatory cells, such as ILC2s, iNKTs

and alternatively activated macrophages (AAM) are activated under low grade inflammation and act to counteract this inflammation (Odegaard *et al.*, 2008, Lynch *et al.*, 2009, Miller *et al.*, 2010, Lynch *et al.*, 2012, Satoh *et al.*, 2012, Schipper *et al.*, 2012, Hams *et al.*, 2013, Molofsky *et al.*, 2013, Lynch, 2014, Venken *et al.*, 2014, Hashiguchi *et al.*, 2015, Lynch *et al.*, 2015). The role of B cells in adipose tissue inflammation is more controversial, as they have been shown to both promote (Winer *et al.*, 2011) and counteract (Nishimura *et al.*, 2013) adipose tissue inflammation. Manipulation of the immune cell composition and protein expression has therefore been the focus for therapeutic interventions of metabolic disease (Lidell *et al.*, 2014). Furthermore, as discussed in chapter 1.3.4, induction of UCP1 expression in adipocytes by a process referred to as beigeing also leads to improved metabolic parameters and could also be used as a target for treatment of metabolic dysregulation.

In addition to the anti-inflammatory effects of immune cells detailed above, adipocytes can also mediate anti-inflammatory signalling within ATs in a paracrine manner. Kwon *et al.* demonstrated that pro-inflammatory signalling involving the protein inhibitor of nuclear factor κ-B kinase subunit β (IKKβ) also induces adipocyte specific expression of IL-13 (Kwon *et al.*, 2014). This can directly inhibit cytokine production by pro-inflammatory cells including Th1 and M1 macrophages.

Finally, in addition to responding to pro-inflammatory cytokines there is growing evidence that immune cells are able to directly respond to markers of nutrient status, PUFA and expression of peroxisome-proliferator-activated receptor δ and γ (PPARδ/γ) (Odegaard *et al.*, 2008, Pal *et al.*, 2012, Lidell *et al.*, 2014). This nutrient-sensing mechanism can either prevent (Odegaard *et al.*, 2008) or drive (Pal *et al.*,

2012) inflammation. Importantly, some have hypothesised this ability could be important for immunity against a variety of pathogens which show a tropism for invasion of ATs, such as human cytomegalovirus (HCMV) or *Mycobacterium tuberculosis* (Man *et al.*, 2017), as infection by these organisms can alter metabolic parameters. This indicates a potential direct link between nutrient status of AT and the activation phenotype of immune cells within them.

In summary, the reciprocal interaction between stromal cells and immune cells in AT has a substantial effect on the metabolic homeostasis both locally and systemically, but also may govern how immune responses within ATs proceed.

1.4. SECONDARY AND TERTIARY LYMPHOID TISSUES

Lymphoid tissues are sites of lymphocyte enrichment and perform a wide variety of functions which are all vital to maintaining a fully functional immune system. Primary lymphoid tissues, including the bone marrow and thymus, are the sites of leukocyte production, termed haematopoiesis. In contrast, SLTs, the main example of which are LNs, are involved in the coordination of immune responses. Following activation, cells of the innate immune system, primarily antigen presenting cells (APCs), migrate to SLT which acts as a 3D structure to facilitate optimal subsequent activation of adaptive immune responses (Cyster, 1999, Forster *et al.*, 1999, Chang and Turley, 2015). Tertiary lymphoid tissues, such as mucosal-associated lymphoid tissues (MALT) and bronchial-associated lymphoid tissues (BALT), appear to serve a similar function to SLTs in coordinating immune responses, but primarily in local tissues (Moyron-Quiroz *et al.*, 2004). This allows faster initiation of adaptive immune responses to local tissues than seen following activation of adaptive immunity within SLTs (Dieu-Nosjean *et al.*, 2014). Finally, the presence of lymphoid clusters within

ATs, referred to as FALC, has been the focus of recent research (Moro *et al.*, 2010, Koyasu and Moro, 2013, Benezech *et al.*, 2015, Cruz-Migoni and Caamano, 2016, Jackson-Jones *et al.*, 2016). The structure and formation of both SLTs (LN) and FALC are described below.

1.4.1. Lymph node formation

Although the general signals required for SLT formation are conserved between tissues, there are subtle differences in the requirement of some genes in the formation of different SLTs, for example peripheral vs. mucosal LN (Cupedo *et al.*, 2004, van de Pavert *et al.*, 2009), or Peyer's patches (Kim *et al.*, 2000, Yoshida *et al.*, 2002). This is evidenced by selective loss of different SLTs in mouse models of gene deletion such as C-X-C motif chemokine ligand 13 deficient ($CXCL13^{-/-}$) mice, which lack peripheral LN but not mucosal LN, and $TRAF6^{-/-}$ mice, which lack LN but not Peyer's patches (Yoshida *et al.*, 2002, van de Pavert *et al.*, 2009). Thus, the description of SLT formation provided below is a generalised overview and is summarised in Figure 1.4.

LN organogenesis is initiated at approximately embryonic day 12.5 (E12.5) in mice, although this varies between different anatomical sites (Blum and Pabst, 2006, van de Pavert *et al.*, 2009, Vondenhoff *et al.*, 2009, Benezech *et al.*, 2010, van de Pavert and Mebius, 2010). The precise mechanism by which LN organogenesis is initiated is a topic of debate; one model proposes that mesenchymal cells receive stimulation from local neurons in the form of RA, which induces the expression of CXCL13 in these mesenchymal cells (van de Pavert *et al.*, 2009). These mesenchymal cells are likely to be the multipotent Pref-1^{+} AP population described in chapter 1.3.2, which express PDGFRα and intermediate levels of the cell adhesion molecules vascular

cell adhesion molecule-1 (VCAM-1) intracellular adhesion molecule-1 (ICAM-1) (Benezech *et al.*, 2012). The CXCL13 gradient results in an initial influx of $CXCR5^+$ haematopoietic cells which are responsible for inducing and driving LN formation, as demonstrated by the lack of peripheral lymphoid tissues when these cells were depleted by the absence of the transcription fact ID2 (Yokota *et al.*, 1999). Therefore, these cells were termed lymphoid tissue inducer cells (LTi). As briefly mentioned in chapter 1.2, subsequent research identified these cells as pre-natal counterparts of a subset of group 3 ILCs, LTi-like cells. These cells are referred to as LTi-like, as their predominant post-natal role appears to be focused on repair of lymphoid tissue following damage and in the maintenance of $CD4^+$ memory cells (Kumar *et al.*, 2010, Withers *et al.*, 2012).

Following recruitment of LTi cells to the forming LN anlage, receptor activator of nuclear factor-kappa-B ligand (RANKL) is expressed by these cells and binds to RANK on the surface of other LTi cells in an autocrine manner (Kim *et al.*, 2000). Downstream signalling leads to the expression of the LTβR ligand LTα1β2 by LTi. (Kim *et al.*, 2000, Yoshida *et al.*, 2002, White *et al.*, 2007). The LTα1β2-LTβR pathway in results in maturation of $CXCL13^+$ stromal cells to a predecessor of mature LN stromal cells (Benezech *et al.*, 2012). These cells are called lymphoid tissue organiser cells (LTo), and their maturation is marked by increased expression of CXCL13, VCAM-1 and ICAM-1, and the additional expression of mucosal vascular addressin cell adhesion molecule-1 (MAdCAM-1) and chemokine (C-C motif) ligand 19 (CCL) and CCL21 (Benezech *et al.*, 2010). Whilst CXCL13, CCL19 and CCL21 stimulates further migration of haematopoietic cells to the forming LN anlage, cell adhesion molecule expression allows for clustering of LTo and retention of

haematopoietic cells, eventually leading to the development of the stromal network and formation of the mature LN (van de Pavert and Mebius, 2010).

Recent data disputes the model described above, instead supporting a sequence of events where endothelial cells in areas of lymph node formation from both the blood and lymphatic vasculature are responsible for the initial clustering of circulating LTi cells by the production of CCL19 (Onder *et al.*, 2017). Interaction between RANK on endothelial cells and RANKL on the surface of LTi cells is crucial for this initial clustering of LTi cells. This was demonstrated by impairment of LN formation in mice deficient in RANK specifically in endothelial cells. In this proposed model, mesenchymal LTo cells are still required for further clustering of LTi cells and LN organogenesis, but act subsequently to initial endothelial cell-LTi cell interactions. Further investigation is required to confirm this and also to elucidate the sequence of events which drive initial endothelial cell expression of CCL19 at specific sites in the lymphatic and blood vasculature which result in the attraction of mesenchymal LTo cells to sites of lymph node formation.

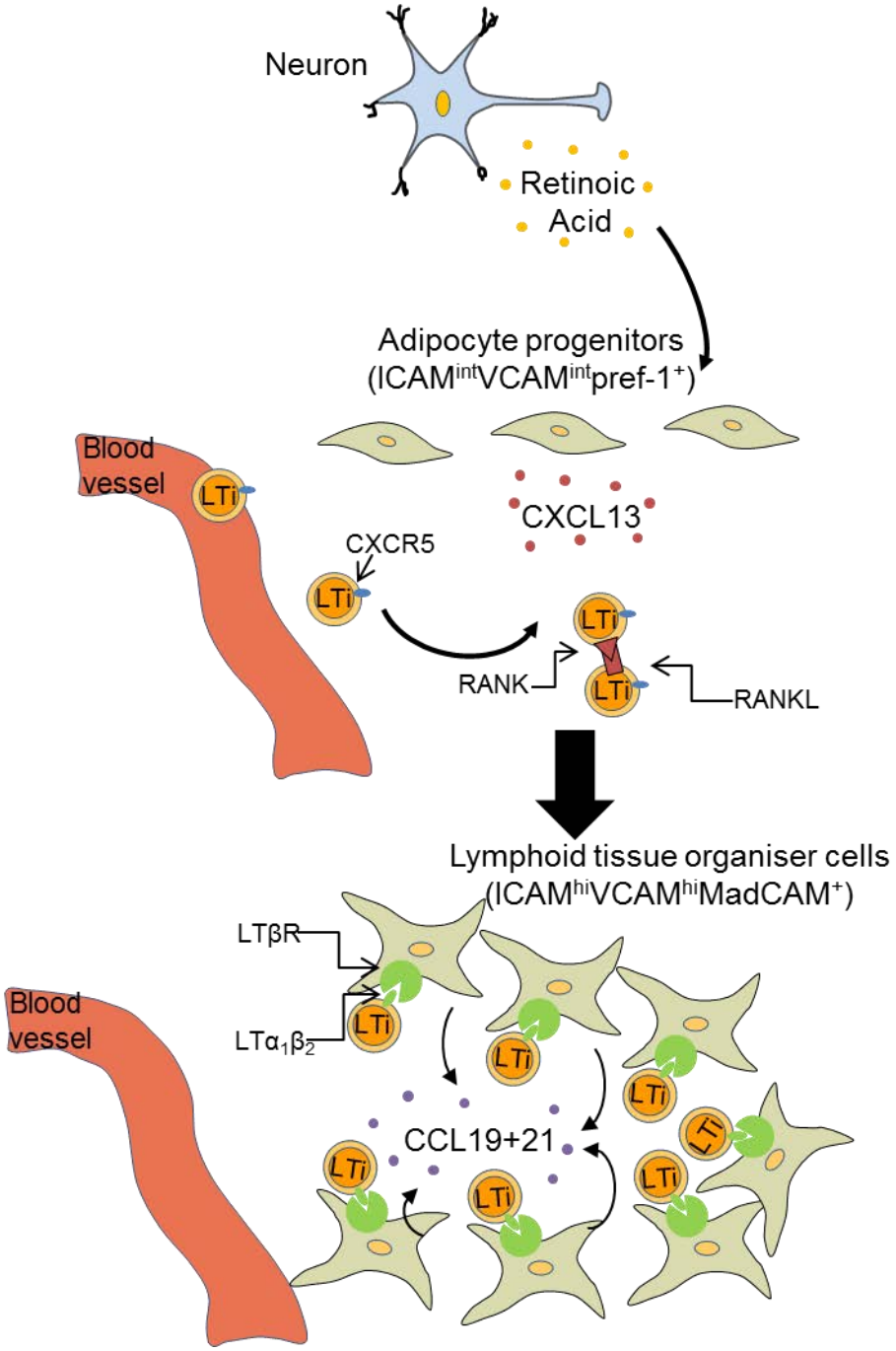

Figure 1.4: Formation of LNs

Schematic based on figure by Van de Pavert and Mebius illustrating signals involved in LN organogenesis (van de Pavert and Mebius, 2010). Neural signals result in the release of RA by local neurones, which in turn stimulates CXCL13 production by mesenchymal AP cells (van de Pavert *et al.*, 2009). This results in the migration of CXCR5 expressing LTi cells from the bloodstream into the developing LN anlage. Autocrine RANK:RANKL signalling on LTi results in these cells expressing LTα1β2 and engaging LTβR on the surface of stromal cells. LTβR activates leads to maturation of stromal cells to mature LTo, which involves the upregulation of ICAM-1 and VCAM-1 and the expression of MAdCAM-1 (Benezech *et al.*, 2010).

1.4.2. Lymph node structure

As discussed above, the structure of the LN facilitates maximal interaction between cells of the innate and adaptive immune systems. Mature stromal cells, which are derived from the LTo stromal cells required for LN formation during embryogenesis, form a three-dimensional network along which haematopoietic cells migrate (Kaldjian *et al.*, 2001, Katakai *et al.*, 2004, Katakai *et al.*, 2008). The stromal cells in the T cell zone express the markers Podoplanin (Gp38), PDGFRα and PDGFRβ (Link *et al.*, 2007). These cells are also negative for the haematopoietic marker CD45 and the blood endothelial marker CD31 (Fletcher *et al.*, 2010, Fletcher *et al.*, 2011, Benezech *et al.*, 2012). These cells are referred to as Fibroblastic Reticular Cells (FRCs). Importantly, these cells express the chemokines CCL19 and CCL21, which are responsible for the chemoattraction of T cells, and IL-7, which is required for T cell survival (Link *et al.*, 2007). Thus, FRC nurture an environment that supports T cell activation (Gunn *et al.*, 1998, Ngo *et al.*, 1998, Bajenoff *et al.*, 2006, Willard-Mack, 2006, Link *et al.*, 2007, Fletcher *et al.*, 2011, Bajenoff, 2012, Malhotra *et al.*, 2013). Similar stromal cells are also found in the B cell follicles, where they instead express the chemokine CXCL13 and are called Follicular Dendritic Cells (FDCs) (Forster *et al.*, 1996, Fletcher *et al.*, 2011, Wang *et al.*, 2011, Bajenoff, 2012). Through the production of CXCL13 and B cell activating factor (BAFF), FDCs support the activation of B-cells (Wang *et al.*, 2011).

Whilst free antigens and activated APCs enter LNs in the lymph through the afferent lymphatic vessels (Randolph *et al.*, 2005, Bajenoff *et al.*, 2006, Willard-Mack, 2006, Roozendaal *et al.*, 2009, Acton *et al.*, 2012, Bajenoff, 2012), lymphocytes predominantly enter the LN through the bloodstream through specialised structures

called high endothelial venules (HEV) (Forster *et al.*, 1996, Bajenoff *et al.*, 2006, Willard-Mack, 2006, Mionnet *et al.*, 2011, Bai *et al.*, 2013, Onder *et al.*, 2013). The migration of both of these cell types requires expression of the C-C motif chemokine receptor 7 (CCR7) and CXCR5 (Randolph, 2016). Upon entry, T cells and B cells migrate to the T cells zone and B cell follicles due to the chemokine production by FRCs and FDCs, respectively (Bajenoff *et al.*, 2006, Willard-Mack, 2006). Antigen-presenting cells, primarily DCs, can migrate to the T cell zone and B cell follicles along the FRC and FDC stromal network and interact with T cells and B cells, leading to activation of adaptive immune responses followed by egress of activated lymphocytes from the LN via efferent lymphatic vessels (Willard-Mack, 2006).

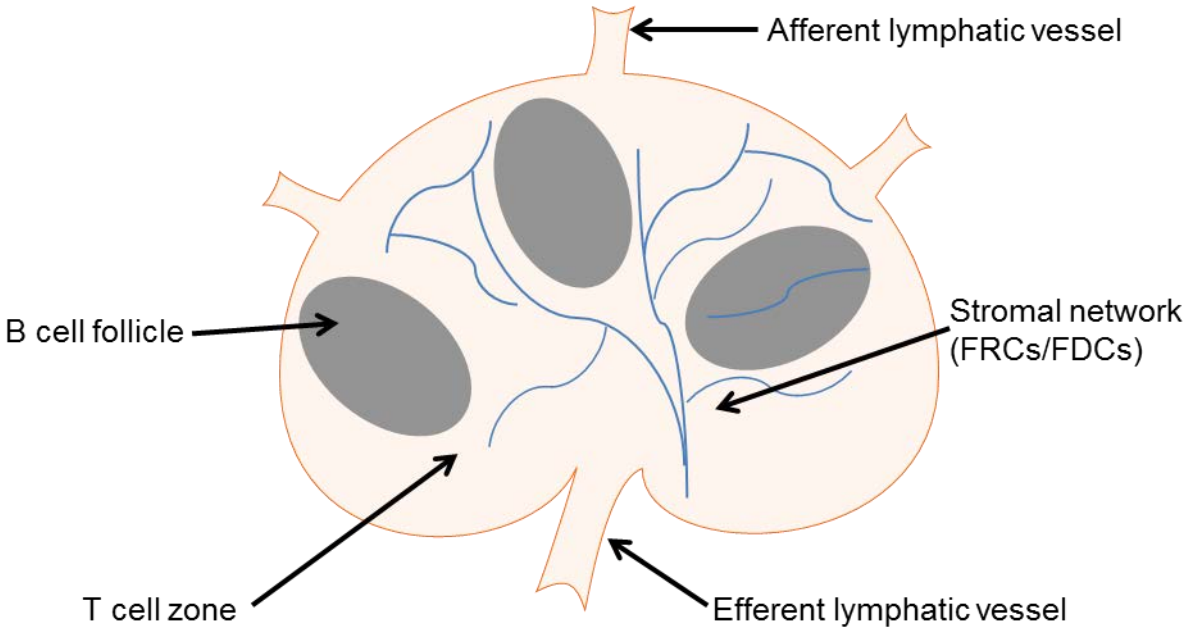

Figure 1.5: LN structure

Illustration of a typical LN structure based on a figure by Chang and Turley (Chang and Turley, 2015). Free antigen or antigen-bearing APCs enter the lymph node via afferent lymphatic vessels. APCs, can then migrate along the stromal network to the B cell follicles or T cell zones. This migration is driven by chemokine gradients; whilst CCL19 and 21 direct cells to the T cell zone, CXCL13 results in migration to the B cell follicles. Interaction of APCs and T cells/ B cells in the respective areas results in activation of these lymphocytes, which then migrate out of the LN through the efferent lymphatics and migrate to sites of infection or inflammation.

1.4.3. FALC formation, structure and function

Unlike the formation of LN, which requires LTβR and LTi cells, FALC do not require these cells for their formation, as the number of FALC identified in mesenteries of *Lta*$^{-/-}$, *Ltβr*$^{-/-}$ and *Rorc*$^{-/-}$ mice was comparable to the number identified in wild type (WT) mice (Benezech *et al.*, 2015). However, deletion of the tumour necrosis factor receptors in *Tnfrsf1a*$^{-/-}$*Tnfrsf1b*$^{-/-}$ animals resulted in a marked decrease in FALC numbers, whilst over-expression of TNF protein (TNF$^{+/\Delta ARE}$ mice) resulted in a large increase in FALC number and size, leading to the conclusion that this pathway was required in the formation of FALC (Benezech *et al.*, 2015). By using irradiated bone marrow chimeras, Bénézech *et al.* demonstrated that this TNF signalling occurred on radiation resistant stromal cells. CD11b^{+}F4/80^{+} cells appeared to be the predominant TNF-expressing cells, which the authors concluded were mostly macrophages. In addition to this, ILC2s and iNKT cells were also involved in the formation of FALC in response to peritoneal inflammation as mice lacking these cells showed reduced FALC numbers following induction of this inflammation. Finally, a requirement for IL-13 in inflammation-induced FALC formation was identified in C57BL/6J, but not BALB/c, mice using IL-4Rα and IL-13 deficient animals, and it was established that this signal is downstream of TNFR signalling. As both ILC2s and iNKT cells are capable of producing IL-13, these cells are the possible source of IL-13 signals during FALC formation.

The purpose of tertiary lymphoid tissues is to mediate faster initiation of adaptive immune responses within local tissues (Dieu-Nosjean *et al.*, 2014). Consistent with this Bénézech *et al.* demonstrated rapid inflammation-induced FALC formation following injection of the yeast glycan zymosan and demonstrated that these

structures supported the development of B cell antibody responses (Benezech *et al.*, 2015). Further work by the same author also illustrated the formation of FALC and induction of B cell responses following a variety of immunological challenges (Jackson-Jones *et al.*, 2016). Thus, consistent with other tertiary lymphoid structures, FALC form rapidly upon initial immune cell activation driven by infection or inflammation and support the induction of adaptive immune responses.

Although investigations of FALC biology have only recently been in the forefront of research (Moro *et al.*, 2010, Koyasu and Moro, 2013, Dieu-Nosjean *et al.*, 2014, Benezech *et al.*, 2015, Jackson-Jones *et al.*, 2016), similar lymphoid clusters to FALCs, were first described in the omentum of rabbits as early as 1863 (V. Recklinghausen, 1863). These clusters appear milky white in colour, resulting in their name, milky spots (MS). As reviewed by both Meza-Perez and Randall and Cruz-Migoni and Caamaño, MS are contained in the adipose region of the omentum in humans and mice and FALC and MS appear to be analogous, although subtle differences exist between the two (Cruz-Migoni and Caamano, 2016, Meza-Perez and Randall, 2017). As such, due to further characterisation of MS structure in the literature, the structure of MS is detailed below.

Like SLTs, distinct clusters of B and T cells including germinal centres are observed and a stromal reticular network exists in MS and FALC (Shimotsuma *et al.*, 1993, Rangel-Moreno *et al.*, 2009, Moro *et al.*, 2010, Benezech *et al.*, 2015, Jackson-Jones *et al.*, 2016, Meza-Perez and Randall, 2017). The segregation of lymphocytes is also a common feature of other lymphoid tissues such as the spleen and Peyer's patches. Similar to what is seen in LNs, the white pulp of the spleen contains segregated regions containing T and B cell with antigen presenting cells predominantly in the T

cell areas (Mebius and Kraal, 2005). Similarly, Peyer's patches, part of the Gut Associated Lymphoid Tissues (GALT), also have strict zones of B cells within follicles and T cells in interfolicular zones (Jung *et al.*, 2010).

However, despite the above similarities between MS and other lymphoid tissues, fundamental differences exist between SLTs and MS/FALC (Shimotsuma *et al.*, 1993, Rangel-Moreno *et al.*, 2009, Moro *et al.*, 2010, Benezech *et al.*, 2015, Jackson-Jones *et al.*, 2016, Meza-Perez and Randall, 2017). Firstly, in contrast to the strict zonation of chemokine expression in SLTs, CCL19 and 21 appear not to be required for clustering of T cells in MS, as the structure of MS was unaffected in mice lacking these chemokines (Rangel-Moreno *et al.*, 2009). Furthermore, although CXCL13 expression has been noted in both the omentum and FALC of the mesenteries, the localisation of $CXCL13^+$ cells, which could be macrophages or stromal cells, are distinct from B cell clusters in the omentum (Ansel *et al.*, 2002, Rangel-Moreno *et al.*, 2009, Benezech *et al.*, 2015). Thus, in contrast to SLTs, where strict segregation of different lymphocyte populations exists due to chemokine gradients, no clear separation of lymphocytes by chemokine gradients is evident in MS.

MS appear to be highly vascularised and T cells appear to be clustered round blood vessels, close to stromal cells expressing markers of HEVs, possibly indicating a conserved mechanism of lymphocyte entry into both SLTs and MS (Rangel-Moreno *et al.*, 2009, Buscher *et al.*, 2016, Meza-Perez and Randall, 2017). Another distinction between SLTs and the omentum is the method by which antigens are collected; whilst SLTs collect free antigens and antigen-expressing cells from the lymph through the afferent lymphatic vessels, gaps in the mesothelial layer of the omentum allow free movement of the peritoneal fluid into the omentum. Thus, the

omentum acts as a key ‘filter’ for the peritoneal cavity (Meza-Perez and Randall, 2017).

In addition to FALC, other aggregates of immune cells have also been noted both in adipose tissues and other tissues (Iannuzzi *et al.*, 2007, Wentworth *et al.*, 2010, Lamps, 2015, Cho *et al.*, 2016, Terziroli Beretta-Piccoli *et al.*, 2018). In adipose tissues of obese humans and mice aggregates of $CD11c^+$ macrophages (M1 macrophages) and dendritic cells, referred to as ‘crown’ structures, form around necrotic adipocytes (Wentworth *et al.*, 2010, Cho *et al.*, 2016). When studied in omental and subcutaneous adipose tissues isolated from obese women, there was a strong correlation between the density of crown structures and degree of insulin resistance (Wentworth *et al.*, 2010). Another example of lymphocyte aggregates found in human tissues is granulomas. Unlike crown structures, granulomas contain many different cell subsets including macrophages, plasma cells, neutrophils and eosinophils along with other stromal cells (Lamps, 2015) and can be found at many anatomical sites including the liver (Lamps, 2015), skin (Terziroli Beretta-Piccoli *et al.*, 2018) and lungs (Iannuzzi *et al.*, 2007). Similar to FALC, the formation of granulomas appears to be driven by inflammation, both through infection and through other aetiologies, such as in the presence of foreign material (Iannuzzi *et al.*, 2007, Lamps, 2015, Terziroli Beretta-Piccoli *et al.*, 2018). However, the key distinction between cellular aggregates, such as granulomas and crown structures, and FALC is that the cells within FALC show a degree of organisation, whilst the distribution of cells within granulomas and crown structures appears to be random.

In summary, although showing some resemblance to the structure of other lymphoid tissues, such as separated B and T cell zones, FALC/MS structure does appear to be

different to that of other lymphoid tissues. Further investigation into the molecular cues which drive FALC/MS formation and how antigen reaches these structures is required.

1.5. AIMS OF THIS STUDY

Obesity is a growing epidemic and is strongly causal in the development of metabolic disease characterised by insulin resistance. There is a growing appreciation of the interaction between adipocytes and immune cells within ATs, and the importance of these interactions in maintaining both local and systemic metabolic homeostasis. Finally, the immune cell composition of adipose tissues has also been linked to the development of cancer and autoimmunity. For this reason we hypothesised that adipose tissues play an important immunological role during immune responses.

To investigate this hypothesis, we sought to characterise some of the immune cell subsets which exist in ATs during homeostasis and infection, and to determine whether immune cells within ATs can contribute to infections in surrounding tissues. Studies indicate that in humans the adiposity of VAT depots is a firmer indicator of metabolic dysfunction than SCAT depots. As such, VAT depots from mice were focused on in this study. Gonadal fat is the most studied VAT depot in mice, so this tissue was examined throughout. However, comparisons with humans indicate that the mesenteries are the most analogous VAT depot between mice and humans, so this tissue was also analysed.

The overall aims of this investigation were to:

1. Establish the immune cell composition in AT during homeostasis and investigate whether this differs from those of other tissues.

2. Examine signals which control AT immune cell composition during homeostasis.

3. Explore whether immune cells within ATs can contribute to infections in surrounding tissues by comparing immune cell composition and phenotype before and after infection.

2. MATERIALS AND METHODS

2.1. MICE

Mice were bred and maintained at [redacted] All WT mice used in this study were generated from in-house mating pairs. All experimental procedures were performed in accordance with Home Office regulations, as of 2017. Unless otherwise specified, all animals used in this study were male and between the ages of 12-20 weeks. Table 2.1 details the different mouse strains used throughout this investigation.

Table 2.1: Mouse strains used in this study

Strain	**Genetic background and CD45 allotype**	**Phenotype**	**Source**
C57BL/6J	C57BL/6J, CD45.2	WT	In-house
BALB/C	BALB/C, CD45.2	WT	In-house
IL-33$^{cit/cit}$	BALB/C, CD45.2	All IL-33^{+} cells produce citrine protein, appearing green under fluorescent light. No functional IL-33 protein is produced (Hardman *et al.*, 2013).	A kind gift from Prof. A McKenzie, MRC LMB, Cambridge, U.K.
p55/p75$^{-/-}$	C57BL/6J, CD45.2	Mice are deficient in TNFR1 and 2, the receptors through which TNF signals (Peschon *et al.*, 1998). As a result mice cannot undergo TNF driven inflammation.	Purchased from Jackson labs, U.K.
TNF$^{+/\Delta ARE}$	C57BL/6J, CD45.2	Mice carrying a deletion in the ARE of the TNF gene, resulting in deregulated expression of	A kind gift from Prof. George

		mRNA and protein. Animals spontaneously develop arthritis and inflammatory bowel disease (Alexopoulou *et al.*, 1997).	Kollias, University of Athens, Greece.

2.2. REAGENTS

2.2.1. Media and buffers

Table 2.2: Media for cell isolation

Reagent	Final concentration	Supplier
Roswell Park Memorial Institute media (RPMI) 1640 with L-glutamine		Gibco (life technologies)
Heat inactivated Fetal Bovine Serum (FBS)	2% v/v	Gibco (life technologies)
Ethylenediaminetetraacetic acid (EDTA)	2 mM	Sigma-Aldrich

Table 2.3: Buffer for flow cytometry staining (FACS buffer)

Reagent	Final concentration (v/v)	Supplier
Dulbecco's Phosphate Buffered Saline (DPBS) with Ca^{2+} and Mg^{2+}		Gibco (life technologies)
FBS	2%	Gibco (life technologies)
EDTA	2mM	Sigma-Aldrich

Table 2.4: Whole-mount staining buffer

Reagent	Final concentration (v/v)	Supplier
DPBS with Ca^{2+} and Mg^{2+}		Gibco (life technologies)
Bovine Serum Albumin (BSA)	2%	Sigma-Aldrich

2.3. GENERATION OF SINGLE CELL SUSPENSIONS

2.3.1. Dissection of tissues

Mice were culled by cervical dislocation and tissues were immediately isolated. Inguinal lymph nodes (ILN), Gonadal fat and omentum were excised directly from mice and placed in cell isolation media (see Table 2.2) on ice in a 6 well tissue culture plate (Fisher Scientific). Mesenteries were excised with the Mesenteric Lymph Node (MLN) intact as described by Moro *et al.* (Moro *et al.*, 2015). After dissection of mesenteries, the SI was isolated from the end of the stomach to the caecum, Peyer's patches were removed and the SI was cut into small pieces approximately 0.5cm in length and placed in Hanks Buffered Saline Solution (HBSS) without Ca^{2+} and Mg^{2+} (HBSS, Sigma-Aldrich) with 2% FBS. To isolate the lungs, 10 ml PBS was injected into the left ventricle of the heart *post mortem*. This causes both lobes of the lungs to inflate, making them easier to dissect.

2.3.2. Isolation of single cell suspensions from lymph nodes

Excess fat was removed from excised LN using a Leica MZ95 stereomicroscope (Leica). Tissue from each animal was treated separately throughout. LN were then placed in fresh cell isolation media in 6 well tissue culture plates (Fisher Scientific) and mechanically disaggregated with forceps, followed by enzymatic digestion with 250 µg/ml Collagenase/Dispase and 25 µg/ml DNase I (Sigma-Aldrich) in an incubator at 37°C. After 20 min the reaction was stopped by addition of 10 mM EDTA (Sigma-Aldrich). Undigested tissue was then removed by passing the suspension through 70µm filters (Fisher Scientific) and a single cell suspension was generated following centrifugation at 1500 revolutions per minute (rpm) for 5 min.

2.3.3. Isolation of single cell suspensions from adipose tissues

Following dissection, ATs (gonadal fat and mesenteries) were checked for contamination of other tissue types using a Leica MZ95 stereomicroscope (Leica) before being finely minced with a scalpel blade (Fisher Scientific). ATs from each animal were treated separately throughout. Following disaggregation, tissue homogenates were digested in 5ml of digestion media containing RPMI 1640 (Gibco) supplemented with 200µg/ml Collagenase P, 800µg/ml Collagenase Dispase, and 100µg/ml DNase I (Sigma-Aldrich). ATs were digested at 37°C with oscillation at 120 rpm for 30 min with additional manual agitation at 10 min intervals. The resulting solution was then filtered into 5 ml RPMI containing 2% FCS and centrifuged at 1500 rpm for 10 min. The supernatant was finally removed and the cell pellet (SVF) was resuspended in FACS buffer (see Table 2.3). Single cell suspensions were then stained for FACS analysis. There was some inter-experiment variation observed in the staining of CD4, CD25 (data not shown) and GATA-3 in both gonadal fat and mesenteries. As a result, in some experiments it was more difficult to identify $CD4^+$ cells and ILC2s (see Figure 2.1A and B). The variation in CD4 and CD25 expression could be due to varying degrees of enzymatic cleavage of surface markers, as gentler enzymatic digestion of AT resulted in better staining for these markers (data not shown). However, as GATA-3 is an intracellular protein, it is doubtful that the variation in ILC GATA-3 expression is due to enzymatic cleavage. It is unclear why this variation in GATA-3 staining occurs and could be either due to genuine biological differences in the tissue, or the variation in staining could be induced by the manipulation of the tissues and downstream processes to obtain a readout of the immune cell composition by flow cytometry. Unfortunately, despite attempts to

optimise the AT digestion process, a compromise between cellular yield and integrity of surface markers was necessary. CD4, CD25 and GATA-3 appeared to be the only markers with inter-experimental variation in staining (data not shown).

2.3.4. Isolation of single cell suspension from lungs

Contaminating tissue was removed from lungs using a stereomicroscope. Tissue from each animal was treated separately throughout. Lungs were then placed in a 1 ml cell isolation media in a small petri dish (Fisher Scientific) and mechanically disaggregated with forceps. The disaggregated lungs were then added to 3 ml cell isolation media (supplemented with 10% FCS, instead of 2%) with a final concentration of 39.7 µg/ml Liberase TM (Roche) and 18.75 µg/ml DNase I and digested for 30 min at 37°C in a oscillating water bath (250 rpm). Subsequent to digestion, lung homogenates were passed through a 70 µm filter and washed three times with RPMI+10% FCS (centrifuged at 1500 rpm for 5 min). Finally, 2 ml of Red Blood Cell Lysis Buffer (Sigma-Aldrich) was added to the cell pellet and incubated at room temperature for 5 min before washing with 5 ml FACS buffer.

2.3.5. Isolation of single cell suspension from small intestine lamina propria

Tissue from each animal was treated separately throughout. Dissected SI was transferred to 20 ml HBSS containing 2 mM EDTA (pre-wared in water bath at 37°C) and incubated in an oscillating water bath at 37°C for 20 min at 250 rpm. After 20 min the supernatant was removed and SI homogenate was incubated for a further 20 min at 37°C in 20 ml fresh HBSS/EDTA solution. The above was then repeated a third time before filtering through nylon mesh (size of pores unspecified, Amazon UK) and

incubating for 10 min at 37°C with 15 ml RPMI/10% FCS containing 1 mg/ml Collagenase VIII (Sigma-Aldrich). The lamina propria (LP) homogenates were subsequently manually shaken for a final 5 min before filtering through 70 µm cell strainers and 2 ml Red Blood Cell Lysis Buffer was added for 5 min before washing with 5 ml FACS buffer.

2.4. STAINING OF CELLS FOR FLOW CYTOMETRY ANALYSIS

2.4.1. Initial preparation of cells

Following digestion, single cell suspensions were seeded in 96 well tissue culture plates (Nunc, Fisher Scientific) at an approximate density of 1-3X10^6 cells total. The cellularity of lung and SI LP was determined using disposable haemocytometer counting slides (Immune Systems).

2.4.2. Live/dead staining

Prior to surface staining, cells were labelled with LIVE/DEAD® fixable Near-IR Viability Dye (1/1000 in DPBS with Ca^{2+} and Mg^{2+}, Invitrogen Life sciences) for 30 min at 4°C in the dark to prevent photobleaching. Cells were then washed three times with FACS buffer. Cells were subsequently incubated with Fc block for 15 min at room temperature (1/50 Purified anti-mouse CD16/CD32; Clone 93 eBioscience), prior to surface staining to reduce non-specific binding of antibodies.

2.4.3. Surface staining with antibodies

Following LIVE/DEAD® staining and Fc block, cells were incubated with a variety of antibodies against the surface antigens listed in Table 2.5 and Table 2.6 by making a combined cocktail of antibodies in FACS buffer (50µl staining cocktail per sample). Antibodies against lineage markers were included as the same fluorochrome to

create a lineage dump channel (Lin) consisting of CD3, CD5, CD11b, CD11c and B220. Fluorescence-minus-one (FMO) controls were performed by staining cells with the same antibody mix, but in which the antibody of interest was absent. Isotype controls were performed similarly to FMO controls, but with the isotype control antibody added as the control fluorochrome.

Table 2.5: Antibodies against surface antigens

Antigen	Fluorochrome	Clone	Manufacturer	Dilution
CD3e	FITC	eBio500A2	eBioscience	1/100
CD3e	PE	145-2C11	eBioscience	1/800
CD3e	APC	145-2C11	eBioscience	1/100
CD4	Brilliant Violet 510™	RM4-5	Biolegend	1/300
CD4	Brilliant Violet 785™	RM4-5	Biolegend	1/300
CD5	FITC	53-7.3	eBioscience	1/100
CD5	PE	53-7.3	eBioscience	1/2000
CD5	APC	53-7.3	eBioscience	1/100
CD11b	FITC	M1/70	eBioscience	1/300
CD11b	PE	M1/70	eBioscience	1/16000
CD11b	APC	M1/70	eBioscience	1/300
CD11c	FITC	N418	eBioscience	1/300
CD11c	PE	N418	eBioscience	1/8000
CD11c	APC	N418	Biolegend	1/300
CD25	Brilliant Violet 650™	PC61	Biolegend	1/200
IL-33R (ST2)	PE	DIH9	Biolegend	1/50
CD45.2	Brilliant Violet 510™	104	Biolegend	1/100
CD45.2	Brilliant Violet 786™	104	Biolegend	1/200
CD45R (B220)	FITC	RA3-6B2	eBioscience	1/300
CD45R (B220)	PE	RA3-6B2	eBioscience	1/800
CD45R (B220)	APC	RA3-6B2	eBioscience	1/300

CD80	Brilliant Violet 605™	16-10A1	Biolegend	1/100
CD127 (IL-7Rα)	PE-Cy7	A7R34	Biolegend	1/100
CD127 (IL-7Rα)	Brilliant Violet 421™	A7R34	Biolegend	1/100
CD186 (CXCR6)	APC	SA051D1	Biolegend	1/100
CD196 (chemokine receptor 6, CCR6)	Brilliant Violet 605™	29-2L17	Biolegend	1/100
CD198 (CCR8)	APC	SA214G2	Biolegend	1/50
CD199 (CCR9)	PE	eBioCW-1.2	eBioscience	1/200
CD278 (Inducible T-cell costimulator, ICOS)	PE-Cy7	C398.4A	Biolegend	1/200
CD335 (NKp46)	Brilliant Violet 605™	29A1.4	Biolegend	1/100
C-C chemokine receptor like 2 (CCRL2)	PE	BZ2E3	BD biosciences	1/100
Killer cell lectin-like receptor G1 (KLRG1)	APC	2F1	Biolegend	1/200
Major histocompatibility complex class II (MHC-class II)	Brilliant Violet 510™	M5/114.15.2	Biolegend	1/500

Table 2.6: Additional reagents used for flow cytometry

Target	Fluorochrome	Source	Dilution
α-Galactosylceramide (α-gal-cer): binds to invariant TCR of iNKT cells.	APC	NIH tetramer facility	1/200

2.4.4. Intracellular/Intranuclear staining of antigens

Following surface staining, cells were washed twice with 200 µl FACS buffer before incubation with 100 µl of Foxp3 fixation solution, diluted as per manufacturer's instructions (eBioscience). Cells were incubated in this solution for 30 min at 4°C before being washed twice with the counterpart permeabilisation buffer (10x stock diluted in distilled water, eBioscience). Cells were then stained with different combinations of antibodies listed in Table 2.7, diluted in permeabilisation buffer.

2.4.5. Intracellular/Intranuclear staining of antigens in IL13$^{+/gfp}$ mice

Following surface staining, cells were washed twice with 200 µl FACS buffer before incubation with 100 µl of BD Cytofix fixation solution (Cytofix/Cytoperm solution, BD biosciences) for 30 min at 4°C. After fixation, cells were washed twice with 200 µl of BD Cytoperm solution diluted one in ten in distilled water before staining with antibodies from Table 2.7 diluted in Cytoperm solution.

Table 2.7: Antibodies against intracellular/intranuclear antigens

Antigen	Fluorochrome	Clone	Manufacturer	Dilution
CD3	Alexa fluor700	17A2	eBioscience	1/100
RORγt	PE	Q31-378	BD bioscience	1/50
IL-5	PE	TRFK5	eBioscience	1/50
IL-13	PE-Cy7	EBio13A	eBioscience	1/50
Ki-67	PE-Cy7	SolA15	eBioscience	1/100
GATA-3	PerCP-efluor710	TWAJ	eBioscience	1/50

2.4.1. FACS acquisition

Subsequent to intracellular staining, cells were washed twice with 200 µl of appropriate permeabilisation buffer (FOXP3 staining kit or BD Cytoperm) before re-suspending in 200 µl of FACS buffer. Cells were then transferred to FACS tubes (BD bioscience) containing 5000, 10.4 µm Accucount Blank particles (Spherotech). Samples were acquired on a LSRFortessa X-20 equipped with red (488 nm), yellow/green (561 nm), blue (488nm) and violet laser (405 nm) using FACS Diva V8 software (BD bioscience). Compensation controls to correct for spectral overlap of fluorochromes were freshly prepared for every experiment performed.

2.5. ADDITIONAL PROCEDURES

2.5.1. Tissue staining for FALC counting

Tissues were isolated as described in chapter 2.3.1 and then placed in 1 ml of whole mount staining buffer (see Table 2.4) containing CD45 FITC diluted at one in two hundred (Clone 30-F11, eBioscience). Samples were incubated in the dark at 4°C, with gentle agitation, for 2 hr. Tissues were then washed with PBS (Gibco). FALCs were counted using a stereofluorescence microscope (Olympus SZX12) equipped with a GFP filter. Images were taken using a linked digital camera (Olympus C50-60). Tissues could subsequently be digested, as described in chapter 2.3.3, to generate a single cell suspension for FACS analysis.

2.5.2. *Ex vivo* stimulation for analysis of cytokine production

Single cell suspensions were generated as described in chapter 2.3. Cells were re-suspended in 1 ml cytokine stimulation media (stimulated, see Table 2.3), or cytokine stimulation media without PMA and Ionomycin (media control), and

incubated in a 24 well plate (Corning) at 37°C for 1 hr. 1 µl Brefeldin A (10 mg/ml in DMSO, Sigma) was then added to all wells to give a final concentration of 10 µg/ml. Cells were incubated for a further 3 hr at 37°C before being washed with 3 ml PBS and transferred to 96 well plates for FACS staining as detailed in chapter 2.4.

2.5.3. Infection of mice with *Heligmosomoides polygyrus*

H.polygyrus L3 larvae were stored long-term at 4ºC, as described by Camberis *et al.* (Camberis *et al.*, 2003). Larvae were counted using a Leica MZ95 stereomicroscope and mice were given either 200 L3 stage larvae, or 200 µl sterile PBS as a control, by oral gavage. Mice were culled five or ten days post infection. SI (from stomach to caecum) were excised with mesenteric tissue intact. Mesenteries and MLN were then separated from the SI and processed as described in chapters 2.3.2 and 2.3.3. Worm burden could be evaluated by counting larvae embedded in the intestinal wall, which were easily identifiable using the aforementioned stereomicroscope.

2.6. DATA ANALYSIS

2.6.1. Flow cytometry data analysis

Flow cytometry data was analysed using FlowJo V10 (TreeStar). Pseudocolour plot axes were displayed as a bi-exponential scale, with the exception of FSC-A and time, which were displayed on a linear scale. For overlaid histograms the modal value was plotted to allow for easier visualisation of populations with vastly different cell numbers. In addition to recording the absolute number and percentage of different cell populations, the Median Fluorescence Intensity (MFI) was also documented for the antibodies used. Although this measure cannot be used to quantify protein expression, it can be a useful tool to compare the relative expression of a marker

between populations. One caveat of this method to note is that the MFI value can be skewed by internalisation of proteins from the cell surface or shedding of proteins by cells. Herein the MFI value is denoted as 'expression', referring to the relative expression of markers between two populations instead of gene expression.

A full gating strategy for the different staining panels is shown in Figure 2.1 and Figure 2.2. Analysis of T cell populations throughout this study consistently used the gating strategy shown in Figure 2.1A. This panel allowed the identification of $CD4^+$ T cells, $CD4^+$ and $CD4^-$ iNKT cells and regulatory T cells (Tregs). Figure 2.1B shows identification of total ILCs, ILC2 and group 3 ILCs (ILC3 and LTi cells) based on transcription factor staining. For staining panels that examined further changes in ILC2s, such as cytokine production or chemokine receptor expression, a similar gating strategy to Figure 2.1B was used (data not shown). Others have reported the majority of ILC2s in MLN and gonadal fat express the IL-33 receptor IL-1 receptor like 1 ((IL1RL1, ST2), (Spits and Cupedo, 2012, Walker and McKenzie, 2013). Consistent with this, Figure 2.1C shows nearly all ILC2s (GATA-3^+ ILCs) express ST2 in gonadal fat.

To maximise the amount of information obtained from each tissue, FALC counting in AT was combined with flow cytometric analysis of tissue immune cell composition. Unfortunately, this reduced the number of markers that could be analysed by flow cytometry. To overcome this, staining panels were designed to allow identification of ILC populations and phenotyping of ILC2 populations based on surface markers alone (Figure 2.2). Both group 2 and group 3 ILCs express the IL-2 receptor (CD25). However, as seen in Figure 2.1B the number of group 3 ILCs in AT is negligible. For this reason it was thought that ILC2s could reliably be identified as $CD25^+CCR6^-$

ILCs (Figure 2.2A). Consistent with transcription factor staining, $CD25^{+}CCR6^{-}$ ILC2s were the predominant ILC population in ATs. However, this method of gating could not be applied to MLN as ILC3s (not LTi) would also be included in the $CD25^{+}CCR6^{-}$ ILC population. Thus, a different gating strategy was devised using ICOS and CCR6, as the majority of ILC2 in MLN express ICOS (Figure 3.6). This modified gating strategy is shown in Figure 2.2B. Similar to what is reported by others (Mackley *et al.*, 2015), a large proportion of ILCs in the MLN were LTi-like cells (Figure 2.2B). CD25 expression on the remaining cells was not sufficiently clear to differentiate between ILC3s and remaining cells (including NK cells and ILC1s, data not shown).

As discussed above, a combination of ST2 and ICOS can be used to identify ILC2s in both AT and MLN. This method was used to phenotype ILC2s where use of transcription factors was not possible (Figure 2.2C). When gating on $ST2^{+}ICOS^{+}$ ILCs, a similar proportion of cells were $KLRG1^{+}$ as seen in $ST2^{+}GATA\text{-}3^{+}$ ILC2s (Figure 2.1C, Figure 2.2C). Moreover, in a separate experiment where transcription factor and surface staining for ILC2s was combined, most of the $ST2^{+}ICOS^{+}$ cells in gonadal fat and mesenteries were also $GATA\text{-}3^{+}$ (gonadal fat median 59.1%, mesenteries median 66.6%, Figure 2.2D).

2.6.2. Statistical analysis

Flow cytometry data was further analysed in Microsoft Excel 2010 (Microsoft), where bead counts were used to convert absolute counts to relative counts, adjusting for proportion of tissue stained. Data was then plotted graphically and statistical analysis was applied using Graph Pad Prism V7 (Graph pad). Statistical significance between single variables was determined using a two-tailed Mann-Whitney T test, where p values <0.05 were determined as statistically significant. Correlation between two

variables was determined using the Spearman's rank test, where r values close to 1 indicate a strong positive correlation, values close to -1 indicate a strong negative correlation and intermediate values indicate a weaker correlation. Assessment of statistical significance between two or more variables was determined using a Kruskal-Wallace test followed by a Dunn's post-hoc test. Comparisons that gave a p value of <0.05 were considered statistically significant using this analysis method. In all cases where no p value is stated, no statistical significance was observed.

Figure 2.1: Gating strategy for staining using transcription factors

FACS plots show representative staining in the gonadal fat isolated from male C57BL/6J animals.

A) FACS plots showing T cell composition analysis leading to identification of $CD4^+$ cells ($CD45.2^+$live/$dead^-$intra$CD3^+CD4^+$α-gal-cer^- cells), $CD4^+$ iNKT ($CD45.2^+$live/$dead^-$intra$CD3^+CD4^+$α-gal-cer^+ cells), $CD4^-$ iNKT ($CD45.2^+$live/$dead^-$intra$CD3^+CD4^-$α-gal-cer^+ cells) and Tregs ($CD45.2^+$live/$dead^-$intra$CD3^+CD4^+$α-gal-cer^-Foxp3^+ cells).

B) FACS plots showing ILC cell composition analysis leading to identification of total ILCs ($CD45.2^+$live/$dead^-$IL-7R$α^+Lin^-$intra$CD3^-$ cells), ILC2s ($CD45.2^+$live/$dead^-$IL-7R$α^+Lin^-$intra$CD3^-$GATA-3^+RORγt^- cells) and ILC3s ($CD45.2^+$live/$dead^-$IL-7R$α^+Lin^-$intra$CD3^-$RORγt^+ cells).

C) FACS plots showing ILC2 phenotype analysis. Expression of KLRG1 and ICOS was assessed on the surface of ILC2s ($CD45.2^+$live/$dead^-$IL-7R$α^+Lin^-$ intra$CD3^-ST2^+$GATA-3^+ cells). Controls were used for KLRG1 staining ($CD45.2^+$live/$dead^-$IL-7R$α^-Lin^{hi}$intra$CD3^-$ cells) and ICOS staining (FMO control) to indicate negative staining.

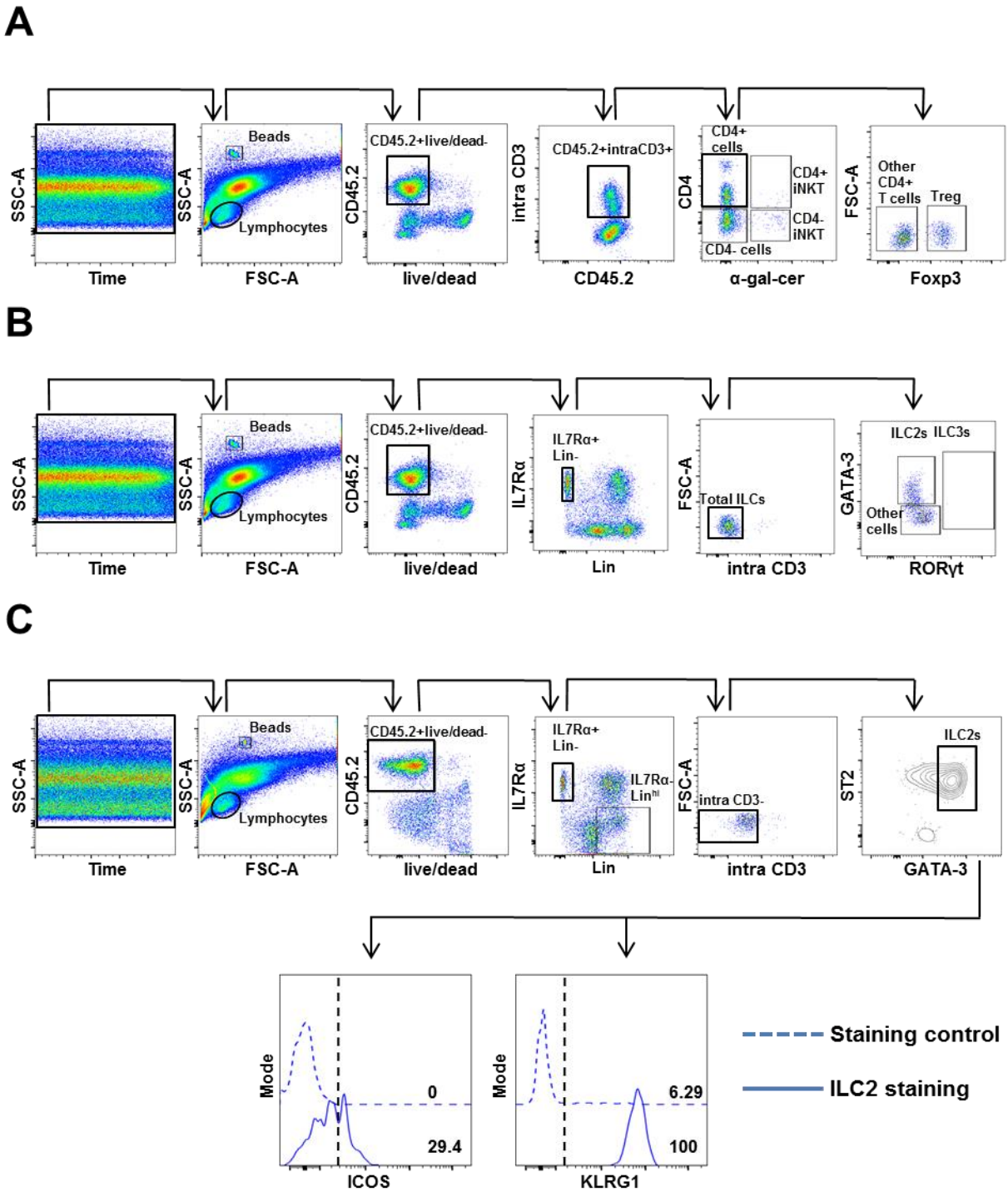
A
SSC-A
Time
Beads
Lymphocytes
FSC-A
CD45.2+live/dead-
CD45.2
live/dead
CD45.2+intraCD3+
intra CD3
CD45.2
CD4+ cells
CD4+ iNKT
CD4- iNKT
CD4- cells
CD4
α-gal-cer
Other CD4+ T cells
Treg
FSC-A
Foxp3
B
SSC-A
Time
Beads
Lymphocytes
FSC-A
CD45.2+live/dead-
CD45.2
live/dead
IL7Rα+ Lin-
IL7Rα
Lin
FSC-A
Total ILCs
intra CD3
ILC2s ILC3s
Other cells
GATA-3
RORγt
C
SSC-A
Time
Beads
Lymphocytes
FSC-A
CD45.2+live/dead-
CD45.2
live/dead
IL7Rα+ Lin-
IL7Rα-
Lin^hi
IL7Rα
Lin
FSC-A
intra CD3-
intra CD3
ILC2s
ST2
GATA-3
Mode
0
29.4
ICOS
Mode
6.29
100
KLRG1
Staining control
ILC2 staining

Figure 2.2: Gating strategy for staining using surface proteins

FACS plots show representative staining in the gonadal fat and MLN isolated from male C57BL/6J animals.

A) FACS plots showing ILC cell composition analysis in gonadal fat leading to identification of total ILCs ($CD45.2^+live/dead^-IL\text{-}7R\alpha^+Lin^-intraCD3^-$ cells), ILC2s ($CD45.2^+live/dead^-IL\text{-}7R\alpha^+Lin^-intraCD3^-CD25^+CCR6^-$ cells) and LTi cells ($CD45.2^+live/dead^-IL\text{-}7R\alpha^+Lin^-intraCD3^-CCR6^+$ cells).

B) FACS plots showing ILC cell composition analysis in MLN leading to identification of total ILCs ($CD45.2^+live/dead^-IL\text{-}7R\alpha^+Lin^-intraCD3^-$ cells), ILC2s ($CD45.2^+live/dead^-IL\text{-}7R\alpha^+Lin^-intraCD3^-ICOS^+CCR6^-$ cells) and LTi cells ($CD45.2^+live/dead^-IL\text{-}7R\alpha^+Lin^-intraCD3^-ICOS^-CCR6^+$ cells).

C) FACS plots showing ILC2 phenotype analysis in gonadal fat. Expression of KLRG1 and ICOS was assessed on the surface of ILC2s ($CD45.2^+live/dead^-IL\text{-}7R\alpha^+Lin^-intraCD3^-ST2^+ICOS^{+/-}$ cells). Controls were used for KLRG1 staining ($CD45.2^+live/dead^-IL\text{-}7R\alpha^-Lin^+intraCD3^-$ cells) to indicate negative staining.

D) FACS plots showing the percentage of GATA-3^+ cells gating on ILC2 surface markers in gonadal fat (left) and mesenteries (right). Numbers in plots indicate percentage of events in gates.

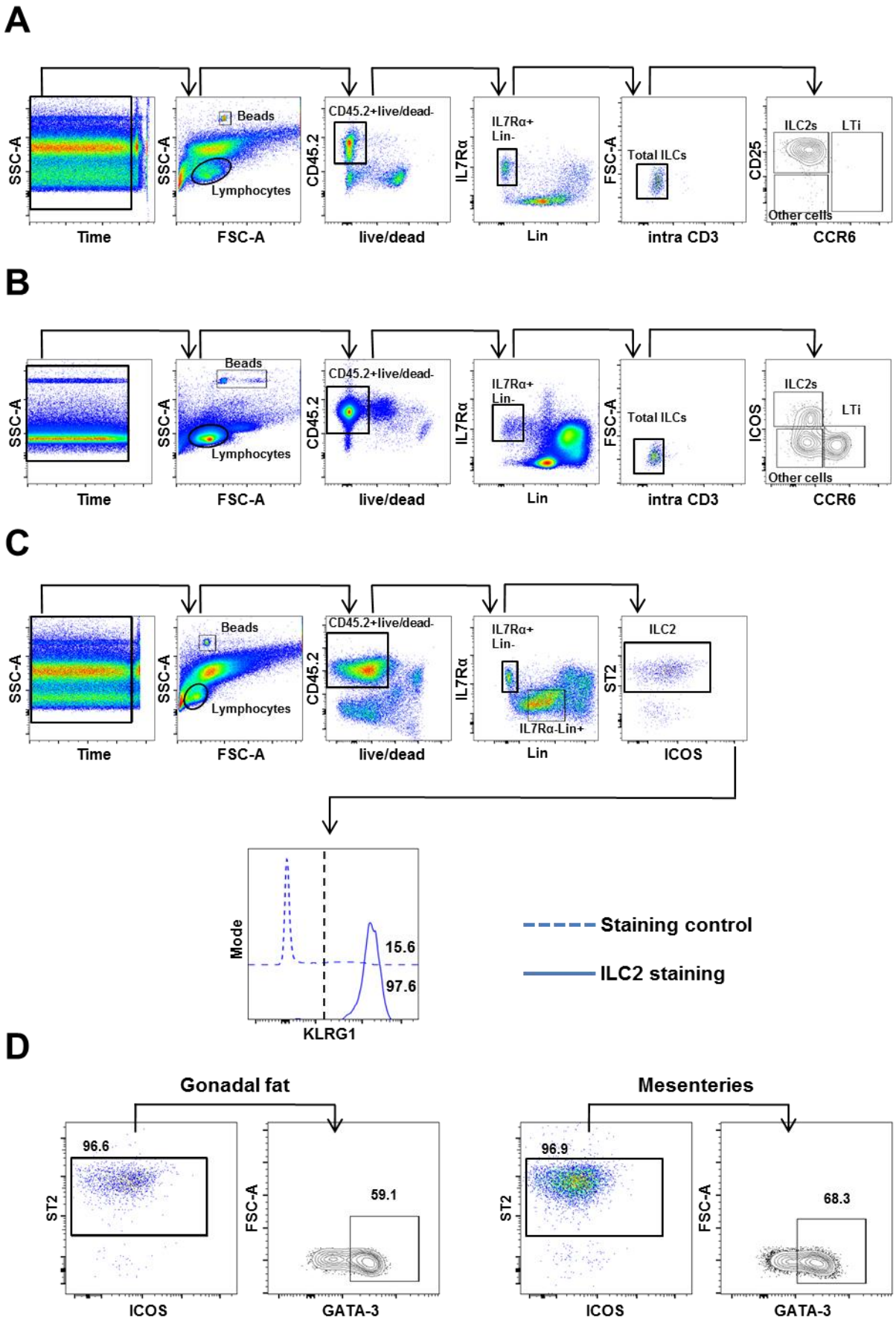
A
SSC-A
Time
Beads
Lymphocytes
FSC-A
CD45.2+live/dead-
CD45.2
live/dead
IL7Rα+
Lin-
IL7Rα
Lin
FSC-A
Total ILCs
intra CD3
CD25
ILC2s
LTi
Other cells
CCR6
B
ICOS
C
ILC2
ST2
IL7Rα-Lin+
Mode
15.6
97.6
KLRG1
Staining control
ILC2 staining
D
Gonadal fat
Mesenteries
96.6
59.1
96.9
68.3
GATA-3

3. CHARACTERISING THE IMMUNE CELL COMPOSITION OF ADIPOSE TISSUES

3.1. INTRODUCTION

ATs are vitally important to the metabolic state of the host due to their role in lipid metabolism and storage. Moreover, the cellular composition of ATs can also have a significant impact on the metabolic state of not just the tissues in which they reside, but also on the whole organism (Man *et al.*, 2017). This impact is exerted through the balance of pro-inflammatory and anti-inflammatory signals within the ATs, orchestrated by both stromal cells and immune cells (Odegaard *et al.*, 2008, Miller *et al.*, 2010, Ouchi *et al.*, 2011, Man *et al.*, 2017).

Recent studies have highlighted that immune cells including iNKT, Th2 and ILC2 are all important in exerting an anti-inflammatory effect and their manipulation can improve overall outcome in mouse models of obesity (Wu *et al.*, 2007, Kintscher *et al.*, 2008, Lynch *et al.*, 2009, Lynch *et al.*, 2012, Satoh *et al.*, 2012, Schipper *et al.*, 2012, Hams *et al.*, 2013, Molofsky *et al.*, 2013, Hashiguchi *et al.*, 2015). ILC2 from ATs have been the particular focus of recent investigations due to their enrichment in these tissues, as compared to lymphoid tissues, such as the ILN, and other non-lymphoid tissues, such as SI and skin (Moro *et al.*, 2010, Molofsky *et al.*, 2013). Furthermore, ILC2s isolated from AT appear to express higher levels of cell surface proteins ST2 and CD25, both of which are important in induction of cytokine production by these cells (Hoyler *et al.*, 2012, Salimi *et al.*, 2013, Molofsky *et al.*, 2015b).

ILC2s respond to alarmins, such as IL-25 and IL-33, which are produced rapidly in response to perturbations in homeostatic conditions, such as in response to infection or inflammation (Griesenauer and Paczesny, 2017). Expression of alarmin receptors allows ILC2s to respond to these early signals by inducing downstream signalling cascades which lead to changes in gene expression and ultimately cytokine production (Fort *et al.*, 2001, Hoyler *et al.*, 2012, Barlow *et al.*, 2013, Molofsky *et al.*, 2015b). In the case of ILC2s, the predominant cytokines produced are IL-5 and IL-13. Expression of cytokines is one known method by which ILC2s can promote immunity and inflammation; for example during helminth infection, whilst IL-13 from ILC2s stimulates goblet cells to produce increased mucus, ILC2-derived IL-5 stimulates eosinophilia (Hashimoto *et al.*, 2009). The net effect of this is increased expulsion of worms.

The majority of established mouse models use the BALB/c or C57BL/6J genetic background to study immune cell function under different conditions. These two strains have slightly differing immune cell compositions, for example peripheral organs from BALB/c mice are enriched in Tregs, as compared to C57BL/6J animals (Chen *et al.*, 2005). Furthermore, cellular responses to certain stimuli can differ at the protein level; research by Watanabe *et al.* demonstrated that following stimulation, macrophage production of key cytokine mediators such as TNF and IL-12 was enhanced in C57BL/6J animals, as compared with BALB/c (Watanabe *et al.*, 2004). Taken together these differences in immune cell composition and activity can have a marked effect on the overall immune response to specific pathogens. This is illustrated in the same study by Watanabe *et al.,* who establish BALB/c mice to be more susceptible than C57BL/6J mice to septic peritonitis, due to impaired bacterial

clearance in the former animals (Watanabe *et al.*, 2004). As such, it is important to consider the immunological features of the different genetic background strains of mice when studying immune cell function. An example of this was demonstrated by Jovicic *et al.*, who found that BALB/c mice were less susceptible to high fat diet (HFD)-induced changes (Jovicic *et al.*, 2015).

In addition to the genetic background of animals, the gender of the animals used can also affect results seen when studying immune cell function, due to the effects of sex hormones on immune cells (Geer and Shen, 2009, Arnold *et al.*, 2016, Klein and Flanagan, 2016, Vom Steeg *et al.*, 2016, Karp *et al.*, 2017). Using a bioinformatics approach, Karp and colleagues found 9.9% of 234 biological traits studied were affected by animal gender. Although it is unclear from this data how many traits examined were associated with immunological function, it is evident that animal gender plays an important role in the overall animal phenotype (Karp *et al.*, 2017).

Finally, the immune cell phenotype can vary vastly between tissues within the same organism, resulting in distinct immunological function. Despite extensive research into the role of immune cell function in ATs (Moro *et al.*, 2010, Molofsky *et al.*, 2013, Lynch, 2014, Benezech *et al.*, 2015, Yeoh and Vijay-Kumar, 2015), direct comparisons of immune cell function between different strains and genders of mice and also different tissues is lacking. Therefore, this chapter aims to establish whether any differences in AT immune cell composition exist between different genetic strains and genders of mice. These results could then be used to inform further investigations into the immunological importance of ATs.

3.2. ADIPOSE TISSUE CELLULAR COMPOSITION IN WT MICE

3.2.1. Comparison of different genetic strains of mice

When initially embarking on this investigation into the immunological importance of ATs, there was little experience of studying the immune cell composition of ATs at The University of Birmingham. For this reason, simple analysis of AT composition was performed alongside the same analysis in MLN, as a control. MLN were chosen for a number of reasons; firstly the immune cell composition of LN in a variety of different mouse models is well established and has been extensively studied at The University of Birmingham. Therefore, this tissue acted as a good control for studying changes in immune cell composition. In addition to the above, MLN were chosen due to the frequently close anatomical localisation of AT and lymphoid tissues (Pond, 2002). More recently, formation of ectopic tertiary lymphoid structures within ATs has also been described (Moro *et al.*, 2010, Koyasu and Moro, 2013, Benezech *et al.*, 2015, Jackson-Jones *et al.*, 2016). As MLN are located within the mesenteric AT depot, it was hypothesised not only that any changes in immune cell composition of ATs may occur within these tertiary lymphoid structures, but may also be mirrored in the MLN too. For this reason, any changes in immune cell composition of MLN were investigated alongside any changes in ATs. Finally, due to their enrichment in ATs, ILCs may be key cells in influencing the homeostasis of ATs. Thus, MLN act as a good control for studying ILCs, as they can be easily identified in MLN.

As discussed above, before assessing changes in AT immune cell composition under conditions of immunological challenge, such as infection, it was important to establish the immune cell composition of ATs in WT, untreated mice. As differences in the immune cell composition of lymphoid tissues are present between C57BL/6J and

BALB/c animals, it was necessary to determine if these differences also arose between the ATs of these two genetic strains. This data would be used to inform the most appropriate genetic background to conduct further investigations into the immunological characteristics of ATs. To explore this, the immune cell composition of ATs and MLN was investigated in adult male (12-20 week of age) BALB/c and C57BL/6J mice by using flow cytometry. Due to technical limitations, it was only possible to investigate a subset of immune cells within AT. As T cells and ILCs both play a role in altering the inflammatory status of AT (Wu *et al.*, 2007, Kintscher *et al.*, 2008, Hams *et al.*, 2013, Molofsky *et al.*, 2013, Boulenouar *et al.*, 2017), these cell types were the focus throughout this investigation. A caveat of this experiment was that, due to issues with availability of age matched animals, analysis of C57BL/6J and BALB/c animals was not performed on the same day. However, analysis of each group was performed as two independent experiments, meaning that there is more confidence that any differences are due to genuine biological differences, rather than inter-experimental variance.

Focusing first on the T-cell compartment, C57BL/6J mice had a higher number of $CD4^+$ T cells in gonadal fat and mesenteries (Figure 3.1A-B) and a higher number of Tregs in the gonadal fat but not mesenteries (Figure 3.1C) when compared to BALB/c animals. This finding contrasts with the findings of Chen, Oppenheim and Howard with regards to the number of Tregs in the lymphoid organs of these animals (Chen *et al.*, 2005). The mesenteries of C57BL/6J animals also had fewer $CD4^+$ and $CD4^-$ iNKTs than seen in the mesenteries of BALB/C animals (Figure 3.1D-E). However, no significant difference in iNKT cell number was seen between gonadal fat isolated from C57BL/6J or BALB/c animals (Figure 3.1D-E).

The expression of different ILC2 cell surface markers was also compared between C57BL/6J and BALB/c tissues. This analysis focused on the expression of ST2 and ICOS, as evidence suggests these markers control ILC2 function through different mechanisms including cytokine production and ILC2 proliferation (Maazi *et al.*, 2015, Molofsky *et al.*, 2015b, Paclik *et al.*, 2015, Rigas *et al.*, 2017). The expression of KLRG1 was also examined, as little is known about the function of this protein with respect to ILC2 biology, although there is some evidence to suggest it is expressed by activated ILC2s (Hoyler *et al.*, 2012, Huang *et al.*, 2015). When the phenotype of the ILC2s from tissues of the two genetic backgrounds was assessed, both the percentage of $ICOS^+$ ILC2s and the expression of ICOS on the surface of ILC2s were lower in ATs isolated from C57BL/6J animals, as compared to BALB/c animals (Figure 3.2B, D-E). There were no differences in the proportion of $KLRG1^+$ ILC2 or the MFI of KLRG1 by ILC2s in the gonadal fat and mesenteries isolated from BALB/c and C57BL/6J animals (Figure 3.2C, F-G). Finally, expression of ST2 by ILC2s was increased in ATs from C57BL/6J animals when compared to BALB/c tissues (Figure 3.2A, H).

A comparison of the ILC composition of ATs and the T cell/ILC composition and ILC2 phenotype of MLN from C57BL/6J and BALB/c animals is shown in the appendix (Figure 7.1-Figure 7.4).

Figure 3.1: Adipose tissue T cell composition in untreated BALB/c and C57BL/6J males

Cells were isolated from the gonadal fat and mesenteries of adult male BALB/c and C57BL/6J mice as described in Materials and Methods. The T cell composition was determined by flow cytometry, as demonstrated previously. Data for each group was obtained from two technical repeats.

Each data point (n=7, 9 for BALB/c and C57BL/6J animals respectively) represents an individual sample with a line indicating the median value. Statistical significance was determined using a Mann-Whitney two-tailed T test, *p<0.05, **p<0.01, ***p<0.001 and ****p<0.0001.

A) FACS plots showing representative T cell composition in gonadal fat (left) and mesenteries (right) from both C57BL/6J (top) and BALB/c (bottom) animals (pre-gated on lymphocytes based on FSC/SSC profile then gated on live/dead-CD45.2$^+$CD3$^+$ cells). Numbers indicate percentage of events in each gate.

B) Graph showing adjusted number of CD4$^+$ cells (CD4$^+$cells/100mg fat) in gonadal fat and mesenteries from BALB/c and C57BL/6J mice (gated on CD45.2+live/dead-intraCD3$^+$CD4$^+$α-gal-cer$^-$ cells).

C) Graph showing adjusted number of regulatory T cells (Tregs/100mg fat) in gonadal fat and mesenteries isolated from BALB/c and C57BL/6J mice (gated on CD45.2$^+$live/dead$^-$intraCD3$^+$CD4$^+$α-gal-cer$^-$Foxp3$^+$ cells).

D) Graph showing adjusted number of CD4$^+$ iNKT cells (CD4$^+$iNKTs/100mg fat) in gonadal fat and mesenteries from BALB/c and C57BL/6J mice (gated on CD45.2$^+$live/dead$^-$intraCD3$^+$CD4$^+$α-gal-cer$^+$ cells).

E) Graph showing adjusted number of CD4$^-$ iNKT cells (CD4$^-$iNKTs/100mg fat) in gonadal fat and mesenteries from BALB/c and C57BL/6J mice (gated on CD45.2$^+$live/dead$^-$intraCD3$^+$CD4$^-$α-gal-cer$^+$ cells).

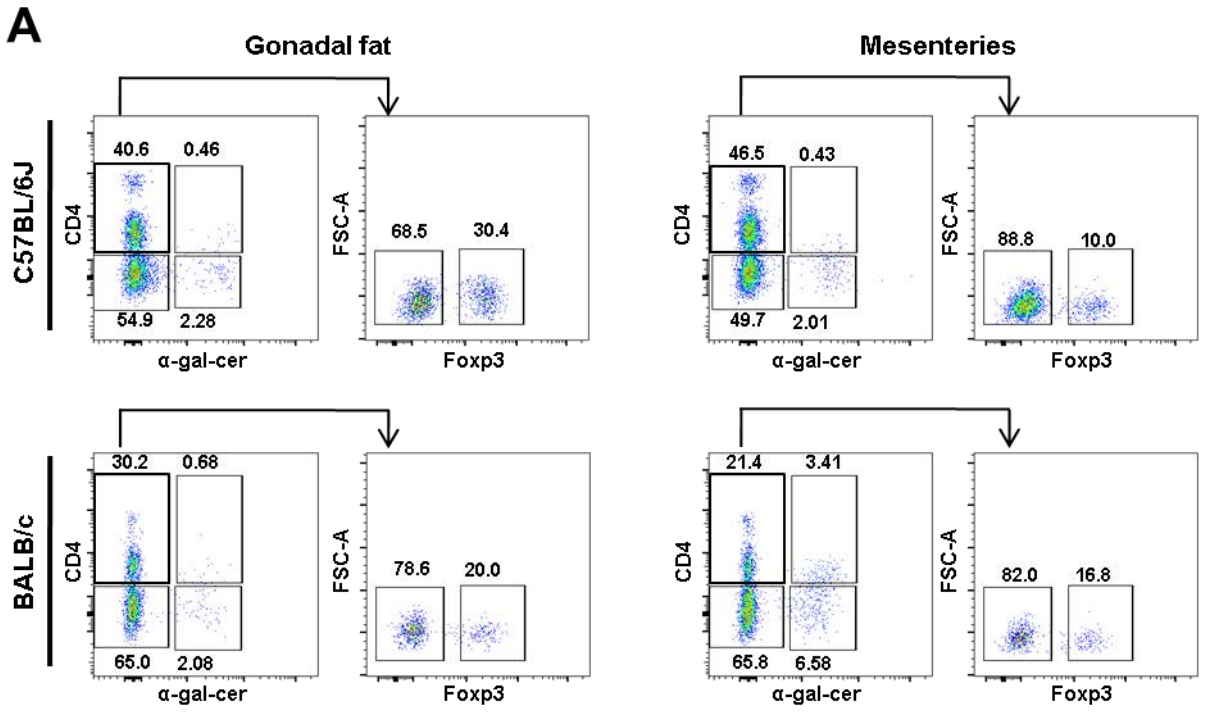
A
Gonadal fat
Mesenteries
C57BL/6J
BALB/c
CD4
α-gal-cer
FSC-A
Foxp3
40.6
0.46
54.9
2.28
68.5
30.4
46.5
0.43
49.7
2.01
88.8
10.0
30.2
0.68
65.0
2.08
78.6
20.0
21.4
3.41
65.8
6.58
82.0
16.8

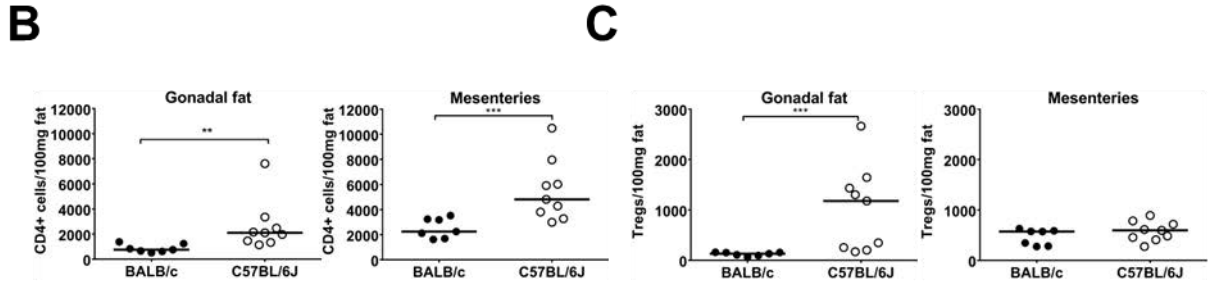
B
C
Gonadal fat
Mesenteries
CD4+ cells/100mg fat
Tregs/100mg fat
BALB/c
C57BL/6J

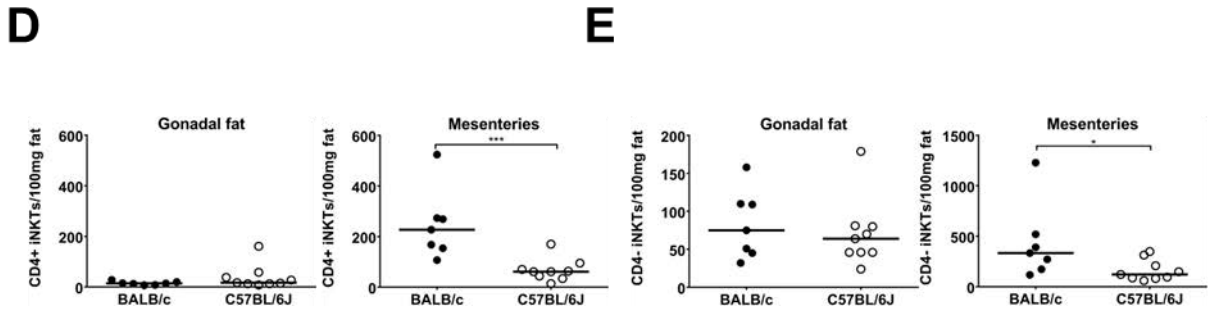
D
E
Gonadal fat
Mesenteries
CD4+ iNKTs/100mg fat
CD4- iNKTs/100mg fat
BALB/c
C57BL/6J

Figure 3.2: Adipose tissue ILC2 phenotype in untreated BALB/c and C57BL/6J males

Cells were isolated from the gonadal fat and mesenteries of adult male BALB/c and C57BL/6J mice, and the ILC2 phenotype was determined by flow cytometry as described in Materials and Methods. Data for each group was obtained from two technical repeats.

Each data point (n=7, 9 for BALB/c and C57BL/6J animals respectively) represents an individual sample with a line indicating the median value. Statistical significance was determined using a Mann-Whitney two-tailed T test, *p<0.05, **p<0.01, ***p<0.001 and ****p<0.0001.

A) FACS plots showing representative ILC2 phenotype in gonadal fat (left) and mesenteries (right) from both C57BL/6J (top) and BALB/c (bottom) animals (pre-gated on live $CD45.2^+$ lymphocytes based on FSC and SSC profile and a viability marker). Numbers indicate percentage of events in each gate.

B) Histogram showing representative ICOS staining in gonadal fat (left panel) or mesenteries (right panel) isolated from BALB/c (red lines) or C57BL/6J (blue lines) animals. Vertical dotted black line indicates positive staining. Solid lines indicate ILC2 staining ($CD45.2^+$live/$dead^-$IL-$7R\alpha^+Lin^-$intra$CD3^-ST2^+GATA\text{-}3^+$ cells), dotted lines indicate ICOS FMO control. Numbers indicate the percentage of $ICOS^+$ cells.

C) Histogram showing representative KLRG1 staining in gonadal fat (left panel) or mesenteries (right panel) isolated from BALB/c (red lines) or C57BL/6J (blue lines) animals. Vertical dotted black line indicates positive staining. Solid lines indicate ILC2 staining ($CD45.2^+$live/$dead^-$IL-$7R\alpha^+Lin^-$intra$CD3^-$ $ST2^+GATA\text{-}3^+$ cells), dotted lines indicate KLRG1 negative control (gated on$CD45.2^+$live/$dead^-$IL-$7R\alpha^-Lin^+$intra$CD3^-$ cells). Numbers indicate the percentage of $KLRG1^+$ cells.

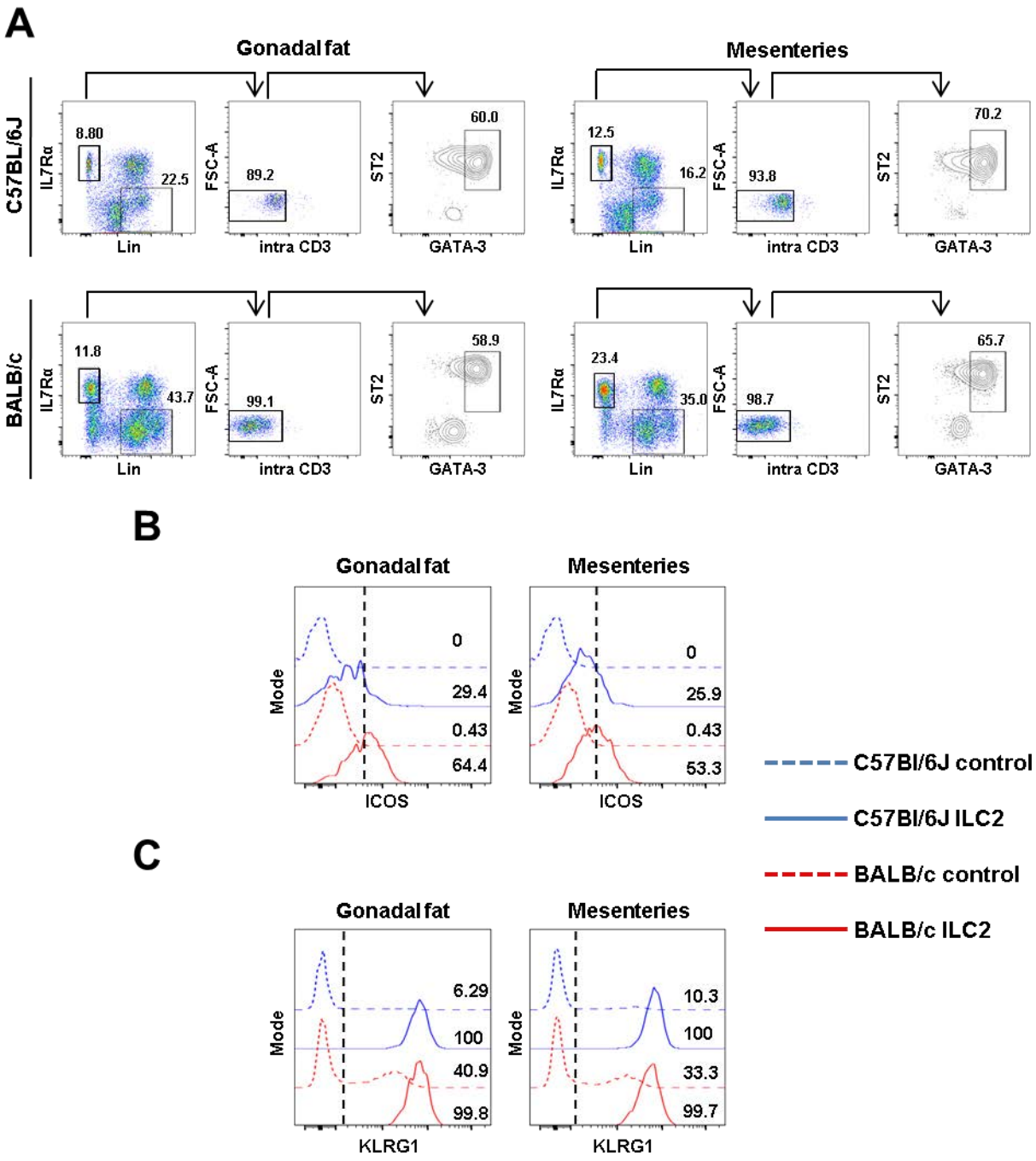
A
Gonadal fat
Mesenteries
C57BL/6J
BALB/c
IL7Rα
Lin
FSC-A
intra CD3
ST2
GATA-3
8.80
22.5
89.2
60.0
12.5
16.2
93.8
70.2
11.8
43.7
99.1
58.9
23.4
35.0
98.7
65.7
B
Gonadal fat
Mesenteries
Mode
ICOS
0
29.4
0.43
64.4
0
25.9
0.43
53.3
C
KLRG1
6.29
100
40.9
99.8
10.3
100
33.3
99.7
C57Bl/6J control
C57Bl/6J ILC2
BALB/c control
BALB/c ILC2

D) Graph showing percentage of ILC2s expressing ICOS in gonadal fat and mesenteries from BALB/c and C57BL/6J mice (gated on live/dead^{-} CD45.2^{+}IL-7Rα^{+}Lin^{-}intraCD3^{-}ST2^{+}GATA-3^{+}ICOS^{+} cells).

E) Graph showing expression of ICOS (median fluorescence) on the surface of ILC2 in gonadal fat and mesenteries from BALB/c and C57BL/6J mice (gated on live/dead^{-}CD45.2^{+}IL-7Rα^{+}Lin^{-}intraCD3^{-}ST2^{+}GATA-3^{+}ICOS^{+}cells).

F) Graph showing percentage of ILC2s expressing KLRG1 in gonadal fat and mesenteries from BALB/c and C57BL/6J mice (gated on live/dead^{-} CD45.2^{+}IL-7Rα^{+}Lin^{-}intraCD3^{-}ST2^{+}GATA-3^{+}KLRG1^{+}cells).

G) Graph showing expression of KLRG1 (median fluorescence) on the surface of ILC2 in gonadal fat and mesenteries from BALB/c and C57BL/6J mice (gated on live/dead^{-}CD45.2^{+}IL-7Rα^{+}Lin^{-}intraCD3^{-}ST2^{+}GATA-3^{+}KLRG1^{+}cells). For both gonadal fat and mesenteries, n=4, 5 for BALB/c and C57BL/6J animals respectively.

H) Graph showing expression of ST2 (median fluorescence) on the surface of ILC2 in gonadal fat and mesenteries from BALB/c and C57BL/6J mice (gated on live/dead^{-}CD45.2^{+}IL-7Rα^{+}Lin^{-}intraCD3^{-}ST2^{+}GATA-3^{+}cells). For both gonadal fat and mesenteries, n=4, 5 for BALB/c and C57BL/6J animals respectively.

D

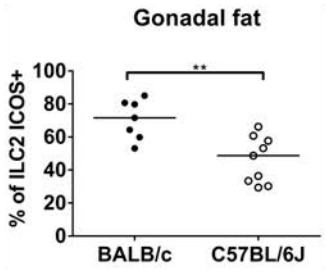
Gonadal fat
% of ILC2 ICOS+
100
80
60
40
20
0
**
BALB/c
C57BL/6J

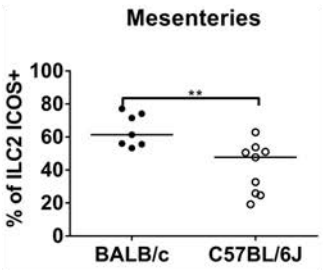
Mesenteries
% of ILC2 ICOS+
100
80
60
40
20
0
**
BALB/c
C57BL/6J

E

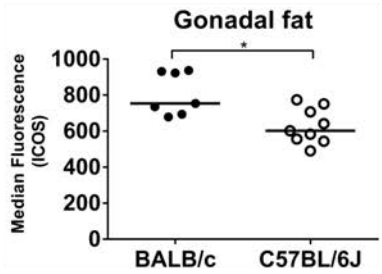
Gonadal fat
Median Fluorescence (ICOS)
1000
800
600
400
200
0
*
BALB/c
C57BL/6J

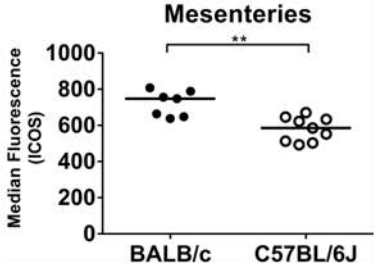
Mesenteries
Median Fluorescence (ICOS)
1000
800
600
400
200
0
**
BALB/c
C57BL/6J

F

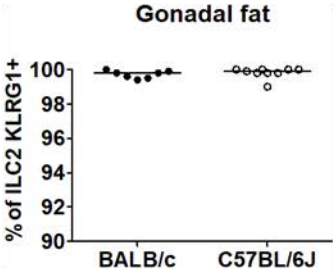
Gonadal fat
% of ILC2 KLRG1+
100
98
96
94
92
90
BALB/c
C57BL/6J

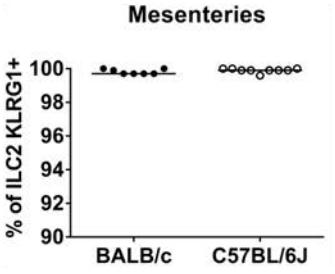
Mesenteries
% of ILC2 KLRG1+
100
98
96
94
92
90
BALB/c
C57BL/6J

G

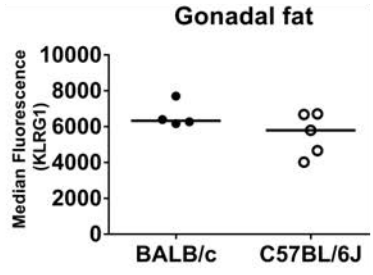
Gonadal fat
Median Fluorescence (KLRG1)
10000
8000
6000
4000
2000
0
BALB/c
C57BL/6J

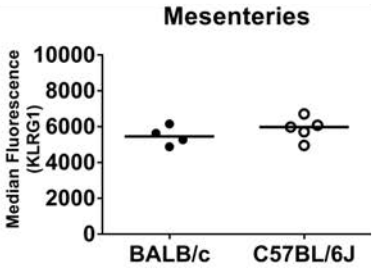
Mesenteries
Median Fluorescence (KLRG1)
10000
8000
6000
4000
2000
0
BALB/c
C57BL/6J

H

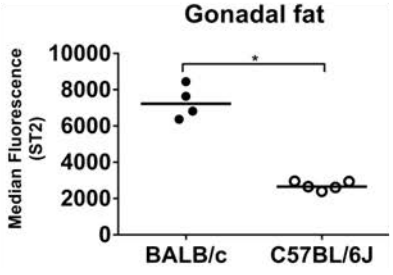
Gonadal fat
Median Fluorescence (ST2)
10000
8000
6000
4000
2000
0
*
BALB/c
C57BL/6J

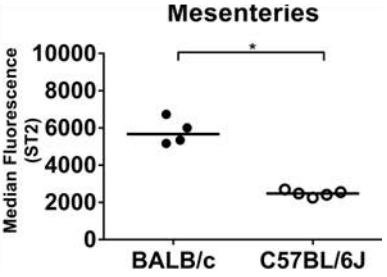
Mesenteries
Median Fluorescence (ST2)
10000
8000
6000
4000
2000
0
*
BALB/c
C57BL/6J

3.2.2. Comparison of male and female BALB/c mice

In addition to the genetic background, the gender of mice has an effect on both lymphoid and AT immune cell composition (Arnold *et al.*, 2016, Klein and Flanagan, 2016, Karp *et al.*, 2017). Therefore, following the investigation of variance between different genetic strains of mice, the immune cell composition of ATs was compared in male and female mice. Unfortunately, whilst performing these experiments only aged matched male and female mice on the BALB/c background were available, therefore the analysis of variance due to gender was performed on mice on the BALB/c background. Furthermore, as with the comparison of C57BL/6J and BALB/c mice, limitations in the availability of mice resulted in analysis of male and female mice being performed in separate experiments. As before, repeating each analysis as two independent experiments should mitigate for any error in interpreting inter-experimental differences as genuine biological differences.

As adiposity varies greatly between males and females in both humans (Demerath *et al.*, 2007, Geer and Shen, 2009) and mice (Macotela *et al.*, 2009, Bruder-Nascimento *et al.*, 2017), it was hypothesised that there are also differences in AT immune cell composition between these genders. As with the analysis of C57BL6J and BALB/c animals, this analysis focused on immune cell types which were likely to play a role in AT homeostasis.

Previous studies have shown that both Tregs and ILC2s have an anti-inflammatory role in prevention of adiposity (Feuerer *et al.*, 2009, Winer *et al.*, 2009, Cipolletta *et al.*, 2011, Hams *et al.*, 2013, Molofsky *et al.*, 2013, Bapat *et al.*, 2015, Kolodin *et al.*, 2015, Donninelli *et al.*, 2017) and that female mice are more resistant to diet induced obesity (Bruder-Nascimento *et al.*, 2017). Gonadal fat isolated from females had

more $CD4^+$ T cells and Tregs than male mice (Figure 3.3A-C) and also a greater number of total ILCs and ILC2s than gonadal fat isolated from males (Figure 3.4B-C). A greater number of these anti-inflammatory cells in the gonadal fat of female mice could indicate a mechanism by which female mice are less susceptible to diet induced obesity than male counterparts. However, these populations did not differ in number in the mesenteries from male and female animals (Figure 3.3A-C, Figure 3.4B-C).

ILC2 phenotype was also examined and compared in the different gender mice. Expression of ICOS was decreased in ATs of male mice compared to female mice, both in terms of percentage and MFI, implying that gender specific signals play a role in determining ILC2 expression of ICOS during steady state conditions (Figure 3.5B, D-E). Both ATs from male mice had a higher percentage of $KLRG1^+$ ILC2s than ILC2s from similar tissues in female mice. Also the expression of KLRG1 on the surface of ILC2s was higher in the ATs of males than in females (Figure 3.5C, F-G). ST2 expression was also higher in ILC2s from all tissues of male animals, as compared to females (Figure 3.5A, H). Whilst a higher ILC2 ST2 expression in males could indicate an increased ability of ILC2s from males to respond to IL-33, it is unclear what the significance of increased ILC2 KLRG1 expression is in the function of ILC2s in male animals.

Comparison of total cellularity of ATs, mass of ATs and differences in certain immune cell populations in ATs and MLN of male and female animals is shown in the appendix (Figure 7.5-Figure 7.8).

Figure 3.3: Adipose tissue T cell composition in untreated BALB/c males and females

Cells were isolated from the gonadal fat and mesenteries of adult male and female BALB/c mice as described in Materials and Methods. The T cell composition was determined by flow cytometry, as demonstrated previously. Data for each group was obtained from two technical repeats.

Each data point (n=7, 6 for males and females respectively) represents an individual sample with a line indicating the median value. Statistical significance was determined using a Mann-Whitney two-tailed T test, *p<0.05, **p<0.01, ***p<0.001 and ****p<0.0001.

A) FACS plots showing representative T cell composition in gonadal fat (left) and mesenteries (right) from both male (top) and female (bottom) animals (pre-gated on lymphocytes based on FSC/SSC profile then gated on live/dead$^-$ CD45.2$^+$CD3$^+$ cells). Numbers indicate percentage of events in each gate.

B) Graph showing adjusted number of CD4$^+$ cells (CD4$^+$cells/100mg fat) in gonadal fat and mesenteries from male and female mice (gated on CD45.2$^+$live/dead$^-$intraCD3$^+$CD4$^+$α-gal-cer$^-$ cells).

C) Graph showing adjusted number of regulatory T cells (Tregs/100mg fat) in gonadal fat and mesenteries isolated from male and female mice (gated on CD45.2$^+$live/dead$^-$intraCD3$^+$CD4$^+$α-gal-cer$^-$Foxp3$^+$ cells).

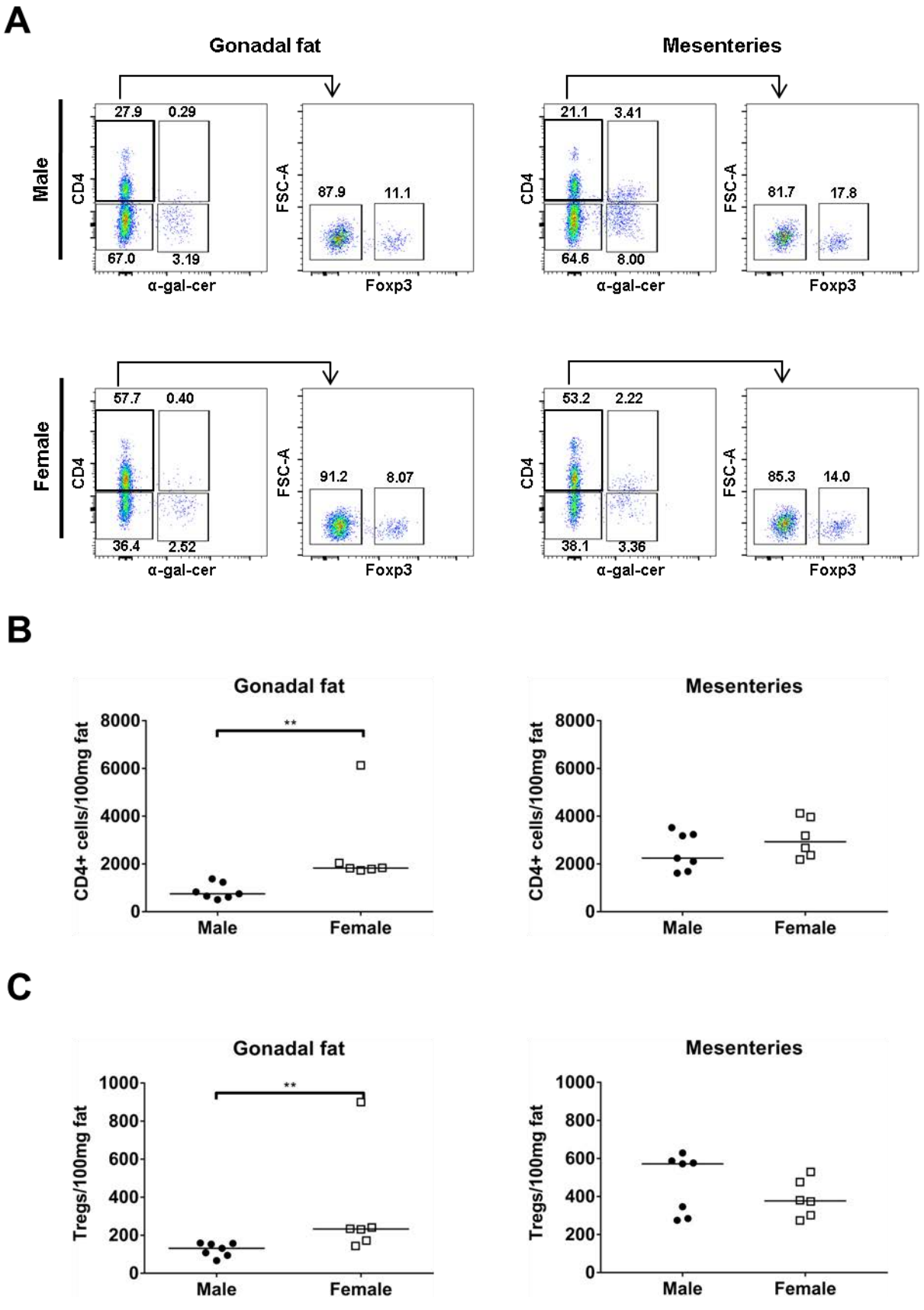
A
Gonadal fat
Mesenteries
Male
Female
CD4
α-gal-cer
FSC-A
Foxp3
27.9
0.29
67.0
3.19
87.9
11.1
21.1
3.41
64.6
8.00
81.7
17.8
57.7
0.40
36.4
2.52
91.2
8.07
53.2
2.22
38.1
3.36
85.3
14.0
B
Gonadal fat
Mesenteries
CD4+ cells/100mg fat
8000
6000
4000
2000
0
**
Male
Female
C
Gonadal fat
Mesenteries
Tregs/100mg fat
1000
800
600
400
200
0
**
Male
Female

Figure 3.4: Adipose tissue ILC composition in untreated BALB/c males and females

Cells were isolated from the gonadal fat and mesenteries of adult male and female BALB/c mice as described in Materials and Methods. The ILC composition was determined by flow cytometry, as demonstrated previously. Data for each group was obtained from two technical repeats.

Each data point (n=7, 6 for males and females respectively) represents an individual sample with a line indicating the median value. Statistical significance was determined using a Mann-Whitney two-tailed T test, *p<0.05, **p<0.01, ***p<0.001 and ****p<0.0001.

A) FACS plots showing representative ILC composition in gonadal fat (left) and mesenteries (right) from both male (top) and female (bottom) animals (pre-gated on live $CD45.2^+$ lymphocytes based on FSC and SSC profile and a viability marker). Numbers indicate percentage of events in each gate.

B) Graph showing adjusted number of total ILCs (total ILCs/100mg fat) in gonadal fat and mesenteries from male and female mice (gated on live/$dead^-$ $CD45.2^+IL\text{-}7R\alpha^+Lin^-$ cells).

C) Graph showing adjusted number of ILC2s (ILC2s/100mg fat) in gonadal fat and mesenteries from male and female mice (gated on live/$dead^-$ $CD45.2^+IL\text{-}7R\alpha^+Lin^-intraCD3^-ROR\gamma t^-GATA\text{-}3^+$ cells).

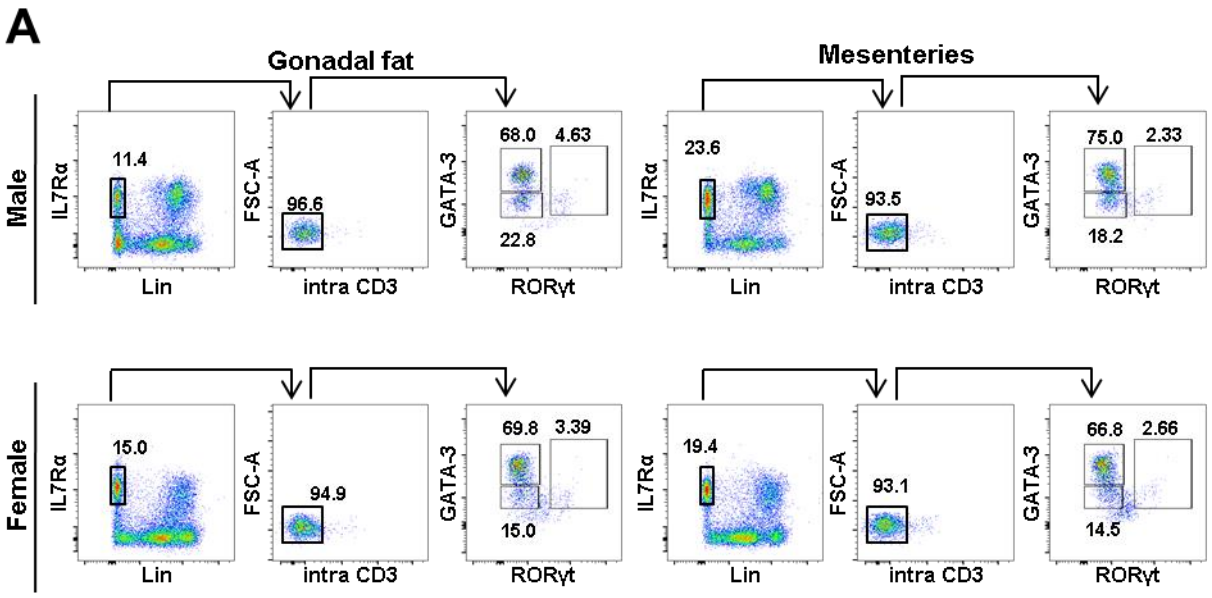
A
Gonadal fat
Mesenteries
Male
Female
IL7Rα
Lin
11.4
FSC-A
intra CD3
96.6
GATA-3
RORγt
68.0
4.63
22.8
23.6
93.5
75.0
2.33
18.2
15.0
94.9
69.8
3.39
15.0
19.4
93.1
66.8
2.66
14.5

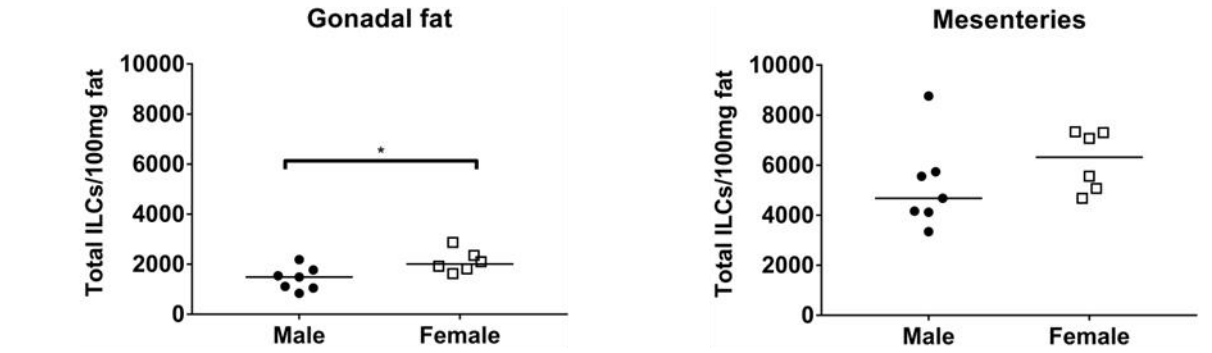
B
Gonadal fat
Mesenteries
Total ILCs/100mg fat
10000
8000
6000
4000
2000
0
*
Male
Female

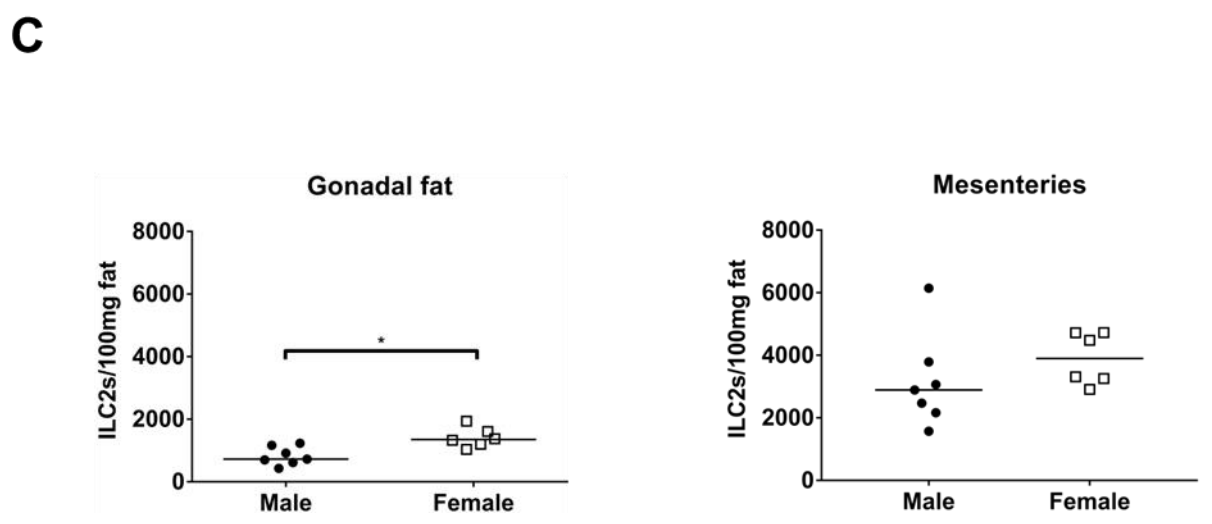
C
Gonadal fat
Mesenteries
ILC2s/100mg fat
8000
6000
4000
2000
0
*
Male
Female

Figure 3.5: Adipose tissue ILC2 phenotype in untreated BALB/c males and females

Cells were isolated from the gonadal fat and mesenteries of adult male and female mice and the ILC2 phenotype was determined by flow cytometry as described in Materials and Methods. Data for each group was obtained from two technical repeats.

Each data point (n=7, 6 for males and females respectively) represents an individual sample with a line indicating the median value. Statistical significance was determined using a Mann-Whitney two-tailed T test, *p<0.05, **p<0.01, ***p<0.001 and ****p<0.0001.

A) FACS plots showing representative ILC2 phenotype in gonadal fat (left) and mesenteries (right) from both male (top) and female (bottom) animals (pre-gated on live $CD45.2^+$ lymphocytes based on FSC and SSC profile and a viability marker). Numbers indicate percentage of events in each gate.

B) Histogram showing representative ICOS staining in gonadal fat (left panel) or mesenteries (right panel) isolated from female (red lines) or male (blue lines) animals. Vertical dotted black line indicates positive staining. Solid lines indicate ILC2 staining ($CD45.2^+$live/$dead^-$IL-$7R\alpha^+Lin^-$intra$CD3^-ST2^+GATA\text{-}3^+$ cells), dotted lines indicate ICOS FMO control. Numbers indicate the percentage of $ICOS^+$ cells.

C) Histogram showing representative KLRG1 staining in gonadal fat (left panel) or mesenteries (right panel) isolated from female (red lines) or male (blue lines) animals. Vertical dotted black line indicates positive staining. Solid lines indicate ILC2 staining ($CD45.2^+$live/$dead^-$IL-$7R\alpha^+Lin^-$intra$CD3^-ST2^+GATA\text{-}3^+$ cells), dotted lines indicate KLRG1 negative control (gated on $CD45.2^+$live/$dead^-$IL-$7R\alpha^-Lin^+$intra$CD3^-$ cells). Numbers indicate the percentage of $KLRG1^+$ cells.

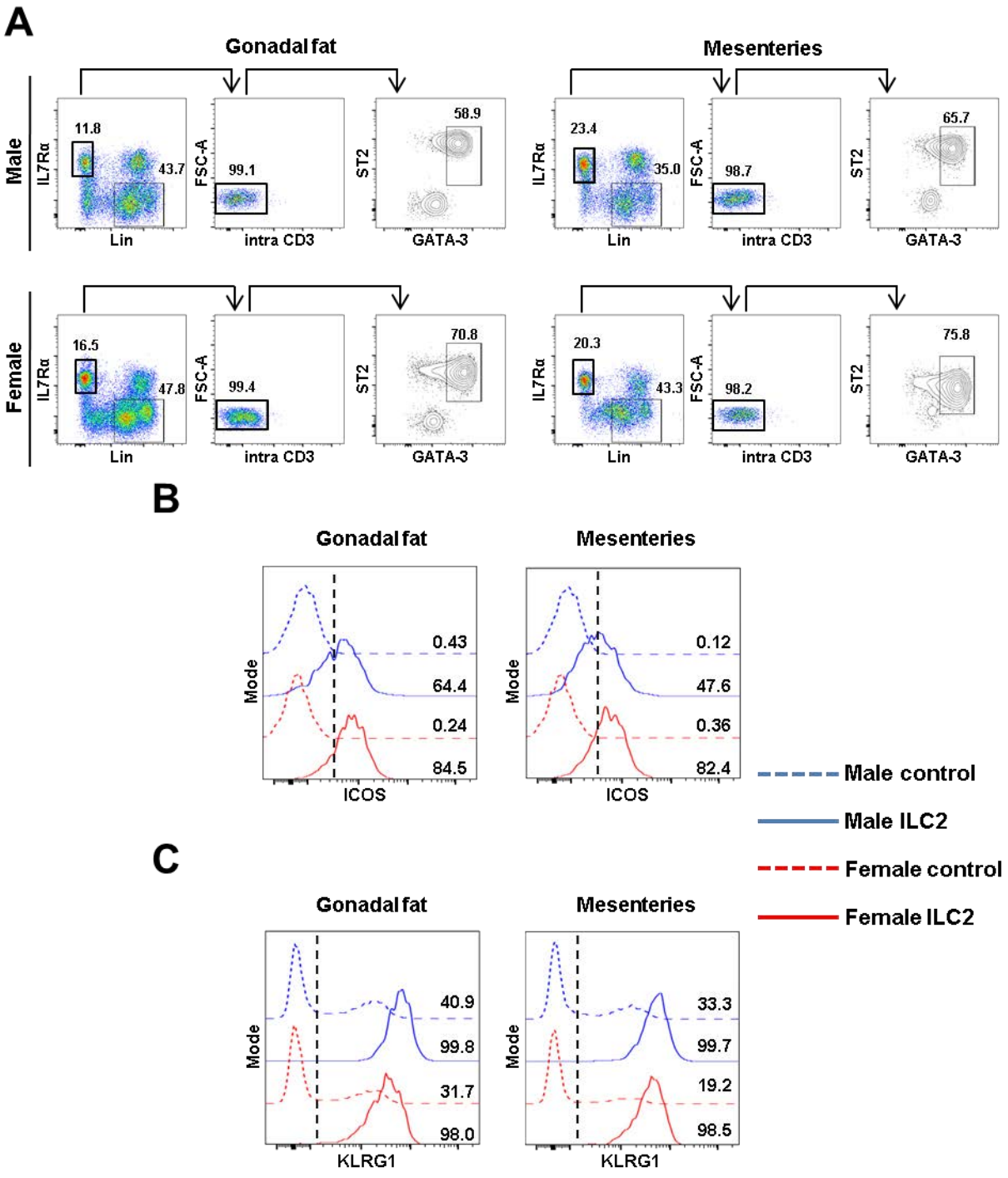
A
Gonadal fat
Mesenteries
Male
Female
IL7Rα
Lin
FSC-A
intra CD3
ST2
GATA-3
11.8
43.7
99.1
58.9
23.4
35.0
98.7
65.7
16.5
47.8
99.4
70.8
20.3
43.3
98.2
75.8
B
Gonadal fat
Mesenteries
Mode
ICOS
0.43
64.4
0.24
84.5
0.12
47.6
0.36
82.4
Male control
Male ILC2
Female control
Female ILC2
C
Gonadal fat
Mesenteries
Mode
KLRG1
40.9
99.8
31.7
98.0
33.3
99.7
19.2
98.5

D) Graph showing percentage of ILC2s expressing ICOS in gonadal fat and mesenteries from male and female mice (gated on live/dead^{-} CD45.2^{+}IL-7Rα^{+}Lin^{-}intraCD3^{-}ST2^{+}GATA-3^{+}ICOS^{+} cells).

E) Graph showing expression of ICOS (median fluorescence) on the surface of ILC2 in gonadal fat and mesenteries from male and female mice (gated on live/dead^{-}CD45.2^{+}IL-7Rα^{+}Lin^{-}intraCD3^{-}ST2^{+}GATA-3^{+}ICOS^{+} cells).

F) Graph showing percentage of ILC2s expressing KLRG1 in gonadal fat and mesenteries from male and female mice (gated on live/dead^{-} CD45.2^{+}IL-7Rα^{+}Lin^{-}intraCD3^{-}ST2^{+}GATA-3^{+}KLRG1^{+} cells).

G) Graph showing expression of KLRG1 (median fluorescence) on the surface of ILC2 in gonadal fat and mesenteries from male and female mice (gated on live/dead^{-}CD45.2^{+}IL-7Rα^{+}Lin^{-}intraCD3^{-}ST2^{+}GATA-3^{+}KLRG1^{+} cells). (n=4, 4).

H) Graph showing expression of ST2 (median fluorescence) on the surface of ILC2 in gonadal fat and mesenteries from male and female mice (gated on live/dead^{-}CD45.2^{+}IL-7Rα^{+}Lin^{-}intraCD3^{-}ST2^{+}GATA-3^{+} cells).

D

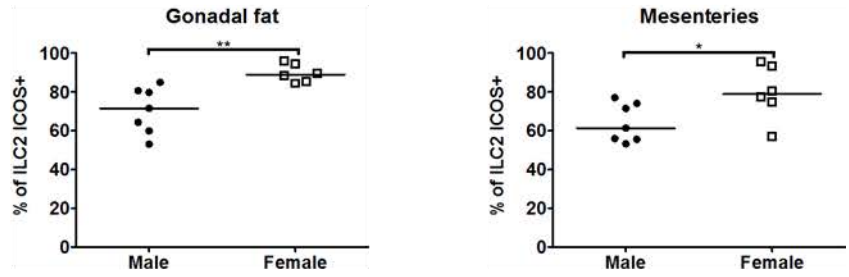
Gonadal fat
% of ILC2 ICOS+
100
80
60
40
20
0
**
Male
Female
Mesenteries
% of ILC2 ICOS+
100
80
60
40
20
0
*
Male
Female

E

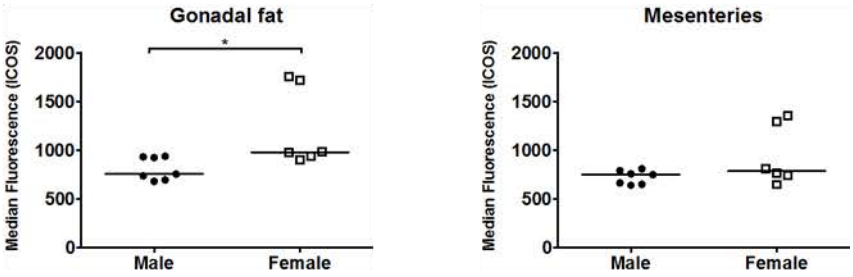
Gonadal fat
Median Fluorescence (ICOS)
2000
1500
1000
500
0
*
Male
Female
Mesenteries
Median Fluorescence (ICOS)
2000
1500
1000
500
0
Male
Female

F

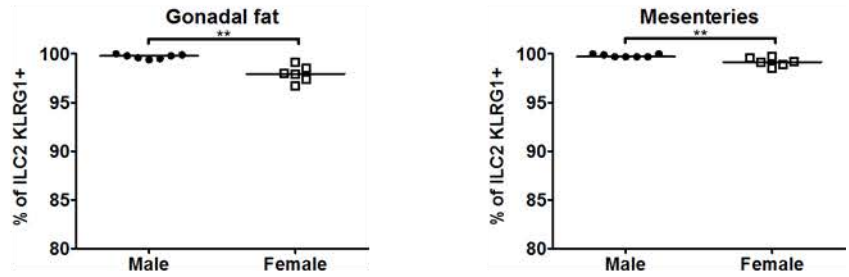
Gonadal fat
% of ILC2 KLRG1+
100
95
90
85
80
**
Male
Female
Mesenteries
% of ILC2 KLRG1+
100
95
90
85
80
**
Male
Female

G

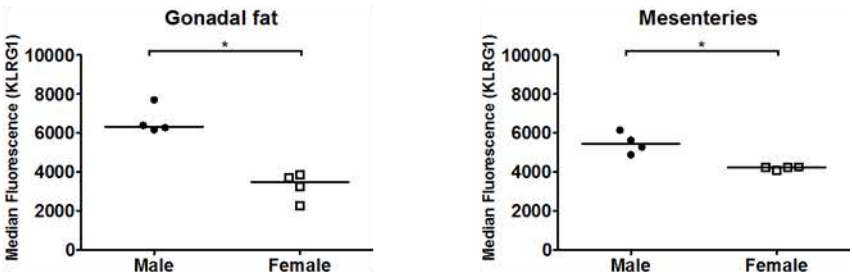
Gonadal fat
Median Fluorescence (KLRG1)
10000
8000
6000
4000
2000
0
*
Male
Female
Mesenteries
Median Fluorescence (KLRG1)
10000
8000
6000
4000
2000
0
*
Male
Female

H

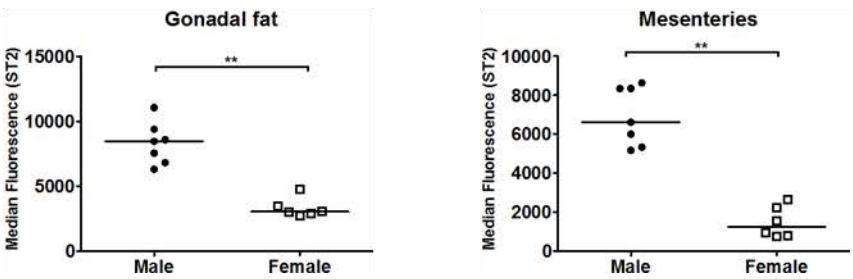
Gonadal fat
Median Fluorescence (ST2)
15000
10000
5000
0
**
Male
Female
Mesenteries
Median Fluorescence (ST2)
10000
8000
6000
4000
2000
0
**
Male
Female

3.3. ILC2 PROTEIN EXPRESSION VARIES BETWEEN TISSUES

3.3.1. ILC2 phenotype differs between adipose tissues and MLN

ILC2s appear to be enriched in ATs, as compared to lymphoid tissues (see Figure 3.2 and Figure 3.5). Others groups have also reported that some markers, such as CD25, are expressed at higher levels by ILC2s isolated from ATs, as compared to ILC2s isolated from other lymphoid and non-lymphoid tissues (Moro *et al.*, 2010, Molofsky *et al.*, 2013, Moro *et al.*, 2015). Many of the proteins expressed on the surface of ILC2s have important contributions to the role ILC2s play during an immune response. Thus, the expression of canonical ILC2 surface proteins was investigated in ILC2 from ATs (gonadal fat and mesenteries) and compared to MLN ILC2s. As previously reported by others (Hams *et al.*, 2013, Molofsky *et al.*, 2013, Molofsky *et al.*, 2015b), whilst cells identified as ILC2s were only a small proportion of the total ILC pool ($CD45.2^{+}IL\text{-}7R\alpha^{+}Lin^{-}intraCD3^{-}$ cells) in MLN, ILC2s represented the majority of ILCs isolated from gonadal fat and mesenteries of C57BL/6J males (Figure 3.6A). Differences were also observed in the proportion of ILC2s expressing different markers between ILC2s from MLN and from ATs; firstly a higher percentage of ILC2s expressed ICOS in MLN than in ATs (Figure 3.6B, D). Furthermore, the level of expression of ICOS was higher on the surface of ILC2s isolated from MLN than ILC2s isolated from ATs (Figure 3.6B, E). ILC2 expression of the ligand for ICOS, ICOSL is reported to be higher in ATs than lymphoid tissues (Molofsky *et al.*, 2015b) and also has been reported to negatively correlate with ICOS expression (Kamachi *et al.*, 2015). Taken together, these pieces of data may illustrate why ILC2 ICOS expression was higher in MLN than ATs.

In contrast to ICOS, a higher percentage of ILC2s isolated from ATs expressed the marker KLRG1 than in the MLN, but there was no significant difference in the level of expression of KLRG1 between these tissues (Figure 3.6C, F-G). As discussed in section 3.2.1, the precise importance of KLRG1 in ILC2 function is unclear, thus it is difficult to interpret the significance of this finding.

Finally, the expression of ST2 was lower on the surface of ILC2s isolated from MLN than those isolated from ATs (Figure 3.6A, H). ST2 is the receptor for IL-33, an alarmin produced early in an immune response to a pathogen. Higher ST2 expression by ILC2s from ATs may reveal a greater propensity of ILC2s from these tissues to respond to IL-33.

No significant differences in percentages or MFI values were observed between gonadal fat and mesenteries (Figure 3.6).

Figure 3.6: ILC2 phenotype in different tissues

Cells were isolated from the MLN, gonadal fat and mesenteries of adult male C57BL/6J mice and the ILC2 phenotype was determined by flow cytometry, as described in Materials and Methods. Data for each group was obtained from two technical repeats.

Each data point (n=10, 9, 9 for MLN, gonadal fat and mesenteries respectively) represents an individual sample with a line indicating the median value. Statistical significance was determined using a Mann-Whitney two-tailed T test, *p<0.05, **p<0.01, ***p<0.001 and ****p<0.0001.

A) FACS plots showing representative ILC2 phenotype in MLN (top), gonadal fat (bottom left) and mesenteries (bottom right) from C57BL/6J males (pre-gated on live CD45.2$^+$ lymphocytes based on FSC and SSC profile and a viability marker). Numbers indicate percentage of events in each gate.

B) Histogram showing representative staining of ICOS in MLN (blue lines), gonadal fat (red lines) or mesenteries (green lines). Vertical dotted black line indicates positive staining. Solid lines indicate ILC2 staining (CD45.2$^+$live/dead$^-$IL-7Rα$^+$Lin$^-$intraCD3$^-$ST2$^+$GATA-3$^+$ cells), dotted lines indicate FMO control staining. Numbers indicate the percentage of positive cells.

C) Histogram showing representative staining of KLRG1 in MLN (blue lines), gonadal fat (red lines) or mesenteries (green lines). Vertical dotted black line indicates positive staining. Solid lines indicate ILC2 staining (CD45.2$^+$live/dead$^-$IL-7Rα$^+$Lin$^-$intraCD3$^-$ST2$^+$GATA-3$^+$ cells), dotted lines indicate negative control staining (CD45.2$^+$live/dead$^-$IL-7Rα$^+$Lin$^-$intraCD3$^-$ST2$^-$ GATA-3$^-$ cells). Numbers indicate the percentage of positive cells.

D) Graph showing the percentage of ILC2s that express ICOS in MLN, gonadal fat and mesenteries (gated on CD45.2$^+$live/dead$^-$IL-7Rα$^+$Lin$^-$intraCD3$^-$ ST2$^+$GATA-3$^+$ICOS$^+$ cells).

E) Graph showing the median fluorescence of ICOS on the surface of ILC2s isolated from MLN, gonadal fat and mesenteries (gated on CD45.2$^+$live/dead$^-$ IL-7Rα$^+$Lin$^-$intraCD3$^-$ST2$^+$GATA-3$^+$ICOS$^+$ cells).

F) Graph showing the percentage of ILC2s that express KLRG1 in MLN, gonadal fat and mesenteries (gated on CD45.2$^+$live/dead$^-$IL-7Rα$^+$Lin$^-$intraCD3$^-$ ST2$^+$GATA-3$^+$KLRG1$^+$ cells).

G) Graph showing the median fluorescence of KLRG1on the surface of ILC2s isolated from MLN, gonadal fat and mesenteries (gated on CD45.2$^+$live/dead$^-$ IL-7Rα$^+$Lin$^-$intraCD3$^-$ST2$^+$GATA-3$^+$KLRG1$^+$ cells).

H) Graph showing the median fluorescence of ST2 on the surface of ILC2s isolated from MLN, gonadal fat and mesenteries (gated on CD45.2$^+$live/dead$^-$ IL-7Rα$^+$Lin$^-$intraCD3$^-$ST2$^+$GATA-3$^+$cells).

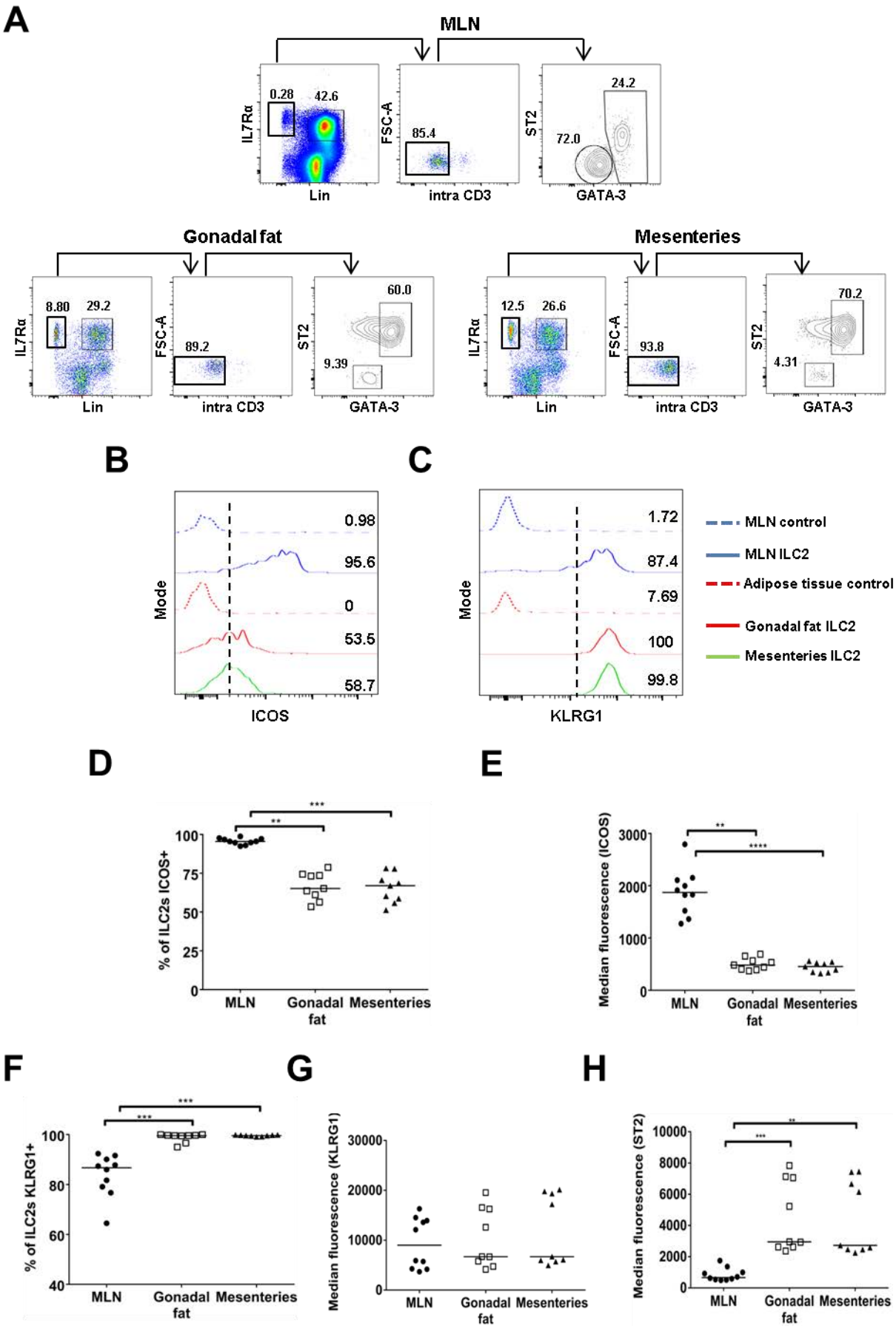
A
MLN
0.28
42.6
IL7Rα
Lin
FSC-A
85.4
intra CD3
ST2
24.2
72.0
GATA-3
Gonadal fat
8.80
29.2
IL7Rα
Lin
FSC-A
89.2
intra CD3
ST2
60.0
9.39
GATA-3
Mesenteries
12.5
26.6
IL7Rα
Lin
FSC-A
93.8
intra CD3
ST2
70.2
4.31
GATA-3
B
Mode
0.98
95.6
0
53.5
58.7
ICOS
C
Mode
1.72
87.4
7.69
100
99.8
KLRG1
MLN control
MLN ILC2
Adipose tissue control
Gonadal fat ILC2
Mesenteries ILC2
D
% of ILC2s ICOS+
MLN
Gonadal fat
Mesenteries
E
Median fluorescence (ICOS)
MLN
Gonadal fat
Mesenteries
F
% of ILC2s KLRG1+
MLN
Gonadal fat
Mesenteries
G
Median fluorescence (KLRG1)
MLN
Gonadal fat
Mesenteries
H
Median fluorescence (ST2)
MLN
Gonadal fat
Mesenteries

3.3.2. ILC2 chemokine receptor expression in different tissues

ILC2s are enriched in ATs compared with MLN. However, mechanisms by which ILCs migrate between tissues have not been determined. Parabiotic models have been used to study recirculation of immune cells in congenic mice. The results from these animals indicate minimal recirculation of ILC subsets within ATs over a long period of time, suggesting ILCs have a low turnover and remain tissue resident following initial establishment within peripheral tissues (Gasteiger *et al.*, 2015, Moro *et al.*, 2016, O'Sullivan *et al.*, 2016, Boulenouar *et al.*, 2017). Moreover, studies investigating the maturation of ILCs from progenitor cells have failed to conclusively demonstrate at what stage of maturation these cells become tissue resident; ILC progenitors initially develop in the bone marrow, but have been also identified in other tissues including ATs (Moro *et al.*, 2016). Cellular migration is predominantly controlled by the expression of C-X-C and C-C motif chemokine receptors in both mice and humans. For this reason, expression of chemokine receptors bearing these motifs may help elucidate the signals which control the migration of immature or mature ILCs into peripheral tissues. In line with this, the expression of chemokine receptors on the surface of mature ILC2s was examined and compared in a number of lymphoid and non-lymphoid tissues. Potential chemokine receptor candidates were chosen based on known expression in T cells, to which ILCs share overlapping functions. Also, recent work by the Immunological Genome Project allowed the analysis of ILC mRNA expression of C-X-C and C-C motif chemokine receptors (Robinette *et al.*, 2015). Finally, the choice of chemokine receptor candidates for investigation was also limited based on the range of commercially available antibodies against these markers. This evaluation led us to explore the potential

expression of the chemokine receptors CCR4, CCR6, CCR8, CCR9, CXCR6 and C-C motif Chemokine Receptor Like 2 (CCRL2). Tissues examined included ILN, MLN, gonadal fat, mesenteries, lung and SILP. ILN and MLN were chosen as they are canonical lymphoid tissues. SILP and lungs were chosen because, like ATs, they are non-lymphoid tissues and have been the focus of previous studies on ILC biology (Chang *et al.*, 2011, Monticelli *et al.*, 2011, Artis and Spits, 2015, Robinette *et al.*, 2015). Therefore, these lymphoid and non-lymphoid tissues helped to dissect whether there were any overlapping patterns determining the migration of ILC2s to lymphoid or non-lymphoid tissues, or to specific tissues.

The proportion of ILC2s varied markedly amongst the tissues examined (Figure 3.7). Higher numbers of ILC2 in MLN compared to ILN have previously been reported by Mackley *et al.* (Mackley *et al.*, 2015). Furthermore, in line with work by others (Moro *et al.*, 2010, Moro *et al.*, 2015, Moro *et al.*, 2016), the proportion of ILC2s was higher in ATs than lung or SILP, suggesting that the enrichment of ILC2s in ATs is not simply a general feature of non-lymphoid tissues.

Representative flow cytometry staining of ILC2 expression of CCR6, CCR8 and CCR9 in the different tissues studied is shown in Figure 3.7 and the percentage of ILC2 expressing each marker is summarised in Figure 3.10C.

CCR6 is expressed on the surface of B cells and Th17 cells (Schutyser *et al.*, 2003). Furthermore, CCR6 is highly expressed specifically by LTi-like cells, but not other group 3 ILCs (Artis and Spits, 2015). CCR6 expression by ILC2s from ILN, MLN, ATs, SILP and lungs was tested. CCR6 expression was minimal in all tissues except the ILN (Figure 3.8A-B). This lack of expression by ILC2s is also reported by others in the literature (Artis and Spits, 2015, Diefenbach, 2015, Mackley *et al.*, 2015).

CCL20, the ligand for CCR6, is expressed by LN FRCs in response to pro-inflammatory signals such as TNF and IL-1β, both of which are associated with the differentiation or effector profile of $CCR6^+$ Th17 cells (Severino *et al.*, 2017). Thus the expression of CCR6 on the surface of ILN ILC2 is unexpected.

CCR8 is expressed on human and mouse NK cells (Inngjerdingen *et al.*, 2000), Th2 cells (Zingoni *et al.*, 1998, Schaerli *et al.*, 2004, Bromley *et al.*, 2008, Islam *et al.*, 2011, Griffith *et al.*, 2014) and Tregs (Bromley *et al.*, 2008, Griffith *et al.*, 2014, Barsheshet *et al.*, 2017). CCR8 expressing cells have been shown to migrate towards the ligand CCL1 and CCL8. Whilst CCL1 is expressed in the thymus, by medullary macrophages, and in the skin during homeostasis, CCL8 is expressed by keratinocytes in the skin during homeostasis (Annunziato *et al.*, 2002, Colantonio *et al.*, 2002, Schaerli *et al.*, 2004, Gombert *et al.*, 2005). Moreover, both CCL1 and CCL8 expression are increased in skin under inflammatory conditions, such as atopic dermatitis (Miller *et al.*, 1989, Islam *et al.*, 2011). CCR9 is also expressed on T cells, however its expression appears to be restricted to a subset of T cells with enhanced homing to the SI (Mora *et al.*, 2003). Furthermore, a paper by Kim and colleagues demonstrate that whilst ILC3 and ILC1 can acquire CCR9 expression in the MLN, ILC2 progenitors acquire CCR9 expression in the bone marrow, allowing the migration of both ILC2 progenitors and mature ILC2s to the SI (Kim *et al.*, 2015a).

The majority of ILC2s in non-lymphoid tissues (ATs, lung and SILP) expressed either CCR8 alone, or co-expressed CCR8 and CCR9 (Figure 3.8C-E). In contrast, a much lower percentage of ILC2s from lymphoid tissues (ILN and MLN) expressed either CCR8 alone or in combination with CCR9, although this difference was only statistically significant when comparing gonadal fat and SI with MLN and ILN (Figure

3.8C-E). Moreover, there was a higher expression of CCR8 on the surface of ILC2s when comparing gonadal fat and lung with ILN and MLN (Figure 3.8F). Conversely, a larger percentage of ILC2s expressed CCR9 alone when gonadal fat and lung ILC2s were compared with MLN ILC2s, and also where gonadal fat ILC2s were compared with ILN ILC2s (Figure 3.8D). Nonetheless, the only difference seen in CCR9 expression was that SILP ILC2s showed a markedly lower expression of CCR9 than ILC2s isolated from lung, ILN and MLN (Figure 3.8G). It is interesting that CCR9 expression, which along with $\alpha_4\beta_7$ is associated as a homing signal for chemotaxis of cells to the SI, is only expressed by a small proportion of ILC2s found in this tissue (Mora *et al.*, 2003, Hoyler *et al.*, 2012, Kim *et al.*, 2015a). The reason for this requires further investigation, but could be due to downregulation once ILC2s migrate to the SI.

The expression of the markers CCRL2, CCR4 and CXCR6 by ILC2s from the different lymphoid and non-lymphoid tissues was also assessed. Representative flow cytometry staining of ILC2 expression of CCR4, CXCR6 and CCRL2 in the different tissues studied is shown in Figure 3.9 and the percentage of ILC2 expressing each marker is summarised in Figure 3.10C.

CCR4 is a GATA-3 target gene and is expressed by Th2 cells and Tregs, especially in the skin (Bonecchi *et al.*, 1998, Islam *et al.*, 2011, Griffith *et al.*, 2014). CCRL2 expression is reported on most cell populations including T cells, neutrophils and monocytes (Yoshimura and Oppenheim, 2011, De Henau *et al.*, 2016). Furthermore, unlike most other chemokine receptors, CCRL2 binding does not appear to induce intracellular signalling. Thus, CCRL2 appears to act as a scavenger receptor, sequestering its ligands CCL5 and CCL19 (Yoshimura and Oppenheim, 2011, De

Henau *et al.*, 2016). In contrast, CXCR6 appears to be preferentially expressed by naïve T cells and also by Th1, Th17 and iNKT cells and Tregs (Thomas *et al.*, 2003, Griffith *et al.*, 2014). Moreover, another study indicates a role of CXCR6 in migration of ILC progenitors to peripheral tissues prior to maturation of these ILC progenitors (Chea *et al.*, 2015). The expression of CCRL2 and CCR4 by ILC2s was determined to be negligible in all tissues, after using isotype controls to identify any non-specific staining (Figure 3.9, see appendix Figure 7.9 for isotype staining). This suggests these receptors are not involved in the migration of mature ILC2s to the tissues studied. Expression of CXCR6 was observed by ILC2s from all tissues examined (Figure 3.9). This is consistent with findings by Chea *et al.*, who hypothesise that CXCR6 expression is induced in later stages of ILC development, but is expressed by all mature ILC subsets (Chea *et al.*, 2015). A marginally higher percentage of ILC2s expressing CXCR6 was observed in the ILN compared to lung and SILP (Figure 3.10A, C). Moreover, there was a higher expression of CXCR6 on the surface of ILC2s isolated from ILN compared with ILC2s from SILP and lung (Figure 3.10B-C). ILC2s isolated from the mesenteries also had a lower expression of CXCR6 than ILC2s isolated from MLN and ILN of the same animals (Figure 3.10B). The reason for these tissue specific differences is unclear. One possibility is that tissues with lower CXCR6 expression on ILC2 contain a greater proportion of mature ILC2s, however this hypothesis requires further testing.

Figure 3.7: ILC2 CCR6, CCR8 and CCR9 staining in different lymphoid and non-lymphoid tissues

Cells were isolated from the ILN, MLN, gonadal fat, mesenteries, lung and SILP of adult male C57BL/6J mice as described in Materials and Methods. The expression of various chemokine receptors on the surface of ILC2s was then assessed by flow cytometry, as demonstrated previously. Data for each group was obtained from two technical repeats.

A) FACS plots showing representative ILC2 expression of CCR6, CCR8 and CCR9 in indicated tissues (pre-gated on live/dead^{-}CD45.2^{+}IL-7Rα^{+}Lin^{-} cells). Numbers indicate percentage of events in each gate.

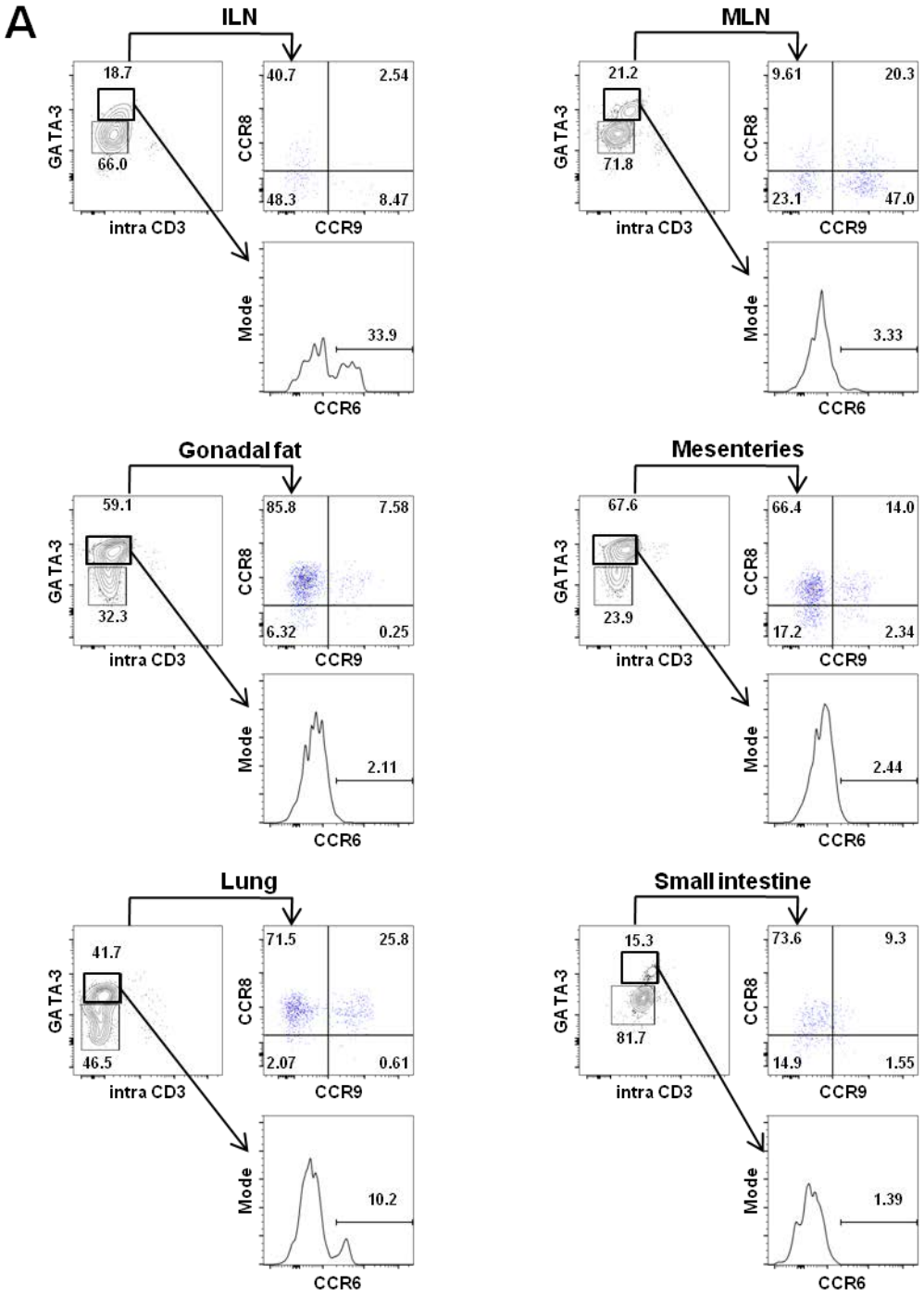
A
ILN
18.7
66.0
GATA-3
intra CD3
40.7
2.54
48.3
8.47
CCR8
CCR9
Mode
33.9
CCR6
MLN
21.2
71.8
9.61
20.3
23.1
47.0
3.33
Gonadal fat
59.1
32.3
85.8
7.58
6.32
0.25
2.11
Mesenteries
67.6
23.9
66.4
14.0
17.2
2.34
2.44
Lung
41.7
46.5
71.5
25.8
2.07
0.61
10.2
Small intestine
15.3
81.7
73.6
9.3
14.9
1.55
1.39

Figure 3.8: ILC2 CCR6, CCR8 and CCR9 expression in different lymphoid and non-lymphoid tissues

Cells were isolated from the ILN, MLN, gonadal fat, mesenteries, lung and SILP of adult male C57BL/6J mice as described in Materials and Methods. The expression of various chemokine receptors on the surface of ILC2s was then assessed by flow cytometry, as demonstrated previously. Data for each group was obtained from two technical repeats.

Each data point (n=5, 5, 5, 5, 3, 6 for gonadal fat, mesenteries, ILN, MLN, lung and SILP respectively) represents an individual sample with a line indicating the median value. Functionally similar tissues grouped and separated with a dotted line. Statistical significance was determined using a Kruskal-Wallis test followed by a Dunn's post-hoc test, *p<0.05, **p<0.01, ***p<0.001 and ****p<0.0001.

A) Graph showing percentage of $CCR6^+$ ILC2 in indicated tissues (gated on $CD45.2^+live/dead^-IL\text{-}7R\alpha^+Lin^-intraCD3^-GATA\text{-}3^+CCR6^+$ cells).

B) Graph showing expression (median fluorescence) of CCR6 on the surface of ILC2s in indicated tissues (gated on $CD45.2^+live/dead^-IL\text{-}7R\alpha$+Lin-$intraCD3^-GATA\text{-}3^+CCR6^+$ cells).

C) Graph showing percentage of $CCR8^+CCR9^-$ ILC2 in indicated tissues (gated on $CD45.2^+live/dead^-IL\text{-}7R\alpha^+Lin^-intraCD3^-GATA\text{-}3^+CCR8^+CCR9^-$ cells).

D) Graph showing percentage of $CCR8^-CCR9^+$ ILC2 in indicated tissues (gated on $CD45.2^+live/dead^-IL\text{-}7R\alpha^+Lin^-intraCD3^-GATA\text{-}3^+CCR8^-CCR9^+$ cells).

E) Graph showing percentage of $CCR8^+CCR9^+$ ILC2 in indicated tissues (gated on $CD45.2^+live/dead^-IL\text{-}7R\alpha^+Lin^-intraCD3^-GATA\text{-}3^+CCR8^+CCR9^+$ cells).

F) Graph showing expression (median fluorescence) of CCR8 on the surface of ILC2s in indicated tissues (gated on $CD45.2^+live/dead^-IL\text{-}7R\alpha^+Lin^-intraCD3^-GATA\text{-}3^+CCR8^+CCR9^{+/-}$ cells).

G) Graph showing expression (median fluorescence) of CCR9 on the surface of ILC2s in indicated tissues (gated on $CD45.2^+live/dead^-IL\text{-}7R\alpha^+Lin^-intraCD3^-GATA\text{-}3^+CCR8^{+/-}CCR9^+$ cells).

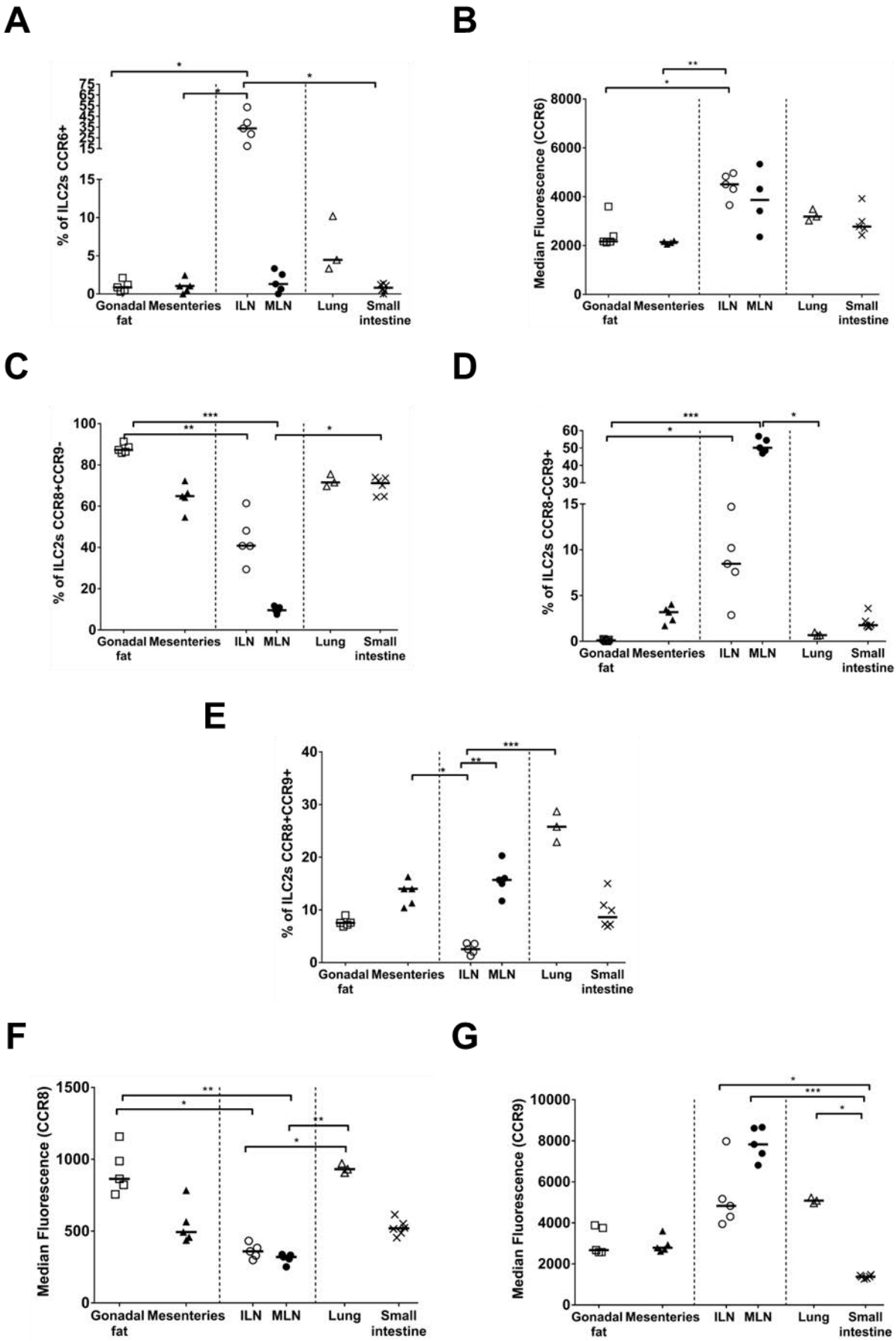
A
% of ILC2s CCR6+
Gonadal fat
Mesenteries
ILN
MLN
Lung
Small intestine
B
Median Fluorescence (CCR6)
C
% of ILC2s CCR8+CCR9-
D
% of ILC2s CCR8-CCR9+
E
% of ILC2s CCR8+CCR9+
F
Median Fluorescence (CCR8)
G
Median Fluorescence (CCR9)

Figure 3.9: ILC2 CXCR6, CCRL2 and CCR4 staining in different lymphoid and non-lymphoid tissues

Cells were isolated from the ILN, MLN, gonadal fat, mesenteries, lung and SILP of adult male C57BL/6J mice as described in Materials and Methods. The expression of various chemokine receptors on the surface of ILC2s was then assessed by flow cytometry, as demonstrated previously. Data for each group was obtained from two technical repeats.

A) FACS plots showing representative ILC2 expression of CXCR6, CCRL2 and CCR4 in indicated tissues (pre-gated on live/dead^{-}CD45.2^{+}IL-7Rα^{+}Lin^{-} cells). Numbers indicate percentage of events in each gate.

A

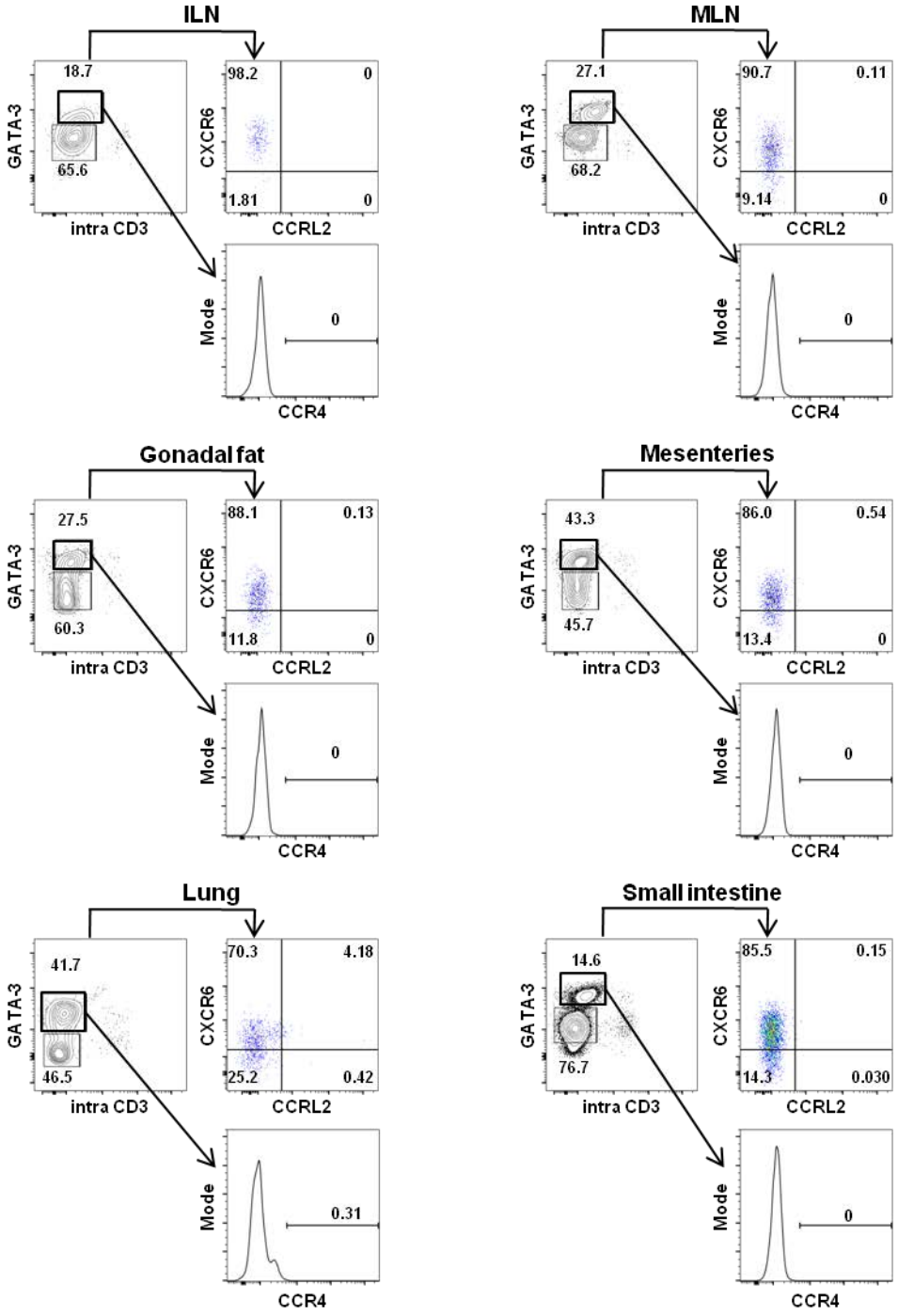
ILN
18.7
65.6
GATA-3
intra CD3
98.2
0
1.81
0
CXCR6
CCRL2
Mode
0
CCR4
MLN
27.1
68.2
GATA-3
intra CD3
90.7
0.11
9.14
0
CXCR6
CCRL2
Mode
0
CCR4
Gonadal fat
27.5
60.3
GATA-3
intra CD3
88.1
0.13
11.8
0
CXCR6
CCRL2
Mode
0
CCR4
Mesenteries
43.3
45.7
GATA-3
intra CD3
86.0
0.54
13.4
0
CXCR6
CCRL2
Mode
0
CCR4
Lung
41.7
46.5
GATA-3
intra CD3
70.3
4.18
25.2
0.42
CXCR6
CCRL2
Mode
0.31
CCR4
Small intestine
14.6
76.7
GATA-3
intra CD3
85.5
0.15
14.3
0.030
CXCR6
CCRL2
Mode
0
CCR4

Figure 3.10: ILC2 CXCR6 expression in different lymphoid and non-lymphoid tissues

Cells were isolated from the ILN, MLN, gonadal fat, mesenteries, lung and SILP of adult male C57BL/6J mice as described in Materials and Methods. The expression of various chemokine receptors on the surface of ILC2s was then assessed by flow cytometry, as demonstrated previously. Data for each group was obtained from two technical repeats.

Each data point (n=6, 6, 6, 6, 3, 6 for gonadal fat, mesenteries, ILN, MLN, lung and SILP respectively) represents an individual sample with a line indicating the median value. Functionally similar tissues are grouped and separated with a dotted line. Statistical significance was determined using a Kruskal-Wallis test followed by a Dunn's post-hoc test, *p<0.05, **p<0.01, ***p<0.001 and ****p<0.0001.

A) Graph showing percentage of $CXCR6^+$ ILC2 in indicated tissues (gated on $CD45.2^+live/dead^-IL\text{-}7R\alpha^+Lin^-intraCD3^-GATA\text{-}3^+CXCR6^+$ cells).

B) Graph showing expression (median fluorescence) of CXCR6 on the surface of ILC2s in indicated tissues (gated on $CD45.2^+live/dead^-IL\text{-}7R\alpha^+Lin^-intraCD3^-GATA\text{-}3^+CXCR6^+$ cells).

C) Table summarising percentage of ILC2 expressing the indicated markers in a variety of tissues. Numbers in table indicates median value.

A

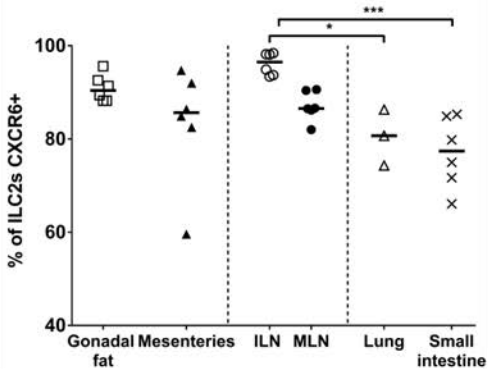

B

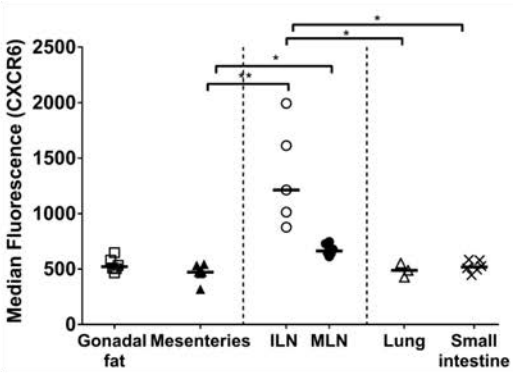

C

	CCR6 (%)	CCR8 (%)	CCR9 (%)	CXCR6 (%)
Gonadal fat	0.9	**total:** 95.7	**total:** 7.7	90.4
		CCR8+CCR9-: 87.3		
		CCR8-CCR9+: 0.1		
		CCR8+CCR9+: 7.5		
Mesenteries	1.0	**total:** 77.3	**total:** 16.4	85.7
		CCR8+CCR9-: 64.9		
		CCR8-CCR9+: 3.2		
		CCR8+CCR9+: 14.0		
ILN	33.9	**total:** 45.8	**total:** 11.0	96.5
		CCR8+CCR9-: 40.8		
		CCR8-CCR9+: 8.5		
		CCR8+CCR9+: 2.5		
MLN	1.3	**total:** 25.6	**total:** 66.2	86.6
		CCR8+CCR9-: 9.6		
		CCR8-CCR9+: 50.2		
		CCR8+CCR9+: 15.7		
Lung	4.5	**total:** 98.4	**total:** 26.4	80.7
		CCR8+CCR9-: 71.5		
		CCR8-CCR9+: 0.7		
		CCR8+CCR9+: 25.8		
Small intestine	0.8	**total:** 80.8	**total:** 10.5	77.4
		CCR8+CCR9-: 71.2		
		CCR8-CCR9+: 1.8		
		CCR8+CCR9+: 8.6		

3.3.3. ILC2 cytokine production in different tissues following ex vivo stimulation

Previous results indicated a higher expression of ST2 by AT ILC2s when compared to MLN ILC2s. Strikingly, IL-33, the ligand for ST2, is more potent at stimulating ILC2 production of IL-5 and IL-13 than other stimuli including IL-25 and TSLP (Doherty *et al.*, 2013, Molofsky *et al.*, 2015b, Moro *et al.*, 2016). Thus, it might appear that IL-33 is a key driver of ILC2 cytokine production. For this reason, it was hypothesised that ILC2 cytokine production may correlate with ST2 expression, and therefore AT-derived ILC2s may have a higher cytokine production compared to MLN ILC2s, due to their higher expression of ST2. To test this hypothesis, ILC2 cytokine production was assessed in single cell suspensions from ATs and MLN of C57BL/6J males by flow cytometry following stimulation of whole single cell suspensions with PMA and Ionomycin (or without stimulation-Figure 3.11, Figure 3.12).

IL-5, but not IL-13, expression was seen in unstimulated ILC2s isolated from all tissues (Figure 3.11A). Moreover, the percentage of ILC2s expressing IL-5 appeared to be markedly higher in ATs than MLN (Figure 3.11A, C). There were no differences in the MFI of ILC2 IL-5 or IL-13 between tissues (Figure 3.11B, D-E). Following stimulation, the majority of ILC2s co-expressed both IL-5 and IL-13 in all tissues examined (Figure 3.12A, D). Despite a markedly higher proportion of IL-5^{+}IL-13^{+} ILC2s in both ATs following stimulation these differences were not statistically significant when compared with MLN ILC2s (Figure 3.12A, D). The total expression of IL-5 by ILC2 was significantly increased in MLN IC2s following stimulation, as was the MFI of IL-13 in gonadal fat and mesenteries following stimulation (Figure 3.12B-C, E-F).

Figure 3.11: Cytokine production by unstimulated WT ILC2s isolated from different tissues

Cells were isolated from the MLN, gonadal fat and mesenteries of adult male C57BL/6J mice as described in Materials and Methods. The *ex vivo* ILC2 cytokine production was determined by flow cytometry following incubation with Brefeldin A alone (media control, See Materials and Methods for details). Data for each group was obtained from three technical repeats.

Each data point (n=9, 9, 6 for gonadal fat, mesenteries, and MLN respectively) represents an individual sample with a line indicating the median value. Statistical significance was determined using a Kruskal-Wallis test with a Dunn's post-hoc test, *p<0.05, **p<0.01, ***p<0.001 and ****p<0.0001.

A) FACS plots showing representative cytokine production by unstimulated cells (media control) isolated from MLN (left), gonadal fat (middle) and mesenteries (right). Top shows ILC2s (pre-gated on CD45.2$^+$live/dead$^-$IL-7Rα$^+$Lin$^-$intraCD3$^-$ GATA-3$^+$ cells), whilst bottom shows control cytokine staining (pre-gated on CD45.2$^+$live/dead$^-$IL-7Rα$^-$Lin$^+$intraCD3$^-$ cells).

B) Histograms showing representative total IL-5 (left) or IL-13(right) staining of ILC2s from MLN (blue), gonadal fat (red) and mesenteries (green).Vertical dotted black line indicates positive staining. Numbers in FACS plots indicate percentage of events in each gate whilst numbers in histograms indicate median fluorescence intensity.

C) Graph showing percentage of ILC2s without stimulation expressing IL-5 only in indicated tissues (media control, gated on CD45.2$^+$live/dead$^-$IL-7Rα$^+$Lin$^-$ intraCD3$^-$GATA-3$^+$IL-5$^+$IL-13$^-$ cells).

D) Graph showing total ILC2s expression of IL-5 (median fluorescence) in indicated tissues without stimulation (media control, pre-gated on CD45.2$^+$live/dead$^-$IL-7Rα$^+$Lin$^-$intraCD3$^-$GATA-3$^+$IL-5$^+$IL-13$^{+/-}$ cells).

E) Graph showing total ILC2s expression of IL-13 (median fluorescence) in indicated tissues without stimulation (media control, pre-gated on CD45.2$^+$live/dead$^-$IL-7Rα$^+$Lin$^-$intraCD3$^-$GATA-3$^+$IL-5$^{+/-}$IL-13$^+$ cells).

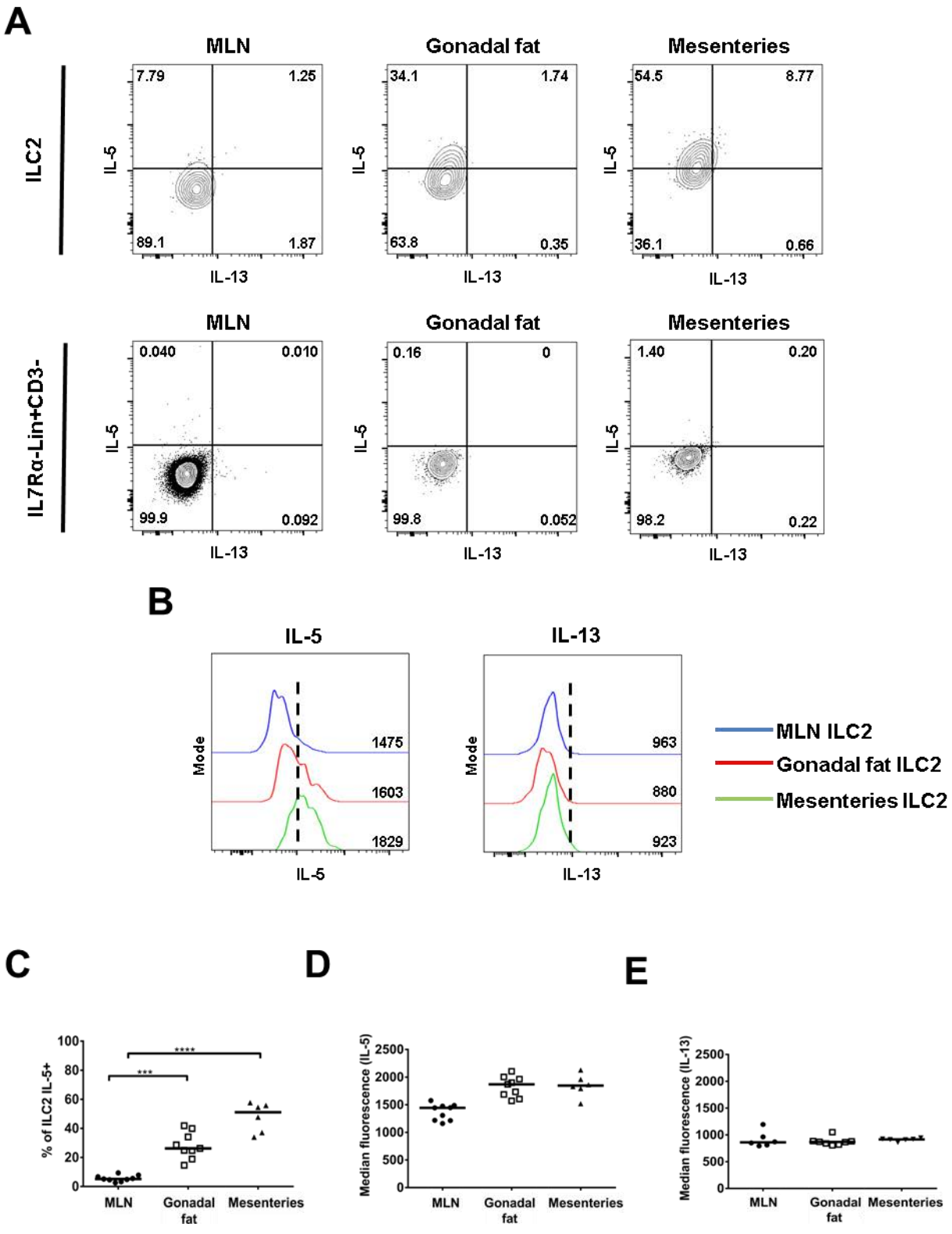
A
MLN
Gonadal fat
Mesenteries
ILC2
IL7Rα-Lin+CD3-
IL-5
IL-13
7.79
1.25
89.1
1.87
34.1
1.74
63.8
0.35
54.5
8.77
36.1
0.66
0.040
0.010
99.9
0.092
0.16
0
99.8
0.052
1.40
0.20
98.2
0.22
B
IL-5
IL-13
Mode
1475
1603
1829
963
880
923
MLN ILC2
Gonadal fat ILC2
Mesenteries ILC2
C
D
E
% of ILC2 IL-5+
Median fluorescence (IL-5)
Median fluorescence (IL-13)
MLN
Gonadal fat
Mesenteries

Figure 3.12: Cytokine production by ILC2s isolated from different tissues following stimulation.

Cells were isolated from the MLN, gonadal fat and mesenteries of adult male C57BL/6J mice as described in Materials and Methods. The *ex vivo* ILC2 cytokine production was determined by flow cytometry following stimulation with PMA and Ionomycin and compared with cells incubated with Brefeldin A alone (See Materials and Methods for details). Data for each group was obtained from three technical repeats.

Each data point (n=9, 9, 9, 9, 6, 7 for gonadal fat control, gonadal fat stimulated, mesentery control, mesentery stimulated, MLN control and MLN stimulated respectively) represents an individual sample with a line indicating the median value. Statistical significance was determined using a Kruskal-Wallis test with a Dunn's post-hoc test, *p<0.05, **p<0.01, ***p<0.001 and ****p<0.0001.

A) FACS plots showing representative cytokine production in MLN (left), gonadal fat (middle) and mesenteries (right) from unstimulated ILC2 (top—see also Figure 3.11A— CD45.2$^+$live/dead$^-$IL-7Rα$^+$Lin$^-$intraCD3$^-$GATA-3$^+$ cells), stimulated ILC2 (middle) and control (bottom, CD45.2$^+$live/dead$^-$IL-7Rα$^-$ Lin$^+$intraCD3$^-$ cells) conditions.

B) Histograms showing representative total IL-5 staining of ILC2s from MLN (blue), gonadal fat (red) and mesenteries (green) in both unstimulated and stimulated conditions, as indicated. Vertical dotted black line indicates positive staining. Numbers in FACS plots indicate percentage of events in each gate whilst numbers in histograms indicate median fluorescence intensity.

C) Histograms showing representative total IL-13 staining of ILC2s from MLN (blue), gonadal fat (red) and mesenteries (green) in both unstimulated and stimulated conditions, as indicated. Vertical dotted black line indicates positive staining. Numbers in FACS plots indicate percentage of events in each gate whilst numbers in histograms indicate median fluorescence intensity.

D) Graph showing percentage of ILC2s expressing both IL-5 and IL-13 in indicated tissues without stimulation (media control, grey circles) and with PMA/Ionomycin stimulation (open circles, gated on CD45.2$^+$live/dead$^-$ IL-7Rα$^+$Lin$^-$intraCD3$^-$GATA-3$^+$IL-5$^+$IL-13$^+$ cells).

E) Graph showing ILC2s expression (median fluorescence) of IL-5 in indicated tissues without stimulation (media control, grey circles) and with PMA/Ionomycin stimulation (open circles, pre-gated on CD45.2$^+$live/dead$^-$ IL-7Rα$^+$Lin$^-$intraCD3$^-$GATA-3$^+$IL-5$^+$IL-13$^{+/-}$ cells).

F) Graph showing ILC2s expression (median fluorescence) of IL-13 in indicated tissues without stimulation (media control, grey circles) and with PMA/Ionomycin stimulation (open circles, pre-gated on CD45.2$^+$live/dead$^-$ IL-7Rα$^+$Lin$^-$intraCD3$^-$GATA-3$^+$IL-5$^{+/-}$IL-13$^+$ cells).

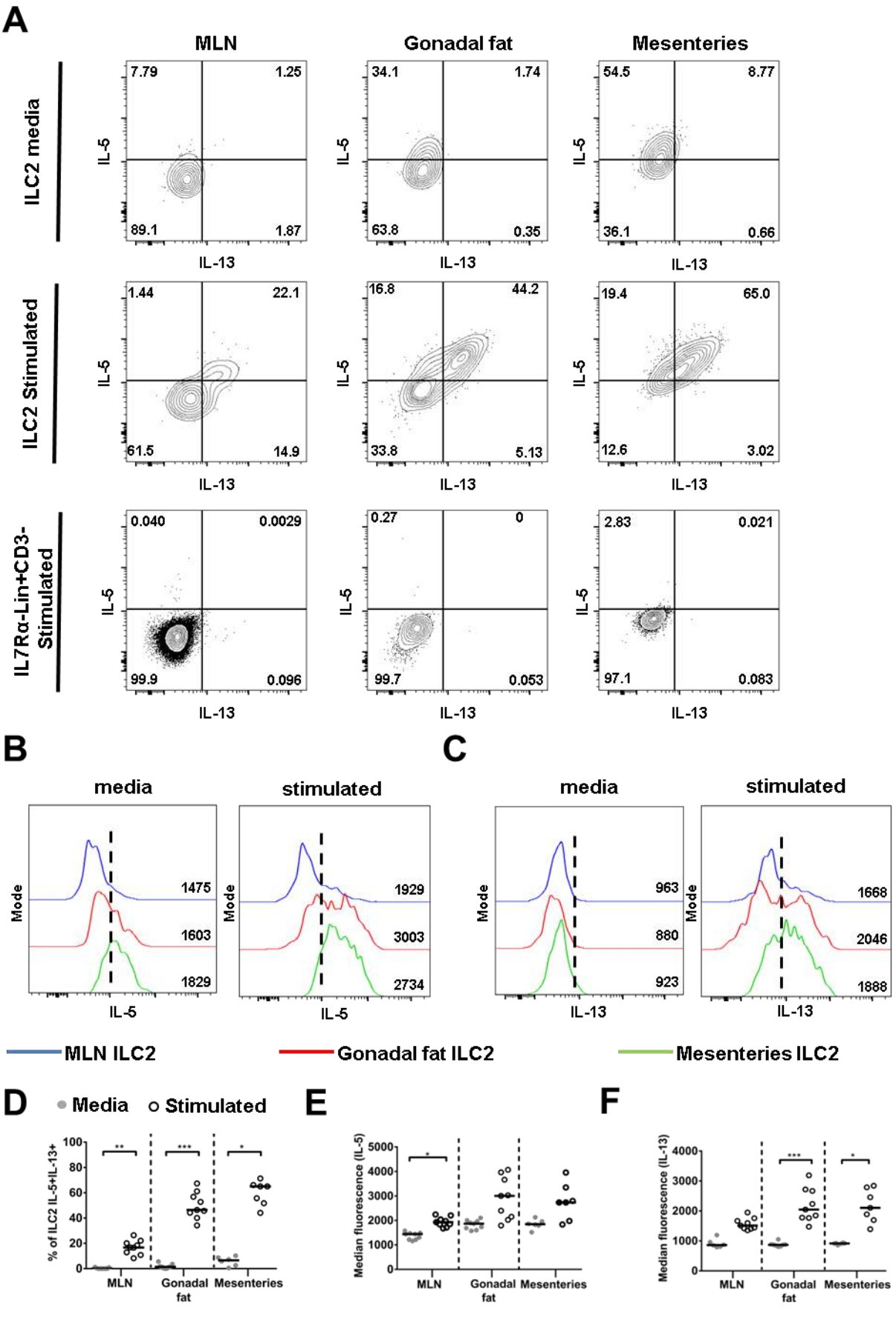
A
MLN
Gonadal fat
Mesenteries
ILC2 media
ILC2 Stimulated
IL7Rα-Lin+CD3-Stimulated
IL-5
IL-13
7.79
1.25
89.1
1.87
34.1
1.74
63.8
0.35
54.5
8.77
36.1
0.66
1.44
22.1
61.5
14.9
16.8
44.2
33.8
5.13
19.4
65.0
12.6
3.02
0.040
0.0029
99.9
0.096
0.27
0
99.7
0.053
2.83
0.021
97.1
0.083
B
media
stimulated
Mode
1475
1603
1829
1929
3003
2734
C
963
880
923
1668
2046
1888
MLN ILC2
Gonadal fat ILC2
Mesenteries ILC2
D
Media
Stimulated
% of ILC2 IL-5+IL-13+
MLN
Gonadal fat
Mesenteries
E
Median fluorescence (IL-5)
F
Median fluorescence (IL-13)

3.4. SUMMARY

ATs are frequently associated with LN, which are important sites for initiation of immune responses (Pond, 2002). Furthermore, there is growing evidence of the presence of ectopic lymphoid tissues within fat, known as FALC (see chapter 4.1 for more detail), which also act as sites for mounting local immune responses (Moro *et al.*, 2010, Koyasu and Moro, 2013, Benezech *et al.*, 2015, Jackson-Jones *et al.*, 2016). Thus, in addition to their important role in lipid storage and metabolic homeostasis, ATs also appear to be immunologically important.

Expertise in the immune cell composition of ATs was initially lacking in the host institution in which this research was conducted. Thus, an initial examination of AT immune cell composition under steady state conditions was necessary.

Animals are important tools in modelling human immune responses, with the two most common mouse genetic background strains used being C57BL/6J and BALB/c. However, these two strains can exhibit different immune responses to the same stimuli due to differing immune cell composition; previous studies have indicated BALB/c mice to be polarised towards more effective type-2 immune responses, with higher numbers of Tregs and iNKT cells reported and preferential production of Immunoglobulin G1 (IgG1) (Chen *et al.*, 2005, Schulte *et al.*, 2008, De Vooght *et al.*, 2010). As a result, BALB/c animals clear parasitic infections (which requires the involvement of type-2 immune responses) faster than their C57BL/6J counterparts (Wahid and Behnke, 1993, Camberis *et al.*, 2003, Reynolds *et al.*, 2012). In contrast C57BL/6J animals are polarised to type 1 immune responses, with higher $CD8^+$ T cells and IgG2a production (Schulte *et al.*, 2008). These animals have a lower tumour incidence than BALB/c animals (Chen *et al.*, 2005). As such, it is important to

use mice of appropriate backgrounds to the response studied. This is illustrated in a study by De Vooght *et al.,* who demonstrated that mice of Th2 polarised genetic background strains showed asthma phenotypes which were more representative of those seen in humans, making these animals better models to study immune responses involved in asthma (De Vooght *et al.*, 2010). Thus, analysis of the immune cell composition of ATs was performed in C57BL/6J and BALB/c strains in order to determine whether there is a difference in AT immune cell composition between these strains. Herein, the composition of gonadal fat, mesenteries and MLN isolated from C57BL/6J and BALB/c males are directly compared.

Higher number of $CD4^+$ and $CD4^-$ iNKT cells were found in the mesenteries of BALB/c animals, compared with C57BL/6J counterparts. This finding is in line with results from others, who found higher numbers of iNKTs in lymphoid tissues of BALB/c mice compared to C57BL/6J animals. However, no differences were observed in the iNKT numbers of gonadal fat isolated from both mouse strains. It is surprising that differences in iNKT cell numbers were only seen between the mesenteries of the two mouse strains, and not the gonadal fat of the same animals. Perhaps this observation highlights differences between the two strains examined that are tissue specific. One possibility is that this tissue specific difference could be due to a differing number of FALC, which are enriched for iNKTs, in gonadal fat and mesenteries (Benezech *et al.*, 2015).

A greater number of $CD4^+$ T cells were identified in gonadal fat and mesenteries from C57BL/6J animals. In contrast to previously published results, gonadal fat from C57BL/6J animals had a larger number of Tregs than in BALB/c animals. However, there were no differences in Treg number between the mesenteries of the two strains

examined. In addition there were no differences in total ILC number or ILC2 number isolated from gonadal fat and mesenteries of the two strains of mice. This suggests that ILC numbers and proportions are unaffected by the genetic differences between C57BL/6J and BALB/c animals. When the mass of gonadal fat and mesenteries isolated from the two strains was compared, there was no difference in gonadal fat mass between C57BL/6J and BALB/c animals, but the mass of mesenteries isolated from C57BL/6J animals was higher than in BALB/c animals. One possible explanation of this is that C57BL/6J mice are more susceptible to diet-induced obesity and therefore may show effects of age-associated adiposity earlier than BALB/c animals (Jovicic *et al.*, 2015).

Finally, when the phenotype of ILC2s was compared between the two strains of animals, ILC2s from gonadal fat and mesenteries of BALB/c animals had a higher expression of ICOS and ST2 and also a higher percentage of $ICOS^+$ ILC2s as compared to C57BL/6J animals. Both ICOS and ST2 have been reported to be important for proliferation and/or survival of ILC2s (Moro *et al.*, 2010, Kamachi *et al.*, 2015, Maazi *et al.*, 2015, Molofsky *et al.*, 2015b, Paclik *et al.*, 2015). This would fit with the consensus that BALB/c animals are type-2 polarised.

As with genetic strains of mice, the gender of mice can also have an impact on immune cell composition. Research by Markle and Fish demonstrated that androgen receptor signalling, which is increased in male animals, has an immunosuppressive effect (Markle and Fish, 2014). Furthermore, adiposity varies between male and female mice and humans (Demerath *et al.*, 2007, Geer and Shen, 2009, Arnold *et al.*, 2016, Bruder-Nascimento *et al.*, 2017). Disruption of metabolic homeostasis, which leads to increased adiposity, can in turn affect the immune cell composition of ATs in

particular. The immune cell composition of ATs and MLN was compared between male and female mice in order to determine any differences between the two genders.

Gonadal fat, but not mesenteries, from females had higher numbers of $CD4^+$ T cells, Tregs and ILC2s compared to male mice, indicating a more anti-inflammatory phenotype of gonadal fat from females. It is unclear why these differences were only noted in gonadal fat and not mesenteries, but it could be due to differing environment-specific signals the tissues are exposed to. ILC2s in gonadal fat and mesenteries from females contained a higher percentage of $ICOS^+$ ILC2 and a higher expression of ICOS by ILC2s than seen in ATs from male animals. ILC2s from both ATs of female mice also had a lower percentage of $KLRG1^+$ ILC2s. The same was true of ILC2 expression of KLRG1 when ILC2s from male tissues were compared with female tissues. Taken together this data is consistent with research by Laffont *et al.*, who showed that bone marrow ILC2 precursors express the androgen receptor, and in male mice androgen receptor signalling leads to decreased ICOS expression and increased KLRG1 expression on the surface of mature lung ILC2s (Laffont *et al.*, 2017). These phenotypic changes correlated with a lower number of mature ILC2s in lung and VAT, due to reduced proliferation. Work by Paclik *et al.* also supported the role of ICOS in controlling ILC2 proliferation (Paclik *et al.*, 2015). Finally, Maazi *et al.* also demonstrated that ICOS expression correlated with the number of ILC2s, but concluded this was due to survival, rather than proliferation (Maazi *et al.*, 2015). This difference, in conclusion, could be due to different models used between these studies (Maazi *et al.*, 2015, Paclik *et al.*, 2015). Results also indicated a higher expression of ST2 on the surface of ILC2s from ATs and MLN in male animals, a

feature also identified in the study by Laffont *et al.* (Laffont *et al.*, 2017). This is counter-intuitive as male ILC2s were found to proliferate less in the study by Laffont *et al.,* whilst other studies have demonstrated ST2 expression positively correlates with the activation and cytokine production by these cells, and IL-33 treatment *in vivo* induces marked ILC2 proliferation (Barlow *et al.*, 2013, Molofsky *et al.*, 2015b, Halim *et al.*, 2016, Moro *et al.*, 2016, Laffont *et al.*, 2017). One possibility is that ST2 signalling stimulates pathways that lead to gene expression of cytokines but does not stimulate cell proliferation programmes. Contrary to what others have published in both mice and humans (Demerath *et al.*, 2007, Arnold *et al.*, 2016), the results shown here indicated that the mass of both gonadal fat and mesenteries isolated from female mice was higher than the ATs isolated from males. This is surprising as the gonadal fat had higher number of anti-inflammatory cells including Tregs and ILC2s, which are thought to counteract the onset of adiposity. Furthermore, female mice are thought to be more resistant to diet induced obesity (Jovicic *et al.*, 2015, Bruder-Nascimento *et al.*, 2017). Differences in animal husbandry procedures, such as the number of animals in each cage and access to food, among other factors, could be one possible reason for the discrepancy seen between the results shown here and the results of animal studies by others. Further investigation is required to explain these different findings. In summary, there appeared to be some differences in immune cell composition of ATs between C57BL/6J and BALB/c mice, and also between male and female mice.

Over recent years a number of studies have focused on AT resident ILC2s, however direct comparisons between different ATs and SLT ILC2s is lacking. The phenotype of ILC2s from the gonadal fat, mesenteries and MLN of C57BL/6J males was

compared. The percentage of $ICOS^+$ ILC2s and the expression of ICOS were higher in MLN than in ATs, whilst ATs had a higher percentage of $KLRG1^+$ and a higher expression of ST2 than MLN ILC2s. The role of KLRG1 in ILC2 biology is controversial; as discussed previously, Laffont *et al*. found higher expression of KLRG1 on ILC2s that had a lower proliferative capacity (Laffont *et al.*, 2017). If this is the case, the lower expression of ICOS and higher expression KLRG1 of AT ILC2s should result in a decreased proliferative capacity of adipose ILC2s compared to MLN ILC2s. However, another study suggests that $KLRG1^{hi}$ cells represent highly activated, inflammatory ILC2s (Huang *et al.*, 2015). A different possibility is that ICOS expression is reduced in ATs as AT-derived ILC2s are reported to have higher expression of ICOSL than lymphoid tissue derived ILC2s, and also that ICOS and ICOSL expression negatively correlate with each other.

Many studies have reported ILC2s from ATs being 'highly activated' due to their ability to produce large amount of cytokine, especially in response to IL-33 (Molofsky *et al.*, 2013, Molofsky *et al.*, 2015b, Moro *et al.*, 2015). This is consistent with the increased expression of ST2 on the surface of ILC2s from ATs. Moreover, ST2 deficient animals are reported to have fewer ILC2s in the VAT than WT controls (Molofsky *et al.*, 2015b). Overall the data indicates that ILC2 phenotype differs between MLN and ATs. There is a range of evidence suggesting ILC subsets differ in number and proportion between tissues, such as MLN contain more ILCs overall and a higher proportion of group 3 ILCs than peripheral LN, such as ILN (Mackley *et al.*, 2015). It therefore makes sense that a difference in ILC2 phenotype exists between ATs and MLN. The ILC2 phenotype of other non-lymphoid tissues, such as skin, lung and SI, should be tested to confirm that this difference in ILC2 phenotype is not just a

feature of comparing lymphoid tissues ILC2s with non-lymphoid tissue ILC2s. In spite of the above, it is important to note that, as discussed in the Materials and Methods section, the MFI values reported by flow cytometry are only semi-quantitative, as differences in protein internalisation or shedding can produce different MFI values where no differences in protein translation exist. As such, other techniques such as qPCR and Western Blotting are required to fully verify whether the trends in MFI discussed above correlate with genuine changes in gene and protein expression. Nevertheless, MFI is still valid as a comparative measure for protein expression when comparing tissues within the same experiment.

Both the data presented here in Figure 3.7, and elsewhere (Moro *et al.*, 2010, Molofsky *et al.*, 2013, Molofsky *et al.*, 2015b), has shown that ILC2s are enriched in ATs, as compared to other lymphoid and non-lymphoid tissues. Mechanisms of how ILCs are seeded within tissues and whether they can migrate to sites of inflammation and infection remain controversial. One known mechanism by which cells migrate between tissues is through chemotaxis by expression of chemokines and their receptors. Chemokine receptor expression of ILC2s was investigated in a variety of lymphoid (ILN and MLN) and non-lymphoid (gonadal fat, mesenteries, lung and SILP) tissues to determine whether differences in chemokine receptor expression exist between tissues. CCR4 and CCRL2 expression by ILC2s was low/absent in all tissues examined. A lack of CCR4 expression by ILC2s is surprising as this chemokine receptor is expressed by Th2 cells, which ILC2s are similar to in many respects, and is a GATA-3 target gene (Bonecchi *et al.*, 1998, Islam *et al.*, 2011, Griffith *et al.*, 2014). The lack of convincing CCRL2 staining was also unexpected, as expression of this chemokine receptor has been reported in many different cell types

(Yoshimura and Oppenheim, 2011, De Henau *et al.*, 2016). CCR6 expression was also minimal in the majority of tissues, with the exception of ILN. This is expected, as CCR6 and its ligand CCL20 is more associated with Th17 and LTi-like ILCs (Eberl *et al.*, 2004, Artis and Spits, 2015, Diefenbach, 2015, Eberl *et al.*, 2015, Mackley *et al.*, 2015). It is unclear why ILC2 CCR6 staining was present in ILN; as ILC plasticity has been described for ILC1 and ILC3 in SI, this CCR6 ILC2 population could represent a transitioning population (Vonarbourg *et al.*, 2010, Klose *et al.*, 2014, Bernink *et al.*, 2015, Serafini *et al.*, 2015). However, this is unlikely, as ILC2 plasticity has only been reported under inflammatory conditions (Bal *et al.*, 2016, Lim *et al.*, 2016, Ohne *et al.*, 2016, Silver *et al.*, 2016).

ILC2 CCR8 expression was expected, as phenotypically similar Th2 cells also express this chemokine receptor. Whilst the majority of ILC2 from non-lymphoid tissues expressed CCR8, either alone or in combination with CCR9, the percentage of ILC2s expressing CCR8 in lymphoid tissues was markedly lower. Thus, CCR8 expression appeared to be enriched in non-lymphoid tissue. CCL1 and CCL8, the ligands for CCR8, are highly expressed in the skin and have previously been reported to act as chemoattractants for Th2 cells, especially in atopic dermatitis (Miller *et al.*, 1989, Annunziato *et al.*, 2002, Colantonio *et al.*, 2002, Gombert *et al.*, 2005, Islam *et al.*, 2011). As ILC2s also play a key role in exacerbation of atopic dermatitis, there may be a link between CCL1/CCL8 and CCR8 expression by ILC2s in other non-lymphoid tissues (Salimi *et al.*, 2013, Saunders *et al.*, 2016). Further analysis of tissue-specific chemokine expression, especially in skin, is required.

In contrast, a high proportion of ILC2s from MLN express CCR9, compared to most non-lymphoid tissues. Previously published data suggests CCR9 is important for

migration of both ILC2 precursors and mature ILC2s and T cells to the SI (Mora *et al.*, 2003, Papadakis *et al.*, 2003, Hoyler *et al.*, 2012, Kim *et al.*, 2015a). Whilst Kim *et al.* also indicated that the majority of mature ILC2s in MLN, the draining LN of the SI, express CCR9, the authors also report a large proportion of ILC2s in the SI also expressing CCR9, which the data presented in this thesis does not show (Kim *et al.*, 2015a). The authors do not show whether CCR9 is expressed in mature ILC2s in other tissues. A possible reason for this discrepancy could be in methods used to isolate cells from the SILP, as the authors do not detail this process.

The majority of ILC2s in all tissues examined expressed the chemokine receptor CXCR6. ILC precursors have been shown to express CXCR6, leading authors to conclude that CXCR6 and its ligand CXCL16 are important for migration of ILC precursors to peripheral tissues (Satoh-Takayama *et al.*, 2014). Despite this, CXCR6 deficient mice still show normal ILC development (Serafini *et al.*, 2015). Research by Satoh-Takayama *et al.* found depletion of Nkp46^{+} ILC3s, but not CD4^{+} LTi-like cells, in the SI of CXCR6 deficient animals (Satoh-Takayama *et al.*, 2014). This could suggest that CXCR6 expression occurs in ILC precursors after commitment to ILC1/ILC2/Nkp46^{+}ILC3 lineage.

In summary, although the expression of the chemokine receptors examined differed between ILC2s from lymphoid and non-lymphoid tissues, none of these receptors appeared to uniquely identify ILC2s from ATs.

As with the phenotype of ILC2s, cytokine production of ILC2s has been noted in the literature in MLN and ATs, but direct comparisons between different ATs and SLTs have not been made (Molofsky *et al.*, 2013, Califano *et al.*, 2015, Molofsky *et al.*, 2015b). Cells were isolated from MLN, gonadal fat and mesenteries of C57BL/6J

males and ILC2 cytokine production was assessed, with and without *ex vivo* stimulation by flow cytometry. ILC2s from all tissues displayed a basal production of IL-5 without re-stimulation. Furthermore, the percentage of IL-5^+ ILC2s without stimulation was higher in ATs than MLN. As reported by others (Hoyler *et al.*, 2012, Moro *et al.*, 2016), following PMA and Ionomycin stimulation, the majority of ILC2s from all tissues produced both IL-5 and IL-13. Following activation with PMA and Ionomycin there was a higher percentage of IL-5^+IL-13^+ ILC2s in ATs compared to MLN, although due to the sample size this difference was not statistically significant. This result suggests a higher production of IL-5 by AT derived ILC2s, although a quantitative approach, such as an Enzyme-linked Immunosorbent Assay (ELISA) on purified ILC2s, is required to confirm this. The difference seen in cytokine response between ILC2s from ATs and MLN could be due to the higher expression of ST2 by AT derived ILC2s. However, this hypothesis cannot be proven by the data shown here and needs further testing. Although this is supported by data from other groups (Molofsky *et al.*, 2015b), further investigation, such as determining whether this tissue difference is still seen in ST2 deficient animals, is required to confirm this.

In conclusion, these data suggests that, in response to exogenous stimulation, a greater percentage of ILC2s produce cytokine when isolated from ATs compared with MLN derived ILC2s. It is important to determine whether this difference in cytokine production is seen in other non-lymphoid tissues, or is unique to ATs. It is also important to determine if this difference is still seen in response to endogenous signals, such as IL-33.

The data presented in this chapter focuses on the use of flow cytometry for identification of cellular composition and protein expression under various conditions.

Whilst this is an informative technique, other methods, including qPCR and histology, could be considered due to their potential to reveal additional information. For example, whilst qPCR can be used to investigate the gene expression of certain genes, such as those encoding cell surface markers in ILC2s, histology can reveal the localisation of cells, including ILC2s, within tissues and suggest interactions with other cell types. Unfortunately, the use of qPCR was limited by an insufficient cellular yield that precluded the use of cell sorting techniques to isolate a pure cell population and immunofluorescence staining on adipose tissues (histology) was not possible due to difficulty in producing frozen sections of these tissues. However, recent advances in ‘whole mount’ staining and immunofluorescence methods, where the entire tissue is labelled with fluorescently labelled antibodies, provides an avenue for future investigation.

4. CHARACTERISING ADIPOSE TISSUE IMMUNE CELL COMPOSITION IN MODELS OF GENETIC DEFICIENCY

4.1. INTRODUCTION

In chapter 3 the immune cell composition of AT was investigated and compared with MLN. Results indicated a differing immune cell composition between AT and MLN. Additionally, there appeared to be differences in ILC2 expression of KLRG1, ICOS and ST2 between MLN and ATs. This indicates that tissue-specific signals occur resulting in disparate immune cell composition and phenotype between tissues. For this reason, in this chapter the signals that are likely to regulate the immune cell composition of ATs are investigated with the aim of determining factors that may lead to this differing immune cell composition between MLN and ATs.

The signals required for maintenance of mature ILC2s within tissues are well established. ILC2 precursors are generated in the bone marrow. Mature ILC2s possess the ability to respond to a number of cytokine and lipid signals which allow for maintenance and cytokine production within tissues, as discussed below. As with other ILCs, ILC2 express IL-7Rα and IL-2Rγ, and homeostatic IL-7 and IL-2 production within tissues allows for maintenance and proliferation of ILC2s within tissues, as demonstrated by their absence in IL-7 and IL-2Rγ deficient animals (Moro *et al.*, 2010, Vonarbourg and Diefenbach, 2012, Roediger *et al.*, 2013, Roediger *et al.*, 2015). Moreover, during infection or inflammation, epithelial derived cytokines including IL-33, IL-25 and TSLP stimulate further production of cytokines by ILC2s, particularly IL-5 and IL-13 (Fort *et al.*, 2001, Mjosberg *et al.*, 2011, Hoyler *et al.*, 2012, Barlow *et al.*, 2013, Califano *et al.*, 2015, Molofsky *et al.*, 2015b, Pelly *et al.*,

2016, Han *et al.*, 2017). Cytokine production by ILC2s appears to be a key function of these cells as it can promote both immunity and inflammation; for example during helminth infection, whilst IL-13 from ILC2s stimulates goblet cells to produce increased mucus, ILC2-derived IL-5 stimulates eosinophilia (Hashimoto *et al.*, 2009). The net effect of this is increased expulsion of worms. In addition to epithelial cytokines, recent evidence indicates that prostaglandins, in particular PGD_2, can also stimulate cytokine production, especially IL-4, from ILC2s (Barnig *et al.*, 2013). In chapter 3, one prominent phenotypic difference between ILC2s isolated from MLN and ATs was a higher expression of ST2 by ILC2s isolated from the latter tissue.

ST2, also known as IL-33R or IL1RL1, can be expressed in four different forms in mice; soluble (sST2, IL1RL1-a) and transmembrane (ST2L, IL1RL1-b) isoforms, and as splice variants of the soluble (ST2V) and transmembrane (ST2VL) isoforms. ST2L has been shown to be selectively expressed by Th2 and not Th1 polarised cells, Tregs and mast cells (Lohning *et al.*, 1998, Schmitz *et al.*, 2005, Kakkar and Lee, 2008, Molofsky *et al.*, 2015b, Griesenauer and Paczesny, 2017). Furthermore, previous studies demonstrate that upon IL-33 binding, signalling through the Mitogen-Activated Protein Kinase (MAPK) and Jun-amino terminal Kinase (JNK) pathways, and ultimately NF-κB, leads to expression of Th2 associated cytokines IL-5 and IL-13 (Kakkar and Lee, 2008, Griesenauer and Paczesny, 2017). Finally, of note, ST2L but not sST2 contains two GATA-3 binding sites in the promoter region, thus GATA-3 expression in Tregs and Th2 cells enhances ST2 expression (Lohning *et al.*, 1998, Griesenauer and Paczesny, 2017).

In contrast to ST2L, sST2 is expressed by stromal cells, such as fibroblasts, and binding of IL-33 does not result in signalling; therefore ST2 acts as a decoy receptor

sequestering free IL-33 (Lohning *et al.*, 1998, Griesenauer and Paczesny, 2017). Furthermore, sST2 expression is not constitutive and is induced by pro-inflammatory cytokines such as tumour necrosis factor (TNF) (Lohning *et al.*, 1998, Griesenauer and Paczesny, 2017). Surprisingly, in obese mice, whilst type-two polarised cells such as ILC2s and Tregs decrease in number, IL-33 production is increased (Miller *et al.*, 2010). One possible reason for this paradox could be an increase in sST2 production due to pro-inflammatory cytokine production, which is prevalent during obesity, resulting in sequestering of the increased amount of IL-33. However, this possibility has not been explored, thus further investigation is required to confirm this. As highlighted above, IL-33 is a key stimulus for ILC2 cytokine production. In this chapter, the ILC2 cytokine production is investigated in the absence of functional IL-33 to test whether the cytokine production by these cells is altered by loss of this crucial stimulus.

As discussed above, crosstalk between stromal cells and immune cells can be mediated through cytokine production, such as by IL-33 production from stromal cells. Pro-inflammatory signalling can also result in a variety of changes to tissue cellular composition through stromal cell and immune cell crosstalk. One of the most studied of these pro-inflammatory pathways is the TNF pathway. This pathway is of particular importance as TNF release by adipocytes is thought to be one of the key driving factors of obesity-associated metabolic disease (Kang *et al.*, 2016).

The tumour necrosis factor superfamily (TNFSF) consists of a number of proteins, all of which signal through receptors of the tumour necrosis factor receptor superfamily (TNFRSF). TNF, an archetypal pro-inflammatory cytokine, signals through the receptors TNFRSF1 (p55) and TNFRSF2 (p75). Whilst p55 is expressed on most

mammalian cells types, the expression of p75 is more restricted to immune cells and endothelial cells (Brenner *et al.*, 2015). The precise fate of cells undergoing TNFR signalling appears to be context dependent. Factors such as expression level of one or both of the receptors, and activation status of the cells, appear to play a role in determining the fate of the cell (Brenner *et al.*, 2015). Therefore, TNFR signalling can lead to either cell survival or cell death depending on these factors.

TNFRSF signalling is crucial in stromal cell biology. Formation of SLTs, which are key sites for coordinating innate and adaptive immune responses, involve the close interaction between stromal cells and haematopoietic cells (Kim *et al.*, 2000, Yoshida *et al.*, 2002, Mebius, 2003, Cupedo *et al.*, 2004, Blum and Pabst, 2006, White *et al.*, 2007, van de Pavert *et al.*, 2009, Vondenhoff *et al.*, 2009, Benezech *et al.*, 2010, van de Pavert and Mebius, 2010, Benezech *et al.*, 2012, Brendolan and Caamano, 2012). TNFRSF signalling, especially involving proteins of the LTβR pathway, by stromal cells is crucial for formation of these SLTs, as demonstrated by varying degrees of defective LN formation in mice deficient in a variety of LTβR pathway proteins (van de Pavert and Mebius, 2010, Benezech *et al.*, 2012). In further support of the importance of TNFRSF signalling in LN development, both p55/p75 signalling and also LTβR signalling drives multipotent stromal precursor cells toward a lymphoid tissue maturation pathway, instead of an adipogenic pathway (Chae and Kwak, 2003, Cawthorn *et al.*, 2007, Benezech *et al.*, 2012).

In addition to its role in SLT formation, TNFRSF signalling has also been implicated in tertiary lymphoid tissue formation of FALC. These tissues appear to solely rely on p55 and p75 signalling, and not LTβR signalling, for their formation (Benezech *et al.*, 2015). FALC are rich in ILC2s, iNKTs and B cells, and recent studies discovered that

these clusters develop in response to inflammation (Benezech *et al.*, 2015) and infection (Moro *et al.*, 2010, Jackson-Jones *et al.*, 2016). Furthermore, TNF overexpression resulted in an increased number of FALC, whilst mice lacking TNFR1 and TNFR2 had fewer FALC. Taken together these data indicate that FALC formation requires TNF-TNFR signalling (Benezech *et al.*, 2015). Bénézech *et al*. also demonstrate that TNF is produced by F4-80^{+} myeloid cells. Furthermore, in a subsequent paper, the same author demonstrates that these clusters are also present in the mediastinum and pleural cavity, and act as important sites for B1 cell Immunoglobulin A (IgA) production during immune responses (Jackson-Jones *et al.*, 2016). Despite the abundance of B cells in FALC and their ability to produce the cytokine TNF, FALC are found in normal numbers in unchallenged *Rag2*$^{-/-}$ mice, as compared to their WT counterparts (Benezech *et al.*, 2015). Therefore, it appears that FALC play a critical role in the recruitment of B cells and their activation, but B cells appear to be dispensable for FALC formation.

Due to the role of these clusters in mediating adaptive immune responses and the importance of TNF signalling in this process, further work, as outlined in this chapter, was performed to characterise any changes in AT immune cell composition following manipulation of the TNF pathway.

4.2. ILC2 CYTOKINE PRODUCTION IN IL-33 DEFICIENCY

In chapter 3.3.3 it was determined that a greater proportion of ILC2 from ATs (both gonadal fat and mesenteries) produced the cytokines IL-5 and IL-13 following *ex vivo* stimulation with the chemicals PMA and Ionomycin.

In vivo ILC2s receive a variety of signals that can induce cytokine production including IL-33, IL-25, TSLP and LTD_4. Whilst LTD_4 is one of the few stimuli that have been shown to induce ILC2 IL-4 *ex vivo* (Doherty *et al.*, 2013), IL-33 appears to be the most potent factor in inducing IL-5 and IL-13 production by purified ILC2s *ex vivo* (Barlow *et al.*, 2013). With this in mind, one potential factor that could result in the increased percentage of cytokine producing ILC2s in ATs, as seen in Figure 3.12, is the higher expression of the ST2 by ILC2s isolated from ATs, as shown in Figure 3.6. ST2 is the receptor for IL-33, an alarmin produced early in an immune response to a pathogen. This increased ST2 expression could mean that ILC2s isolated from ATs are in a more 'primed' state, with regards to cytokine production, and therefore these cells are more able to produce cytokine when re-stimulated *ex vivo*. To test this hypothesis, the ILC2 cytokine production following *ex vivo* stimulation was compared between IL-$33^{cit/cit}$ tissues and WT tissues (both on the BALB/c background). In IL-$33^{cit/cit}$ animals all cells that transcribe the gene for *IL33* only express the citrine protein, meaning no functional IL-33 protein is produced.

Where ILC2s received no stimulation there was no difference in the percentage of IL-5 expressing ILC2 between WT and IL-$33^{cit/cit}$ animals (Figure 4.1).

As seen in WT ILC2 from C57BL/6J (Figure 3.12), *ex vivo* stimulation of WT BALB/c ILC2s resulted in the majority of ILC2s producing both IL-5 and IL-13 (Figure 4.2). A small but significant reduction in the percentage of IL-5^{+}IL-13^{+} ILC2s was seen in the mesenteries of IL-$33^{cit/cit}$ mice compared to WT mesentery ILC2s following stimulation, but not in any other tissues (Figure 4.2B).

Analysis of IL-5 and IL-13 MFI of unstimulated and stimulated ILC2s is shown in the appendix (Figure 7.10).

Figure 4.1: Cytokine production by unstimulated ILC2s isolated from WT and IL-33$^{cit/cit}$ animals

Cells were isolated from the MLN, gonadal fat and mesenteries of adult male BALB/c and IL-33$^{cit/cit}$ mice (also on BALB/c background) as described in Materials and Methods. The ILC2 cytokine production *ex vivo* was determined by flow cytometry following incubation with Brefeldin A alone (media control, see Materials and Methods for details). Data for each group was obtained from two technical repeats.

Each data point (n=4, 6 for WT and IL-33$^{cit/cit}$ animals respectively) represents an individual sample with a line indicating the median value. Statistical significance was determined using a Mann-Whitney two-tailed T test, *p<0.05, **p<0.01, ***p<0.001 and ****p<0.0001.

A) FACS plots showing representative ILC2 cytokine production by unstimulated cells (media control) isolated from MLN (left), gonadal fat (middle) and mesenteries (right) of WT (top) and IL-33$^{cit/cit}$ (bottom) animals (pre-gated on CD45.2$^+$live/dead$^-$IL-7Rα$^+$Lin$^-$intraCD3$^-$GATA-3$^+$ cells). Numbers in FACS plots indicate percentage of events in each gate.

B) Histograms showing representative total IL-5 (top) or IL-13 (bottom) staining of ILC2s from MLN (blue), gonadal fat (red) and mesenteries (green). Vertical dotted black line indicates positive staining. Numbers in histograms indicate median fluorescence intensity.

C) Graph showing percentage of ILC2s without stimulation expressing IL-5 only in MLN, gonadal fat and mesenteries from WT and IL-33$^{cit/cit}$ mice (media control, gated on CD45.2$^+$live/dead$^-$IL-7Rα$^+$Lin$^-$intraCD3$^-$GATA-3$^+$ cells).

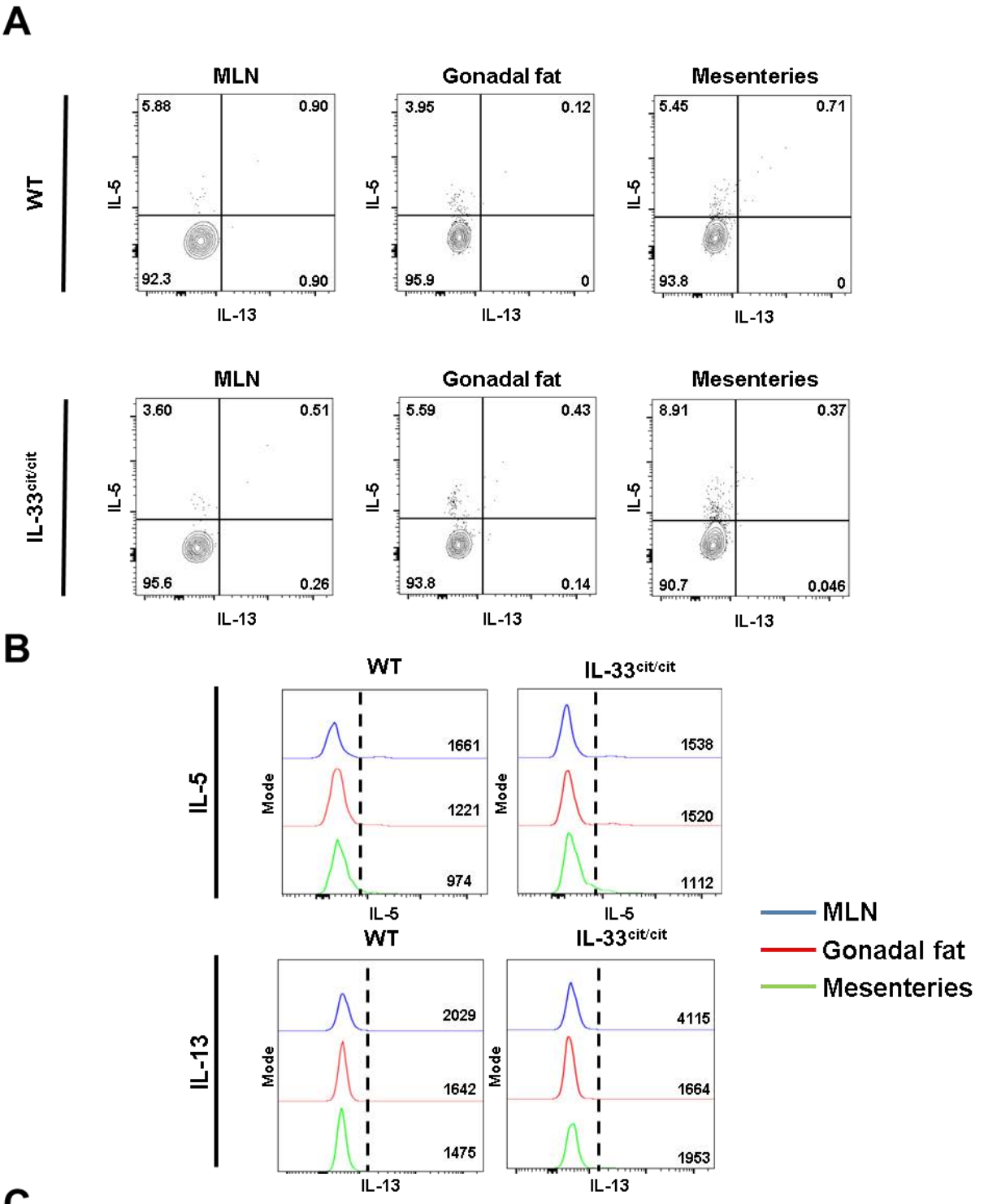
A
MLN
Gonadal fat
Mesenteries
WT
IL-33cit/cit
IL-5
IL-13
5.88
0.90
92.3
0.90
3.95
0.12
95.9
0
5.45
0.71
93.8
0
3.60
0.51
95.6
0.26
5.59
0.43
93.8
0.14
8.91
0.37
90.7
0.046
B
WT
IL-33cit/cit
Mode
1661
1221
974
1538
1520
1112
2029
1642
1475
4115
1664
1953
MLN
Gonadal fat
Mesenteries
C
% of ILC2 IL-5+
WT
IL-33 cit/cit

Figure 4.2: Cytokine production by stimulated ILC2s isolated from WT and IL-33$^{cit/cit}$ animals.

Cells were isolated from the MLN, gonadal fat and mesenteries of adult male BALB/c and IL-33$^{cit/cit}$ mice (also on BALB/c background) as described in Materials and Methods. The ILC2 cytokine production *ex vivo* was determined by flow cytometry following incubation with PMA, Ionomycin and Brefeldin A (see Materials and Methods for details). Data for each group was obtained from two technical repeats.

Each data point (n=4, 6 for WT and IL-33$^{cit/cit}$ animals respectively) represents an individual sample with a line indicating the median value. Statistical significance was determined using a Mann-Whitney two-tailed T test, **p*<0.05, ***p*<0.01, ****p*<0.001 and *****p*<0.0001.

A) FACS plots showing representative ILC2 cytokine production by stimulated cells isolated from MLN (left), gonadal fat (middle) and mesenteries (right) from WT (top) and IL-33$^{cit/cit}$ (bottom) animals (pre-gated on CD45.2^{+}live/dead^{-} IL-7Rα^{+}Lin^{-}intraCD3^{-}GATA-3^{+} cells). Histograms show representative total IL-5 (left) or IL-13 (right) staining of ILC2s from MLN (blue), gonadal fat (red) and mesenteries (green).Vertical dotted black line indicates positive staining. Numbers in FACS plots indicate percentage of events in each gate whilst numbers in histograms indicate median fluorescence intensity.

B) Graph showing percentage of ILC2s expressing IL-5 and IL-13 in MLN, gonadal fat and mesenteries from WT and IL-33$^{cit/cit}$ mice following stimulation (gated on CD45.2^{+}live/dead^{-}IL-7Rα^{+}Lin^{-}intraCD3^{-}GATA-3^{+} cells).

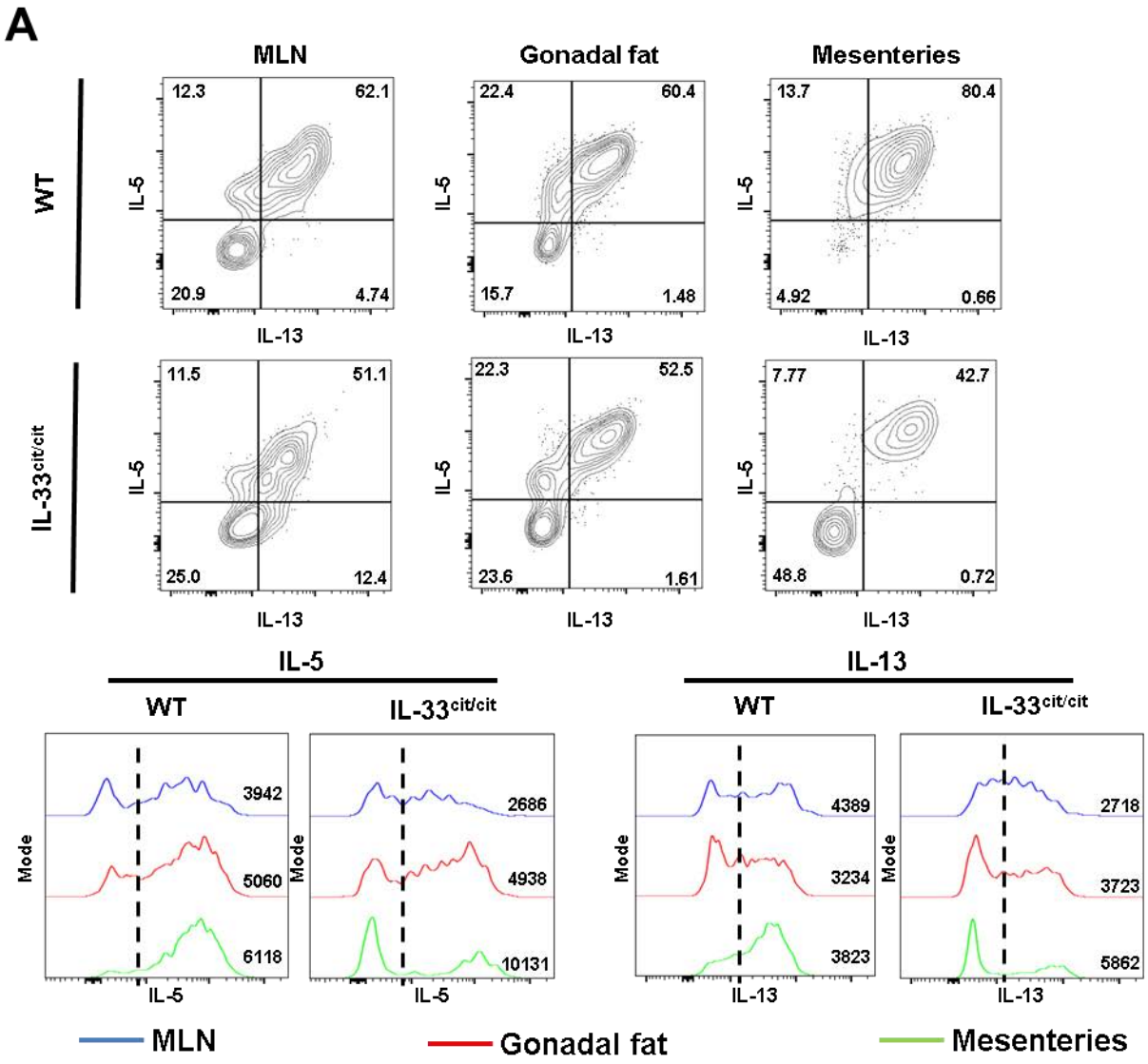
A
MLN
Gonadal fat
Mesenteries
WT
IL-33cit/cit
IL-5
IL-13
12.3
62.1
20.9
4.74
22.4
60.4
15.7
1.48
13.7
80.4
4.92
0.66
11.5
51.1
25.0
12.4
22.3
52.5
23.6
1.61
7.77
42.7
48.8
0.72
IL-5
IL-13
WT
IL-33cit/cit
Mode
3942
5060
6118
2686
4938
10131
4389
3234
3823
2718
3723
5862
MLN
Gonadal fat
Mesenteries

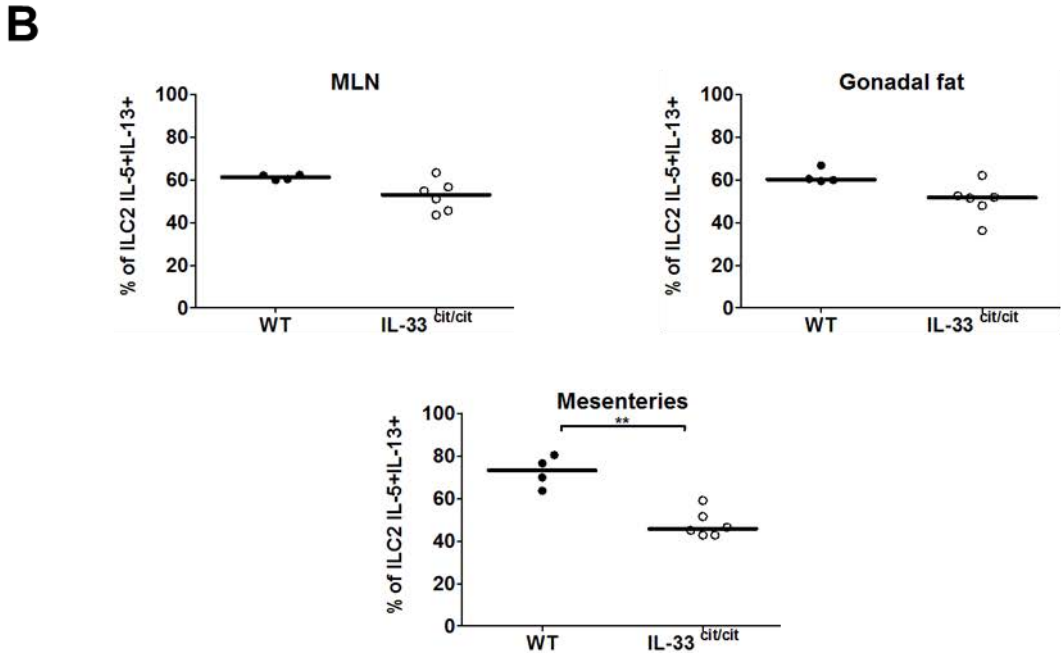
B
MLN
Gonadal fat
Mesenteries
% of ILC2 IL-5+IL-13+
100
80
60
40
20
0
WT
IL-33 cit/cit
**

4.3. ROLE OF TNF-SUPERFAMILY PROTEINS IN GOVERNING TISSUE IMMUNE CELL COMPOSITION

4.3.1. TNFRSF1a/b deficient animals

The balance of anti-inflammatory and pro-inflammatory signals (usually mediated via cytokines), and the cells which mediate these signals, are crucial in determining the immune cell composition of ATs (Odegaard *et al.*, 2008, Man *et al.*, 2017). As a result, these signals can have a crucial impact on the inflammatory status of the tissue, and on immune responses within the tissue. An example of this is during obesity; insulin resistance leads to release of pro-inflammatory cytokines, such as TNF (Hotamisligil *et al.*, 1993, Czech, 2017). This subsequently results in activation of pro-inflammatory cell subsets, such as M1-polarised macrophages and T cells, driving inflammation of ATs with the net effect of metabolic dysregulation and increased fat mass (Wu *et al.*, 2007, Kintscher *et al.*, 2008, Nishimura *et al.*, 2009, Wentworth *et al.*, 2010, McLaughlin *et al.*, 2014, Cho *et al.*, 2016, Kumamoto *et al.*, 2016).

As highlighted above, one pro-inflammatory cytokine that can influence AT immune cell composition, and therefore the immune responses within these tissues, is TNF. TNF signals through the TNFRSF1a (p55) and TNFRSF1b (p75) receptors. Previous work by Bénézech *et al.* highlighted an important role for TNF signalling for FALC formation during homeostasis and inflammation (Benezech *et al.*, 2015). The authors demonstrated a marked decrease in FALC numbers in the mesenteries of TNFRSF1a/b deficient mice and concomitantly an increased FALC formation in this tissue by overexpression of TNF using $TNF^{+/\Delta ARE}$ mice. The role of TNF in other adipose depots was not explored. Therefore, to examine the effect TNF signalling

has on the immune cell composition of ATs, the mass and immune cell composition of these tissues was investigated using mice deficient in both TNFRs (p55/p75$^{-/-}$ mice). TNFR deficiency resulted in a reduced number of FALC in gonadal fat and mesenteries and in the number of MS in the omentum (Figure 4.3A-B-pictures indicate representative density of FALC, not the full number of FALC seen in the tissues). Pictures of gonadal fat were not included as no FALC were reliably found in p55/p75$^{-/-}$ mice. Consistent with this, in a study by Bénézech *et al.* the authors also show a reduction in the number of FALC in mesenteries of p55/p75$^{-/-}$ mice compared to WT animals (Benezech *et al.*, 2015). p55/p75$^{-/-}$ mice also had significantly higher masses of gonadal fat, mesenteries and omentum than WT animals (Figure 4.3C). This is unexpected as TNF is a key driver of AT inflammation during obesity (Kang *et al.*, 2016).

Due to technical limitations, it was not possible to assess ILC composition simultaneously based on transcription factor staining alongside enumeration of FALCs. Thus, as described in the Materials and Methods section, ILC composition of ATs and MLN was determined by flow cytometry based on expression of the surface markers CD25 and CCR6.

The total cellularity of mesenteries from p55/p75$^{-/-}$ mice was reduced compared to WT mesenteries (Figure 4.4B). This could signify that TNF signalling is required for the maintenance of some cell types in the mesenteries. However, there were no differences in the total cellularity of gonadal fat from p55/p75$^{-/-}$ and WT mice (Figure 4.4B). Furthermore, there were no differences in the number of total AT ILCs or ILC2s between WT and p55/p75$^{-/-}$ mice (Figure 4.4C-D), indicating that TNF signalling was not required for the maintenance of these cells within ATs. There also

appeared to be a decrease in the number of $CD4^-$ iNKTs in mesenteries of $p55/p75^{-/-}$ mice compared to WT mice, but the fold change in $CD4^-$ cells was approximately 1.8 fold, the same as the fold decrease in total cellularity of the mesenteries of $p55/p75^{-/-}$ mice, suggesting the number of these cells is unaffected in the absence of TNFR signalling (Figure 4.5C). This difference was not seen in the gonadal fat of the same mice (Figure 4.5C).

As discussed in the Materials and Methods section, there was some degree of inter-experimental variation in CD4 staining, making clear identification of the $CD4^+$ population difficult. Nevertheless, by using a consistent gating strategy throughout all experiments, an increase in the number of $CD4^+$ cells and Tregs was seen in the gonadal fat of $p55/p75^{-/-}$ mice, compared with WT mice, but not in the mesenteries of the same animals (Figure 4.6A-C). There is a possibility that the trend seen in $CD4^+$ cells could be affected by the variable CD4 staining, resulting in inadvertent inclusion of $CD4^-$ cells. As the majority of CD4- cells are likely to be $CD8^+$ T cells, inclusion of the marker CD8 could help verify the accuracy of the CD4+ gate and ensure genuine changes in the $CD4^+$ population.

The percentage of $KLRG1^+$ ILC2s was similar between $p55/p75^{-/-}$ and WT mice for both ATs, but the expression of KLRG1 by ILC2s was lower in the gonadal fat from $p55/p75^{-/-}$ mice compared to WT mice (Figure 4.7B-D). There was also a higher expression of ST2 by ILC2s from gonadal fat of $p55/p75^{-/-}$ mice compared to WT animals (Figure 4.12E). However, these differences in KLRG1 and ST2 expression were very small, so are unlikely to be of biological significance.

The immune cell composition of MLN from WT and $p55/p75^{-/-}$ mice is shown in the appendix (Figure 7.11-Figure 7.13).

Figure 4.3: FALC/ MS numbers in WT and p55/p75$^{-/-}$ animals

The mesenteries and omentum were isolated from adult male WT and TNFRSF1a/b deficient (p55/p75$^{-/-}$) mice (both on C57BL/6J background) and stained with antibodies against CD45 as described in Materials and Methods. FALC and MS numbers were enumerated using a fluorescent dissecting microscope. Data for each group was obtained from two technical repeats.

Each data point (n=4, 5 for WT and p55p/75$^{-/-}$ animals respectively) represents an individual sample with a line indicating the median value. Statistical significance was determined using a Mann-Whitney two-tailed T test. *p<0.05, **p<0.01, ***p<0.001 and ****p<0.0001.

A) Images showing representative FALC/MS staining in mesenteries (top) and omentum (bottom) from both WT (left) and p55/p75$^{-/-}$ (right) animals. Images taken at 20X magnification. White arrows indicate FALC/MS.

B) Graph showing adjusted number of FALC (number FALC/100mg fat) in gonadal fat, mesenteries and omentum from WT and p55/p75$^{-/-}$ animals.

C) Graph showing mass of gonadal fat, mesenteries and omentum isolated from WT and p55/p75$^{-/-}$ animals.

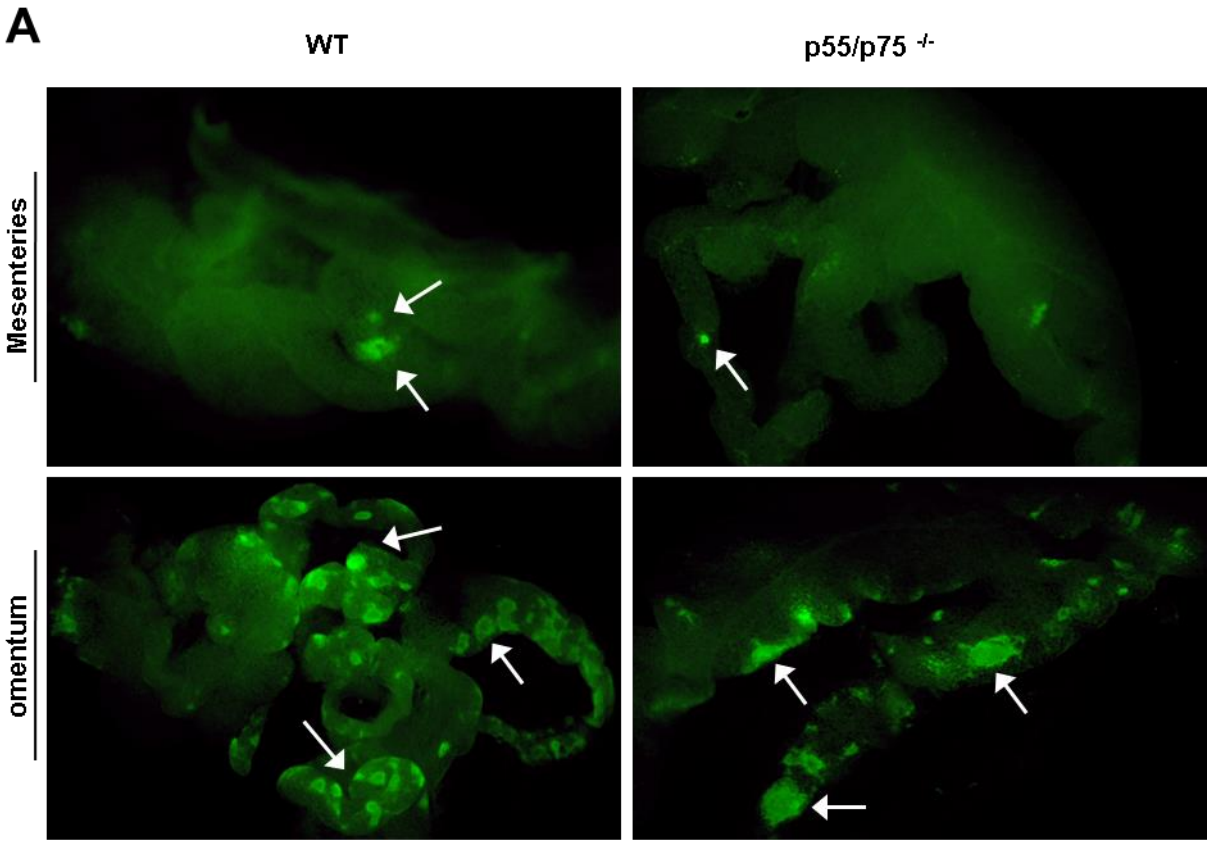
A
WT
p55/p75 -/-
Mesenteries
omentum

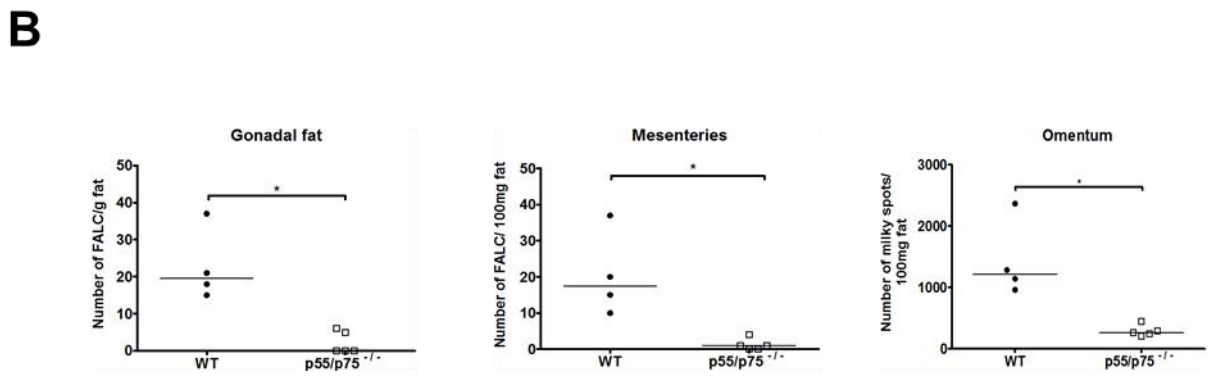
B
Gonadal fat
Number of FALC/g fat
WT
p55/p75 -/-
Mesenteries
Number of FALC/ 100mg fat
Omentum
Number of milky spots/ 100mg fat

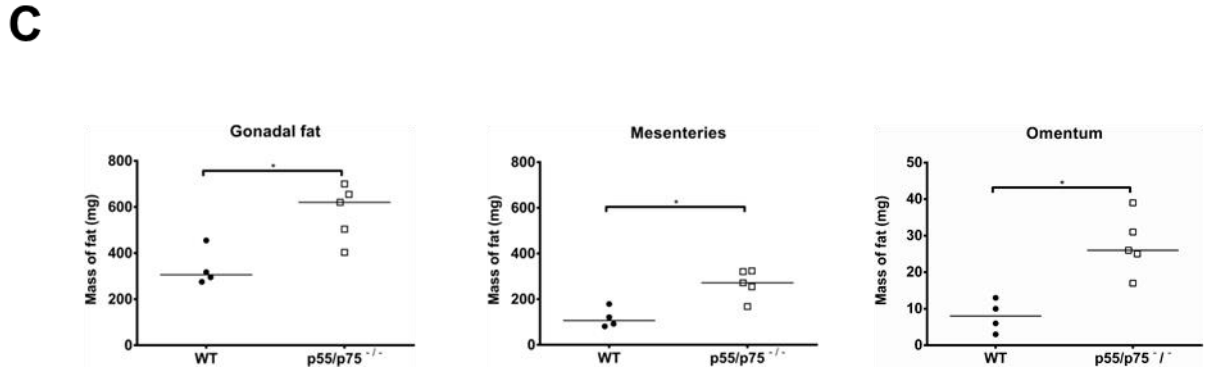
C
Gonadal fat
Mass of fat (mg)
WT
p55/p75 -/-
Mesenteries
Omentum

Figure 4.4: Adipose tissue ILC composition in WT and p55/p75$^{-/-}$ animals

Cells were isolated from the gonadal fat and mesenteries of adult male WT and p55/p75$^{-/-}$ mice (both on C57BL/6J background) as described in Materials and Methods. The ILC composition was determined by flow cytometry, as demonstrated previously. Data for each group was obtained from two technical repeats.

Each data point (n=4, 5 for WT and p55p/75$^{-/-}$ animals respectively) represents an individual sample with a line indicating the median value. Statistical significance was determined using a Mann-Whitney two-tailed T test, *p<0.05, **p<0.01, ***p<0.001 and ****p<0.0001.

A) FACS plots showing representative ILC composition in gonadal fat (left) and mesenteries (right) from both WT (top) and p55/p75$^{-/-}$ (bottom) animals (pre-gated on live CD45.2^{+} lymphocytes based on FSC and SSC profile and a viability marker). Numbers indicate percentage of events in each gate.

B) Graph showing adjusted number of total live cells (Total cellularity/100mg fat) in gonadal fat and mesenteries from WT and p55/p75$^{-/-}$ animals (gated on live/dead^{-} cells).

C) Graph showing adjusted number of total ILCs (Total ILCs/100mg fat) in gonadal fat and mesenteries from WT and p55/p75$^{-/-}$ mice (gated on CD45.2^{+}live/dead^{-}IL-7Rα^{+}Lin^{-} cells).

D) Graph showing adjusted number of ILC2s (number ILC2s/100mg fat) in gonadal fat and mesenteries from WT and p55/p75$^{-/-}$ animals (gated on CD45.2^{+}live/dead^{-}IL-7Rα^{+}Lin^{-}intraCD3^{-}CD25^{+}CCR6^{-} cells).

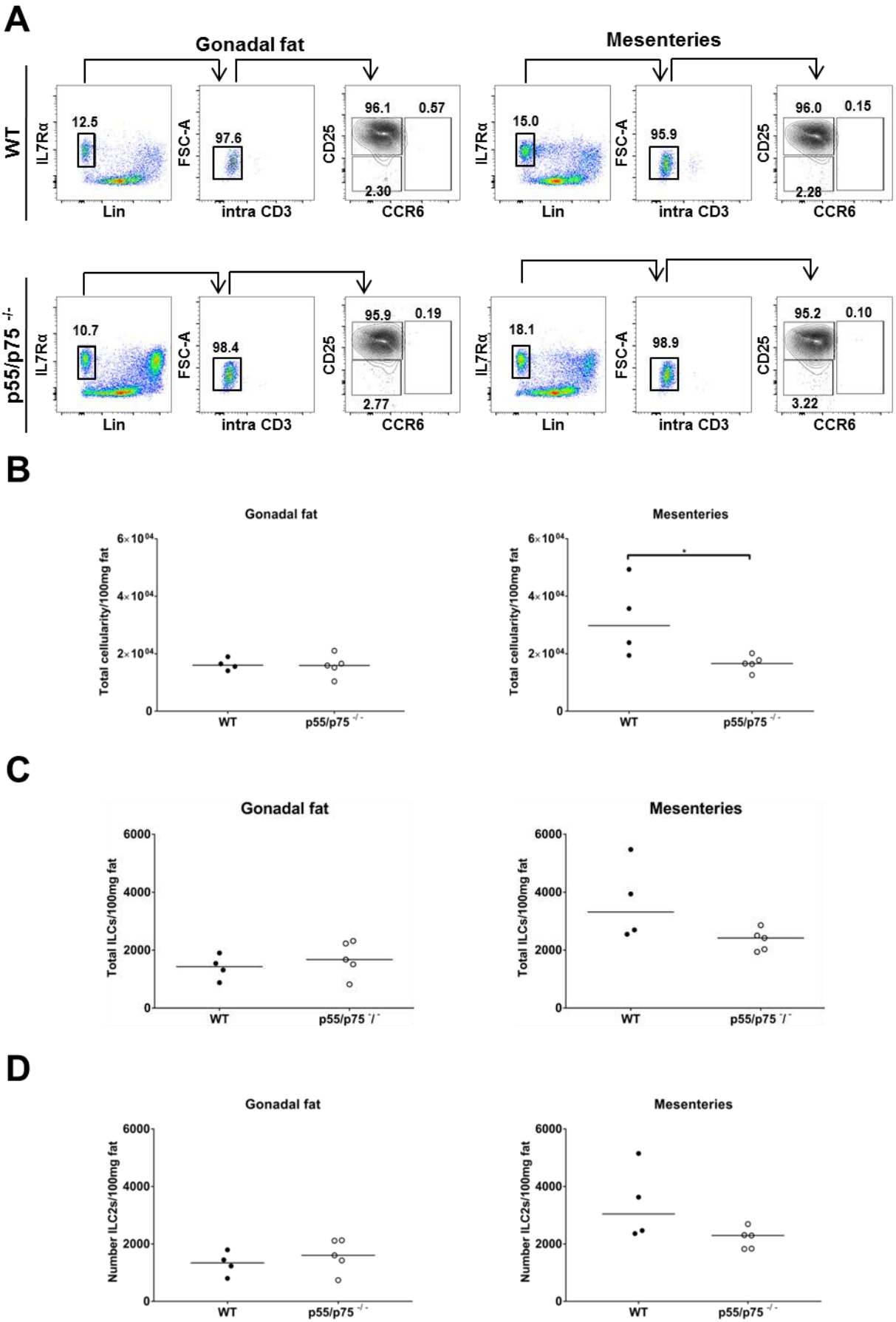
A
Gonadal fat
Mesenteries
WT
p55/p75 -/-
IL7Rα
Lin
12.5
FSC-A
intra CD3
97.6
CD25
CCR6
96.1
0.57
2.30
15.0
95.9
96.0
0.15
2.28
10.7
98.4
95.9
0.19
2.77
18.1
98.9
95.2
0.10
3.22
B
Gonadal fat
Mesenteries
Total cellularity/100mg fat
6×10^04
4×10^04
2×10^04
0
WT
p55/p75 -/-
*
C
Gonadal fat
Mesenteries
Total ILCs/100mg fat
6000
4000
2000
0
WT
p55/p75 -/-
D
Gonadal fat
Mesenteries
Number ILC2s/100mg fat
6000
4000
2000
0
WT
p55/p75 -/-

Figure 4.5: Adipose tissue iNKT cell composition in WT and p55/p75$^{-/-}$ animals

Cells were isolated from the gonadal fat and mesenteries of adult male WT and p55/p75$^{-/-}$ mice (both on C57BL/6J background) as described in Materials and Methods. The iNKT composition was determined by flow cytometry, as demonstrated previously. Data for each group was obtained from two technical repeats.

Each data point (n=4, 5 for WT and p55p/75$^{-/-}$ animals respectively) represents an individual sample with a line indicating the median value. Statistical significance was determined using a Mann-Whitney two-tailed T test, *p<0.05, **p<0.01, ***p<0.001 and ****p<0.0001.

A) FACS plots showing representative T cell composition in gonadal fat and mesenteries from both WT (left) and p55/p75$^{-/-}$ (right) animals (pre-gated on live CD45.2^{+} lymphocytes based on FSC and SSC profile and a viability marker). Numbers indicate percentage of events in each gate.

B) Graph showing adjusted number of CD4^{+}iNKT cells (number CD4^{+}iNKT cells/100mg fat) in gonadal fat and mesenteries from WT and p55/p75$^{-/-}$ animals (gated on CD45.2^{+}live/dead^{-}intraCD3^{+}CD4^{+}α-gal-cer^{+} cells).

C) Graph showing adjusted number of CD4^{-} iNKT cells (number CD4^{-} iNKT cells/100mg fat) in gonadal fat and mesenteries isolated from WT and p55/p75$^{-/-}$ animals (gated on CD45.2^{+}live/dead^{-}intraCD3^{+}CD4^{-}α-gal-cer^{+} cells).

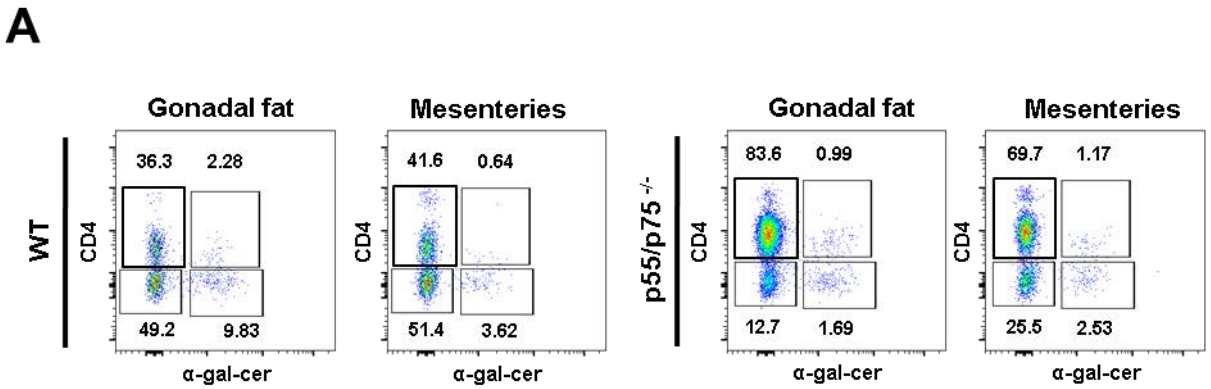
A
Gonadal fat
Mesenteries
Gonadal fat
Mesenteries
WT
p55/p75 -/-
CD4
36.3
2.28
49.2
9.83
41.6
0.64
51.4
3.62
83.6
0.99
12.7
1.69
69.7
1.17
25.5
2.53
α-gal-cer

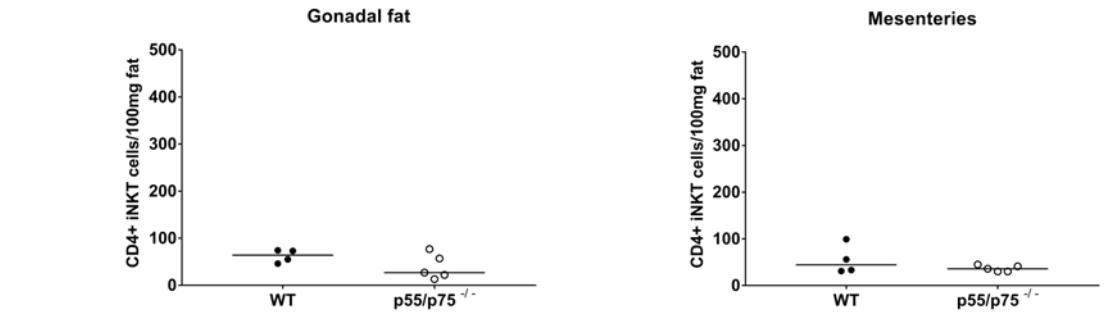
B
Gonadal fat
Mesenteries
CD4+ iNKT cells/100mg fat
0
100
200
300
400
500
WT
p55/p75 -/-

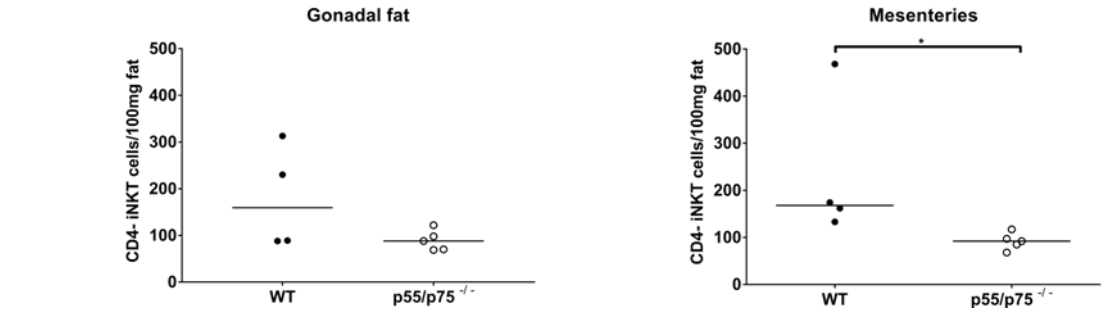
C
Gonadal fat
Mesenteries
CD4- iNKT cells/100mg fat
0
100
200
300
400
500
*
WT
p55/p75 -/-

Figure 4.6: Adipose tissue T cell composition in WT and p55/p75$^{-/-}$ animals

Cells were isolated from the gonadal fat and mesenteries of adult male WT and p55/p75$^{-/-}$ mice (both on C57BL/6J background) as described in Materials and Methods. The T cell composition was determined by flow cytometry, as demonstrated previously. Data for each group was obtained from two technical repeats.

Each data point (n=4, 5 for WT and p55p/75$^{-/-}$ animals respectively) represents an individual sample with a line indicating the median value. Statistical significance was determined using a Mann-Whitney two-tailed T test, *p<0.05, **p<0.01, ***p<0.001 and ****p<0.0001.

A) As in Figure 4.5A, FACS plots showing representative T cell composition in gonadal fat (left) and mesenteries (right) from both WT (top) and p55/p75$^{-/-}$ (bottom) animals (pre-gated on live CD45.2^{+} lymphocytes based on FSC and SSC profile and a viability marker). Numbers indicate percentage of events in each gate.

B) Graph showing adjusted number of CD4^{+} cells (number CD4^{+} cells/100mg fat) in gonadal fat and mesenteries from WT and p55/p75$^{-/-}$animals (gated on CD45.2^{+}live/dead^{-}intraCD3^{+}CD4^{+}α-gal-cer^{-} cells).

C) Graph showing adjusted number of regulatory T cells (number Tregs/100mg fat) in gonadal fat and mesenteries from WT and p55/p75$^{-/-}$animals (gated on CD45.2^{+}live/dead^{-}intraCD3^{+}CD4^{+}α-gal-cer^{-}Foxp3^{+} cells).

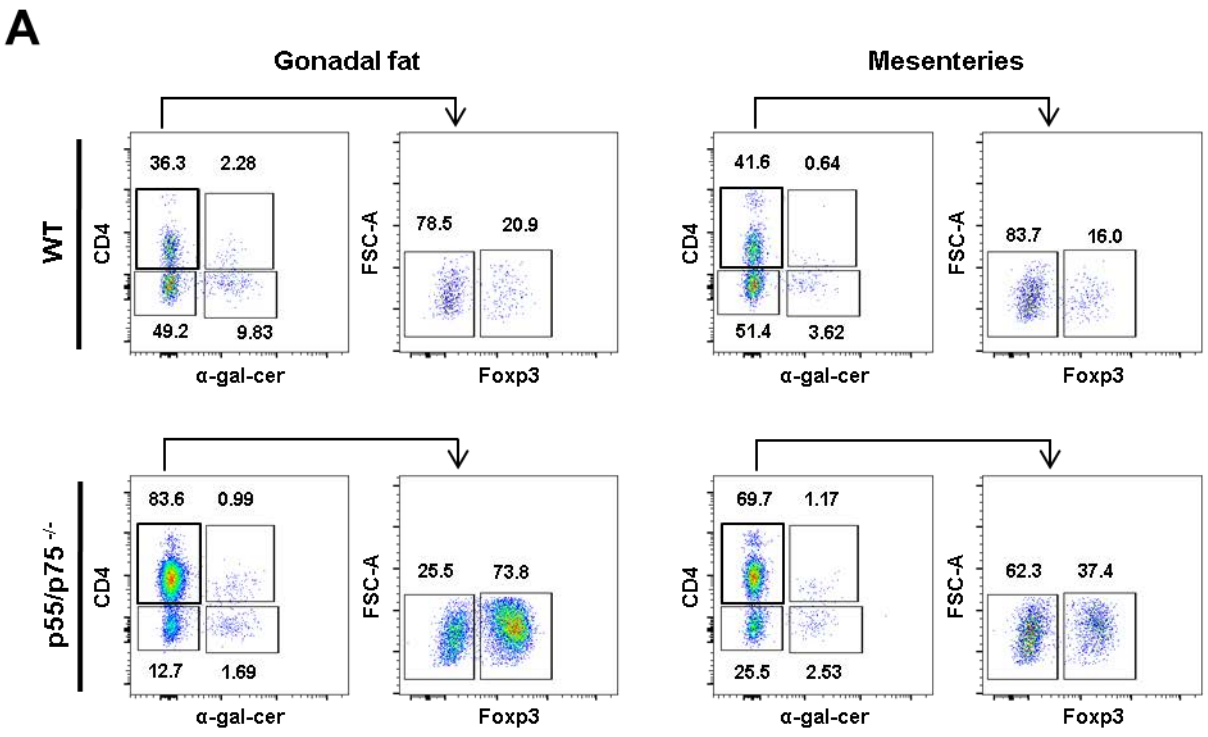
A
Gonadal fat
Mesenteries
WT
p55/p75 -/-
CD4
α-gal-cer
FSC-A
Foxp3
36.3
2.28
49.2
9.83
78.5
20.9
41.6
0.64
51.4
3.62
83.7
16.0
83.6
0.99
12.7
1.69
25.5
73.8
69.7
1.17
25.5
2.53
62.3
37.4

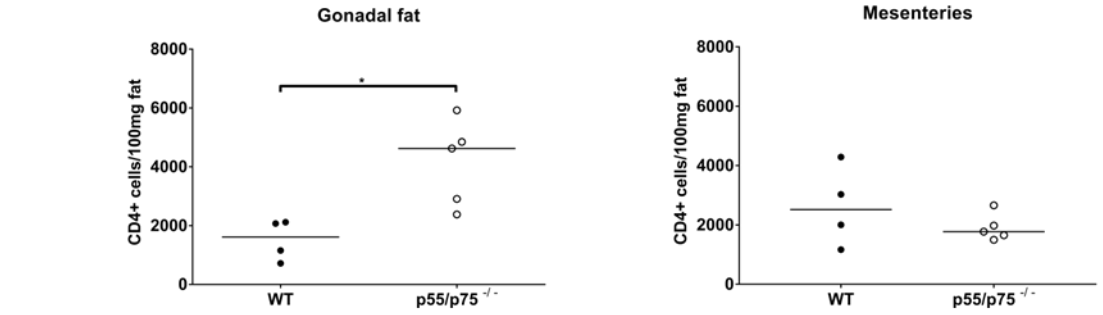
B
Gonadal fat
Mesenteries
CD4+ cells/100mg fat
8000
6000
4000
2000
0
*
WT
p55/p75 -/-

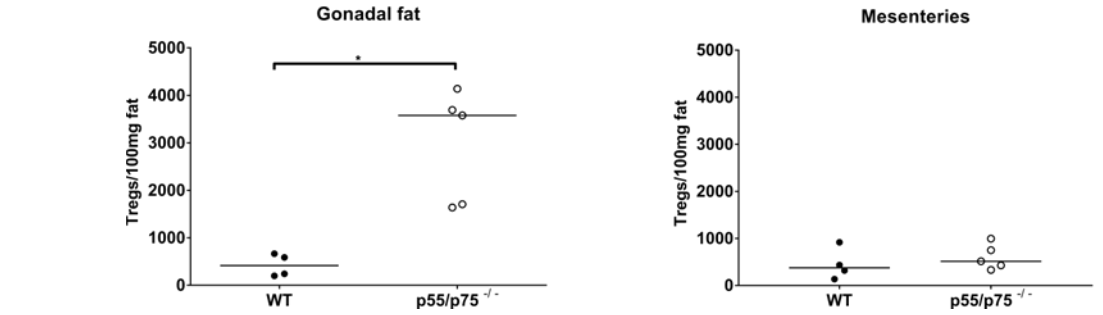
C
Gonadal fat
Mesenteries
Tregs/100mg fat
5000
4000
3000
2000
1000
0
*
WT
p55/p75 -/-

Figure 4.7: Adipose tissue ILC2 phenotype in WT and p55/p75$^{-/-}$ animals

Cells were isolated from the gonadal fat and mesenteries of adult male WT and p55/p75$^{-/-}$ mice (both on C57BL/6J background) as described in Materials and Methods. The ILC2 phenotype was determined by flow cytometry as described in the Materials and Methods. Data for each group was obtained from two technical repeats.

Each data point (n=4, 5 for WT and p55p/75$^{-/-}$ animals respectively) represents an individual sample with a line indicating the median value. Statistical significance was determined using a Mann-Whitney two-tailed T test, *p<0.05, **p<0.01, ***p<0.001 and ****p<0.0001.

A) FACS plots showing representative ILC2 phenotype in gonadal fat (left) and mesenteries (right) from both WT (top) and p55/p75$^{-/-}$ (bottom) animals (pre-gated on live CD45.2^{+} lymphocytes based on FSC and SSC profile and a viability marker). Numbers indicate percentage of events in each gate.

B) Histogram showing representative KLRG1 staining in gonadal fat (left panel) or mesenteries (right panel) isolated from p55/p75$^{-/-}$ (red lines) or WT (blue lines) animals. Vertical dotted black line indicates positive staining. Solid lines show ILC2 staining (CD45.2^{+}live/dead^{-}IL-7Rα^{+}Lin^{-}intraCD3^{+}ST2^{+}ICOS$^{+/-}$ cells), dotted lines show negative control staining (CD45.2^{+}live/dead^{-}IL-7Rα^{-} Lin^{+}intraCD3^{-}cells). Numbers indicate the percentage of KLRG1^{+} cells.

C) Graph showing the percentage of ILC2s expressing KLRG1 in gonadal fat and mesenteries from WT and p55/p75$^{-/-}$ mice (gated on CD45.2^{+}live/dead^{-} IL-7Rα^{+}Lin^{-}intraCD3^{-}ST2^{+}ICOS$^{+/-}$KLRG1^{+} cells).

D) Graph showing the expression of KLRG1 on the surface of ILC2s in gonadal fat and mesenteries from WT and p55/p75$^{-/-}$ mice (gated on CD45.2^{+}live/dead^{-} IL-7Rα^{+}Lin^{-}intraCD3^{-}ST2^{+}ICOS$^{+/-}$KLRG1^{+} cells).

E) Graph showing the expression of ST2 on the surface of ILC2s in gonadal fat and mesenteries from WT and p55/p75$^{-/-}$ mice (gated on CD45.2^{+}live/dead^{-} IL-7Rα^{+}Lin^{-}intraCD3^{-}ST2^{+}ICOS$^{+/-}$ cells).

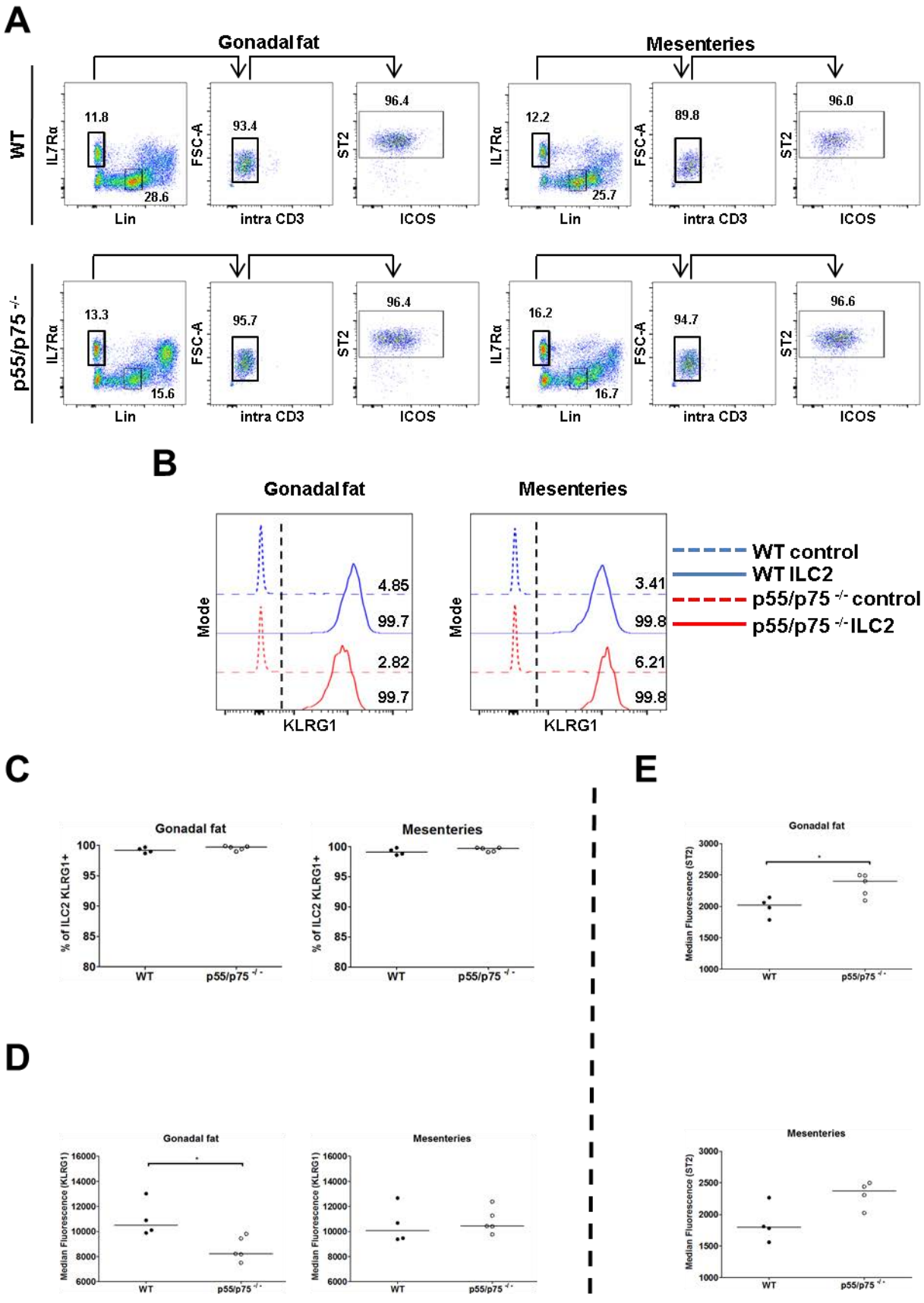
A
Gonadal fat
Mesenteries
WT
p55/p75 -/-
IL7Rα
FSC-A
ST2
Lin
intra CD3
ICOS
11.8
28.6
93.4
96.4
12.2
25.7
89.8
96.0
13.3
15.6
95.7
96.4
16.2
16.7
94.7
96.6
B
Gonadal fat
Mesenteries
Mode
KLRG1
4.85
99.7
2.82
99.7
3.41
99.8
6.21
99.8
WT control
WT ILC2
p55/p75 -/- control
p55/p75 -/- ILC2
C
Gonadal fat
Mesenteries
% of ILC2 KLRG1+
WT
p55/p75 -/-
D
Gonadal fat
Mesenteries
Median Fluorescence (KLRG1)
E
Gonadal fat
Mesenteries
Median Fluorescence (ST2)

4.3.2. Overexpression of TNF

In section 4.3.1 the role of TNFR1a and 1b in determining AT immune cell composition was investigated. Despite having an effect on FALC number and total cellularity of mesenteries, few differences in immune cell composition was seen in both gonadal fat and mesenteries from TNFR1a/b deficient mice. To further assess the role of the TNF pathway in influencing the immune cell composition of ATs, the same parameters were examined in mice that overexpress the TNF protein ($TNF^{+/\Delta ARE}$) and were compared with WT littermate controls. As with $p55/p75^{-/-}$ mice, ILC composition in $TNF^{+/\Delta ARE}$ mice was determined based on surface protein staining and did not include intracellular CD3.

Higher numbers of FALC were identified in the gonadal fat and mesenteries of $TNF^{+/\Delta ARE}$ mice, as compared to WT mice (Figure 4.8A-B). These results are consistent with other studies, which have demonstrated an increased number of FALC in the mesenteries of $TNF^{+/\Delta ARE}$ mice (Benezech *et al.*, 2015). The mass of gonadal fat and mesenteries isolated from $TNF^{+/\Delta ARE}$ mice was lower than the mass isolated from WT animals, but there was no difference in omental mass between WT and $TNF^{+/\Delta ARE}$ mice (Figure 4.8C). This directly opposes the differences seen in $p55/p75^{-/-}$ animals, suggesting that TNFR signalling truly does have an effect on AT mass. As TNF signalling has been reported to block adipogenesis, it is likely that decreased fat mass seen in $TNF^{+/\Delta ARE}$ mice is a downstream effect of this (Chae and Kwak, 2003, Cawthorn *et al.*, 2007).

The total cellularity was higher in gonadal fat (~ three fold) and mesenteries (~10 fold) than in the same tissues from WT animals (Figure 4.9A-B). Taking this into account, the number of total ILCs and ILC2 in gonadal fat and mesenteries of TNF

mutants was not specifically higher than in WT animals i.e. the fold difference in number of these populations was not more than the total fold difference in total cellularity, so the number of these populations as a proportion of the total cells remained the same (Figure 4.9). The same was true of $CD4^+$ cells, $CD4^+$ iNKTs and Tregs in gonadal fat and mesenteries (Figure 4.10A-B, Figure 4.11). However, $CD4^-$ iNKT were 7.7 fold higher in gonadal fat from $TNF^{+/\Delta ARE}$ mice than WT mice, whilst the total cellularity was only ~ 3 times higher in the gonadal fat from these animals compared to WT mice, indicating that this population was specifically higher in gonadal fat (Figure 4.10C). Data from Bénézech *et al.* indicates a key role of iNKT in the formation of FALC, although they do not specify whether these cells express CD4 (Benezech *et al.*, 2015). Thus, an increase in iNKT cells in ATs of $TNF^{+/\Delta ARE}$ mice might be expected due to an increased number of FALC in these animals (Benezech *et al.*, 2015). This trend was not seen in the mesenteries of $TNF^{+/\Delta ARE}$ mice compared to WT (Figure 4.10C), which was the tissue assessed in the study by Bénézech *et al.* (Benezech *et al.*, 2015).

Finally, ILC2s from mesenteries, but not gonadal fat, of $TNF^{+/\Delta ARE}$ mice had a higher expression, but not percentage, of KLRG1 than seen on the surface of ILC2s from the same tissues of WT mice (Figure 4.12B-D). However, as with the differences seen in ILC2 phenotype in $p55/p75^{-/-}$ animals, the difference seen in ILC2 KLRG1 expression between WT and $TNF^{+/\Delta ARE}$ animals is unlikely to be biologically relevant. No variation was seen in ILC2 expression of ST2 between WT and $TNF^{+/\Delta ARE}$ mice in either AT (Figure 4.12E).

The immune cell composition of MLN from WT and $TNF^{+/\Delta ARE}$ mice is shown in the appendix (Figure 7.14-Figure 7.16).

Figure 4.8: FALC/ MS numbers in WT and $TNF^{+/\Delta ARE}$ mice

The mesenteries and omentum were isolated from adult male WT and $TNF^{+/\Delta ARE}$ mice (both on C57BL/6J background) and stained with antibodies against CD45 as described in Materials and Methods. FALC and MS numbers were enumerated using a fluorescent dissecting microscope. Data for each group was obtained from five technical repeats.

Each data point (n=10, 7 for WT and $TNF^{+/\Delta ARE}$ animals respectively) represents an individual sample with a line indicating the median value. Statistical significance was determined using a Mann-Whitney two-tailed T test, *p<0.05, **p<0.01, ***p<0.001 and ****p<0.0001.

A) Images showing representative FALC/MS staining in gonadal fat (top), mesenteries (middle) and omentum (bottom) from both WT (left) and $TNF^{+/\Delta ARE}$ (right) animals. Images taken at 20X magnification. White arrows indicate FALC/MS.

B) Graph showing adjusted number of FALC (number FALC/100mg fat) in gonadal fat, mesenteries and omentum from WT and $TNF^{+/\Delta ARE}$ animals. For omentum n=9, 7 WT and $TNF^{+/\Delta ARE}$ animals respectively.

C) Graph showing mass of gonadal fat, mesenteries and omentum isolated from WT and $TNF^{+/\Delta ARE}$ animals. For omentum n=9, 7 WT and $TNF^{+/\Delta ARE}$ animals respectively.

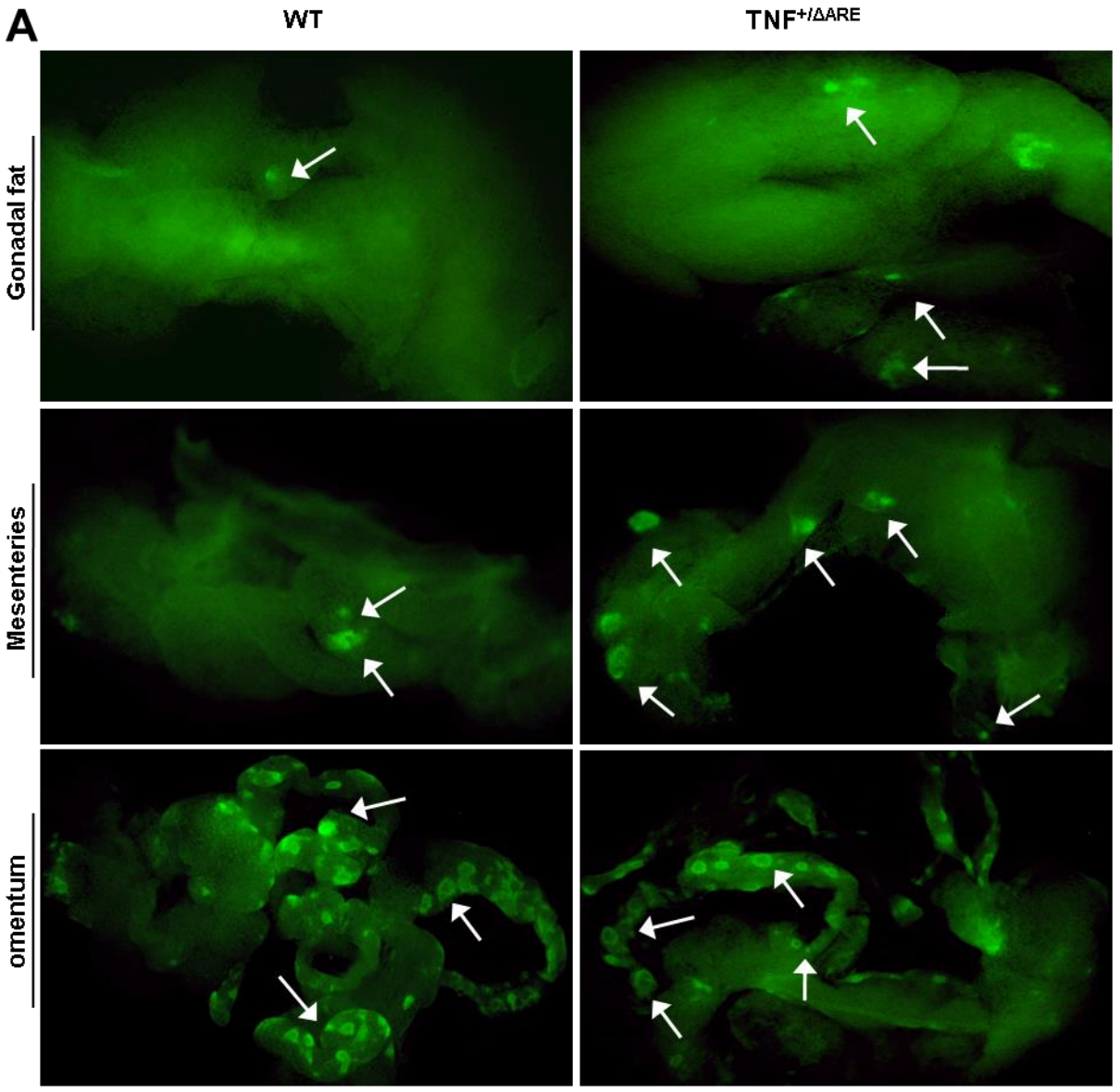
A
WT
TNF+/ΔARE
Gonadal fat
Mesenteries
omentum

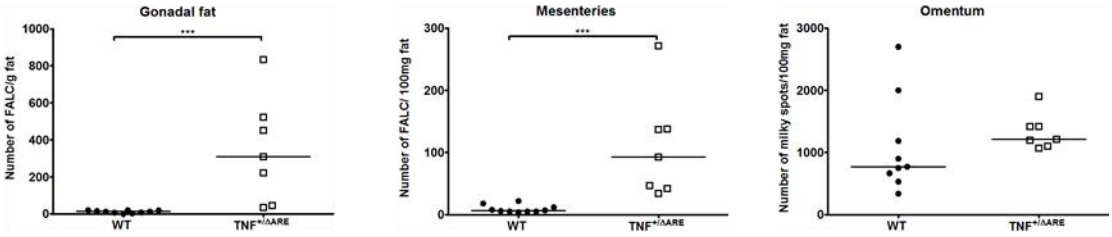
B
Gonadal fat
Number of FALC/g fat
1000
800
600
400
200
0
***
WT
TNF+/ΔARE
Mesenteries
Number of FALC/ 100mg fat
300
200
100
0
***
WT
TNF+/ΔARE
Omentum
Number of milky spots/100mg fat
3000
2000
1000
0
WT
TNF+/ΔARE

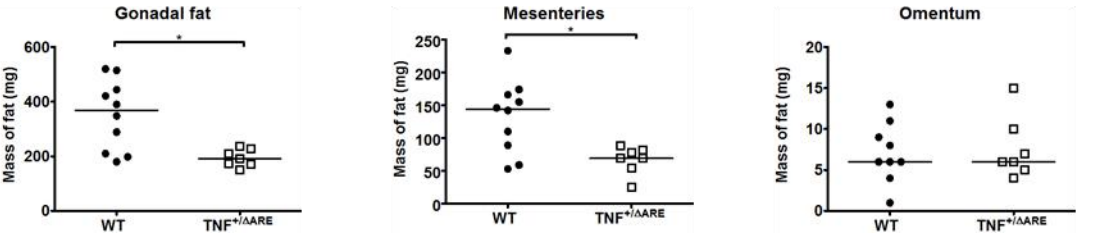
C
Gonadal fat
Mass of fat (mg)
600
400
200
0
*
WT
TNF+/ΔARE
Mesenteries
Mass of fat (mg)
250
200
150
100
50
0
*
WT
TNF+/ΔARE
Omentum
Mass of fat (mg)
20
15
10
5
0
WT
TNF+/ΔARE

Figure 4.9: Adipose tissue ILC composition in WT and $TNF^{+/\Delta ARE}$ mice

Cells were isolated from the gonadal fat and mesenteries of adult male WT and $TNF^{+/\Delta ARE}$ mice (both on C57BL/6J background) as described in Materials and Methods. The ILC composition was determined by flow cytometry, as demonstrated previously. Data for each group was obtained from four technical repeats.

Each data point (n=7, 6 for WT and $TNF^{+/\Delta ARE}$ animals respectively) represents an individual sample with a line indicating the median value. Statistical significance was determined using a Mann-Whitney two-tailed T test, *p<0.05, **p<0.01, ***p<0.001 and ****p<0.0001.

A) FACS plots showing representative ILC composition in gonadal fat (left) and mesenteries (right) from both WT (top) and $TNF^{+/\Delta ARE}$ (bottom) animals (pre-gated on live $CD45.2^+$ lymphocytes based on FSC and SSC profile and a viability marker). Numbers indicate percentage of events in each gate.

B) Graph showing adjusted number of total live cells (Total cellularity/100mg fat) in gonadal fat and mesenteries from WT and $TNF^{+/\Delta ARE}$ animals (gated on live/$dead^-$ cells).

C) Graph showing adjusted number of total ILCs (Total ILCs/100mg fat) in gonadal fat and mesenteries from WT and $TNF^{+/\Delta ARE}$ animals (gated on $CD45.2^+$live/$dead^-$$IL\text{-}7R\alpha^+Lin^-$ cells).

D) Graph showing adjusted number of ILC2s (ILC2s/100mg fat) in gonadal fat and mesenteries from WT and $TNF^{+/\Delta ARE}$ animals (gated on $CD45.2^+$live/$dead^-$ $IL\text{-}7R\alpha^+Lin^-$intra$CD3^-GATA\text{-}3^+CCR6^-$ cells).

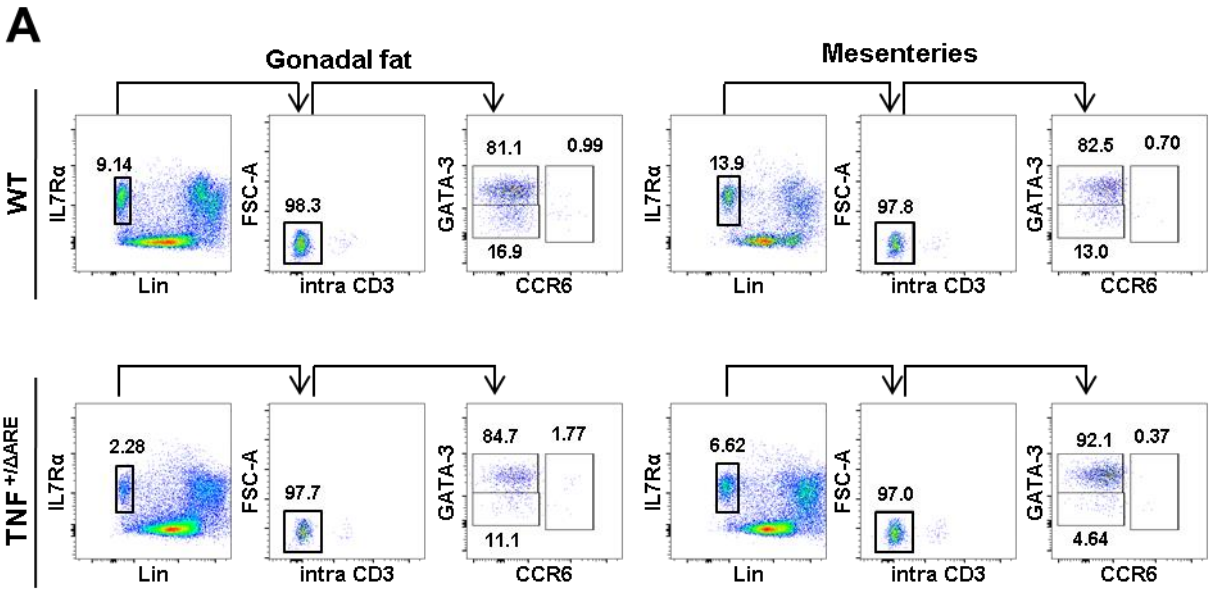
A
Gonadal fat
Mesenteries
WT
TNF+/ΔARE
IL7Rα
Lin
9.14
FSC-A
intra CD3
98.3
GATA-3
CCR6
81.1
0.99
16.9
13.9
97.8
82.5
0.70
13.0
2.28
97.7
84.7
1.77
11.1
6.62
97.0
92.1
0.37
4.64

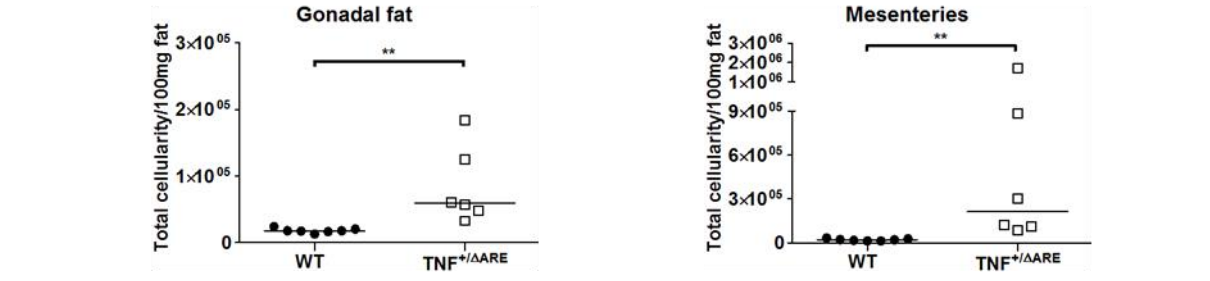
B
Gonadal fat
Mesenteries
Total cellularity/100mg fat
WT
TNF+/ΔARE
**

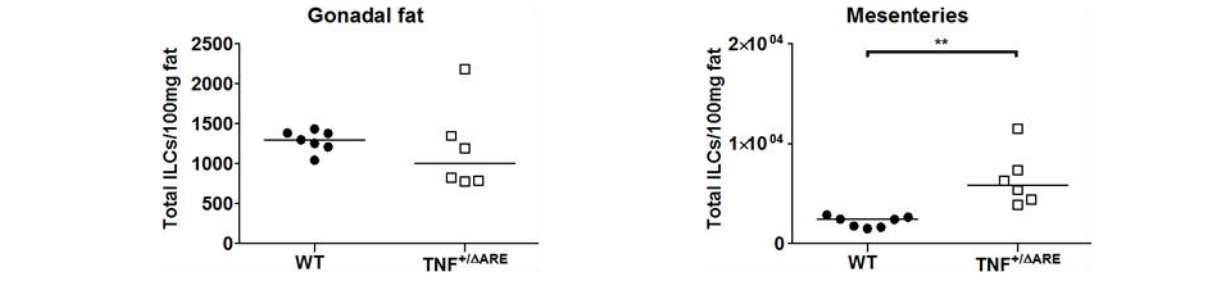
C
Gonadal fat
Mesenteries
Total ILCs/100mg fat
WT
TNF+/ΔARE
**

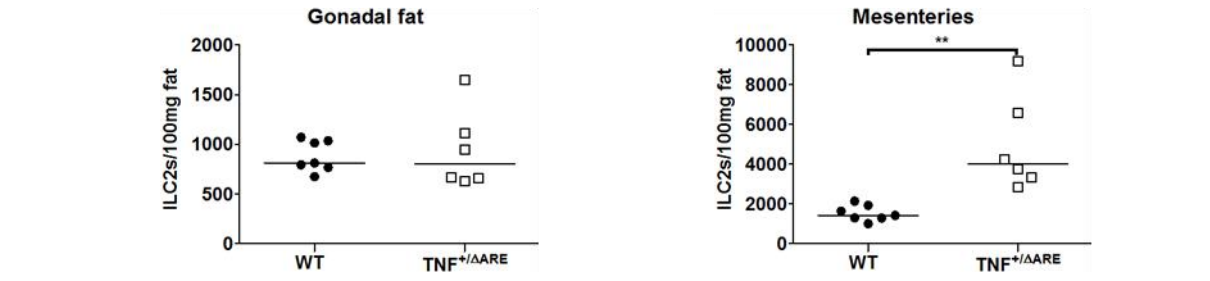
D
Gonadal fat
Mesenteries
ILC2s/100mg fat
WT
TNF+/ΔARE
**

Figure 4.10: Adipose tissue iNKT cell composition in WT and TNF$^{+/\Delta ARE}$ mice

Cells were isolated from the gonadal fat and mesenteries of adult male WT and TNF mutant TNF$^{+/\Delta ARE}$ mice (both on C57BL/6J background) as described in Materials and Methods. The iNKT composition was determined by flow cytometry, as demonstrated previously. Data for each group was obtained from four technical repeats.

Each data point (n=7, 6 for WT and TNF$^{+/\Delta ARE}$ animals respectively) represents an individual sample with a line indicating the median value. Statistical significance was determined using a Mann-Whitney two-tailed T test, *p<0.05, **p<0.01, ***p<0.001 and ****p<0.0001.

A) FACS plots showing representative T cell composition in gonadal fat (left) and mesenteries (right) from both WT (top) and TNF$^{+/\Delta ARE}$ (bottom) animals (pre-gated on live CD45.2^{+} lymphocytes based on FSC and SSC profile and a viability marker). Numbers indicate percentage of events in each gate.

B) Graph showing adjusted number of CD4^{+}iNKT cells (number CD4^{+}iNKT cells/100mg fat) in gonadal fat and mesenteries from WT and TNF$^{+/\Delta ARE}$ animals (gated on CD45.2^{+}live/dead^{-}intraCD3^{+}CD4^{+}α-gal-cer^{+} cells).

C) Graph showing adjusted number of CD4^{-} iNKT cells (number CD4^{-} iNKT cells/100mg fat) in gonadal fat and mesenteries isolated from WT and TNF$^{+/\Delta ARE}$ animals (gated on CD45.2^{+}live/dead^{-}intraCD3^{+}CD4^{-}α-gal-cer^{+} cells).

A

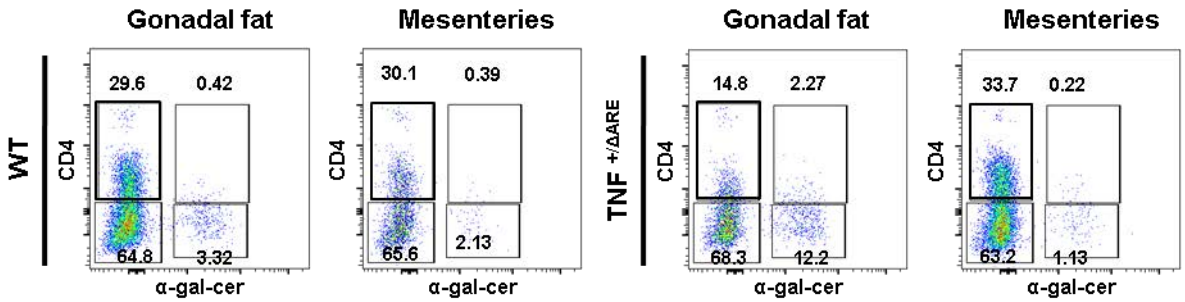
Gonadal fat
Mesenteries
Gonadal fat
Mesenteries
WT
TNF +/ΔARE
CD4
29.6
0.42
64.8
3.32
30.1
0.39
65.6
2.13
14.8
2.27
68.3
12.2
33.7
0.22
63.2
1.13
α-gal-cer

B

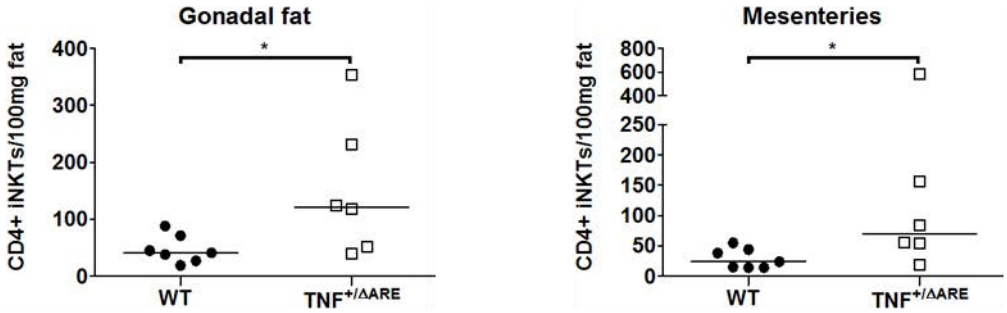
Gonadal fat
Mesenteries
CD4+ iNKTs/100mg fat
400
300
200
100
0
800
600
400
250
200
150
100
50
*
WT
TNF+/ΔARE

C

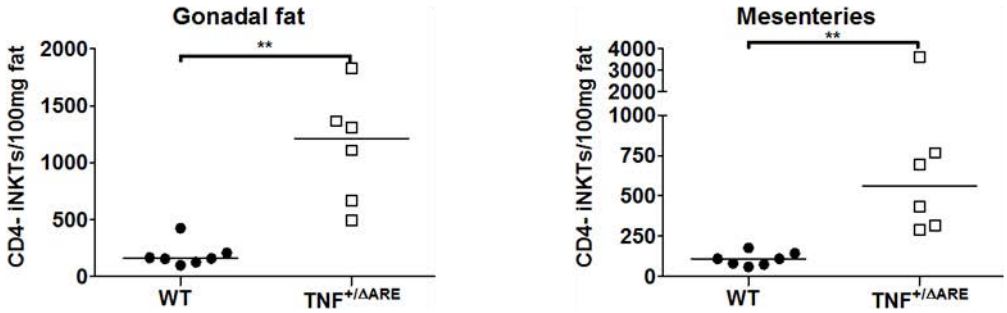
Gonadal fat
Mesenteries
CD4- iNKTs/100mg fat
2000
1500
1000
500
0
4000
3000
2000
1000
750
500
250
**
WT
TNF+/ΔARE

Figure 4.11: Adipose tissue T cell composition in WT and TNF$^{+/\Delta ARE}$ mice

Cells were isolated from the gonadal fat and mesenteries of adult male WT and TNF mutant TNF$^{+/\Delta ARE}$ mice (both on C57BL/6J background) as described in Materials and Methods. The T cell composition was determined by flow cytometry, as demonstrated previously. Data for each group was obtained from four technical repeats.

Each data point (n=7, 6 for WT and TNF$^{+/\Delta ARE}$ animals respectively) represents an individual sample with a line indicating the median value. Statistical significance was determined using a Mann-Whitney two-tailed T test, *p<0.05, **p<0.01, ***p<0.001 and ****p<0.0001.

A) As in Figure 4.10A, FACS plots showing representative T cell composition in gonadal fat (left) and mesenteries (right) from both WT (top) and TNF$^{+/\Delta ARE}$ (bottom) animals (pre-gated on live CD45.2$^+$ lymphocytes based on FSC and SSC profile and a viability marker). Numbers indicate percentage of events in each gate.

B) Graph showing adjusted number of CD4$^+$ cells (number CD4$^+$ cells/100mg fat) in gonadal fat and mesenteries from WT and TNF$^{+/\Delta ARE}$ animals (gated on CD45.2$^+$live/dead$^-$intraCD3$^+$CD4$^+$α-gal-cer$^-$ cells).

C) Graph showing adjusted number of regulatory T cells (number Tregs/100mg fat) in gonadal fat and mesenteries from WT and TNF$^{+/\Delta ARE}$ animals (gated on CD45.2$^+$live/dead$^-$intraCD3$^+$CD4$^+$α-gal-cer$^-$Foxp3$^+$ cells).

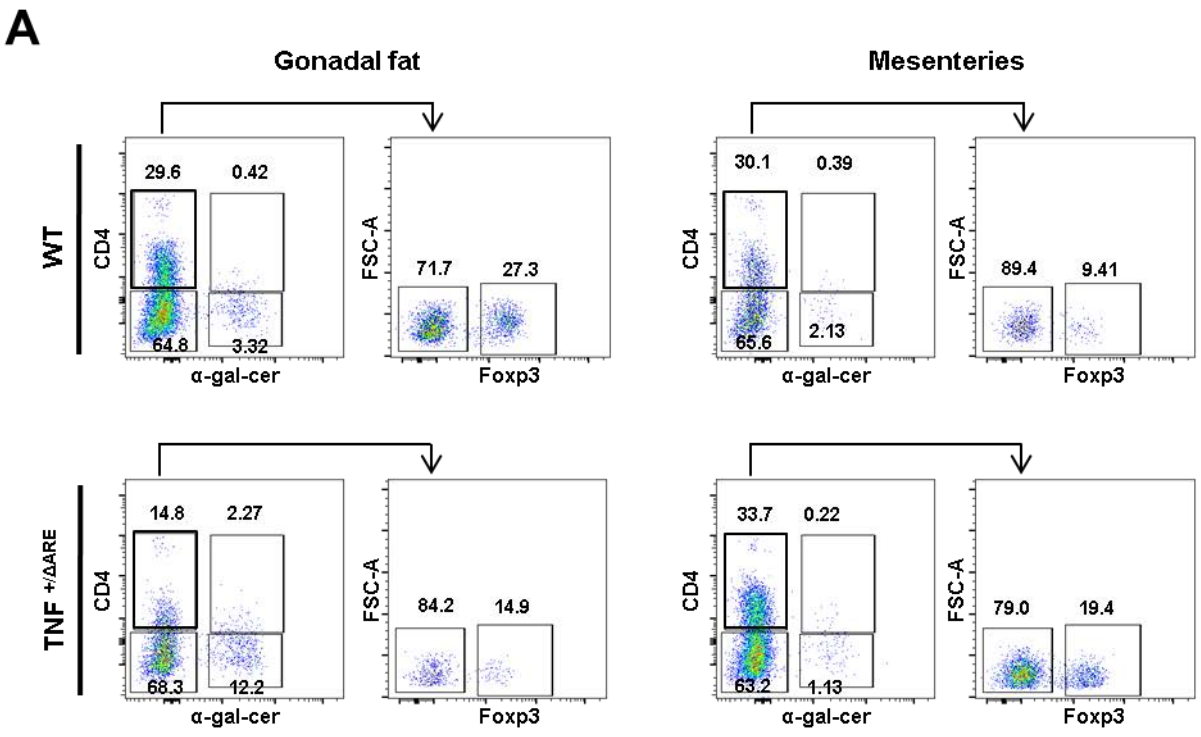
A
Gonadal fat
Mesenteries
WT
TNF +/ΔARE
CD4
α-gal-cer
FSC-A
Foxp3
29.6
0.42
64.8
3.32
71.7
27.3
30.1
0.39
65.6
2.13
89.4
9.41
14.8
2.27
68.3
12.2
84.2
14.9
33.7
0.22
63.2
1.13
79.0
19.4

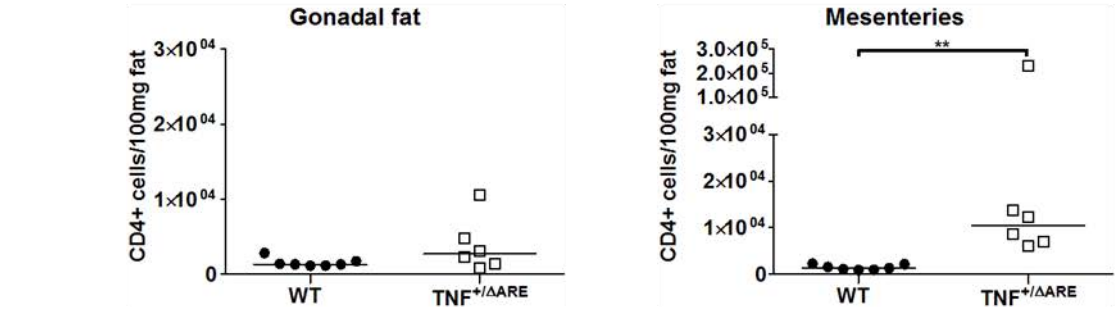
B
Gonadal fat
Mesenteries
CD4+ cells/100mg fat
WT
TNF+/ΔARE
**

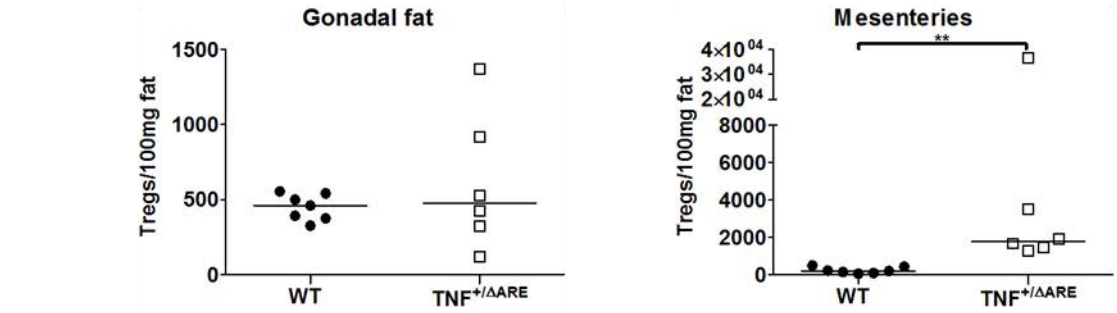
C
Gonadal fat
Mesenteries
Tregs/100mg fat
WT
TNF+/ΔARE
**

Figure 4.12: Adipose tissue ILC2 phenotype in WT and TNF$^{+/\Delta ARE}$ mice

Cells were isolated from the gonadal fat and mesenteries of adult male WT and TNF$^{+/\Delta ARE}$ mice (both on C57BL/6J background) as described in Materials and Methods. The ILC2 phenotype was determined by flow cytometry as described in Materials and Methods. Data for each group was obtained from four technical repeats.

Each data point (n=9, 6 for WT and TNF$^{+/\Delta ARE}$ animals respectively) represents an individual sample with a line indicating the median value. Statistical significance was determined using a Mann-Whitney two-tailed T test, *p<0.05, **p<0.01, ***p<0.001 and ****p<0.0001.

A) FACS plots showing representative ILC2 phenotype in gonadal fat (left) and mesenteries (right) from both WT (top) and TNF$^{+/\Delta ARE}$ (bottom) animals (pre-gated on live CD45.2$^+$ lymphocytes based on FSC and SSC profile and a viability marker). Numbers indicate percentage of events in each gate.

B) Histogram showing representative KLRG1 staining in gonadal fat (left panel) or mesenteries (right panel) isolated from TNF$^{+/\Delta ARE}$ (red lines) or WT (blue lines) animals. Vertical dotted black line indicates positive staining. Solid lines show ILC2 staining (CD45.2$^+$live/dead$^-$IL-7Rα$^+$Lin$^-$intraCD3$^-$ST2$^+$ICOS$^{+/-}$ cells), dotted lines show negative control staining (CD45.2$^+$live/dead$^-$IL-7Rα$^-$ Lin$^+$intraCD3$^-$ cells). Numbers indicate the percentage of KLRG1$^+$ cells.

C) Graph showing the percentage of ILC2s expressing KLRG1 in gonadal fat and mesenteries from WT and TNF$^{+/\Delta ARE}$ mice (gated on CD45.2$^+$live/dead$^-$ IL-7Rα$^+$Lin$^-$intraCD3$^-$ST2$^+$ICOS$^{+/-}$KLRG1$^+$ cells). For mesenteries n=8, 6 for WT and TNF$^{+/\Delta ARE}$ animals respectively.

D) Graph showing the expression of KLRG1 on the surface of ILC2s in gonadal fat and mesenteries from WT and TNF$^{+/\Delta ARE}$ mice (gated on CD45.2$^+$live/dead$^-$ IL-7Rα$^+$Lin$^-$intraCD3$^-$ST2$^+$ICOS$^{+/-}$KLRG1$^+$ cells). For mesenteries n=8, 6 for WT and TNF$^{+/\Delta ARE}$ animals respectively.

E) Graph showing the expression of ST2 on the surface of ILC2s in gonadal fat and mesenteries from WT and TNF$^{+/\Delta ARE}$ mice (gated on CD45.2$^+$live/dead$^-$ IL-7Rα$^+$Lin$^-$intraCD3$^-$ST2$^+$ICOS$^{+/-}$ cells). For mesenteries n=8, 6 for WT and TNF$^{+/\Delta ARE}$ animals respectively.

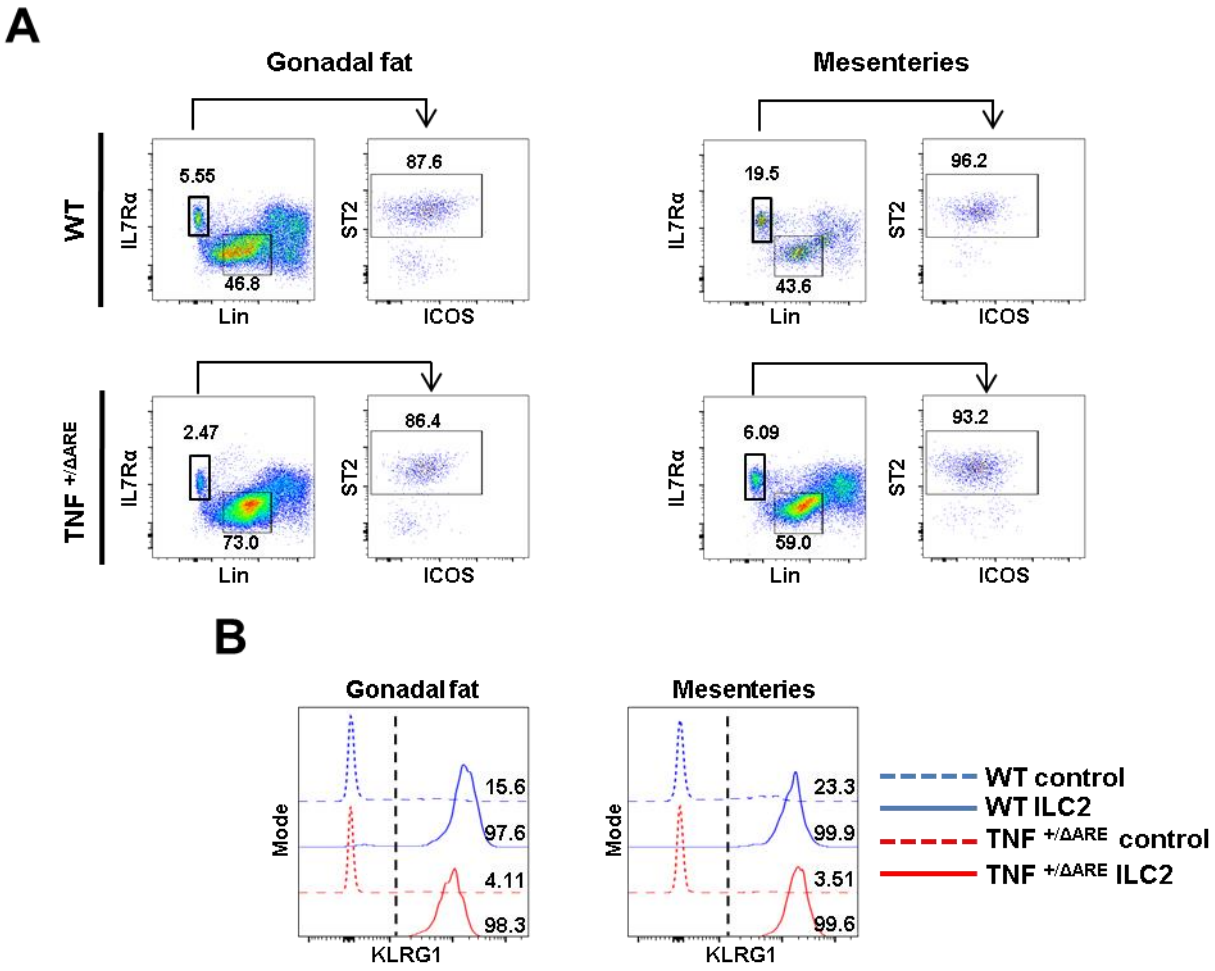
A
Gonadal fat
Mesenteries
WT
TNF +/ΔARE
IL7Rα
Lin
ST2
ICOS
5.55
46.8
87.6
19.5
43.6
96.2
2.47
73.0
86.4
6.09
59.0
93.2
B
Gonadal fat
Mesenteries
Mode
KLRG1
15.6
97.6
4.11
98.3
23.3
99.9
3.51
99.6
WT control
WT ILC2
TNF +/ΔARE control
TNF +/ΔARE ILC2
C
Gonadal fat
Mesenteries
% of ILC2 KLRG1+
WT
TNF+/ΔARE
E
Gonadal fat-ST2
Median Fluorescence (ST2)
D
Gonadal fat-KLRG1
Mesenteries-KLRG1
Median Fluorescence (KLRG1)
Mesenteries-ST2

4.4. SUMMARY

Crosstalk between stromal cells and immune cells, through mediators such as cytokines, are vital in determining the cellular composition of tissues. Likewise, the immune cell composition of tissues, and the resulting plethora of anti-inflammatory and pro-inflammatory signals which they produce, also has an important role in the resulting physiology of the tissues. One such example of this is in obesity, where pro-inflammatory signals drive the influx of cells, which amplifies inflammation within the tissue and results in metabolic dysregulation (Hotamisligil *et al.*, 1993, Leff and Granneman, 2010, Ouchi *et al.*, 2011, Kang *et al.*, 2016). This indicates that the immune cell composition, and the inflammatory balance within tissues, can therefore have an impact on immune responses within ATs. Thus, signals which control coordination between stromal cells and immune cells, and therefore control cellular composition and phenotype in ATs, were investigated.

Previous results indicated that ILC2s isolated from AT had both a higher expression of ST2 (see chapter 3.3.1) and a higher production of cytokines (see chapter 3.3.3) than MLN derived ILC2s. To determine the importance of IL-33 signals in the induction of ILC2 derived cytokines, cells from ATs of WT and IL-33 deficient (IL-33$^{cit/cit}$) were stimulated *ex vivo* and the ILC2 cytokine production was compared between animals. There were no differences in the percentages or MFI of IL-5 and IL-13 between WT and IL-33$^{cit/cit}$ ILC2s. In addition to this, there were no differences in cytokine production between ILC2s from the MLN and gonadal fat of WT and IL-33$^{cit/cit}$ mice. Although there was a statistically significant reduction in percentage of IL-5^{+}IL-13^{+} ILC2s isolated from the mesenteries of IL-33$^{cit/cit}$ mice following *ex vivo* stimulation, this difference was small. Other groups have reported ST2 expression is

independent of type-2 cytokine production, as ST2 expression was unaffected in mice deficient in IL-4, IL-5, IL-10 or IL-13, suggesting that ST2 provides an early signal in cytokine production (Lohning *et al.*, 1998, Griesenauer and Paczesny, 2017). However, in addition to IL-33, a number of signals which induce ILC2 cytokine expression have been identified including IL-9, TSLP, IL-25 and PGD_2 (Fort *et al.*, 2001, Barlow *et al.*, 2013, Barnig *et al.*, 2013, Doherty *et al.*, 2013, Han *et al.*, 2017, Rauber *et al.*, 2017). Thus, whilst data from others has demonstrated that IL-33 is the most potent activator of ILC2 cytokine production (Barlow *et al.*, 2013), it is conceivable that some redundancy exists in the signals that elicit cytokine production from ILC2s, which may be why no discernible differences were observed in the data from gonadal fat and MLN shown here. The fact that a difference was seen in the mesenteries and not in the gonadal fat or MLN of IL-$33^{cit/cit}$ could be due to variances in expression of these other cytokine-inducing signals between the different tissues examined. In conclusion, the data shown here suggests that, at least in gonadal fat and MLN, IL-33 signalling is dispensable for ILC2 cytokine production, but does not rule out that increased ST2 expression by AT ILC2s endows these ILC2s with a greater capacity for cytokine production. Further examination is required to confirm whether this redundancy in cytokine-inducing signals exists *in vivo*. Moreover, further models, such as *in vitro* or *in vivo* models which specifically alter the expression of ST2, are required to characterise the importance of ST2 expression in AT ILC2 cytokine production.

TNF is a key pro-inflammatory molecule with many disparate effects. Research by others has demonstrated a role for TNF and TNFR signalling in formation of FALC and that these FALC act as sites for the development of innate and adaptive

immunity, and thus can contribute to immune responses during infection and inflammation (Moro *et al.*, 2010, Benezech *et al.*, 2015, Jackson-Jones *et al.*, 2016). To further investigate the effects of TNFR signalling in controlling AT immune cell composition, ATs were examined in both the absence of TNFR signalling and in the overexpression of TNF. Consistent with the results reported by Bénézech *et al*. (Benezech *et al.*, 2015), an increased number of FALC were observed in the mesenteries of $TNF^{+/\Delta ARE}$ mice, and a decreased number in the mesenteries of $p55/p75^{-/-}$ animals. These trends were also replicated in gonadal fat for both mutant strains and for the omentum of $p55/p75^{-/-}$ mice. Whilst the mass of all three tissues was increased in $p55/p75^{-/-}$ mice, the mass of gonadal fat and mesenteries was decreased in $TNF^{+/\Delta ARE}$ mice. TNFR signalling has been reported to block adipogenic differentiation of precursor cells (Chae and Kwak, 2003, Cawthorn *et al.*, 2007). Additionally, a study by Kim *et al.* noted hypothalamic release of TNF during bacterial infection resulted in increased lipolysis (Kim *et al.*, 2015b). This could explain trends observed in tissue mass. Moreover, consistent with this report, an increase in the number of total lymphocytes was also noted in AT and MLN of $TNF^{+/\Delta ARE}$ mice, as compared to WT mice. Surprisingly, whilst there was a slight decrease in the total cellularity of mesenteries from $p55/p75^{-/-}$ animals compared to WTs, the MLN from $p55/p75^{-/-}$ animals contained four times more total cells (data shown in the appendix). This finding is in contrast to the findings of Peschon *et al.*, who indicate that the cellularity of thymi and peripheral lymphoid organs from these animals was comparable to control animals (Peschon *et al.*, 1998). The reasons for this are unclear but these differences could be attributed to tissue specific differences in the

importance of TNFR1 and 2 in delivering survival or apoptotic signals (Locksley *et al.*, 2001).

In p55/p75$^{-/-}$ animals an increase in the number of CD4^{+} T cells and Tregs was seen in the gonadal fat, whilst a decrease in the number of CD4^{-} iNKTs was noted in the mesenteries, when compared to WT animals, although the change in iNKT number was very small. In contrast, TNF$^{+/\Delta ARE}$ mice had almost 8 fold more CD4^{-} iNKT cells in the gonadal fat compared with WT animals. Results published by Bénézech *et al*. indicate that iNKT are partially required for the formation of FALC and, by using p55/p75$^{-/-}$ animals, show that TNFR signalling in both stromal cells and iNKT is required for FALC formation in response to inflammation (Benezech *et al.*, 2015). As such, there may be a link between the requirement of iNKT in FALC formation and the increase seen here in the number of iNKT cells in the mesenteries of TNF$^{+/\Delta ARE}$ mice, which have a greater number of FALC than WT counterparts. However, it is surprising that an overall change in iNKT number was not also seen in the mesenteries of TNF$^{+/\Delta ARE}$ animals. One possible cause of these tissue specific differences between gonadal fat and mesenteries could be due to the different quantity of FALC in these tissues. Our own unpublished data indicates that when FALC were removed from tissues by dissection, the ILC composition of the ATs was unaffected, suggesting that, in WT mice, the contents of FALC have a minimal impact on the proportions of immune cells in ATs as a whole. However, this may not be true in conditions where FALC numbers are increased, such as during infection or inflammation. Thus, a more elegant model of specifically preventing FALC formation, such as genetic deletion, is required to fully explore this possibility.

No differences were observed in the number of total ILCs and ILC2s in ATs of p55/p75$^{-/-}$vs. WT mice and TNF$^{+/\Delta ARE}$ vs. WT mice, suggesting that these cells do not respond to signals from TNFR signalling for survival or apoptosis.

ILC2 isolated from p55/p75$^{-/-}$ gonadal fat had a lower expression of KLRG1 compared to WT ILC2s, whilst ILC2s from mesenteries and MLN of TNF$^{+/\Delta ARE}$ mice had a higher expression KLRG1 than WT ILC2s. Taken together this could indicate a role of TNFR signalling in controlling ILC2 KLRG1 expression, however, the functional significance of this is unclear without further knowledge of the role KLRG1 plays in ILC2 biology, and also the change in expression was minimal. Finally, ST2 expression on ILC2s was higher in the gonadal fat of p55/p75$^{-/-}$ animals than WT animals, further implying that TNFR signals may alter ILC2 phenotype.

The microbiota are thought, in part, to be required for early *de novo* FALC formation under non-inflammatory conditions, as demonstrated by the notable reduction of FALC in germ free mice (Benezech *et al.*, 2015). The signals through which the microbiota drive this FALC formation are currently unknown, however it is likely that colonisation of the gut during early development in mice results in signalling, such as the production of TNF, between stromal and immune cells. Finally, whether the microbiota plays a role in inflammation-induced FALC formation requires investigation.

In conclusion, consistent with data published by others (Benezech *et al.*, 2015), TNF signalling induced the formation of FALC. In line with their role in FALC formation, CD4^{-} iNKT were increased in the gonadal fat, but not the mesenteries, of TNF$^{+/\Delta ARE}$ mice. TNF overexpression also appeared to induce changes in ILC2 phenotype but further investigation is required to fully elucidate this.

5. MEASURING IMMUNE RESPONSES IN ADIPOSE TISSUES

5.1. INTRODUCTION

In chapters 3 and 4 the immune cell composition of mouse ATs was characterised and some investigation into signals which control the immune cell composition was performed. As previously mentioned, ATs are routinely found in close association with SLT (Pond, 2002). SLTs are important sites for initiating adaptive immune responses. Activated APCs migrate from peripheral sites in the lymph and enter the LN through afferent lymphatics (Randolph *et al.*, 2005, Acton *et al.*, 2012, Bajenoff, 2012). Stromal cells called FRCs and FDCs then facilitate the optimal interaction of T cells and B cells respectively with APCs in specialised areas known as the T zone and B cell follicles (Forster *et al.*, 1996, Forster *et al.*, 1999, Bajenoff *et al.*, 2006, Link *et al.*, 2007, Wang *et al.*, 2011, Chang and Turley, 2015). This results in activation of T and B cell responses. The crucial role of SLT in initiating adaptive immune responses, and the co-localisation of ATs led to the hypothesis that ATs play a role in immune responses (Pond, 2002). Research by Bénézech *et al.,* indicated that under inflammatory conditions, namely overexpression of TNF, tertiary lymphoid structures (FALC) are formed within ATs (Benezech *et al.*, 2015). Moreover, Bénézech *et al.* further demonstrated that these FALC were enriched for B1 cells and the number of FALC in response to peritoneal inflammation induced by immunisation with the yeast glucan zymosan (Benezech *et al.*, 2015). More recent work by the same author also showed increased lymphoid cluster formation and the production of IgM by lymphoid cluster-associated B cells in response to the pleural nematode *Litomosoides sigmodontis* and in response to lung inflammation following infection with *Alternaria alternata* (Jackson-Jones *et al.*, 2016). As discussed in chapter 1.4.3, FALC and MS

appear to be analogous structures. Taken together, both the close anatomical association of SLTs and ATs, and also the inflammation-induced formation of tertiary lymphoid tissues within ATs, which support local B cell proliferation, substantiates the hypothesis that ATs may play a role in initiating, or maintaining adaptive immune responses. In order to explore this further, it was necessary to determine an appropriate infection model based on the ATs analysed throughout this study. Helminth infection was determined to be the best model for studying immune responses within peritoneal ATs, as outlined below.

Helminth infections are the most common disease reported in humans from developing countries (Hotez *et al.*, 2008). In order to further the understanding of the immune cell response to these parasites, and to develop methods to treat helminth infections, a number of murine models of intestinal helminth infection have been established, the predominant models using the natural rodent parasites *Nippostrongylus brasiliensis* and *Heligmosomoides polygyrus* (Monroy and Enriquez, 1992, Camberis *et al.*, 2003).

H.polygyrus is an intestinal nematode naturally found within mice. Upon ingestion, the infectious stage 3 larvae (L3 larvae) embed into the duodenum of the SI within 24 hours, where they mature to adult worms by undergoing two stages of moulting in the process (L4 stage). L4 larvae emerge into the intestinal lumen at day seven to eight post infection (Monroy and Enriquez, 1992, Camberis *et al.*, 2003, Maizels *et al.*, 2012, Reynolds *et al.*, 2012). At day eight to ten post infection, following mating, the adult parasites produce eggs. These eggs can be found in the faeces and used to isolate and culture *H.polygyrus* larvae to L3 stage for use in animal models (Monroy and Enriquez, 1992, Camberis *et al.*, 2003, Reynolds *et al.*, 2012). Depending on the

genetic background (see below), full eradication of *H.polygyrus* larvae can occur anywhere from eight weeks to many months post infection (Wahid and Behnke, 1993, Camberis *et al.*, 2003).

In contrast to *H.polygyrus*, *N.brasiliensis* L3 larvae initially infect the lungs of host animals, where they mature to the L4 stage after 24 hours, before migrating to the SI two to three days post infection (Monroy and Enriquez, 1992, Camberis *et al.*, 2003, Maizels *et al.*, 2012). Eggs are produced by adult worms at day six to nine post infection and the worms are usually fully cleared from the host by day eleven post infection (Monroy and Enriquez, 1992, Camberis *et al.*, 2003, Filbey *et al.*, 2014).

It is important to note that genetic background, gender and the age of mice used have all been shown to have an impact on the time taken for clearance of both *H.polygyrus* and *N.brasiliensis* (Monroy and Enriquez, 1992, Wahid and Behnke, 1993, Camberis *et al.*, 2003, Filbey *et al.*, 2014). Female mice clear both infections faster than their male counterparts (Van Zandt *et al.*, 1973, Monroy and Enriquez, 1992, Wahid and Behnke, 1993, Camberis *et al.*, 2003, Filbey *et al.*, 2014). Furthermore, younger mice and animals on the BALB/c background clear both helminth infections faster than males and animals on the C57BL/6J background (Van Zandt *et al.*, 1973, Monroy and Enriquez, 1992, Wahid and Behnke, 1993, Camberis *et al.*, 2003, Filbey *et al.*, 2014, Morimoto *et al.*, 2015). Differences in rate of clearance between BALB/c and C57BL/6J animals are thought to be due to the Th2 bias of BALB/c animals, as the immune response to these helminths requires Th2-mediated immunity, as detailed below (Maizels *et al.*, 2012, Reynolds *et al.*, 2012, Filbey *et al.*, 2014).

Despite the notable differences in the life cycle of *H.polygyrus* and *N.brasiliensis* detailed above, the immunological response to these parasites within mice appears to be broadly similar, as would be expected, given they are taxonomically related. Initial studies revealed that immune responses to both *N.brasiliensis* and *H.polygyrus* involve expression of Th2-associated cytokines IL-4, IL-5 and IL-13 by cells within the MLN and SI (Urban *et al.*, 1995, Camberis *et al.*, 2003, Price *et al.*, 2010, Neill and McKenzie, 2011, Maizels *et al.*, 2012, Reynolds *et al.*, 2012, Filbey *et al.*, 2014, Nair and Herbert, 2016, Pelly *et al.*, 2016). This was also found to be the case in human helminth infections (Turner *et al.*, 2003, Jackson *et al.*, 2004). Treating *N.brasiliensis* infected animals with IL-12, which drives Th1 differentiation and cytokine production, led to a delay in worm clearance (Finkelman *et al.*, 1994). Given that Th1 cytokines directly counteract Th2 cytokines, this finding further illustrates the importance of Th2 cytokines in clearance of helminths. Effector immune cells downstream of these Th2 cytokines include B cells, macrophages and eosinophils (Reynolds *et al.*, 2012, Esser-von Bieren *et al.*, 2013). Whilst B cells produce IgE in response to IL-4, eosinophils are directly responsible for the killing and clearance of helminths in an IL-5 dependent manner (Reynolds *et al.*, 2012, Esser-von Bieren *et al.*, 2013). Finally, IL-13 induces increased mucus production, which helps facilitate worm clearance (Hashimoto *et al.*, 2009).

Although similarities exist in the immune response to helminths, as highlighted above, some differences in the relative contribution of different immune cell subsets have been established. Whilst IL-4 deficient mice had reduced clearance of worms in *H.polygyrus* infections, *N.brasiliensis* clearance was only reduced in mice deficient in the IL-4 receptor (IL-4Rα) and signal transducer and activator of transcription 6

(STAT6), and not in IL-4 deficient mice (Urban *et al.*, 1991, Urban *et al.*, 1998, Camberis *et al.*, 2003). This suggests a greater dependence of IL-4 in clearance of *H.polygyrus* whilst *N.brasiliensis* immunity shows redundancy of IL-4 and IL-13, which both signal through IL-4Rα (Urban *et al.*, 1998). Interestingly IL-4 treatment in *H.polygyrus* increased the rate of worm clearance even when anti-CD4 antibodies were administered, suggesting an additional innate contribution to this effect (Urban *et al.*, 1991). Through use of adoptive transfer models in T cell and cytokine deficient mice, more recent studies have identified these innate cells to be ILC2s, which also produce the canonical Th2 cytokines IL-4, IL-5 and IL-13 (Voehringer *et al.*, 2006, Price *et al.*, 2010, Neill and McKenzie, 2011, Pelly *et al.*, 2016). Finally, data by Hepworth *et al.* and Shimokawa *et al.* indicates that mast cells are also important in coordinating IL-25, IL-33 and TSLP production early in response to *H.polygyrus* and *N.brasiliensis* infection (Hepworth *et al.*, 2012, Shimokawa *et al.*, 2017). These epithelial cytokines are crucial for initiation of ILC2 responses.

The results discussed above have focused on the immune responses that occur in MLN and SI during helminth infection. However, there is a very limited range of research exploring how helminth infection alters the immune cell composition of ATs (Wu *et al.*, 2011, Moro *et al.*, 2016). Whilst Moro *et al.* demonstrate that adoptive transfer of ILC2s from mesentery-derived FALC were sufficient to induce goblet cell hyperplasia in $gc^{-/-}Rag2^{-/-}$ animals (these animals lack adaptive immunity and ILCs), the authors did not explore how these cells responded in ATs of WT animals following infection (Moro *et al.*, 2010). Recent research by Wu *et al.* demonstrated improved glucose tolerance in HFD-fed animals following infection with *N.brasiliensis* (Wu *et al.*, 2011). With further research into the mechanisms which drive this

process, this could be a potential therapeutic strategy not only for intervention of metabolic dysregulation and obesity, but also for other diseases where type two cytokine production may be therapeutically beneficial (Yang *et al.*, 2013, Guigas and Molofsky, 2015, Hussaarts *et al.*, 2015, Finlay *et al.*, 2016, Ramanan *et al.*, 2016). With this in mind, the changes in immune cell composition following helminth infection were investigated with the aim to progress the knowledge of how immune cells within ATs contribute to immune responses.

5.2. ADIPOSE TISSUE COMPOSITION AT DAY TEN FOLLOWING *HELIGMOSOMOIDES POLYGYRUS* INFECTION

Whilst the role of AT immune cells during inflammatory settings, such as in obesity, has been extensively studied (Weisberg *et al.*, 2003, Lumeng *et al.*, 2007, Wu *et al.*, 2007, Kintscher *et al.*, 2008, Odegaard *et al.*, 2008, Miller *et al.*, 2010, Lynch *et al.*, 2012, Satoh *et al.*, 2012, Schipper *et al.*, 2012, Molofsky *et al.*, 2013, Kang *et al.*, 2016, O'Neill and Pearce, 2016, Donninelli *et al.*, 2017, Man *et al.*, 2017), little is known about whether the immune cells within these tissues contribute to immune responses to local infections. The presence of tertiary lymphoid structures (FALC) within ATs which support B cell responses have been noted and these FALC increased in size and number following a variety of infectious and inflammatory challenges (Benezech *et al.*, 2015, Jackson-Jones *et al.*, 2016). Taken together, these data suggests that ectopic lymphoid structures within AT, and their immune cell components, might contribute to the initiation, or feed into the development of, immune responses in SLTs following infection or inflammation. To test these hypotheses the immune cell composition of ATs was examined following helminth infection. The best established animal models to study helminth infection use the

parasites *H.polygyrus* and *N.brasiliensis* (Camberis *et al.*, 2003). Whilst both helminths migrate to the SI, initiating an adaptive immune response in the MLN (the draining LN), *N.brasiliensis* initially migrates to the host lungs before migrating to the SI, resulting in an influx of immune cells in lungs (Camberis *et al.*, 2003). As the previous investigations within this thesis focuses on AT within the peritoneal cavity, further investigations were carried out using *H.polygyrus,* rather than *N.brasiliensis*. Furthermore, *H.polygyrus* is a natural murine parasite and the L3 larvae can be stored for many months at 4°C, whilst *N.brasiliensis* is a natural parasite of rats and the L3 larvae can only be viably maintained for a few weeks (Camberis *et al.*, 2003). Thus, *H.polygyrus* was used as a model in an attempt to decipher the contribution of AT-resident immune cells in the immune response to local infection.

Whilst it appears that MS of the omentum receive antigenic material by passive diffusion from the peritoneal cavity, research on how antigen enters the FALC is lacking (Meza-Perez and Randall, 2017). Recent work from my laboratory shows that MS and FALCs are located very close to collecting lymphatic vessels, or sitting on top of lymphatic capillaries, indicating that antigen diffusion from the lymphatic vasculature may reach the clusters and could possibly be a mechanism by which antigen reaches the FALC (Cruz-Migoni, S. unpublished observations, University of Birmingham, U.K.).

As described in chapter 5.1, *H.polygyrus* L4 stage larvae emerge from the intestinal wall into the intestinal lumen at roughly day seven post infection and produce eggs at around days eight to ten post infection (Camberis *et al.*, 2003). This coincides with the peak of the immune response, i.e. when the greatest number of responding immune cells is found in the draining LN, the MLN (Urban *et al.*, 1991, Monroy and

Enriquez, 1992, Wahid and Behnke, 1993, Urban *et al.*, 1995, Camberis *et al.*, 2003, Finney *et al.*, 2007, Price *et al.*, 2010, Wu *et al.*, 2011, Maizels *et al.*, 2012, Mackley *et al.*, 2015, Pelly *et al.*, 2016). For this reason, initial comparisons of the immune cell composition of ATs in infected and uninfected mice were performed at day ten post infection.

In this instance, to maximise the range of immune cell subsets studied within ATs, analysis of FALC number in ATs of infected and uninfected animals was performed separately from any other analysis, unlike previous analyses where FALC analysis was performed alongside FACS analysis of ATs (see chapter 4.3.1 and 4.3.2).

Whilst the number of MS was increased in the omentum of infected animals, no differences were seen in the number of FALC in the gonadal fat or mesenteries of control and infected animals at day ten post infection (Figure 5.1A). This could indicate that either antigen can reach tissues surrounding the SI, or that systemic signals are released into the surrounding tissue, leading to activation of tissue resident immune cells. However, when normalised to tissue weight, the number of MS in the omentum of infected animals was not significantly higher than in the control omenta (Figure 5.1B). Despite this, the MS number was higher in the majority of infected animals, when compared to control animals, so the lack of statistical significance may be due to insufficient numbers of animals used for this comparison. In addition to the above, when normalised to tissue weight, there was no significant differences in FALC number between the gonadal fat of control and infected animals but there was an increase in the number of FALC in the mesenteries of infected animals compared to control animals (Figure 5.1B). Although not statistically significant, the mass of the mesenteries from the majority of infected animals was

lower than the mass of this tissue when isolated from control animals (Figure 5.1C). In contrast, a small but statistically significant increase in the mass of the omentum from infected animals compared with controls was observed (Figure 5.1C). However, this difference may have only reached statistical significance due to outlying values in the infected animals, and thus is unlikely to indicate any biological relevance without further repeats to verify this trend.

As minimal changes were observed in gonadal fat FALC number or tissue mass, FACS analysis was focused on the immune cell composition of mesenteries. Consistent with reports that the MLN acts as the draining LN for the SI, a three-fold increase in total cellularity of the MLN was observed in infected mice compared with control animals (Figure 5.1D). The existence of an ongoing infection was also confirmed in by the presence of worms in the SI (Figure 5.1E). This is consistent with reports by other researchers at day seven post infection (Mackley *et al.*, 2015, Pelly *et al.*, 2016).

No statistically significant differences were observed in the number of total ILCs or ILC2 in the ATs of control and infected animals (Figure 5.2A-C). In spite of this, the number of ILC2s was marginally higher in the majority of mesenteries from infected mice when compared with control mice. Thus, following infection, there may be subtle changes in the number of ILCs in the mesenteries, but an absence of a sufficient number of animals meant that the statistical power to detect these changes was lacking. Unfortunately, access to both helminths and sufficient numbers of WT animals was limited, preventing repeats of the above experiments to increase animal number in each group.

Like ILCs, the number of $CD4^+$ cells and the number of Tregs were unchanged following infection (Figure 5.3A-C). Moreover, $CD4^+$ and $CD4^-$ iNKT cells in the mesenteries were similar in number between control and infected animals (Figure 5.3D-E). As such, the data suggests that the T cell compartment within ATs is not overtly changed in response to infection in surrounding tissues. However, subtle changes cannot be ruled out by the data.

The phenotype of ILC2s from ATs of control and infected animals was also examined at day ten post infection with *H.polygyrus*. No differences in the expression of ICOS or KLRG1 (percentage or MFI) were observed in mesentery ILC2s following infection (Figure 5.4A-G). Again, this data only rules out any obvious changes in these parameters and further repeats are required to confirm that subtle differences in ICOS or KLRG1 do not occur. In contrast, the expression of ST2 on the surface of ILC2s isolated from infected animals was half the expression seen on ILC2s from control animals (Figure 5.4H). Given that ST2 signalling is one of the mechanisms by which ILC2s are stimulated to produce cytokines, this decreased ST2 expression could mark a pathway by which ILC2s might be negatively regulated following activation. Taken together, this data suggests that ILC2s from AT may contribute to local immune responses, but might act earlier in the immune response than examined here.

Analysis of the MLN immune cell composition following infection with *H.polygyrus* is shown in the appendix (Figure 7.17-Figure 7.19).

Figure 5.1: FALC numbers and tissue mass at day ten following *H.polygyrus* infection

C57BL/6J males were either infected with *H.polygyrus* larvae (infected), or given PBS as a control, and the mesenteries and omentum were isolated ten days post infection (see Materials and Methods for details). Tissues were stained with antibodies against CD45 as described in the Materials and Methods section. FALC and MS numbers were enumerated using a fluorescent dissecting microscope. Data for each group was obtained from two technical repeats. N.B. data for A) and B) were obtained from the same set of experiments, whilst data for C-E) was generated from a different set of animals.

Each data point (n=7, 6 for control and infected animals respectively) represents an individual sample with a line indicating the median value. Statistical significance was determined using a Mann-Whitney two-tailed T test, *p<0.05, **p<0.01, ***p<0.001 and ****p<0.0001.

A) Graph showing adjusted total number of FALC/MS in gonadal fat, mesenteries and omentum from control and infected animals. For gonadal fat n=7, 5 and for omentum n=6, 4 control and infected animals, respectively.

B) Graph showing adjusted number of FALC (number FALC/100mg fat) in gonadal fat, mesenteries and omentum from control and infected animals. For gonadal fat n=7, 5 and for omentum n=6, 4 control and infected animals, respectively.

C) Graph showing mass of gonadal fat (left), mesenteries (right) and omentum (bottom) isolated from control and infected animals.

D) Graph showing total live cells in MLN from infected and control mice (gated on live/dead$^-$ cells). For control and infected animals, n=4, 5, respectively.

E) Graph showing worm burden of SI at day ten following *H.polygyrus* infection.

A

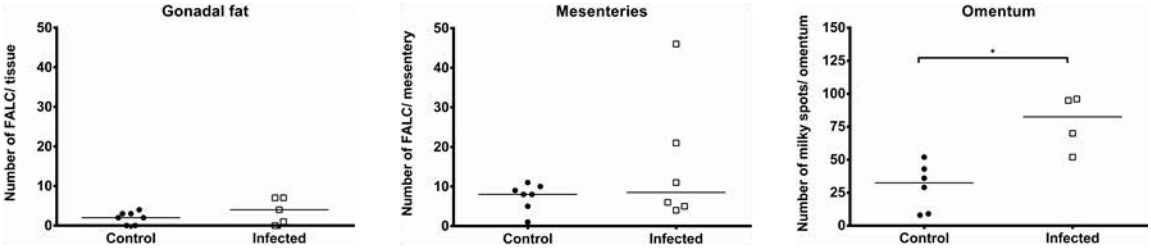
Gonadal fat
Number of FALC/ tissue
Control
Infected
Mesenteries
Number of FALC/ mesentery
Control
Infected
Omentum
Number of milky spots/ omentum
*
Control
Infected

B

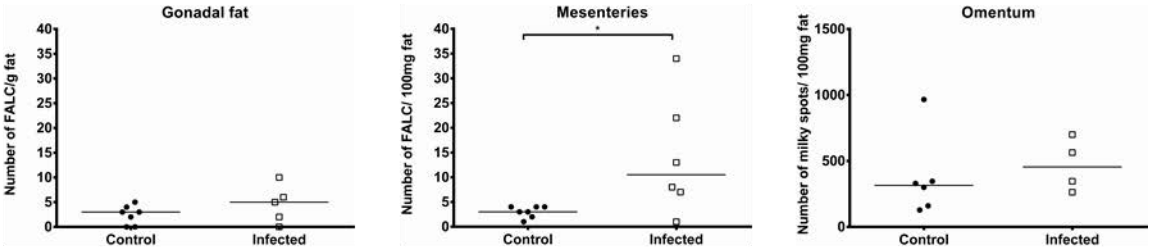
Gonadal fat
Number of FALC/g fat
Control
Infected
Mesenteries
Number of FALC/ 100mg fat
*
Control
Infected
Omentum
Number of milky spots/ 100mg fat
Control
Infected

C

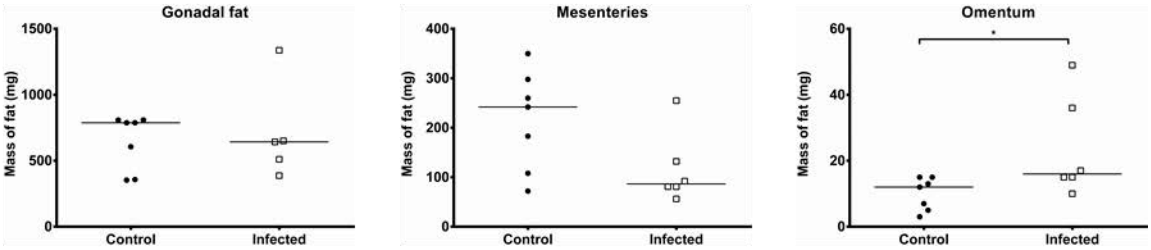
Gonadal fat
Mass of fat (mg)
Control
Infected
Mesenteries
Mass of fat (mg)
Control
Infected
Omentum
Mass of fat (mg)
*
Control
Infected

D

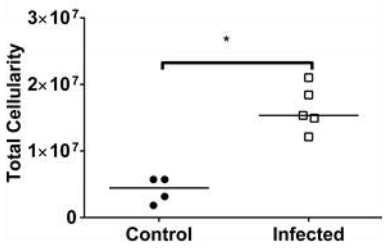
Total Cellularity
*
Control
Infected

E

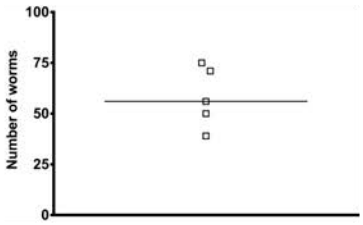
Number of worms

Figure 5.2: Adipose tissue ILC composition at day ten following *H.polygyrus* infection

C57BL/6J males were either infected with *H.polygyrus* larvae (infected), or given PBS as a control, and cells were isolated from mesenteries ten days post infection (see Materials and Methods for details). The ILC composition was determined by flow cytometry, as demonstrated previously. Data for each group was obtained from two technical repeats.

Each data point (n=4, 4 for control and infected animals respectively) represents an individual sample with a line indicating the median value. Statistical significance was determined using a Mann-Whitney two-tailed T test, *p<0.05, **p<0.01, ***p<0.001 and ****p<0.0001.

A) FACS plots showing representative ILC composition in mesenteries from both control (top) and infected (bottom) animals (pre-gated on live CD45.2$^+$ lymphocytes based on FSC and SSC profile and a viability marker). Numbers indicate percentage of events in each gate.

B) Graph showing adjusted total live cells (Total cellularity/100mg fat) in mesenteries from control and infected mice (gated on live/dead$^-$ cells).

C) Graph showing adjusted number of ILC2s (ILC2s/100mg fat) in mesenteries from control and infected mice (gated on live/dead$^-$CD45.2$^+$IL-7Rα$^+$Lin$^-$ intraCD3$^-$RORγt$^-$GATA-3$^+$ cells).

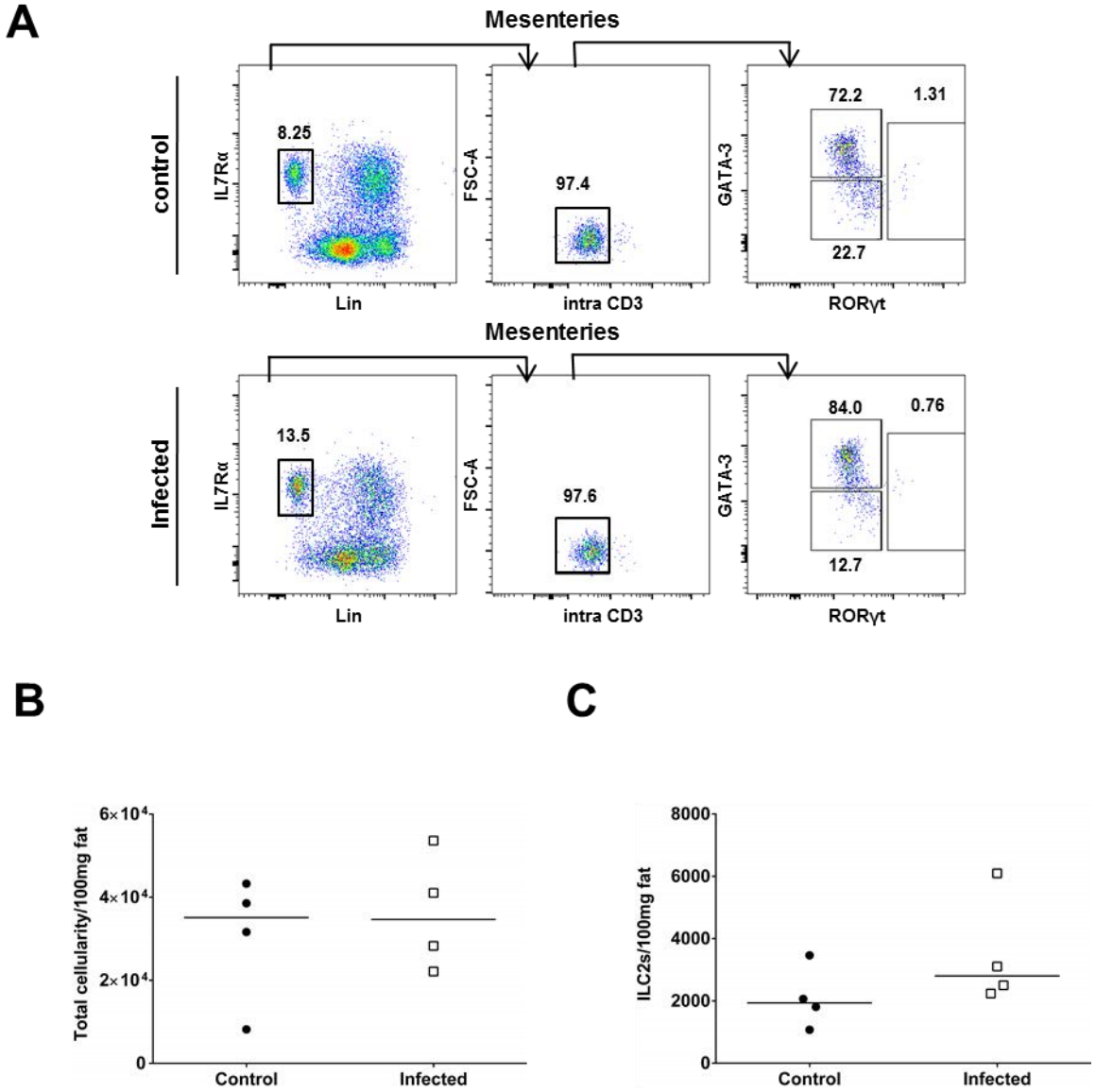
A
Mesenteries
control
IL7Rα
Lin
8.25
FSC-A
intra CD3
97.4
GATA-3
RORγt
72.2
1.31
22.7
Mesenteries
Infected
IL7Rα
Lin
13.5
FSC-A
intra CD3
97.6
GATA-3
RORγt
84.0
0.76
12.7
B
Total cellularity/100mg fat
6×10⁴
4×10⁴
2×10⁴
0
Control
Infected
C
ILC2s/100mg fat
8000
6000
4000
2000
0
Control
Infected

Figure 5.3: Adipose tissue T cell composition at day ten following *H.polygyrus* infection

C57BL/6J males were either infected with *H.polygyrus* larvae (infected), or given PBS as a control, and cells were isolated from mesenteries ten days post infection (see Materials and Methods for details). The T cell composition was determined by flow cytometry, as demonstrated previously. Data for each group was obtained from two technical repeats.

Each data point (n=4, 4 for control and infected animals respectively) represents an individual sample with a line indicating the median value. Statistical significance was determined using a Mann-Whitney two-tailed T test, *p<0.05, **p<0.01, ***p<0.001 and ****p<0.0001.

A) FACS plots showing representative T cell composition in mesenteries from both control (left) and infected (right) animals (pre-gated on live CD45.2$^+$ lymphocytes based on FSC and SSC profile and a viability marker). Numbers indicate percentage of events in each gate.

B) Graph showing adjusted number of CD4$^+$ cells (CD4$^+$cells/100mg fat) in mesenteries from control and infected mice (gated on CD45.2$^+$live/dead$^-$ intraCD3$^+$CD4$^+$α-gal-cer$^-$ cells).

C) Graph showing adjusted number of regulatory T cells (Tregs/100mg fat) in mesenteries isolated from control and infected mice (gated on CD45.2$^+$live/dead$^-$intraCD3$^+$CD4$^+$α-gal-cer$^-$FOXP3$^+$ cells).

D) Graph showing adjusted number of CD4$^+$ iNKT cells (CD4$^+$iNKTs/100mg fat) in mesenteries from control and infected mice (gated on CD45.2$^+$live/dead$^-$ intraCD3$^+$CD4$^+$α-gal-cer$^+$ cells).

E) Graph showing adjusted number of CD4$^-$ iNKT cells (CD4$^-$iNKTs/100mg fat) in mesenteries from control and infected mice (gated on CD45.2$^+$live/dead$^-$ intraCD3$^+$CD4$^-$α-gal-cer$^+$ cells).

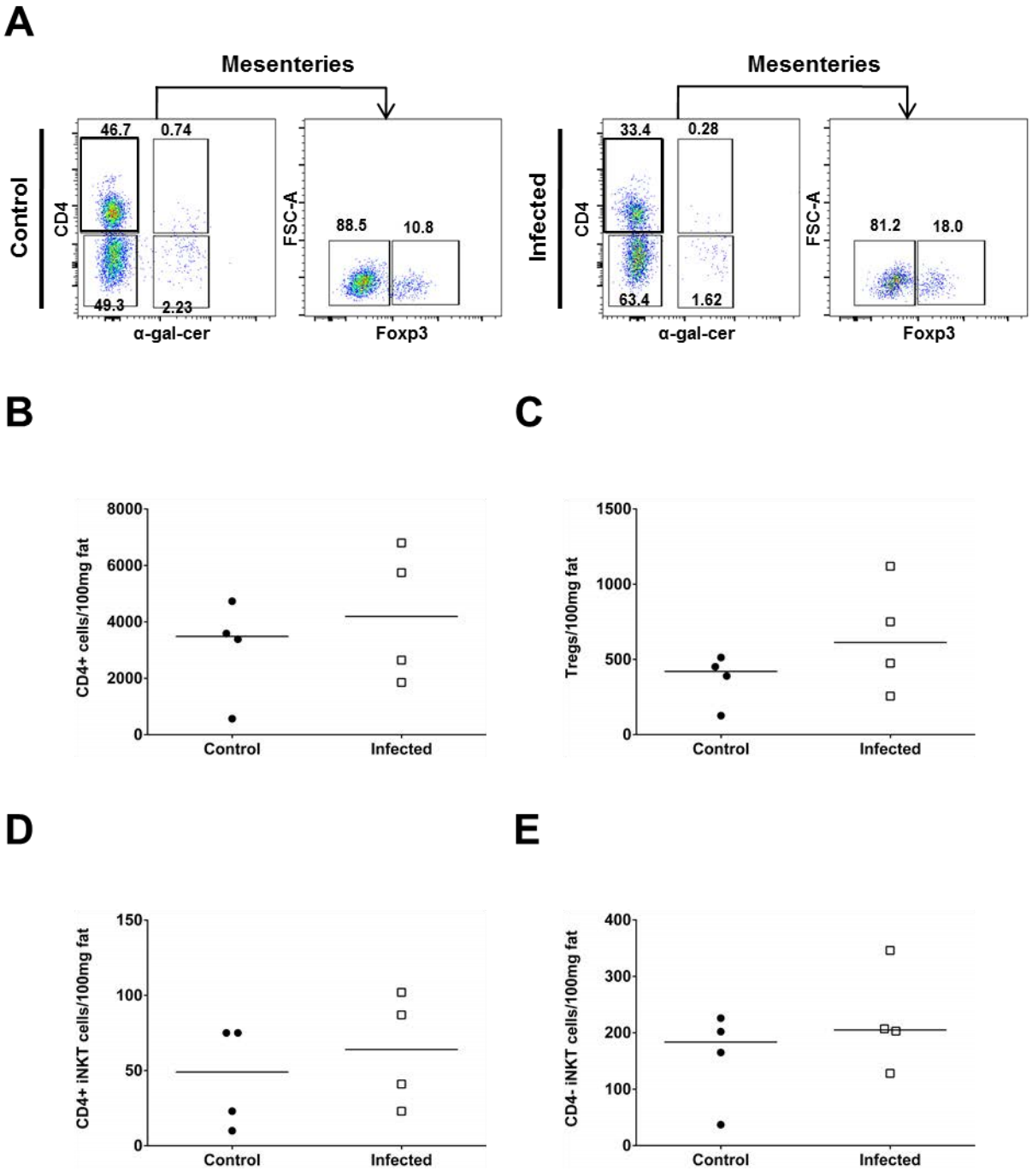
A
Mesenteries
Control
CD4
46.7
0.74
49.3
2.23
α-gal-cer
FSC-A
88.5
10.8
Foxp3
Mesenteries
Infected
CD4
33.4
0.28
63.4
1.62
α-gal-cer
FSC-A
81.2
18.0
Foxp3
B
CD4+ cells/100mg fat
8000
6000
4000
2000
0
Control
Infected
C
Tregs/100mg fat
1500
1000
500
0
Control
Infected
D
CD4+ iNKT cells/100mg fat
150
100
50
0
Control
Infected
E
CD4- iNKT cells/100mg fat
400
300
200
100
0
Control
Infected

Figure 5.4: Adipose tissue ILC2 phenotype at day ten following *H.polygyrus* infection

C57BL/6J males were either infected with *H.polygyrus* larvae (infected), or given PBS as a control, and cells were isolated from mesenteries ten days post infection (see Materials and Methods for details). The ILC2 phenotype was determined by flow cytometry, as demonstrated previously. Data for each group was obtained from two technical repeats.

Each data point (n=4, 4 for control and infected animals respectively) represents an individual sample with a line indicating the median value. Statistical significance was determined using a Mann-Whitney two-tailed T test, *p<0.05, **p<0.01, ***p<0.001 and ****p<0.0001.

A) FACS plots showing representative ILC2 staining in mesenteries from both control (top) and infected (bottom) animals (pre-gated on live CD45.2$^+$ lymphocytes based on FSC and SSC profile and a viability marker). Numbers indicate percentage of events in each gate.

B) Histogram showing representative ICOS staining in mesenteries isolated from infected (red line) or control (blue line) animals. Vertical dotted line indicates positive staining. Solid lines show ILC2 staining (gated on CD45.2$^+$live/dead$^-$ IL-7Rα$^+$Lin$^-$intraCD3$^-$ST2$^+$GATA-3$^+$ cells), dotted green line shows ICOS FMO control. Numbers indicate the percentage of ICOS$^+$ cells.

C) Histogram showing representative KLRG1 staining in mesenteries isolated from infected (red lines) or control (blue lines) animals. Vertical dotted line indicates positive staining. Solid lines show ILC2 staining (gated on CD45.2$^+$live/dead$^-$IL-7Rα$^+$Lin$^-$intraCD3$^-$ST2$^+$GATA-3$^+$ cells), dotted lines show KLRG1 negative control (gated onCD45.2$^+$live/dead$^-$IL-7Rα$^-$Lin$^+$intraCD3$^-$ cells). Numbers indicate the percentage of KLRG1$^+$ cells.

D) Graph showing percentage of ILC2s expressing ICOS in mesenteries from control and infected mice (gated on live/dead$^-$CD45.2$^+$IL-7Rα$^+$Lin$^-$intraCD3-ST2$^+$GATA-3$^+$ICOS$^+$ cells).

E) Graph showing expression of ICOS (median fluorescence) on the surface of ILC2 in mesenteries from control and infected mice (gated on live/dead$^-$ CD45.2$^+$IL-7Rα$^+$Lin$^-$intraCD3-ST2$^+$GATA-3$^+$ICOS$^+$ cells).

F) Graph showing percentage of ILC2s expressing KLRG1 in mesenteries from control and infected mice (gated on live/dead$^-$CD45.2$^+$IL-7Rα$^+$Lin$^-$intraCD3-ST2$^+$GATA-3$^+$KLRG1$^+$ cells).

G) Graph showing expression of KLRG1 (median fluorescence) on the surface of ILC2 in mesenteries from control and infected mice (gated on live/dead$^-$ CD45.2$^+$IL-7Rα$^+$Lin$^-$intraCD3-ST2$^+$GATA-3$^+$KLRG1$^+$ cells).

H) Graph showing expression of ST2 (median fluorescence) on the surface of ILC2 in mesenteries from control and infected mice (gated on live/dead$^-$ CD45.2$^+$IL-7Rα$^+$Lin$^-$intraCD3-ST2$^+$GATA-3$^+$cells).

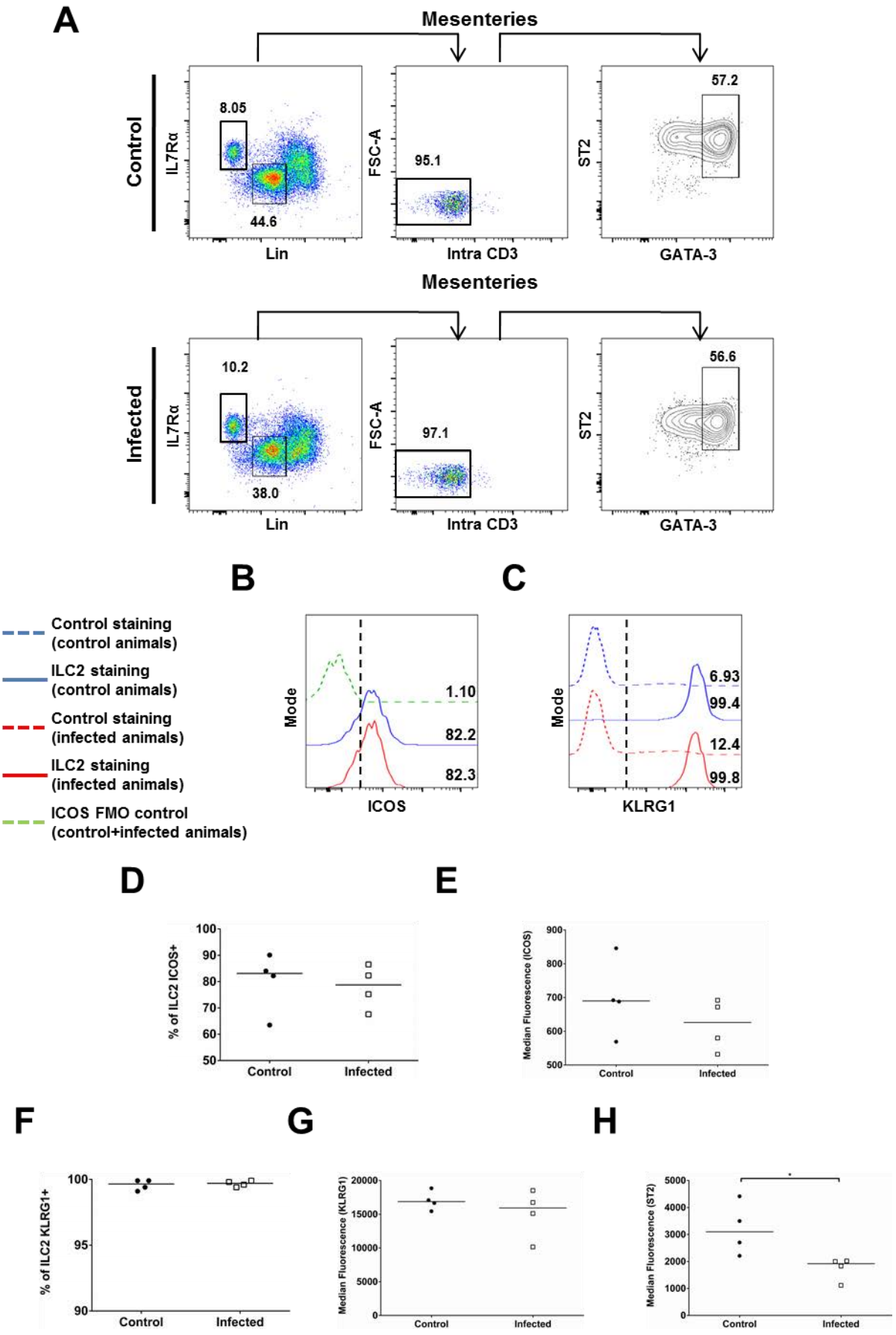
A
Mesenteries
Control
IL7Rα
8.05
44.6
Lin
FSC-A
95.1
Intra CD3
ST2
57.2
GATA-3
Mesenteries
Infected
IL7Rα
10.2
38.0
Lin
FSC-A
97.1
Intra CD3
ST2
56.6
GATA-3
B
C
Control staining (control animals)
ILC2 staining (control animals)
Control staining (infected animals)
ILC2 staining (infected animals)
ICOS FMO control (control+infected animals)
Mode
1.10
82.2
82.3
ICOS
Mode
6.93
99.4
12.4
99.8
KLRG1
D
E
% of ILC2 ICOS+
100
90
80
70
60
50
Control
Infected
Median Fluorescence (ICOS)
900
800
700
600
500
Control
Infected
F
G
H
% of ILC2 KLRG1+
100
95
90
Control
Infected
Median Fluorescence (KLRG1)
20000
15000
10000
5000
0
Control
Infected
Median Fluorescence (ST2)
5000
4000
3000
2000
1000
0
Control
Infected

5.3. ADIPOSE TISSUE COMPOSITION AT DAY FIVE FOLLOWING *HELIGMOSOMOIDES POLYGYRUS* INFECTION

In chapter 5.2 the AT immune composition was examined in animals infected with the parasite *H.polygyrus* and compared with uninfected control animals with the aim of determining the contribution of AT resident immune cells in local immune responses. Few differences were observed between control and infected animals, with the exception of an increased number of FALC and a decreased expression of ST2 by ILC2s in the mesenteries following infection. The latter result indicated a possible negative regulation pathway of ILC2s following activation. Based on this it was hypothesised that ILC2s from ATs may contribute to the immune responses to infection in local tissues at an earlier time point than day ten. Data by Pelly *et al.* indicates that ILC2 numbers were significantly increased in the MLN and SI of infected animals as early as day five post infection with *H.polygyrus* (Pelly *et al.*, 2016). For this reason the same analysis of AT immune composition was performed at day five post infection with *H.polygyrus*.

FALC/MS numbers in the mesenteries and omentum were compared between uninfected and infected animals five days post infection with *H.polygyrus*. Both the mesenteries and the omentum showed an increased number of FALC/MS in infected animals compared to control animals, with a four-fold difference in mesenteries and a two-fold difference in the omentum (Figure 5.5A). More FALC and MS were detected in the mesenteries and omentum of control animals at day five post infection compared with previous data at day ten post infection with *H.polygyrus* (Figure 5.1A and Figure 5.5B). It should be noted that a refinement in the technique for counting FALCs was used in the analysis of D5 post infection; initially FALC/MS numbers for samples at day ten post infection were counted following fixation and permeabilisation with paraformaldehyde and triton. However, it was subsequently

discovered that antibodies against CD45 could be used to directly stain for FALC and MS without prior fixation and permeabilisation. This technique was therefore applied to the analysis of FALC/MS number in samples from mice at day five post infection with *H.polygyrus,* but additional mice and helminths were not available to repeat this analysis using the refined technique on samples at day ten post infection.

When normalised to tissue weight there was still greater than a four-fold higher number of FALC in the mesenteries of infected animals at five days post infection with *H.polygyrus*, compared with control animals (Figure 5.5B). However, when normalised to tissue weight there was no difference in the number of MS between control and infected omenta (Figure 5.5B). One reason for this discrepancy could be an increased weight masking changes in MS number; whilst the mass of omentum isolated from infected mice was higher than controls, there was a large amount of variation and so this difference was not statistically significant (Figure 5.5C). As the bulk of the omentum in mice is predominantly MS (Cruz-Migoni and Caamano, 2016), it is conceivable that an increase in MS number, as seen in Figure 5.5A, could have a significant impact on the overall tissue weight.

As minimal changes were seen in the immune cell composition of gonadal fat following infection with *H.polygyrus* at day ten post infection, analysis of AT immune cell composition at day five post infection was focused on the mesenteries.

As seen at day ten post infection, at day five post infection with *H.polygyrus* a significant increase was observed in the total cellularity of MLN from infected mice, compared with their uninfected control, and worms were observable in the SI in comparable numbers to day ten post infection (Figure 5.5D-E). In addition, mesenteries isolated from infected animals had double the total cellularity of control animals (Figure 5.6A-B). The number of total ILCs and ILC2s was also higher in the mesenteries of infected animals, as compared with controls (Figure 5.6C-D). This

finding indicates that ILC2s within ATs are involved in the immune response to *H.polygyrus* in the local environment. As seen at day ten post infection, no differences were observed in the number of $CD4^+$ cells, Tregs, $CD4^+$ iNKT cells or $CD4^-$ iNKT cells in the mesenteries of control and infected animals at day five post infection with *H.polygyrus* (Figure 5.7A-E). This suggests that the T cell/iNKT compartment in ATs might not undergo changes during the immune response to *H.polygyrus* in surrounding tissues.

Finally, ILC2 phenotype was also investigated in the mesenteries of control and infected animals at day five post infection. ILC2s isolated from the mesenteries of infected animals had a higher proportion of ILC2s which were $ICOS^+$ and the expression of ICOS was also higher in these ILC2s, when compared with control-derived ILC2s (Figure 5.8B, D-E). Taken together with the previous data of an increased number of ILC2s in the mesenteries following infection, this data is suggestive of ILC2 activation within ATs following infection. In contrast, no changes were observed in the percentage of $KLRG1^+$ ILC2s, or the MFI of ILC2 KLRG1 expression when comparing control and infected animals (Figure 5.8C, F-G). The significance of this is unclear, as the precise role of KLRG1 expression on ILC2 function has not been fully elucidated. Finally, as seen at day ten post infection, ILC2s isolated from the mesenteries of infected animals had a lower expression of ST2 than control ILC2s when analysed five days post infection (Figure 5.8H). As before, this could illustrate a mechanism of negative regulation to limit ILC2 activation. This change in ST2 expression could be linked to the changes seen in ICOS, or could be independent.

Analysis of the MLN immune cell composition following infection with *H.polygyrus* is shown in the appendix (Figure 7.20-Figure 7.22).

Figure 5.5: FALC numbers and tissue mass at day five following *H.polygyrus* infection

C57BL/6J males were either infected with *H.polygyrus* larvae (infected), or given PBS as a control, and the mesenteries and omentum were isolated five days post infection (see Materials and Methods for details). Tissues were stained with antibodies against CD45 as described in the Materials and Methods section. FALC and MS numbers were enumerated using a fluorescent dissecting microscope. Data for each group was obtained from three technical repeats.

Each data point (n=6, 6 for control and infected animals respectively) represents an individual sample with a line indicating the median value. Statistical significance was determined using a Mann-Whitney two-tailed T test, *p<0.05, **p<0.01, ***p<0.001 and ****p<0.0001.

A) Graph showing number of FALC in mesenteries and omentum from control and infected animals.

B) Graph showing adjusted number of FALC (number FALC/100mg fat) in mesenteries and omentum from control and infected animals.

C) Graph showing mass of mesenteries and omentum isolated from control and infected animals.

D) Graph showing adjusted number of total viable cells in MLN from infected and control mice (gated on live/dead$^-$CD45.2$^+$ cells). n=7, 7 for control and infected animals, respectively.

E) Graph showing worm burden of SI at day five following *H.polygyrus* infection.

A

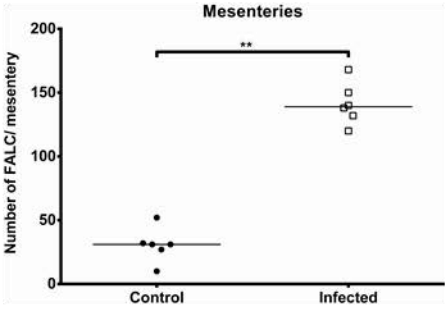
Mesenteries
Number of FALC/ mesentery
200
150
100
50
0
**
Control
Infected

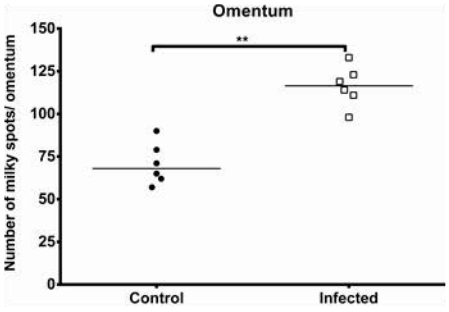
Omentum
Number of milky spots/ omentum
150
125
100
75
50
25
0
**
Control
Infected

B

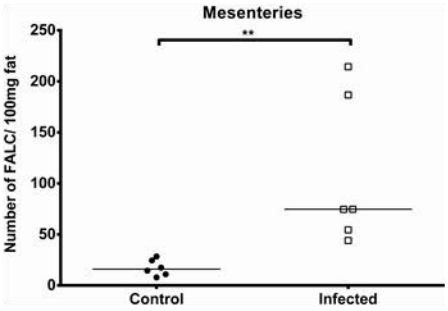
Mesenteries
Number of FALC/ 100mg fat
250
200
150
100
50
0
**
Control
Infected

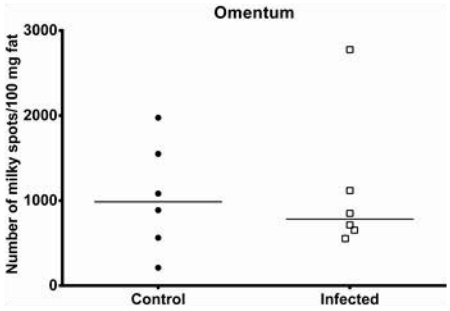
Omentum
Number of milky spots/100 mg fat
3000
2000
1000
0
Control
Infected

C

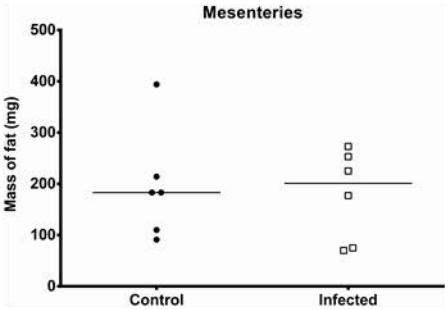
Mesenteries
Mass of fat (mg)
500
400
300
200
100
0
Control
Infected

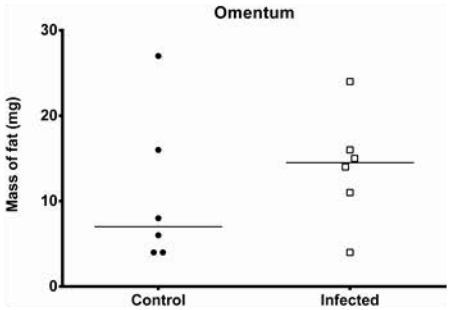
Omentum
Mass of fat (mg)
30
20
10
0
Control
Infected

D

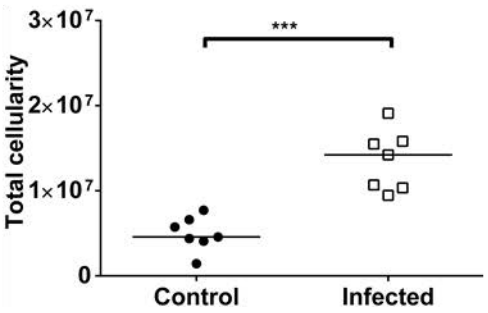
Total cellularity
3×10^7
2×10^7
1×10^7
0
***
Control
Infected

E


Number of worms
200
150
100
50
0

Figure 5.6: Adipose tissue ILC composition at day five following *H.polygyrus* infection

C57BL/6J males were either infected with *H.polygyrus* larvae (infected), or given PBS as a control, and cells were isolated from mesenteries five days post infection (see Materials and Methods for details). The ILC composition was determined by flow cytometry, as demonstrated previously. Data for each group was obtained from three technical repeats.

Each data point (n=6, 7 for control and infected animals respectively) represents an individual sample with a line indicating the median value. Statistical significance was determined using a Mann-Whitney two-tailed T test, *p<0.05, **p<0.01, ***p<0.001 and ****p<0.0001.

A) FACS plots showing representative ILC composition in mesenteries from both control (top) and infected (bottom) animals (pre-gated on live CD45.2$^+$ lymphocytes based on FSC and SSC profile and a viability marker). Numbers indicate percentage of events in each gate.

B) Graph showing adjusted number of viable cells (Total cellularity/100mg fat) in mesenteries from control and infected mice (gated on live/dead$^-$CD45.2$^+$ cells).

C) Graph showing adjusted number of total ILCs (total ILCs/100mg fat) in mesenteries from control and infected mice (gated on live/dead$^-$ CD45.2$^+$IL-7Rα$^+$Lin$^-$ cells).

D) Graph showing adjusted number of ILC2s (ILC2s/100mg fat) in mesenteries from control and infected mice (gated on live/dead$^-$CD45.2$^+$IL-7Rα$^+$Lin$^-$ intraCD3$^-$RORγt$^-$GATA-3$^+$ cells).

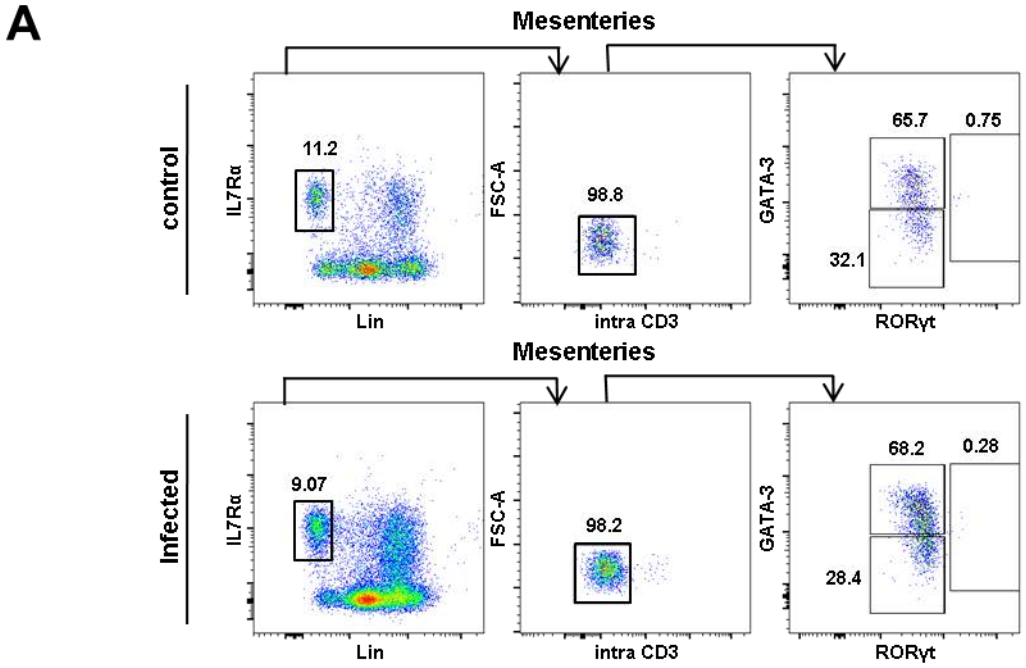
A
Mesenteries
control
IL7Rα
Lin
11.2
FSC-A
intra CD3
98.8
GATA-3
RORγt
65.7
0.75
32.1
Mesenteries
Infected
IL7Rα
Lin
9.07
FSC-A
intra CD3
98.2
GATA-3
RORγt
68.2
0.28
28.4

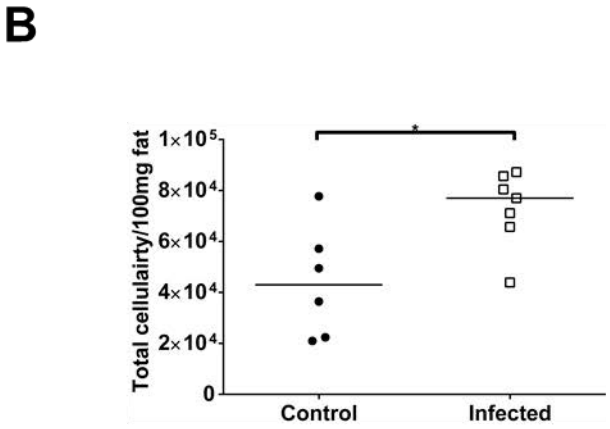
B
Total cellulairty/100mg fat
1×10⁵
8×10⁴
6×10⁴
4×10⁴
2×10⁴
0
*
Control
Infected

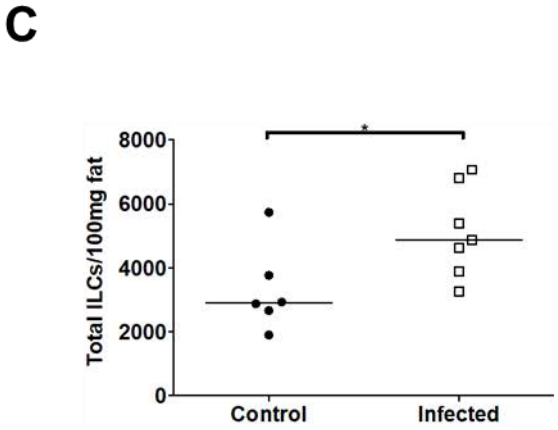
C
Total ILCs/100mg fat
8000
6000
4000
2000
0
*
Control
Infected

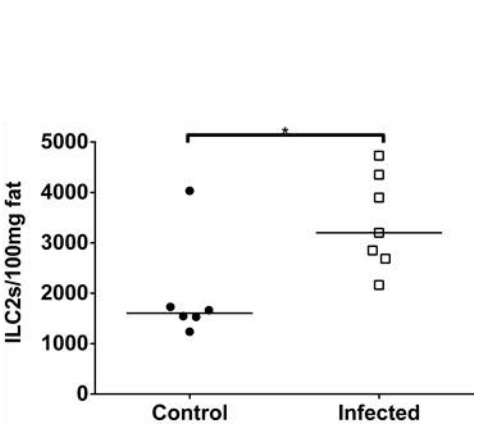
D
ILC2s/100mg fat
5000
4000
3000
2000
1000
0
*
Control
Infected

Figure 5.7: Adipose tissue T cell composition at day five following *H.polygyrus* infection

C57BL/6J males were either infected with *H.polygyrus* larvae (infected), or given PBS as a control, and cells were isolated from mesenteries five days post infection (see Materials and Methods for details). The T cell composition was determined by flow cytometry, as demonstrated previously. Data for each group was obtained from three technical repeats.

Each data point (n=6, 7 for control and infected animals respectively) represents an individual sample with a line indicating the median value. Statistical significance was determined using a Mann-Whitney two-tailed T test, *p<0.05, **p<0.01, ***p<0.001 and ****p<0.0001.

A) FACS plots showing representative T cell composition in mesenteries from both control (left) and infected (right) animals (pre-gated on live CD45.2$^+$ lymphocytes based on FSC and SSC profile and a viability marker). Numbers indicate percentage of events in each gate.

B) Graph showing adjusted number of CD4$^+$ cells (CD4$^+$cells/100mg fat) in mesenteries from control and infected mice (gated on CD45.2$^+$live/dead$^-$ intraCD3$^+$CD4$^+$α-gal-cer$^-$ cells).

C) Graph showing adjusted number of regulatory T cells (Tregs/100mg fat) in mesenteries isolated from control and infected mice (gated on CD45.2$^+$live/dead$^-$intraCD3$^+$CD4$^+$α-gal-cer$^-$FOXP3$^+$ cells).

D) Graph showing adjusted number of CD4$^+$ iNKT cells (CD4$^+$iNKTs/100mg fat) in mesenteries from control and infected mice (gated on CD45.2$^+$live/dead$^-$ intraCD3$^+$CD4$^+$α-gal-cer$^+$ cells).

E) Graph showing adjusted number of CD4$^-$ iNKT cells (CD4$^-$iNKTs/100mg fat) in mesenteries from control and infected mice (gated on CD45.2$^+$live/dead$^-$ intraCD3$^+$CD4$^-$α-gal-cer$^+$ cells).

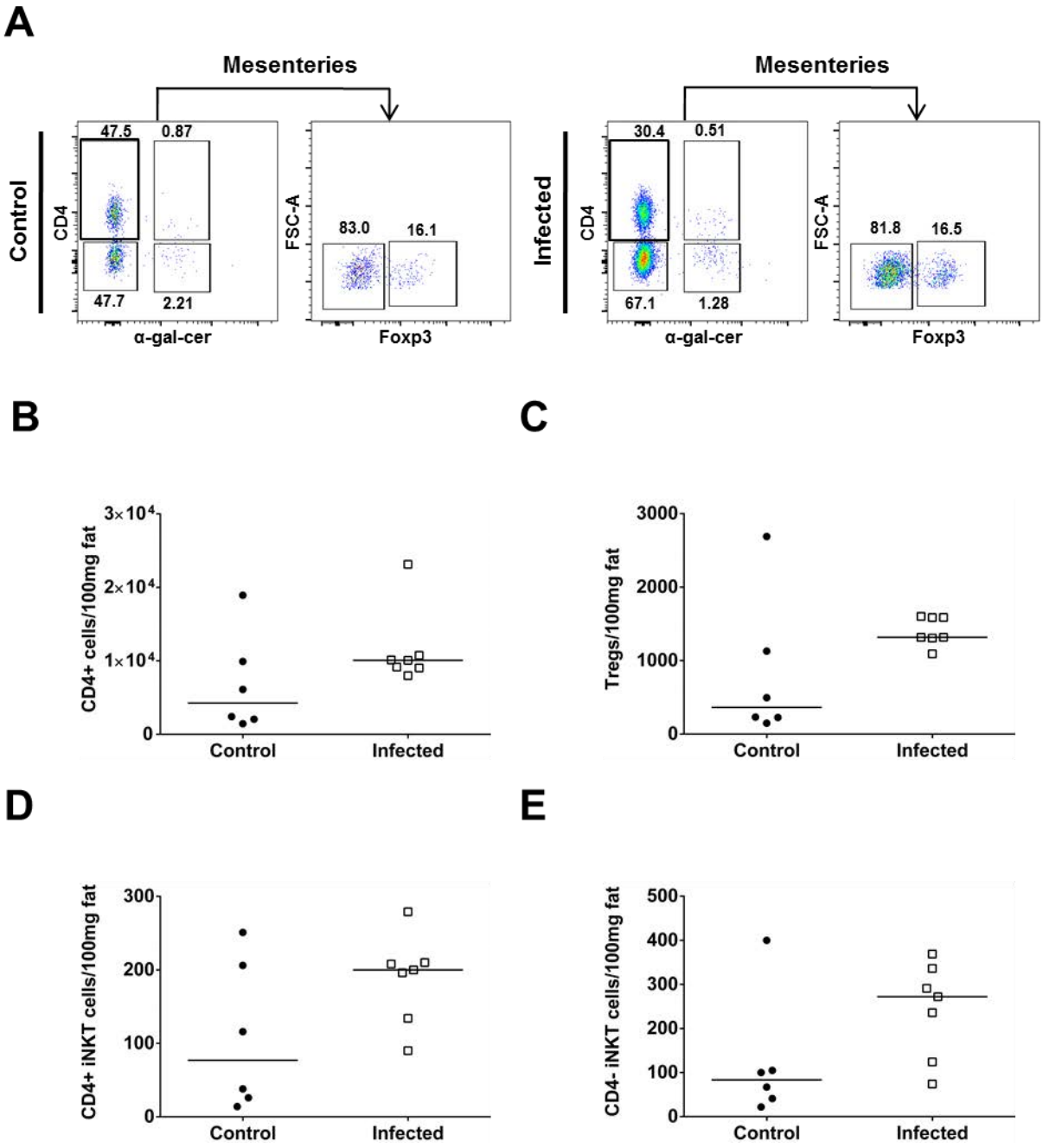
A
Mesenteries
Control
CD4
47.5
0.87
47.7
2.21
α-gal-cer
FSC-A
83.0
16.1
Foxp3
Mesenteries
Infected
CD4
30.4
0.51
67.1
1.28
α-gal-cer
FSC-A
81.8
16.5
Foxp3
B
CD4+ cells/100mg fat
3×10⁴
2×10⁴
1×10⁴
0
Control
Infected
C
Tregs/100mg fat
3000
2000
1000
0
Control
Infected
D
CD4+ iNKT cells/100mg fat
300
200
100
0
Control
Infected
E
CD4- iNKT cells/100mg fat
500
400
300
200
100
0
Control
Infected

Figure 5.8: Adipose tissue ILC2 phenotype at day five following *H.polygyrus* infection

C57BL/6J males were either infected with *H.polygyrus* larvae (infected), or given PBS as a control, and cells were isolated from mesenteries five days post infection (see Materials and Methods for details). The ILC2 phenotype was determined by flow cytometry, as demonstrated previously. Data for each group was obtained from three technical repeats.

Each data point (n=6, 7 for control and infected animals respectively) represents an individual sample with a line indicating the median value. Statistical significance was determined using a Mann-Whitney two-tailed T test, *p<0.05, **p<0.01, ***p<0.001 and ****p<0.0001.

A) FACS plots showing representative ILC2 staining in mesenteries from both control (top) and infected (bottom) animals (pre-gated on live CD45.2$^+$ lymphocytes based on FSC and SSC profile and a viability marker). Numbers indicate percentage of events in each gate.

B) Histogram showing representative ICOS staining in mesenteries isolated from infected (red line) or control (blue line) animals. Vertical dotted line indicates positive staining. Solid lines show ILC2 staining (gated on CD45.2$^+$live/dead$^-$ IL-7Rα$^+$Lin$^-$intraCD3$^-$ST2$^+$GATA-3$^+$ cells), dotted green line shows ICOS FMO control. Numbers indicate the percentage of ICOS$^+$ cells.

C) Histogram showing representative KLRG1 staining in mesenteries isolated from infected (red lines) or control (blue lines) animals. Vertical dotted line indicates positive staining. Solid lines show ILC2 staining (gated on CD45.2$^+$live/dead$^-$IL-7Rα$^+$Lin$^-$intraCD3$^-$ST2$^+$GATA-3$^+$ cells), dotted lines show KLRG1 negative control (gated onCD45.2$^+$live/dead$^-$IL-7Rα$^-$Lin$^+$intraCD3$^-$ cells). Numbers indicate the percentage of KLRG1$^+$ cells.

D) Graph showing percentage of ILC2s expressing ICOS in mesenteries from control and infected mice (gated on live/dead$^-$CD45.2$^+$IL-7Rα$^+$Lin$^-$intraCD3$^-$ ST2$^+$GATA-3$^+$ICOS$^+$ cells).

E) Graph showing expression of ICOS (median fluorescence) on the surface of ILC2 in mesenteries from control and infected mice (gated on live/dead$^-$ CD45.2$^+$IL-7Rα$^+$Lin$^-$intraCD3$^-$ST2$^+$GATA-3$^+$ICOS$^+$ cells).

F) Graph showing percentage of ILC2s expressing KLRG1 in mesenteries from control and infected mice (gated on live/dead$^-$CD45.2$^+$IL-7Rα$^+$Lin$^-$intraCD3$^-$ ST2$^+$GATA-3$^+$KLRG1$^+$ cells).

G) Graph showing expression of KLRG1 (median fluorescence) on the surface of ILC2 in mesenteries from control and infected mice (gated on live/dead$^-$ CD45.2$^+$IL-7Rα$^+$Lin$^-$intraCD3$^-$ST2$^+$GATA-3$^+$KLRG1$^+$ cells).

H) Graph showing expression of ST2 (median fluorescence) on the surface of ILC2 in mesenteries from control and infected mice (gated on live/dead$^-$ CD45.2$^+$IL-7Rα$^+$Lin$^-$intraCD3$^-$ST2$^+$GATA-3$^+$cells).

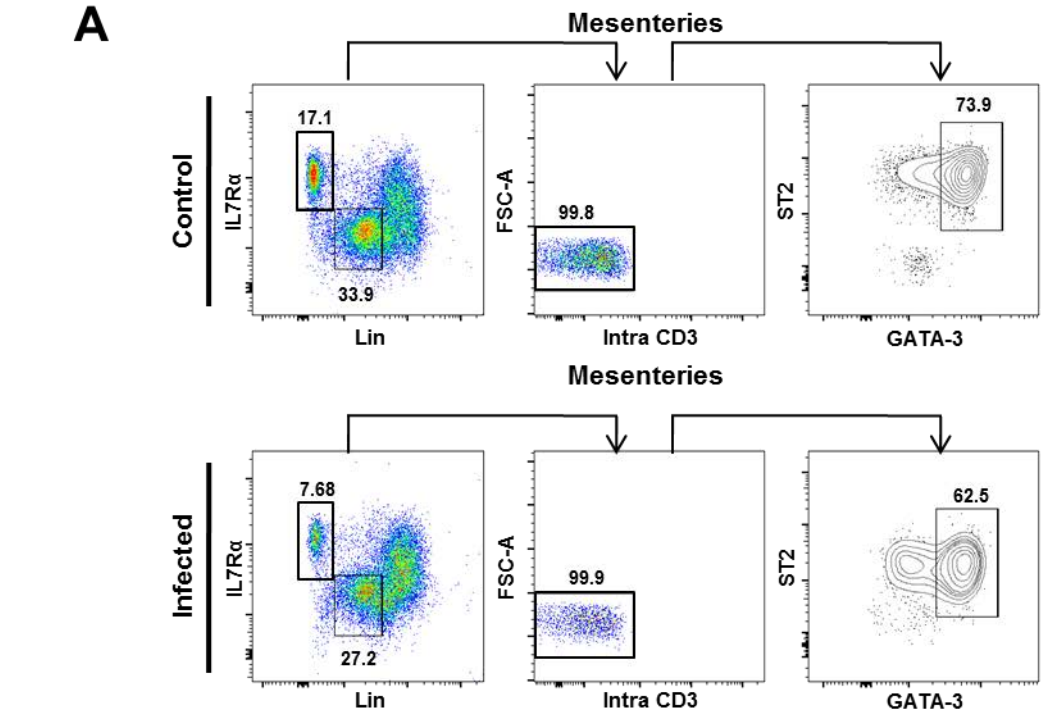
A
Mesenteries
Control
IL7Rα
17.1
33.9
Lin
FSC-A
99.8
Intra CD3
ST2
73.9
GATA-3
Mesenteries
Infected
IL7Rα
7.68
27.2
Lin
FSC-A
99.9
Intra CD3
ST2
62.5
GATA-3

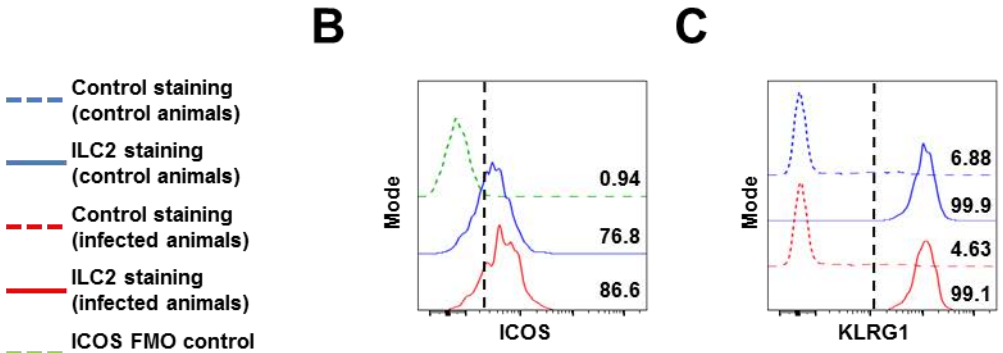
B
C
Control staining (control animals)
ILC2 staining (control animals)
Control staining (infected animals)
ILC2 staining (infected animals)
ICOS FMO control (control+infected animals)
Mode
0.94
76.8
86.6
ICOS
Mode
6.88
99.9
4.63
99.1
KLRG1

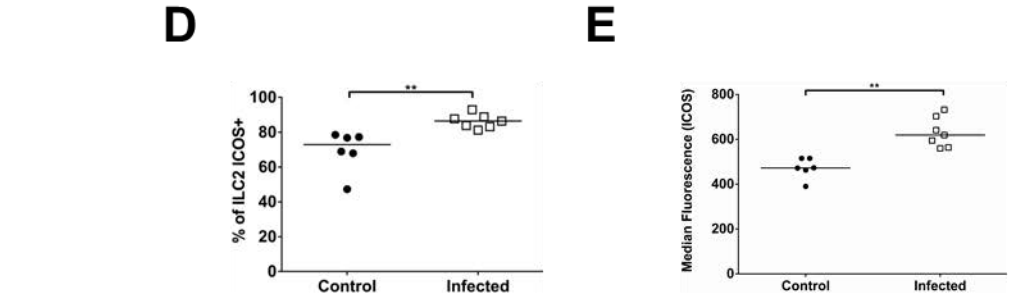
D
E
% of ILC2 ICOS+
Control
Infected
Median Fluorescence (ICOS)
Control
Infected

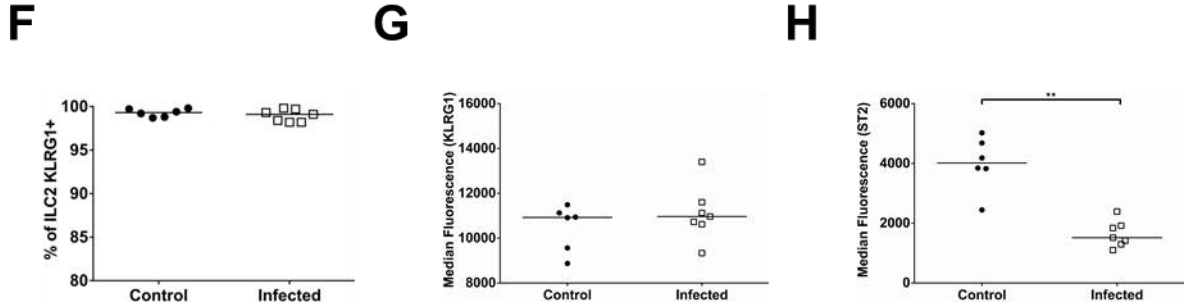
F
G
H
% of ILC2 KLRG1+
Control
Infected
Median Fluorescence (KLRG1)
Control
Infected
Median Fluorescence (ST2)
Control
Infected

5.4. PHENOTYPE OF ADIPOSE TISSUE ILC2 AT DAY FIVE FOLLOWING *HELIGMOSOMOIDES POLYGYRUS* INFECTION

Although few changes in AT immune cell composition were seen at day ten post infection with *H.polygyrus*, changes in both ILC2 number and phenotype were observed in the mesenteries of infected animals when analysed at day five post infection. These results suggested that ILC2s were becoming activated and may therefore contribute to the immune responses occurring during infection of local tissues. It was decided to assess further indicators of ILC2 activation to confirm this finding.

As previously discussed, one of the primary functions of ILC2s which has been established is to coordinate the involvement of further cells in localised immune responses by production of cytokines. Thus, cytokine production can be used as an indicator of ILC2 activation. However, ILC2 cytokine production was undetectable *ex vivo*, even in infected animals, without re-stimulation. As a result ILC2 proliferation was investigated instead, as this is another surrogate sign of ILC2 activation.

IL-2 induces ILC2 proliferation but not cytokine production through the expression of the IL-2Rα and associated downstream signalling (Moro *et al.*, 2016). In addition to this, the epithelial cytokine IL-33 can also stimulate ILC2 proliferation, as well as activating cytokine production (Moro *et al.*, 2016). As IL-33 expression is increased in MLN and SILP following *H.polygyrus* infection (Pelly *et al.*, 2016), it is likely that ILC2s from ATs are proliferating, hence the increased number of ILC2s observed in mesenteries at five days post infection with *H.polygyrus*. The Ki-67 protein is found in the nucleus of proliferating mammalian cells, but is not detectable in the nucleus of non-proliferating (quiescent) cells (Bruno and Darzynkiewicz, 1992, Darzynkiewicz *et*

al., 2015). Thus, antibodies against this marker can be used to assess, by flow cytometry, the proportion of a cell population that is proliferating. As the expression of the Ki-67 protein varies depending on the stage of the cell cycle, the MFI values are not informative for the purposes of comparing the rate of proliferation of different cell populations (Bruno and Darzynkiewicz, 1992, Darzynkiewicz *et al.*, 2015). As such, in order to further investigate ILC2 activation following *H.polygyrus* infection, the Ki-67 expression of AT derived ILC2s was measured by flow cytometry at five days post infection with *H.polygyrus*.

During infection, the expression of certain chemokines in the infected tissue is increased to stimulate migration of further immune cell subsets to amplify the immune response against the pathogen (Griffith *et al.*, 2014). The signals generated within inflamed or infected tissues, especially cytokines, can also alter chemokine receptor expression on peripheral immune cells, resulting in migration of these cells into the inflamed tissue (Griffith *et al.*, 2014). Earlier results indicated ongoing immune responses in the mesenteries surrounding the SI. Cells within AT might become activated before migrating to the site of infection. For this reason, in addition to the proliferation, ILC2 chemokine receptor expression was examined in the gonadal fat and mesenteries of control and infected animals at day five post infection with *H.polygyrus*.

Analysis of chemokine receptor expression showed no change in the proportion of ILC2s expressing CCR8 or CCR9 following infection with *H.polygyrus* (Figure 5.9A-D). These results may indicate that chemokine receptor expression (CCR8/CCR9) on ILC2s within AT does not change in response to helminth infection

at this time point. However, changes in the expression of other chemokine receptors on ILC2s in response to *H.polygyrus* cannot be ruled out.

Consistent with the previously reported increase in ILC2 number in mesenteries following *H.polygyrus* infection, total ILC2 proliferation, as measured by the proportion of Ki-67 cells, was increased by roughly three-fold in both gonadal fat and mesenteries at day five post infection with *H.polygyrus* (Figure 5.10A-B). This further supports the hypothesis that ILC2s from ATs are activated in response to *H.polygyrus* infection in surrounding tissues at day five post infection. The proliferation of both $CCR8^{+}CCR9$- and $CCR8^{+}CCR9^{+}$ ILC2 subsets was increased in infected animals (gonadal fat and mesenteries) compared to control animals (Figure 5.10C-D). Of note, following infection, a greater proportion of $CCR8^{+}CCR9^{+}$ ILC2s were proliferating, as compared with $CCR8^{+}CCR9^{-}$ ILC2s (Figure 5.10C-D); in the mesenteries the percentage of $Ki\text{-}67^{+}CCR8^{+}CCR9^{+}$ ILC2s increased by 3.5 fold, whilst the percentage of $Ki\text{-}67^{+}CCR8^{+}CCR9^{-}$ ILC2 increased by approximately 2.5 fold following infection. There were too few $CCR8^{-}CCR9^{+}$ ILC2s in gonadal fat to analyse Ki-67 expression, so this data was excluded for both tissues. Furthermore, in the MLN there was no notable change in the expression of Ki-67 by $CCR8^{+}CCR9^{-}$ ILC2s following infection, whilst there was an increased proportion of Ki-67 expression in both $CCR8^{-}CCR9^{+}$ by $CCR8^{+}CCR9^{+}$ ILC2s (Figure 7.25C-E). Taken together, this may signify that CCR9 expressing ILC2s are activated to a greater extent following *H.polygyrus* infection. However, there was approximately a 3.5 fold increase in Ki-67 expression by both $CCR8^{+}CCR9^{-}$ and $CCR8^{+}CCR9^{+}$ ILC2s in gonadal fat following infection.

Overall this data indicates that at day five post infection, ILC2s proliferation is increased in response to *H.polygyrus* infection and $CCR8^{+}CCR9^{+}$ ILC2s appear to proliferate to a greater extent than $CCR8^{+}CCR9^{-}$ ILC2s following infection.

AT isotype controls for CCR8 and CCR9 staining, along with analysis of MLN ILC2 proliferation and chemokine receptor staining is shown in the appendix (Figure 7.23-Figure 7.25). A comparison of ILC2 proliferation and T cell proliferation is also contained with the appendix (Figure 7.26).

Figure 5.9: Adipose tissue ILC2 chemokine receptor expression at day five following *H.polygyrus* infection

C57BL/6J males were either infected with *H.polygyrus* larvae, or given PBS as a control, and cells were isolated from the gonadal fat and mesenteries five days post infection (see Materials and Methods). The ILC2 chemokine receptor expression was determined by flow cytometry, as demonstrated previously. Data for each group was obtained from two technical repeats.

Each data point (n=5, 6 for control and infected animals respectively) represents an individual sample with a line indicating the median value. Statistical significance was determined using a Mann-Whitney two-tailed T test, *p<0.05, **p<0.01, ***p<0.001 and ****p<0.0001.

A) FACS plots showing representative ILC2 chemokine receptor staining in gonadal fat (left) and mesenteries (right) from both control (top) and infected (bottom) animals (pre-gated on CD45.2$^+$live/dead$^-$IL-7Rα$^+$Lin$^-$ cells). Numbers indicate percentage of events in each gate.

B) Graph showing percentage of CCR8$^+$CCR9$^-$ ILC2s in gonadal fat and mesenteries from control and infected mice (gated on CD45.2$^+$live/dead$^-$ IL-7Rα$^+$Lin$^-$intraCD3$^-$GATA-3$^+$ CCR8$^+$CCR9$^-$ cells).

C) Graph showing percentage of CCR8$^-$CCR9$^+$ ILC2s in gonadal fat and mesenteries from control and infected mice (gated on CD45.2$^+$live/dead$^-$ IL-7Rα$^+$Lin$^-$intraCD3$^-$GATA-3$^+$ CCR8$^-$CCR9$^+$ cells).

D) Graph showing percentage of CCR8$^+$CCR9$^+$ ILC2s in gonadal fat and mesenteries from control and infected mice (gated on CD45.2$^+$live/dead$^-$ IL-7Rα$^+$Lin$^-$intraCD3$^-$GATA-3$^+$ CCR8$^+$CCR9$^+$ cells).

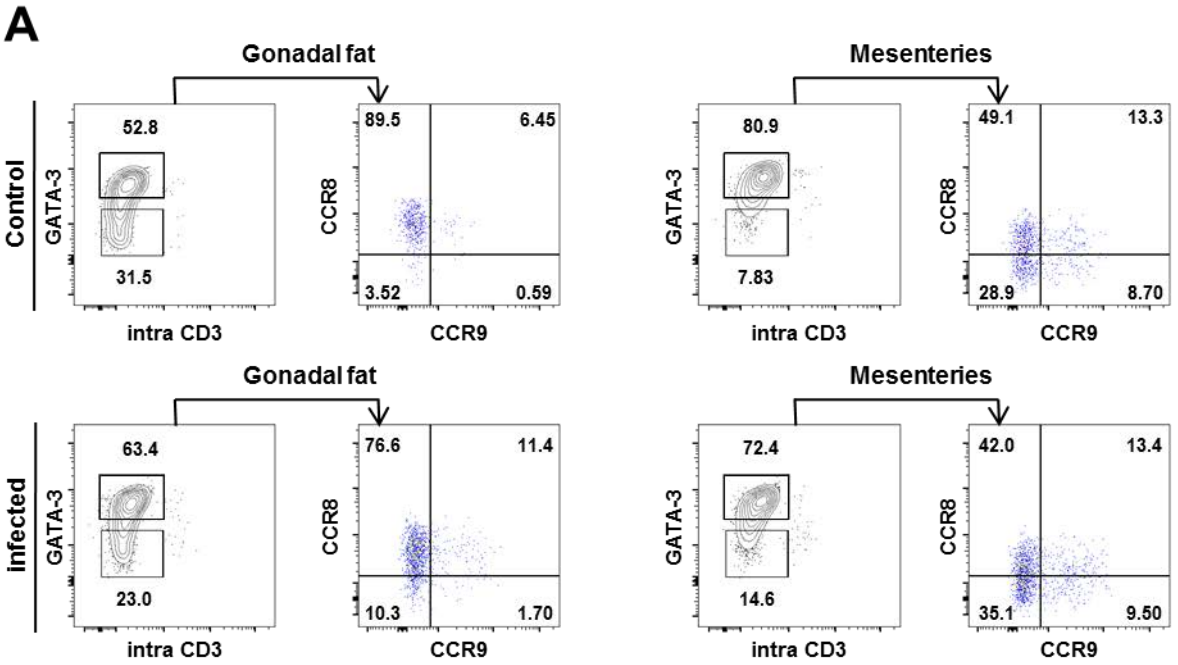
A
Gonadal fat
Mesenteries
Control
Infected
GATA-3
intra CD3
CCR8
CCR9
52.8
31.5
89.5
6.45
3.52
0.59
80.9
7.83
49.1
13.3
28.9
8.70
63.4
23.0
76.6
11.4
10.3
1.70
72.4
14.6
42.0
13.4
35.1
9.50

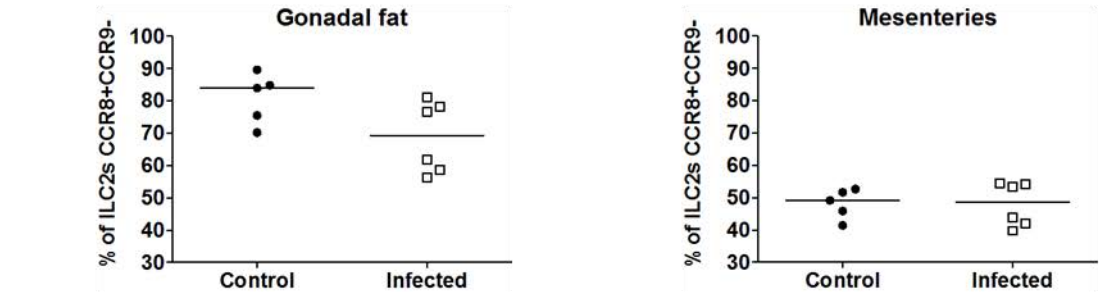
B
Gonadal fat
Mesenteries
% of ILC2s CCR8+CCR9-
Control
Infected

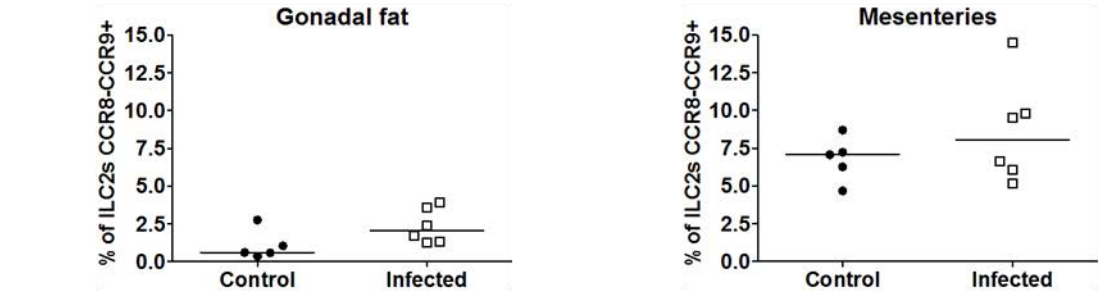
C
Gonadal fat
Mesenteries
% of ILC2s CCR8-CCR9+
Control
Infected

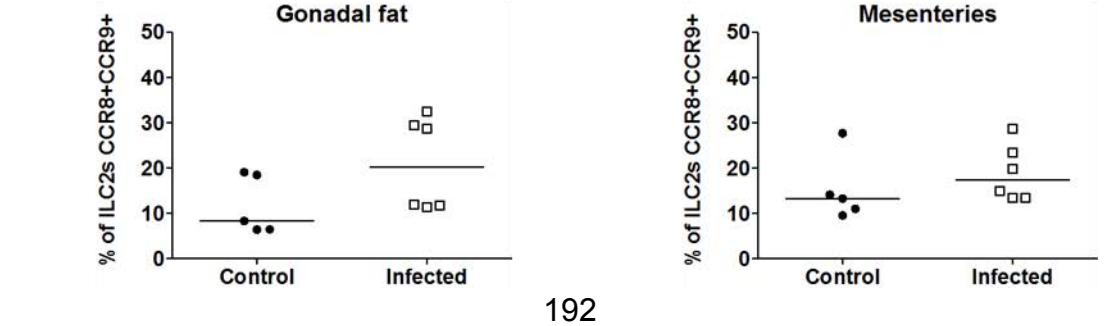
D
Gonadal fat
Mesenteries
% of ILC2s CCR8+CCR9+
Control
Infected

Figure 5.10: Adipose tissue ILC2 proliferation at day five following *H.polygyrus* infection

C57BL/6J males were either infected with *H.polygyrus* larvae, or given PBS as a control, and cells were isolated from the gonadal fat and mesenteries five days post infection (see Materials and Methods for details). The ILC2 proliferation was measured by flow cytometry and quantified in different chemokine receptor profiles. Data for each group was obtained from two technical repeats.

Each data point (n=5, 6 for control and infected animals respectively) represents an individual sample with a line indicating the median value. Statistical significance was determined using a Mann-Whitney two-tailed T test, *p<0.05, **p<0.01, ***p<0.001 and ****p<0.0001.

A) Flow cytometry analysis showing representative total ILC2 Ki-67 staining (black line) and Ki-67 staining in different ILC2 chemokine receptor subsets in gonadal fat (left) and mesenteries (right) from both control (top) and infected (bottom) animals (pre-gated on CD45.2$^+$live/dead$^-$IL-7Rα$^+$Lin$^-$GATA-3$^+$ cells). Numbers indicate percentage of events in each gate. Dotted vertical black line indicates positive events.

B) Graph showing percentage of ILC2s which are Ki-67$^+$ in gonadal fat and mesenteries from control and infected mice (gated on CD45.2$^+$live/dead$^-$ IL-7Rα$^+$Lin$^-$intraCD3$^-$GATA-3$^+$Ki-67$^+$ cells).

C) Graph showing percentage of CCR8$^+$CCR9$^-$ ILC2s which are Ki-67$^+$ in gonadal fat and mesenteries from control and infected mice (gated on CD45.2$^+$live/dead$^-$IL-7Rα$^+$Lin$^-$intraCD3$^-$GATA-3$^+$CCR8$^+$CCR9$^-$ Ki-67$^+$ cells).

D) Graph showing percentage of CCR8$^+$CCR9$^+$ ILC2s which are Ki-67$^+$ in gonadal fat and mesenteries from control and infected mice (gated on CD45.2$^+$live/dead$^-$IL-7Rα$^+$Lin$^-$intraCD3$^-$GATA-3$^+$CCR8$^+$CCR9$^+$ Ki-67$^+$ cells).

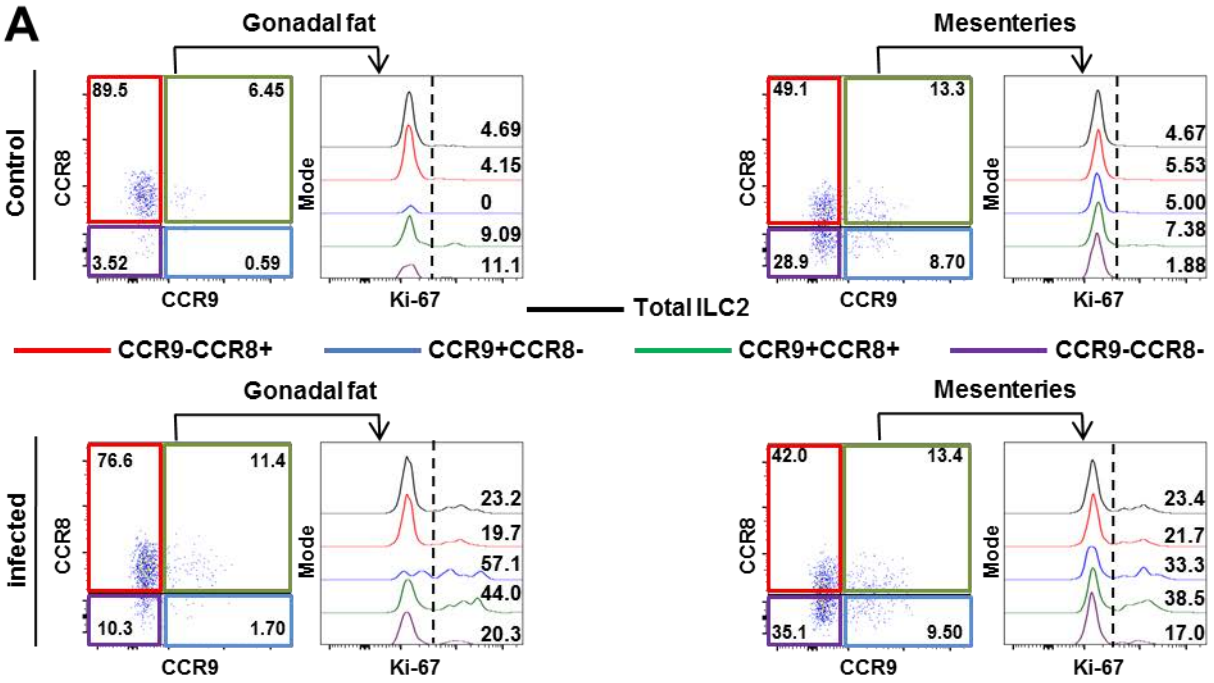
A
Gonadal fat
Mesenteries
Control
CCR8
CCR9
Mode
Ki-67
89.5
6.45
3.52
0.59
4.69
4.15
0
9.09
11.1
49.1
13.3
28.9
8.70
4.67
5.53
5.00
7.38
1.88
Total ILC2
CCR9-CCR8+
CCR9+CCR8-
CCR9+CCR8+
CCR9-CCR8-
Infected
76.6
11.4
10.3
1.70
23.2
19.7
57.1
44.0
20.3
42.0
13.4
35.1
9.50
23.4
21.7
33.3
38.5
17.0

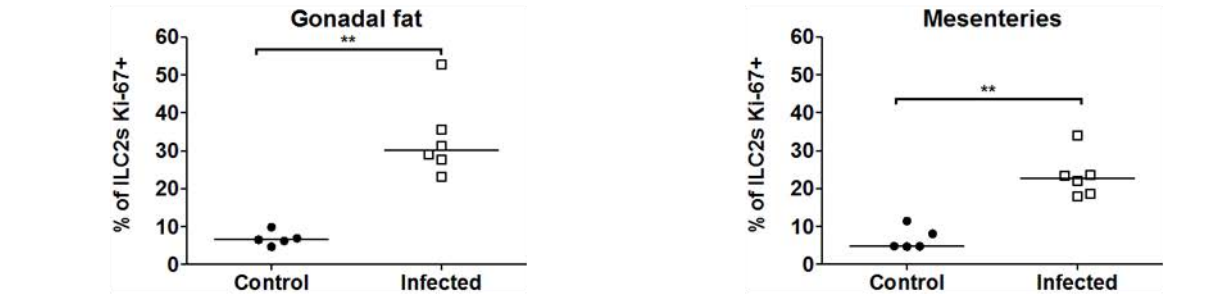
B
Gonadal fat
Mesenteries
% of ILC2s Ki-67+
Control
Infected
**

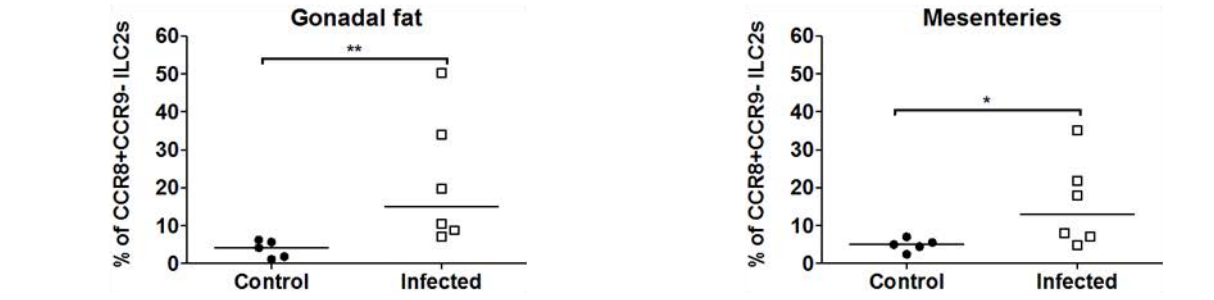
C
Gonadal fat
Mesenteries
% of CCR8+CCR9- ILC2s
Control
Infected
**
*

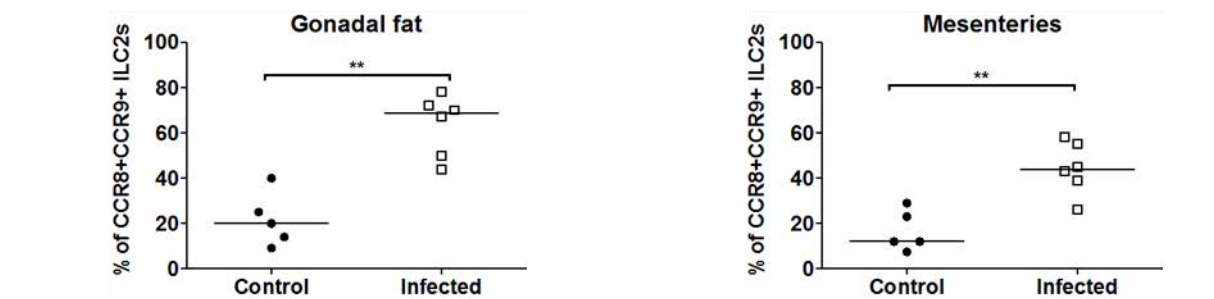
D
Gonadal fat
Mesenteries
% of CCR8+CCR9+ ILC2s
Control
Infected
**

5.5. SUMMARY

The overarching aim of this project was to explore the role of AT immune cells in immune responses. The rationale for investigating this was due to the observation that ATs and SLTs are frequently co-localised anatomically (Pond, 2002). Furthermore, previous research by a number of groups indicated the presence of tertiary lymphoid clusters, known as FALC, within ATs (Moro *et al.*, 2010, Koyasu and Moro, 2013, Benezech *et al.*, 2015, Jackson-Jones *et al.*, 2016). The number of these FALC increased in response to both inflammation and infection and FALC supported the development of antigen-specific B cells (Benezech *et al.*, 2015, Jackson-Jones *et al.*, 2016). These changes in FALC were all observed in ATs peripheral to the site of infection. All of the above therefore supports the hypothesis that immune cells in ATs can contribute to immune responses in surrounding tissues.

As the mesentery depot has been one of the main AT depots studied within this thesis, a model of murine helminthiasis was utilised in order to investigate this hypothesis. *H.polygyrus* was chosen, as this parasite is a natural murine parasite and it is an easier mouse model to use over a longer period of time, as the infective L3 larvae can be stored for many months at 4°C (Camberis *et al.*, 2003).

Initially, the AT FALC number and immune cell composition was investigated at day ten post infection, as this is approximately when the peak of the immune response occurs. Following infection with *H.polygyrus* the number of MS was increased in the omenta of infected animals, but there was no difference in the number of FALC in gonadal fat or mesenteries in control and infected animals. However, when normalised to tissue weight, the number of FALC/MS was increased in mesenteries, but not omentum or gonadal fat, of infected mice compared with controls. Outlying

values could explain the inconsistency in the trends of total mesentery FALC number and mesentery FALC number/100 mg fat following infection.

Data by Pelly *et al.* indicated an increase in T cells in the MLN as early as day seven post infection (Pelly *et al.*, 2016). Moreover, expansion of Tregs has been reported in the MLN of infected animals, reaching significance between day seven and day fourteen post infection (Finney *et al.*, 2007, Rausch *et al.*, 2008). Whilst some of these differences were observed herein in the MLN of infected animals (see Figure 7.18 and Figure 7.21), when the immune cell composition of the mesenteries from infected animals was compared with control animals following *H.polygyrus* infection no differences were observed in $CD4^+$ cells, Tregs or iNKT cells. This could indicate that the T cell compartment does not significantly contribute to the immune responses to *H.polygyrus* in this tissue at the time point investigated. However, a significant increase in proliferation was seen by IL-$7R\alpha^+CD3^+$ cells, the majority of which are likely to be T cells, following infection in all tissues examined.

In a model of *N.brasiliensis,* Van Dyken *et al.* demonstrated that Th2 cells, but not ILC2s, in the lung require priming in the draining LN in order to generate effector immune responses in the former tissue (Van Dyken *et al.*, 2016). It is unclear whether the T cells within ATs are activated, or whether they require similar priming. This could be an avenue for future investigation. However, iNKTs can proliferate and produce cytokine very rapidly (Carnaud *et al.*, 1999, Fujii *et al.*, 2003). Furthermore, iNKTs can respond to IL-33, which is produced in large amounts during *H.polygyrus* infection, and have been shown to play a role in clearance of the helminth *Schistosoma japonicum* (Smithgall *et al.*, 2008). Taken together, these findings may suggest that, although iNKT cell numbers were unchanged between the mesenteries

of control and infected animals at ten days post infection, changes in iNKT cell number may be seen earlier in the response.

No statistically significant changes were seen in total ILCs number or ILC2 number in the mesenteries at day ten following infection, although in the majority of samples the mesenteries of infected animals had a greater number of ILC2s than the same tissues in control animals. ILC2 phenotype was also investigated following infection with *H.polygyrus* at day ten post infection and no overt changes were seen in the expression of ICOS or KLRG1 by ILC2s following infection. However, as highlighted above, a limited number of WT animals were available whilst performing these experiments, such that sufficient statistical power to detect subtle changes in these markers was lacking. Moreover, like iNKT cells, ILC2s also can produce cytokine rapidly following activation, therefore this result does not completely exclude the involvement of AT derived ILC2s in the immune response to *H.polygyrus*. This theory is supported by a report by Pelly *et al.*, who show an increased number of ILC2s in the SILP and MLN at day five post infection with *H.polygyrus*, whilst T cells are increased later at day seven post infection (Pelly *et al.*, 2016). Mackley *et al.* also show an increased number of ILC2s and ILC3s in the MLN of infected animals seven days after infection with *H.polygyrus* (Mackley *et al.*, 2015).

A decrease in the expression of ST2 in ILC2s from the mesenteries of infected animals was identified at day ten post infection. This could be a mechanism of negative regulation for preventing over-activation of ILC2s, which could lead to autoimmunity. However, data by Pelly *et al.* does not support this supposition, as IL-5 and IL-13 mRNA was maintained in the SILP at day ten post infection with

H.polygyrus, although this could be due to the T cell contribution to these cytokines (Pelly *et al.*, 2016).

In summary, no substantial changes in the immune cell composition of ATs were seen at day ten post infection with *H.polygyrus*, however some of the immune cells studied may act earlier in the immune response. For this reason the FALC number and immune cell composition of ATs was examined at day five post infection with *H.polygyrus*.

At day five post infection both the mesenteries and omentum of infected animals had increased numbers of FALC/MS. The increase in the number of FALC/MS clearly demonstrates that these clusters are responding to the infection, although it is unclear whether antigens reach them by passive diffusion, or are transported by APCs (Meza-Perez and Randall, 2017). Further investigation is necessary to determine the mechanisms by which *de novo* FALC and MS formation is induced following *H.polygyrus* infection and by other systemic signals released during infection or inflammation along with characterisation of the pathways of antigen transport to the clusters.

Despite an increase in total number of FALC and MS following infection, when normalised to tissue weight, this trend was only significant for the mesenteries of infected animals. One possibility to explain this discrepancy could be that the increased MS number contributes to an increased mass of the omentum; as the omentum is a very small tissue, no more than 20 mg in mass in WT animals, it is conceivable that a large increase in MS numbers could have an impact on the overall tissue weight. If this were the case then increases in MS numbers may be masked when normalised to tissue weight. Whilst the majority of omenta isolated from

infected animals were heavier than the same tissue from control animals, there was a large variation in mass of the omentum for both groups, thus this difference did not reach statistical significance.

It is surprising that mesentery mass was unaffected by *H.polygyrus* infection as reports have shown beneficial metabolic effects, such as improved insulin sensitivity, to HFD-fed mice following helminth infection (Yang *et al.*, 2013, Hussaarts *et al.*, 2015, Van Dyken *et al.*, 2016). One possibility is that the improvement seen could only be relevant in a situation of metabolic dysregulation, such as obesity, and may not have an effect on lean mass. Furthermore, these reports study these metabolic parameters much later in the course of helminthiasis (Yang *et al.*, 2013, Hussaarts *et al.*, 2015, Van Dyken *et al.*, 2016). Therefore, beneficial metabolic effects may only be evident after a chronic infection has been established.

As seen at day ten post infection, when $CD4^+$ cells, Tregs and iNKT cell numbers were compared between control and infected animals at day five post infection, no differences were observed in the mesenteries. This suggests that these cells, in the context of ATs, do not contribute to immune responses in local tissues as these cells were all increased in the MLN of infected animals. Although iNKT cells did not increase in the mesenteries following infection, iNKT can rapidly produce cytokines in the absence of proliferation following activation by glycolipids (Matsuda *et al.*, 2008, Jukes *et al.*, 2012). Thus, iNKTs are likely still involved in the formation of FALC seen here in response to helminth infection.

Similar to what others have shown in MLN (Mackley *et al.*, 2015, Pelly *et al.*, 2016), the number of ILC2s was increased in the mesenteries of infected animals at day five post infection.

When ILC2 phenotype was examined at day five post infection, an increased expression of ICOS by ILC2s from infected mesenteries was observed. ICOS is expressed predominantly in activated T cells and is required for optimal T cell terminal differentiation through co-stimulation (Hutloff *et al.*, 1999, Dong *et al.*, 2001). Of note, activation of Th2 responses appears to have a greater dependence on ICOS expression than Th1 responses (Dong *et al.*, 2001). ICOS expression has also been reported on the surface of ILC2s and some ILC3s in the SI (Artis and Spits, 2015, Eberl *et al.*, 2015, Paclik *et al.*, 2015, Robinette *et al.*, 2015, Klose and Artis, 2016). Although many ILCs functions mirror those of T cells, as ILCs lack antigen specific receptors, it is unclear whether the costimulatory role of ICOS is equally as applicable for ILC2s (Kamachi *et al.*, 2015, Paclik *et al.*, 2015). Research by Kamachi *et al.* demonstrated that ICOS on ILC2s can bind to its ligand, ICOSL, on the surface of DCs, leading to cytokine production and blocking of this interaction abrogated ILC2 mediated responses to papain-induced lung inflammation (Kamachi *et al.*, 2015). Furthermore, interaction between ICOS on ILC2s and ICOSL on Tregs was found to be vital for survival of ILC2s through STAT5 activation and mice deficient in ICOS had reduced ILC2 responses in a model of ILC2-induced asthma (Maazi *et al.*, 2015, Molofsky *et al.*, 2015b). In summary, these reports demonstrate an important role of ICOS in regulating ILC2 function through interaction with both the innate and adaptive immune system. Thus, the increase in ICOS expression by mesentery ILC2s following infection may be suggestive of activation of these cells.

As seen at later time points, ILC2 expression of ST2 was also lower in the mesenteries of infected animals at day five post infection. ILC2 cytokine production is crucial to the immune response to *H.polygyrus* (Urban *et al.*, 1998). Taken together,

both the increased number of ILC2s and the changes in phenotype of these cells suggests that ILC2s from ATs can therefore play a vital role in mounting an immune response to parasitic infection in neighbouring tissues. It is still unclear whether the ILC2s are distributed throughout the mesenteries, or are located within the FALC, which are reported to be enriched in these cells (Moro *et al.*, 2010, Benezech *et al.*, 2015). The function of ILC2 within FALC is currently unknown, so these ILC2s may contribute to the function of FALC in mediating adaptive immune responses, as reported by Jackson-Jones *et al.* (Jackson-Jones *et al.*, 2016).

ILC2 chemokine receptor expression and proliferation were then investigated at day five post infection with *H.polygyrus*, with the aim of better establishing the role of ILC2s in the immune response to this parasite. No differences in ILC2 CCR8 or CCR9 expression were observed between control and infected mesenteries. As discussed earlier, CCR9 expression is required for migration to the SI (Mora *et al.*, 2003, Hoyler *et al.*, 2012, Kim *et al.*, 2015a). Lack of changes in CCR9 expression could suggest that ILC2-mediated effects on the immune response to *H.polygyrus* are coordinated from within ATs, and not after migration to the SI. Consistent with the increased number of ILC2s in mesenteries following infection, the proliferation of ILC2s, as determined by Ki-67 expression, was greater in mesenteries isolated from infected animals, as compared to control animals. However, $CCR8^{+}CCR9^{+}$ ILC2s in all tissues appeared to proliferate to a greater extent the $CCR8^{+}CCR9^{-}$ ILC2s. It is unclear whether expression of these chemokine receptors marks different functional subsets of ILC2s with ATs. Future investigations could identify whether $CCR9^{+}$ and $CCR9^{-}$ ILC2s differ in expression of key proteins, such as ICOS, KLRG1, IL-5 and IL-13. ILC2 proliferation by Ki-67 expression has also been reported at day seven

post infection elsewhere (Mackley *et al.*, 2015). This finding could be confirmed by additional staining with Bromodeoxyuridine (BrdU), which is another marker used to determine cellular proliferation. Although the changes in Ki-67 indicate that ILC2s are proliferating in adipose tissues following infection, it is not possible to determine from the data presented herein whether these ILC2s migrate into the adipose tissues from peripheral sites, or are derived from local precursor populations. Analysis of the ILC progenitor compartment within adipose tissues following infection would help identify this. Furthermore, a technique that could be used in future analysis to investigate whether migration of ILC2s occurs during infection is the Kaede mouse model, where cells are photoconvertible upon exposure to UV light, allowing the monitoring of cellular migration (Tomura and Kabashima, 2013).

In summary, FALC numbers in the mesenteries were increased as early as day five following infection with *H.polygyrus*. No overt changes were observed in the immune cell subsets examined from the mesenteries of control and infected animals at day ten post infection, suggesting that these cells within ATs did not contribute to the immune responses to *H.polygyrus* in surrounding tissues at this time point. However, limitations in statistical power, due to the number of animals used, means that this possibility cannot completely be ruled out. Despite this, ILC2 numbers and proliferation were increased at day five post infection with *H.polygyrus*, suggesting that adipose-derived ILC2s can contribute early in the immune response to this helminth.

6. DISCUSSION

Over the last four years, during which this study has been conducted, there has been an increased interest in investigating the functional role of immune cells within ATs. This research has predominantly focused on the role that these cells play in controlling metabolic homeostasis, especially in the context of obesity (Hams *et al.*, 2013, Molofsky *et al.*, 2013, Brestoff *et al.*, 2015, Hashiguchi *et al.*, 2015, Lynch *et al.*, 2016, O'Sullivan *et al.*, 2016). In addition to this, the presence of tertiary lymphoid clusters, known as FALC, have been identified within ATs, and recent data indicates that these FALC are important in supporting innate and adaptive immunity in response to infection and inflammation of surrounding tissues (Moro *et al.*, 2010, Koyasu and Moro, 2013, Benezech *et al.*, 2015, Jackson-Jones *et al.*, 2016).

The main function of ATs is the coordination of systemic metabolism; whilst WAT functions as a site for storage of energy, and is found readily distributed across a number of depots in both humans and mice (Seale *et al.*, 2008, Azeez *et al.*, 2014, Chusyd *et al.*, 2016), BAT uses energy to generate heat, referred to as thermogenesis, but is rare in adult humans or in mice (Seale *et al.*, 2008).

Obesity is a risk factor for a number of diseases in humans, including cancer and viral infections, due to impairment of immune cell function (Milner and Beck, 2012, Okwan-Duodu *et al.*, 2013). Thus, in addition to the metabolic role of these tissues, there is growing evidence that ATs can also interact with the host immune system.

WAT can be subdivided into SCAT and VAT, based on anatomical location. The relative contribution of these depots to obesity and metabolic disease in humans is controversial; whilst the majority of human studies suggest that VAT is the main

indicator of insulin sensitivity (Koster *et al.*, 2010, Bjorndal *et al.*, 2011, Strissel *et al.*, 2014), some groups argue that SCAT adiposity can also drive metabolic dysregulation (Geer and Shen, 2009). Inter-depot discrepancies are also seen in mouse studies. The majority of studies investigating beigeing of WAT, a process by which adipocytes within WAT acquire the ability to perform thermogenesis through UCP1 expression, identify this process to occur almost exclusively in the SCAT of mice and either note that this process does not occur in VAT, or fail to investigate this process in VAT (Qiu *et al.*, 2014, Brestoff *et al.*, 2015, Lee *et al.*, 2015a, Lynch *et al.*, 2016). In contrast, some groups demonstrate UCP-1 expression, and indications of beigeing, in VAT following cold-exposure (Rao *et al.*, 2014, Suarez-Zamorano *et al.*, 2015). Furthermore, whilst the majority of studies focus on epididymal and inguinal fat as representative VAT and SCAT depots respectively, a number of reviews have noted that these depots are dissimilar from human VAT and SCAT depots. Research should instead focus on the mesenteries of mice, as this is most analogous depot to intra-abdominal VAT found in humans, the adiposity of which has a strong correlation with metabolic dysregulation. With this in mind, it is difficult to predict whether targeting this beigeing pathway with the aim to improve insulin sensitivity in humans with metabolic disease will be beneficial.

Within this investigation the immune cell composition of mesenteries and epididymal (gonadal) VAT was examined both in the steady state, following gene ablation/over expression and in response to helminth infection. BAT and SCAT immune cell composition was not explored in these settings due to the predominance of evidence supporting the changes in immune cell composition in WAT during obesity and other infectious or inflammatory challenges (Moro *et al.*, 2010, Lynch *et al.*, 2012, Satoh *et*

al., 2012, Hams *et al.*, 2013, Molofsky *et al.*, 2013, Benezech *et al.*, 2015, Hashiguchi *et al.*, 2015, Jackson-Jones *et al.*, 2016, Boulenouar *et al.*, 2017).

In the steady state distinct differences were observed in the immune cell composition between ATs and MLN, used as a representative SLT throughout. This included enrichment for iNKTs, ILC2s and Tregs in ATs compared with MLN. Furthermore, the expression of the surface proteins ICOS, KLRG1 and ST2 differed between ILC2s isolated from MLN and ATs. Whilst the role of ST2 and ICOS in ILC2 biology as a stimuli for cell proliferation and cytokine production is well established (Neill *et al.*, 2010, Hoyler *et al.*, 2012, Barlow *et al.*, 2013, Doherty *et al.*, 2013, Califano *et al.*, 2015, Kamachi *et al.*, 2015, Maazi *et al.*, 2015, Paclik *et al.*, 2015, Halim *et al.*, 2016, Han *et al.*, 2017), the cellular function of KLRG1 is less well established.

In a study by Huang *et al.* the authors identified an ILC-like subset expressing high levels of KLRG1 following IL-25 treatment and further investigation led the authors to conclude that KLRG1 is an inflammatory marker, which is expressed by activated, cytokine producing ILC2s (Huang *et al.*, 2015). However, whilst this study showed the majority of ILC2s in untreated WT mice to be KLRG1 negative, data within this thesis demonstrates that the majority of ILC2s in both SLTs and ATs express KLRG1. In support of the latter data, Hoyler *et al.* demonstrated ubiquitous expression of KLRG1 by GATA-3^{hi} ILC2s, and IL-5 and IL-13 expression was only found in $KLRG1^{+}$ cells (Hoyler *et al.*, 2012).

KLRG1 has been reported as a maturation marker in both NK cells and $CD8^{+}$ T cells, and in both cell subsets KLRG1 expression corresponded with increasing replicative senescence and inhibition of functional cytokine production (Voehringer *et al.*, 2001, Robbins *et al.*, 2002, Grundemann *et al.*, 2006, Huntington *et al.*, 2007,

Schwartzkopff *et al.*, 2007, Tessmer *et al.*, 2007). The ligand for KLRG1, E-cadherin, is expressed on most epithelial cells, but expression has also been demonstrated on APCs (Grundemann *et al.*, 2006, Tessmer *et al.*, 2007, Henson *et al.*, 2009). Taken together, as discussed in a review by Henson and Akbar, these findings could suggest a role of KLRG1 in the negative regulation of lymphocytes (Henson and Akbar, 2009). Similar to the findings in NK cells and T cells, Hoyler *et al.* also found KLRG1 expression to positively correlate with the maturation state of ILC2s from SILP (Hoyler *et al.*, 2012). Finally, unpublished work by Kazuyo Moro also shows ILC2 KLRG1 expression to be a maturation marker for AT ILC2s, with pre-natal ILC progenitors expressing low/negligible levels of KLRG1, and mature ILC2s stably expressing high levels of KLRG1 (Moro group, RIKEN Centre for Integrative Medical Sciences, Japan). However, neither group have identified whether this impacts the proliferative or cytokine capacity of ILC2s.

Of particular interest was the apparent increase in cytokine production by ILC2s isolated from ATs as compared with MLN. A number of reports have also described differential protein expression by adipose ILC2s and have illustrated the importance of these cells in maintaining metabolic homeostasis and preventing obesity (Donninelli *et al.*, 2017). *In vitro* data suggests that IL-33 is the most potent of the alarmins in inducing type two cytokine production by ILC2s (Hoyler *et al.*, 2012, Barlow *et al.*, 2013, Califano *et al.*, 2015, Molofsky *et al.*, 2015b). Both adipocytes and AP cells express IL-33, and IL-33 expression is increased during obesity, presumably as a stress response by hypertrophic adipocytes ((Wood *et al.*, 2009, Miller *et al.*, 2010), unpublished work, Beth McKendrick, Caamaño group, University of Birmingham, U.K.). Therefore IL-33 might be a link between the metabolic status

of AT and activation of anti-inflammatory pathways by ILC2s. In accordance with this, mice lacking the receptor for IL-33, ST2, had increased weight gain and insulin resistance following HFD (Miller *et al.*, 2010).

In support of the above hypothesis, the expression of ST2 was higher on AT ILC2s, as compared to MLN ILC2s. This could therefore be a mechanism by which AT ILC2s are endowed with higher cytokine production, but further evidence is required to confirm this. However, when cytokine production was compared between WT mice and mice lacking IL-33 (IL-$33^{cit/cit}$ mice), only a small difference in *ex vivo* ILC2 cytokine production was observed in the mesenteries. This could be due to redundancy in signals which activate ILC2s, such as IL-25, TSLP, cysteinyl leukotrienes and PGD_2. A more refined approach is required to fully assess the importance of the IL-33/ST2 axis in the observed increased ILC2 cytokine production in ATs.

The type-two cytokines IL-5 and IL-13 are thought to play a crucial role in maintaining the homeostasis of ATs and counteracting the onset of obesity (Hams *et al.*, 2013, Molofsky *et al.*, 2013, Brestoff *et al.*, 2015, Hashiguchi *et al.*, 2015, Lee *et al.*, 2015a). Not only are ILC2s enriched in response to AT inflammation, but also eosinophils, AAM and iNKTs, all of which produce type-two cytokines and restore insulin sensitivity (Lynch *et al.*, 2012, Satoh *et al.*, 2012, Schipper *et al.*, 2012, Hams *et al.*, 2013, Molofsky *et al.*, 2013, Hashiguchi *et al.*, 2015). Recent research has identified a cellular circuit involving IL-5 and IL-13 leading to downstream UCP-1 expression by WAT adipocytes, and ultimately resulting in improved metabolic function (Qiu *et al.*, 2014, Brestoff *et al.*, 2015, Lee *et al.*, 2015a). IL-33 treatment induces protective effects against obesity and Miller *et al.* demonstrate that *ex vivo* treatment of adipose

tissue cultures with IL-33 induces type-2 cytokines (Miller *et al.*, 2010). Thus, the increased production of IL-5 and IL-13 by WT ILC2s within ATs, and the anti-inflammatory role these cytokines play in the immune system may be key to the ascribed role of these cells in maintaining metabolic balance (Molofsky *et al.*, 2013, Donninelli *et al.*, 2017). It is important to verify whether this increased cytokine production is unique to AT ILC2s and not a caveat of comparing lymphoid and non-lymphoid tissues. This can be achieved by performing the same comparisons with ILC2s derived from other non-lymphoid tissues, such as skin, lungs and SILP. Furthermore, in this report cytokine expression was analysed following *ex vivo* stimulation with an exogenous stimulus. It is important to confirm these findings with endogenous ligands, such as IL-33, and ideally under more physiological conditions *in vivo*. Once such method would be to use cytokine reporter animals, such as described in papers by Neill *et al.*, to compare ILC2 cytokine production both under steady state conditions and following *in vivo* activation of ILC2s (Neill *et al.*, 2010).

Some differences in the immune cell composition of ATs were observed between different genders and genetic background strains of animals. This was anticipated, as gender is thought to affect both the metabolic function of ATs and the function of immune cells (Demerath *et al.*, 2007, Geer and Shen, 2009, Macotela *et al.*, 2009, Arnold *et al.*, 2016, Klein and Flanagan, 2016, Bruder-Nascimento *et al.*, 2017, Karp *et al.*, 2017). As such, mice of the same gender (male) and genetic background (C57BL/6J) were used throughout, unless otherwise stated.

It was hypothesised that changes in chemokine receptor expression could contribute to the increased composition of ILC2s in ATs, as compared with many other lymphoid and non-lymphoid tissues, due to enhanced homing to ATs, or improved

retention of ILC2 in these tissues. When the expression of chemokine receptors CCR4, CCR6, CCR8, CCR9, CXCR6 and CCRL2 were investigated in a variety of lymphoid and non-lymphoid tissues, non-lymphoid tissues had a higher expression of CCR8 and a lower expression of CCR9 than lymphoid tissues. However, there were minimal differences in expression of these chemokine receptors on the surface of ILC2s between ATs and other non-lymphoid tissues. Thus, this perhaps suggests that these chemokine receptors may not be responsible for the increased ILC2 composition of ATs. In addition to chemokines, another molecule that can induce migration of ILC2s into tissues is PGD_2 (Xue *et al.*, 2014, Wojno *et al.*, 2015). Expression of the receptor for PGD_2, CRTH2, has been demonstrated on both mouse and human ILC2s and the migratory effect of PGD_2 was dependent on the expression of this receptor (Xue *et al.*, 2014, Wojno *et al.*, 2015). Furthermore, as discussed in chapter 1.2.3, PGD_2 can also induce cytokine production in ILC2s. PGD_2, which is produced from lipid precursors, is increased in these tissues early in obesity (Hams *et al.*, 2013, Molofsky *et al.*, 2013, Hashiguchi *et al.*, 2015). PGD_2 therefore represent an important signal linking the metabolic status of ATs and ILC2 composition.

A number of reviews compare the distribution of fat depots between humans and mice (Bjorndal *et al.*, 2011, Chusyd *et al.*, 2016). These reviews highlight that whilst mesenteries of mice are the most physiologically analogous fat depots to human intra-abdominal VAT, the gonadal fat from mice does not have a functionally analogous fat depot in humans (Bjorndal *et al.*, 2011, Chusyd *et al.*, 2016). There is evidence for metabolic differences between SCAT and VAT both in mice (Macotela *et al.*, 2009) and humans (Geer and Shen, 2009, Bjorndal *et al.*, 2011, Tchkonia *et*

al., 2013, Chusyd *et al.*, 2016), and also in cellular composition between these depots in mice (Prunet-Marcassus *et al.*, 2006, Feuerer *et al.*, 2009, Winer *et al.*, 2009). In further support of tissue-specific variation in cellular composition, research by Lee *et al.* indicates that tissue localisation directs the cytokine profile of iNKT cells (Lee *et al.*, 2015b). However, the mesenteries and gonadal fat both represent VAT depots. Although there is evidence to support metabolic and cellular differences between omental and mesenteric depots in humans (Edens *et al.*, 1993, Fried *et al.*, 1993, Caserta *et al.*, 2001, Tchkonia *et al.*, 2006), limited comparisons have been made between VAT depots within mice (Kirkland *et al.*, 1990, Moro *et al.*, 2010) Taken together these data suggest functional heterogeneity between VAT depots, at least in humans. Therefore, it is conceivable that immune cell composition and function differs within these tissues.

The majority of research into the role of immune cells within VAT has focused on gonadal fat (Lynch *et al.*, 2012, Satoh *et al.*, 2012, Schipper *et al.*, 2012, Hams *et al.*, 2013, Molofsky *et al.*, 2013, Lynch, 2014, Hashiguchi *et al.*, 2015). However, in light of the fact this depot is not analogous to human VAT, the mesenteries was additionally included in all experiments, such that any findings may be extrapolated to humans. Interestingly, minimal differences in immune cell composition and protein expression were observed between gonadal fat and mesenteries under steady state conditions. However, following manipulation, such as gene ablation or infection, tissue specific differences arose. One factor which could lead to a differing composition between mesenteries and gonadal fat is the contrasting distribution of FALC. Whilst mesenteries have around ten to twenty FALC in adult mice, dependent on the age and gender of animals, they are barely detectable in gonadal fat under

steady state conditions (usually less than five). In support of this, data by Moro *et al.* observed differences in ILC2 composition between different AT depots (Moro *et al.*, 2010). It is important to note that, whilst in studies by Moro *et al*. and Bénézech *et al.* some analysis of FALC composition was performed by immunofluorescence staining, demonstrating the presence of B cells, T cells ($CD3^+$ or $CD4^+$ cells) and ILC2s, when flow cytometry analysis was performed in these studies, the single cell suspension of the whole mesenteries plus FALC was analysed (Moro *et al.*, 2010, Koyasu and Moro, 2013, Benezech *et al.*, 2015, Jackson-Jones *et al.*, 2016). Therefore, changes seen may be in AT composition, rather than FALC composition. This argument is equally applicable to the data shown in this report with regards to changes in AT composition following infections; the changes seen herein may reflect AT-derived cell changes or FALC-derived cell changes. Furthermore, whole mount immunofluorescence staining is only sensitive enough to detect larger FALC, and thus gonadal fat may contain many smaller FALC that are not detectable by current techniques. The exact contribution that FALC has to the total cellularity of tissues has not been fully characterised, and is important in determining the significance of the caveat described above. Under steady state conditions, removal of easily visible FALC did not result in any difference in ILC populations within the mesenteries (unpublished data, Beth McKendrick, University of Birmingham), suggesting that immune cells within FALC may not represent a significant proportion of the total immune cellularity within mesenteries. However, this method is technically challenging and removes only clearly visible FALC and not smaller ones. Further refinement in techniques for labelling and identification of FALC of all sizes is required. One method that could overcome this would be to analyse changes in

FALC immune cell composition by immunofluorescence staining. In this respect, the use of the recently developed method described by Gerner *et al.* of histo-cytometry and clearing-enhanced tri-dimensional microscopy, which allows quantitative analysis of up to five different antibodies, might be useful in further establishing the immune cell composition of these clusters (Gerner *et al.*, 2012, Li *et al.*, 2017). Whilst Bénézech *et al.* showed reduction in FALC formation in mice lacking iNKT these cells were also lacking in other tissues (Benezech *et al.*, 2015). One method to test whether the formation of FALC is required for immune responses to helminth infection would be to compare responses in the absence of signals required for FALC formation. An example of this is TNF; the immune response following helminth infection could be compared between mice treated with antagonistic TNFR antibodies and untreated counterparts.

The data within this thesis focuses on the composition of adipose tissue and the number of FALC following infection with the helminth *H.polygyrus.* A future line of investigation would be not only to examine whether similar results are seen with other helminth infections, such as with *N.brasiliensis*, but also to determine whether FALC numbers change following other types of infection including bacterial, fungal and viral infections. Work by Bénézech *et al.,* demonstrated FALC formation in the adipose tissues of the pleural cavity following infection with the fungus *Alternaria alternata*, indicating that FALC formation can also occur at anatomical sites not examined within this thesis in response to fungal infection (Jackson-Jones *et al.*, 2016). Furthermore, unpublished work at The University of Birmingham indicates that the number of omental milky spots increase following infection with the bacterium *Salmonella typhimurium* (D18 P.I.). These results are interesting, as *S. typhimurium*

induces a Th1 polarised response, providing the first evidence that FALC formation occurs not only in Th2 polarised responses, but also in Th1 responses. Finally, there is evidence to support the formation of FALCs in murine models of systemic lupus erythematosus (Elewa *et al.*, 2016, Elewa *et al.*, 2017). Taken together, these data reinforce the crucial role of FALC in supporting a wide variety of adaptive immune responses.

In conclusion, it is clear from this study that the immune cell composition and phenotype is different between ATs and SLTs. Changes within ATs during infection of local tissues indicate that ILC2s, if not other cells within ATs, can contribute to immune responses. Questions that remain unanswered include whether differences between AT and SLT ILC2 phenotype, including the functional role that ILC2 surface proteins play in ILC2 biology, and cytokine production have a physiologically important role. Furthermore, following infection changes in ILC2 protein expression were observed in adipose tissues. Again, it would be of benefit to further investigate whether these changes result in functional changes (i.e. in cytokine production) to ILC2 within adipose tissues.

Finally, it is important to determine whether the contribution of AT-derived immune cells to immune responses is strictly limited to cells found within FALC. Whilst the role of FALC in supporting adaptive immune responses has been clearly demonstrated during artificial models of inflammation and also following helminth infection, future research should determine what is the mechanisms of FALC formations and their function following fungal, bacterial and viral infections and under other inflammatory conditions, such as during cancer and autoimmunity. A greater understanding of the role FALCs play in shaping immune responses could lead to

future developments in our ability to manipulate immune responses and prevent disease.

In order to fully investigate the above, better methods of dissociating FALC and remaining AT-resident immune cells are required.

7. APPENDIX

7.1. COMPARISON OF DIFFERENT GENETIC STRAINS (SEE CHAPTER 3.2.1)

Figure 7.1: Adipose tissue ILC composition in untreated BALB/c and C57BL/6J males

Cells were isolated from the gonadal fat and mesenteries of adult male BALB/c and C57BL/6J mice as described in Materials and Methods. The ILC composition was determined by flow cytometry, as demonstrated previously. Data for each group was obtained from two technical repeats.

Each data point (n=7, 9 for BALB/c and C57BL/6J animals respectively) represents an individual sample with a line indicating the median value. Statistical significance was determined using a Mann-Whitney two-tailed T test, *p<0.05, **p<0.01, ***p<0.001 and ****p<0.0001.

C) FACS plots showing representative ILC composition in gonadal fat (left) and mesenteries (right) from both C57BL/6J (top) and BALB/c (bottom) animals (pre-gated on live $CD45.2^+$ lymphocytes based on FSC and SSC profile and a viability marker). Numbers indicate percentage of events in each gate.

D) Graph showing adjusted number of total live cells (Total cellularity/100mg fat) in gonadal fat and mesenteries from BALB/c and C57BL/6J mice (gated on live/$dead^-$ cells).

E) Graph showing adjusted number of total ILCs (total ILCs/100mg fat) in gonadal fat and mesenteries from BALB/c and C57BL/6J mice (gated on live/$dead^-CD45.2^+$IL-$7R\alpha^+Lin^-$ cells).

F) Graph showing adjusted number of ILC2s (ILC2s/100mg fat) in gonadal fat and mesenteries from BALB/c and C57BL/6J mice (gated on live/$dead^-$ $CD45.2^+$IL-$7R\alpha^+Lin^-$intra$CD3^-RoR\gamma t^-GATA\text{-}3^+$ cells).

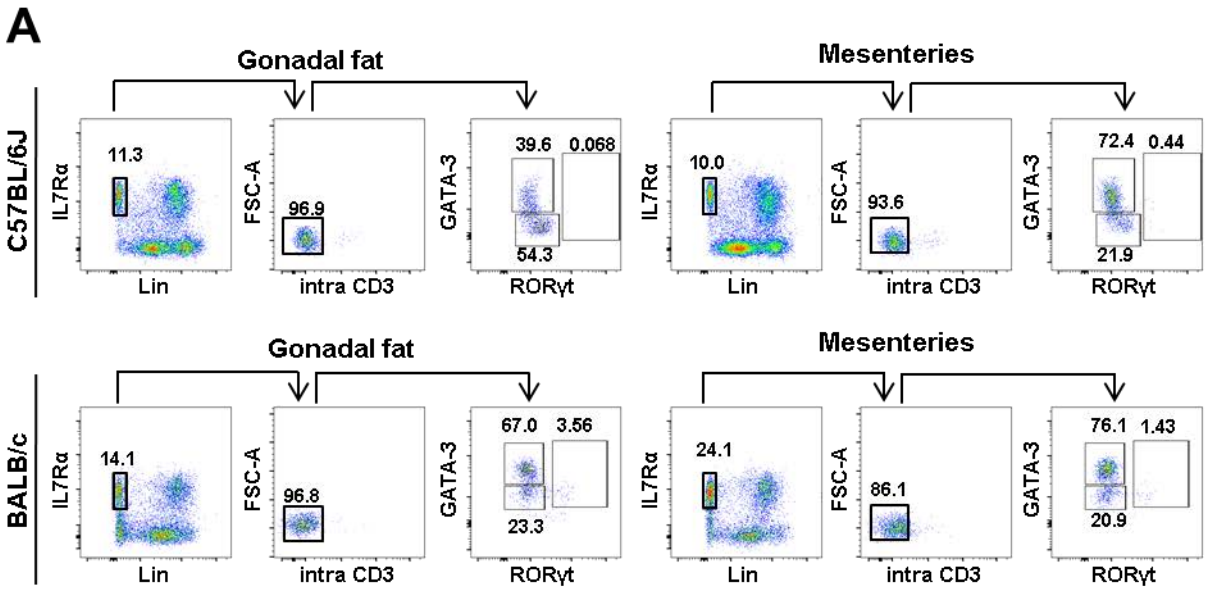
A
Gonadal fat
Mesenteries
C57BL/6J
IL7Rα
Lin
11.3
FSC-A
intra CD3
96.9
GATA-3
RORγt
39.6
0.068
54.3
10.0
93.6
72.4
0.44
21.9
BALB/c
14.1
96.8
67.0
3.56
23.3
24.1
86.1
76.1
1.43
20.9

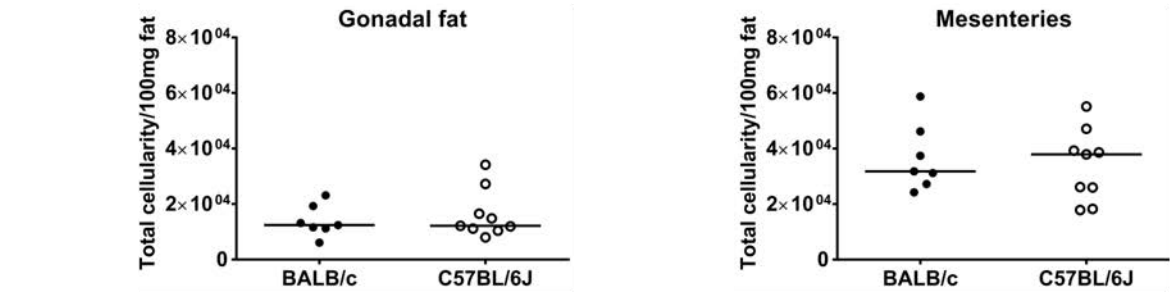
B
Gonadal fat
Mesenteries
Total cellularity/100mg fat
8×10^04
6×10^04
4×10^04
2×10^04
0
BALB/c
C57BL/6J

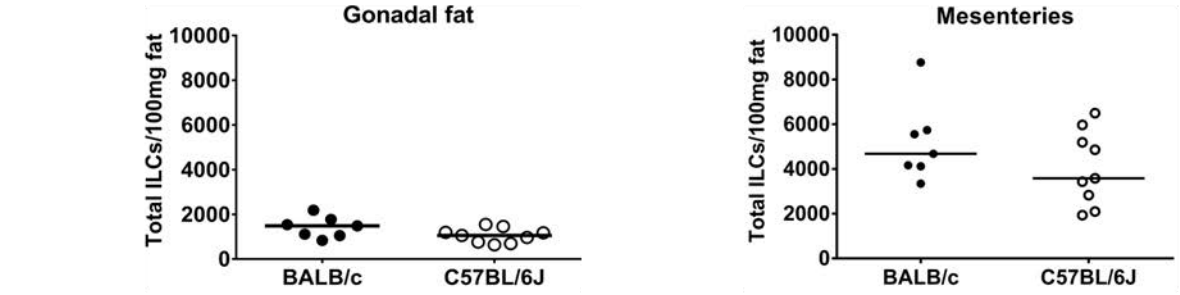
C
Gonadal fat
Mesenteries
Total ILCs/100mg fat
10000
8000
6000
4000
2000
0
BALB/c
C57BL/6J

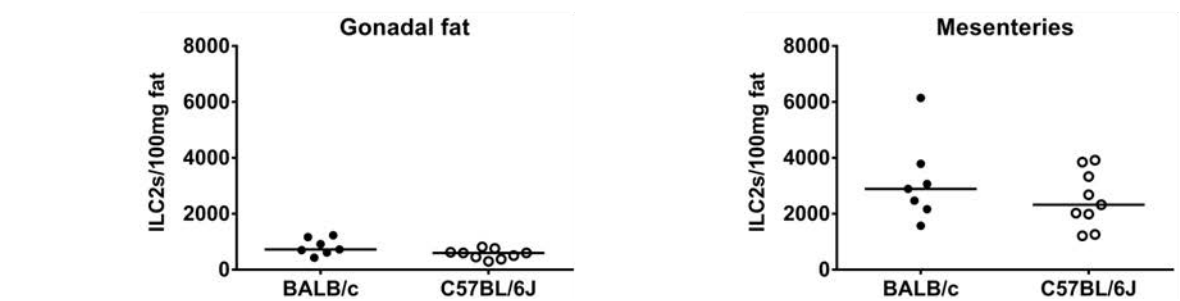
D
Gonadal fat
Mesenteries
ILC2s/100mg fat
8000
6000
4000
2000
0
BALB/c
C57BL/6J

Figure 7.2: MLN T cell composition in untreated BALB/c and C57BL/6J males

Cells were isolated from the MLN of adult male BALB/c and C57BL/6J mice, and the T cell composition was determined by flow cytometry as described in Materials and Methods. Data for each group was obtained from two technical repeats.

Each data point (n=7, 10 for BALB/c and C57BL/6J animals respectively) represents an individual sample with a line indicating the median value. Statistical significance was determined using a Mann-Whitney two-tailed T test, *p<0.05, **p<0.01, ***p<0.001 and ****p<0.0001.

A) FACS plots showing representative T cell composition in MLN isolated from both C57BL/6J (left) and BALB/c (right) animals (pre-gated on lymphocytes based on FSC/SSC profile then gated on live/dead$^-$CD45.2$^+$CD3$^+$ cells). Numbers indicate percentage of events in each gate.

B) Graph showing absolute number of CD4$^+$ cells in MLN from BALB/c and C57BL/6J mice (gated on CD45.2$^+$live/dead$^-$intraCD3$^+$CD4$^+$α-gal-cer$^-$ cells).

C) Graph showing adjusted number of regulatory T cells in MLN from BALB/c and C57BL/6J mice (gated on CD45.2$^+$live/dead$^-$intraCD3$^+$CD4$^+$α-gal-cer$^-$Foxp3$^+$ cells).

D) Graph showing absolute number of CD4$^+$ iNKT cells in MLN from BALB/c and C57BL/6J mice (gated on CD45.2$^+$live/dead$^-$intraCD3$^+$CD4$^+$α-gal-cer$^+$ cells).

E) Graph showing absolute number of Total ILCs in MLN from BALB/c and C57BL/6J mice (gated on CD45.2$^+$live/dead$^-$IL-7Rα$^+$Lin$^-$ cells).

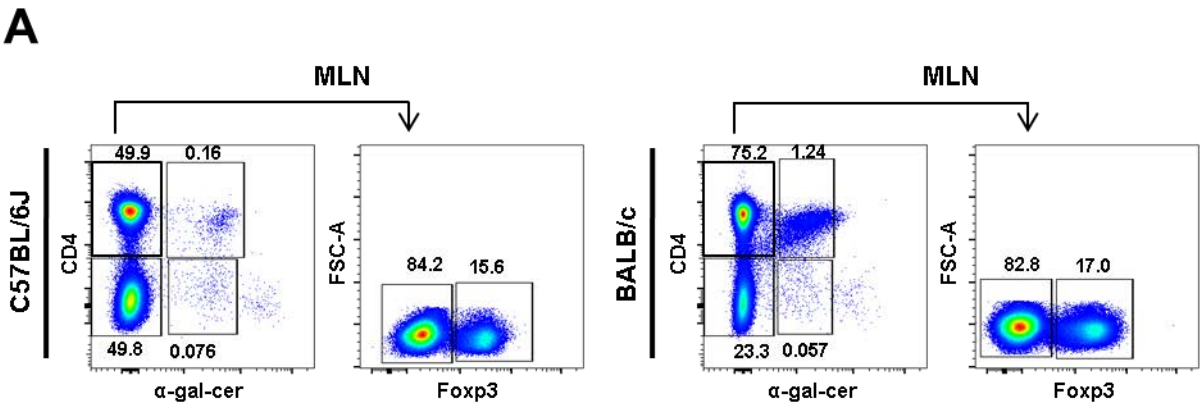
A
MLN
C57BL/6J
CD4
49.9
0.16
49.8
0.076
α-gal-cer
FSC-A
84.2
15.6
Foxp3
MLN
BALB/c
CD4
75.2
1.24
23.3
0.057
α-gal-cer
FSC-A
82.8
17.0
Foxp3

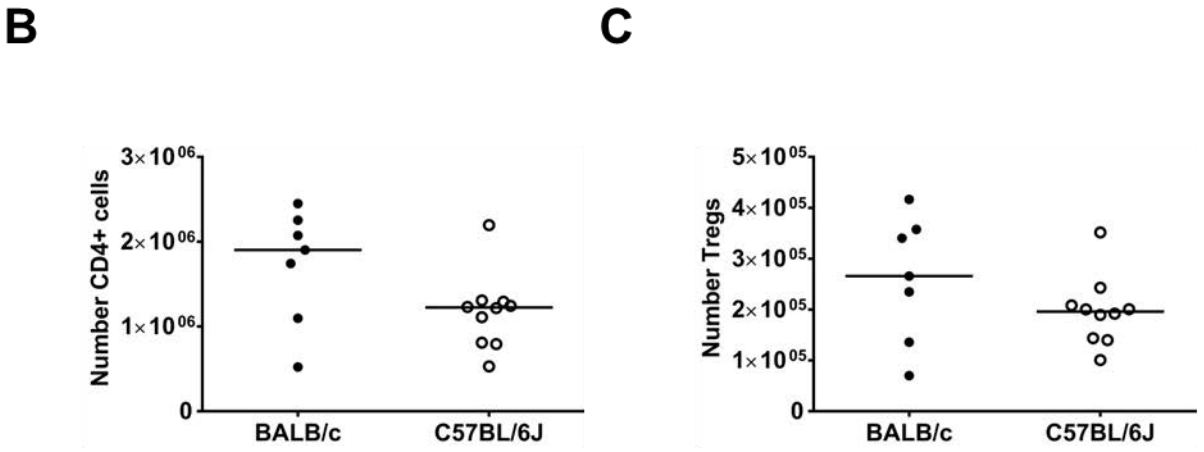
B
Number CD4+ cells
3×10^06
2×10^06
1×10^06
0
BALB/c
C57BL/6J
C
Number Tregs
5×10^05
4×10^05
3×10^05
2×10^05
1×10^05
0
BALB/c
C57BL/6J

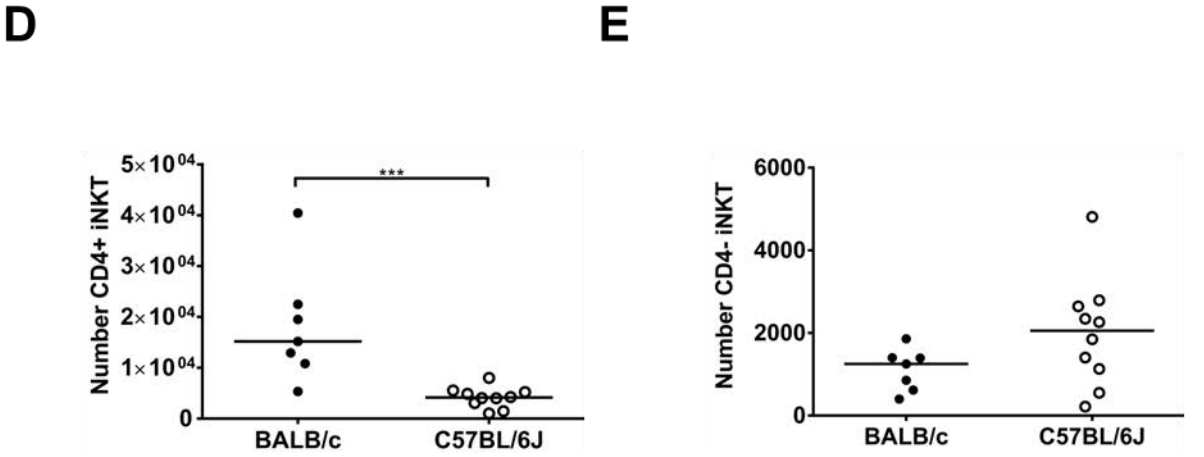
D
Number CD4+ iNKT
5×10^04
4×10^04
3×10^04
2×10^04
1×10^04
0
***
BALB/c
C57BL/6J
E
Number CD4- iNKT
6000
4000
2000
0
BALB/c
C57BL/6J

Figure 7.3: MLN ILC composition in untreated BALB/c and C57BL/6J males

Cells were isolated from the MLN of adult male BALB/c and C57BL/6J mice, and the ILC composition was determined by flow cytometry as described in Materials and Methods. Data for each group was obtained from two technical repeats.

Each data point (n=7, 10 for BALB/c and C57BL/6J animals respectively) represents an individual sample with a line indicating the median value. Statistical significance was determined using a Mann-Whitney two-tailed T test, *p<0.05, **p<0.01, ***p<0.001 and ****p<0.0001.

A) FACS plots showing representative ILC composition in MLN isolated from both C57BL/6J (top) and BALB/c (bottom) animals (pre-gated on live CD45.2$^+$ lymphocytes based on FSC and SSC profile and a viability marker). Numbers indicate percentage of events in each gate.

B) Graph showing absolute number of Total viable cells (Total cellularity) in MLN from BALB/c and C57BL/6J mice (gated on live/dead$^-$ cells).

C) Graph showing absolute number of Total ILCs in MLN from BALB/c and C57BL/6J mice (gated on CD45.2$^+$live/dead$^-$IL-7Rα$^+$Lin$^-$ cells).

D) Graph showing absolute number of ILC2s in MLN from BALB/c and C57BL/6J mice (gated on CD45.2$^+$live/dead$^-$IL-7Rα$^+$Lin$^-$intraCD3$^-$GATA-3$^+$RoRγt$^-$ cells).

E) Graph showing absolute number of group 3 ILCs in MLN from BALB/c and C57BL/6J mice (gated on CD45.2$^+$live/dead$^-$IL-7Rα$^+$Lin$^-$intraCD3$^-$RoRγt$^+$ cells).

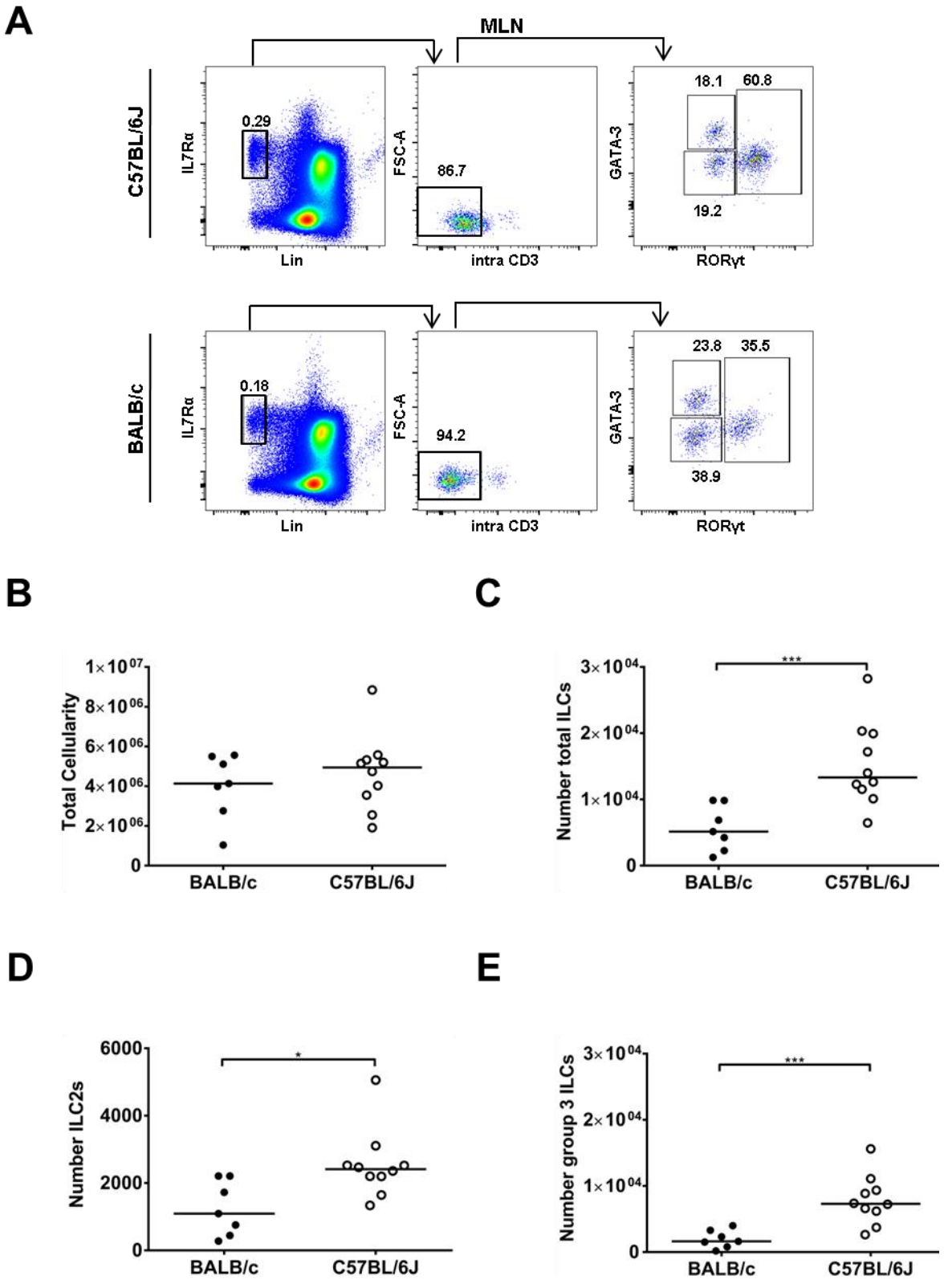
A
MLN
C57BL/6J
IL7Rα
Lin
0.29
FSC-A
intra CD3
86.7
GATA-3
RORγt
18.1
60.8
19.2
BALB/c
IL7Rα
Lin
0.18
FSC-A
intra CD3
94.2
GATA-3
RORγt
23.8
35.5
38.9
B
Total Cellularity
1×10^07
8×10^06
6×10^06
4×10^06
2×10^06
0
BALB/c
C57BL/6J
C
Number total ILCs
3×10^04
2×10^04
1×10^04
0
***
BALB/c
C57BL/6J
D
Number ILC2s
6000
4000
2000
0
*
BALB/c
C57BL/6J
E
Number group 3 ILCs
3×10^04
2×10^04
1×10^04
0
***
BALB/c
C57BL/6J

Figure 7.4: MLN ILC2 phenotype in untreated BALB/c and C57BL/6J males

Cells were isolated from the MLN of adult male BALB/c and C57BL/6J mice, and the ILC2 phenotype was determined by flow cytometry as described in Materials and Methods. Data for each group was obtained from two technical repeats.

Each data point (n=7, 10 for BALB/c and C57BL/6J animals respectively) represents an individual sample with a line indicating the median value. Statistical significance was determined using a Mann-Whitney two-tailed T test, *p<0.05, **p<0.01, ***p<0.001 and ****p<0.0001.

A) FACS plots showing representative ILC2 staining in MLN isolated from both C57BL/6J (top) and BALB/c (bottom) animals (pre-gated on live $CD45.2^+$ lymphocytes based on FSC and SSC profile and a viability marker). Numbers indicate percentage of events in each gate.

B) Histogram showing representative ICOS staining in MLN isolated from BALB/c (red lines) or C57BL/6J (blue lines) animals. Solid lines ILC2 staining ($CD45.2^+$live/$dead^-$$IL\text{-}7R\alpha^+Lin^-$$intraCD3^+ST2^{+/-}GATA\text{-}3^+$ cells), dotted lines ICOS FMO control. Numbers indicate the percentage of $ICOS^+$ cells.

C) Histogram showing representative KLRG1 staining in MLN isolated from BALB/c (red lines) or C57BL/6J (blue lines) animals. Vertical dotted black line indicates positive staining. Solid lines indicate ILC2 staining ($CD45.2^+$live/$dead^-$$IL\text{-}7R\alpha^+Lin^-$$intraCD3^-ST2^+GATA\text{-}3^+$ cells), dotted lines indicate KLRG1 negative control (gated on$CD45.2^+$live/$dead^-$$IL\text{-}7R\alpha^-$ $Lin^+intraCD3^-$ cells). Numbers indicate the percentage of $KLRG1^+$ cells.

D) Graph showing the percentage of ILC2s that are $ICOS^+$ in MLN from BALB/c and C57BL/6J mice (gated on $CD45.2^+$live/$dead^-$$IL\text{-}7R\alpha^+Lin^-$$intraCD3^-ST2^{+/-}$ $GATA\text{-}3^+ICOS^+$ cells).

E) Graph showing the expression of ICOS on the surface of ILC2s in MLN from BALB/c and C57BL/6J mice (gated on $CD45.2^+$live/$dead^-$$IL\text{-}7R\alpha^+Lin^-$$intraCD3^-$ $ST2^{+/-}GATA\text{-}3^+ICOS^+$ cells).

F) Graph showing the percentage of ILC2s that are $KLRG1^+$ in MLN from BALB/c and C57BL/6J mice (gated on $CD45.2^+$live/$dead^-$$IL\text{-}7R\alpha^+Lin^-$$intraCD3^-ST2^{+/-}$ $GATA\text{-}3^+KLRG1^+$cells).

G) Graph showing the expression of KLRG1 on the surface of ILC2s in MLN from BALB/c and C57BL/6J mice (gated on $CD45.2^+$live/$dead^-$$IL\text{-}7R\alpha^+Lin^-$$intraCD3^-$ $ST2^{+/-}GATA\text{-}3^+KLRG1^+$ cells). n=4, 5 for BALB/c and C57BL/6J animals respectively.

H) Graph showing the expression of ST2 on the surface of ILC2s in MLN from BALB/c and C57BL/6J mice (gated on $CD45.2^+$live/$dead^-$$IL\text{-}7R\alpha^+Lin^-$$intraCD3^-$ $ST2^{+/-}GATA\text{-}3^+$ cells). n=4, 5 for BALB/c and C57BL/6J animals respectively.

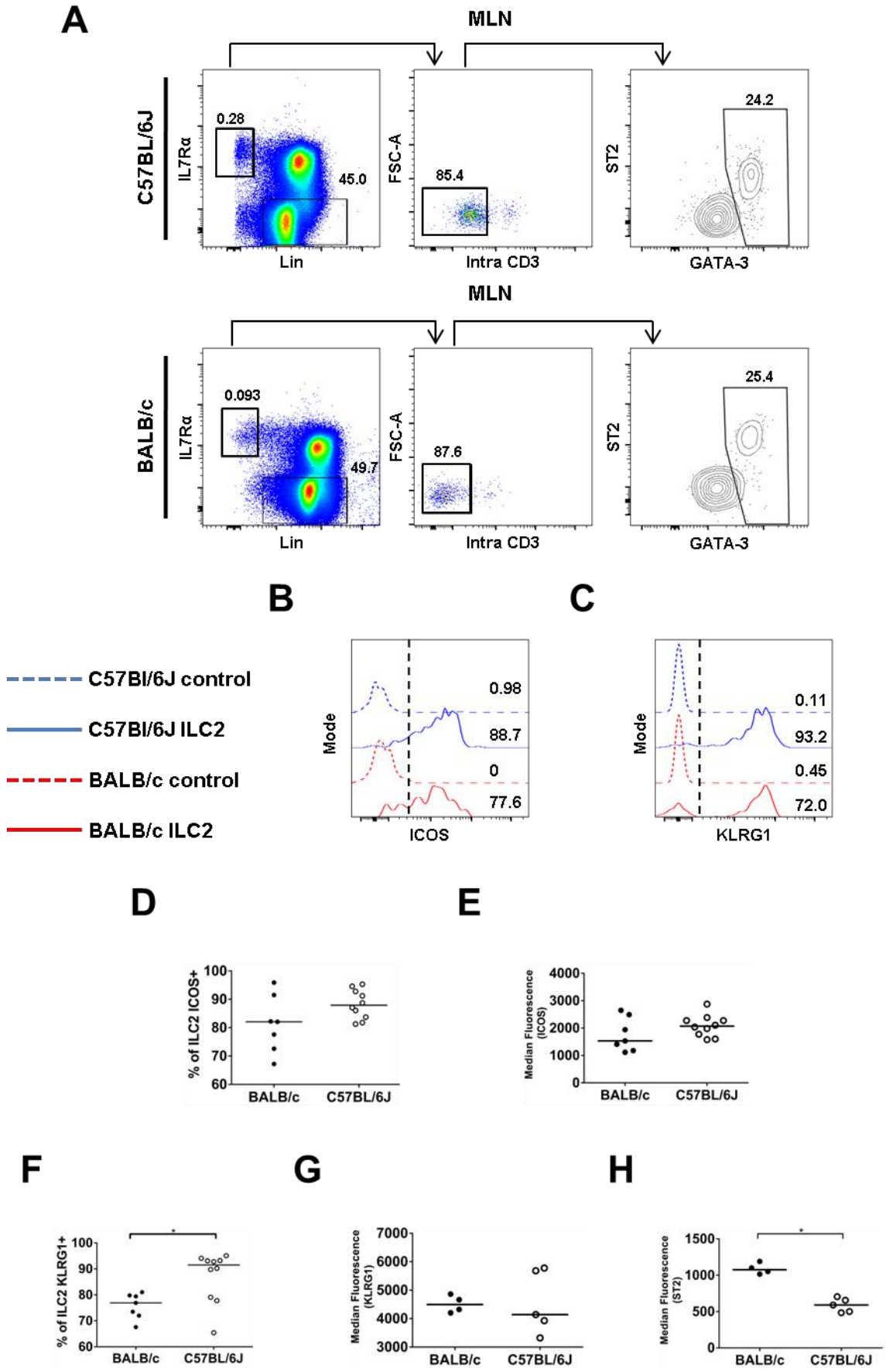
A
MLN
C57BL/6J
IL7Rα
Lin
0.28
45.0
FSC-A
Intra CD3
85.4
ST2
GATA-3
24.2
MLN
BALB/c
IL7Rα
Lin
0.093
49.7
FSC-A
Intra CD3
87.6
ST2
GATA-3
25.4
B
C
C57Bl/6J control
C57Bl/6J ILC2
BALB/c control
BALB/c ILC2
Mode
ICOS
0.98
88.7
0
77.6
Mode
KLRG1
0.11
93.2
0.45
72.0
D
E
% of ILC2 ICOS+
BALB/c
C57BL/6J
Median Fluorescence (ICOS)
BALB/c
C57BL/6J
F
G
H
% of ILC2 KLRG1+
BALB/c
C57BL/6J
Median Fluorescence (KLRG1)
BALB/c
C57BL/6J
Median Fluorescence (ST2)
BALB/c
C57BL/6J

7.2. COMPARISON OF MALE AND FEMALE MICE (SEE CHAPTER 3.2.2)

Figure 7.5: Adipose tissue iNKT cell composition in untreated BALB/c males and females

Cells were isolated from the gonadal fat and mesenteries of adult male and female BALB/c mice as described in Materials and Methods section. The iNKT cell composition was determined by flow cytometry, as demonstrated previously. Data for each group was obtained from two technical repeats.

Each data point (n=7, 6 for males and females respectively) represents an individual sample with a line indicating the median value. Statistical significance was determined using a Mann-Whitney two-tailed T test, *p<0.05, **p<0.01, ***p<0.001 and ****p<0.0001.

A) FACS plots showing representative iNKT cell composition in gonadal fat (left) and mesenteries (right) from both male (top) and female (bottom) animals (pre-gated on lymphocytes based on FSC/SSC profile then gated on live/dead$^-$ CD45.2$^+$CD3$^+$cells). Numbers indicate percentage of events in each gate.

B) Graph showing adjusted number of total live cells (Total cellularity/100mg fat) in gonadal fat and mesenteries from male and female mice (gated on live/dead$^-$ cells).

C) Graph showing adjusted number of CD4$^+$ iNKT cells (CD4$^+$iNKTs/100mg fat) in gonadal fat and mesenteries from male and female mice (gated on CD45.2$^+$live/dead$^-$intraCD3$^+$CD4$^+$α-gal-cer$^+$ cells).

D) Graph showing adjusted number of CD4$^-$ iNKT cells (CD4$^-$iNKTs/100mg fat) in gonadal fat and mesenteries from male and female mice (gated on CD45.2$^+$live/dead$^-$intraCD3$^+$CD4$^-$α-gal-cer$^+$ cells).

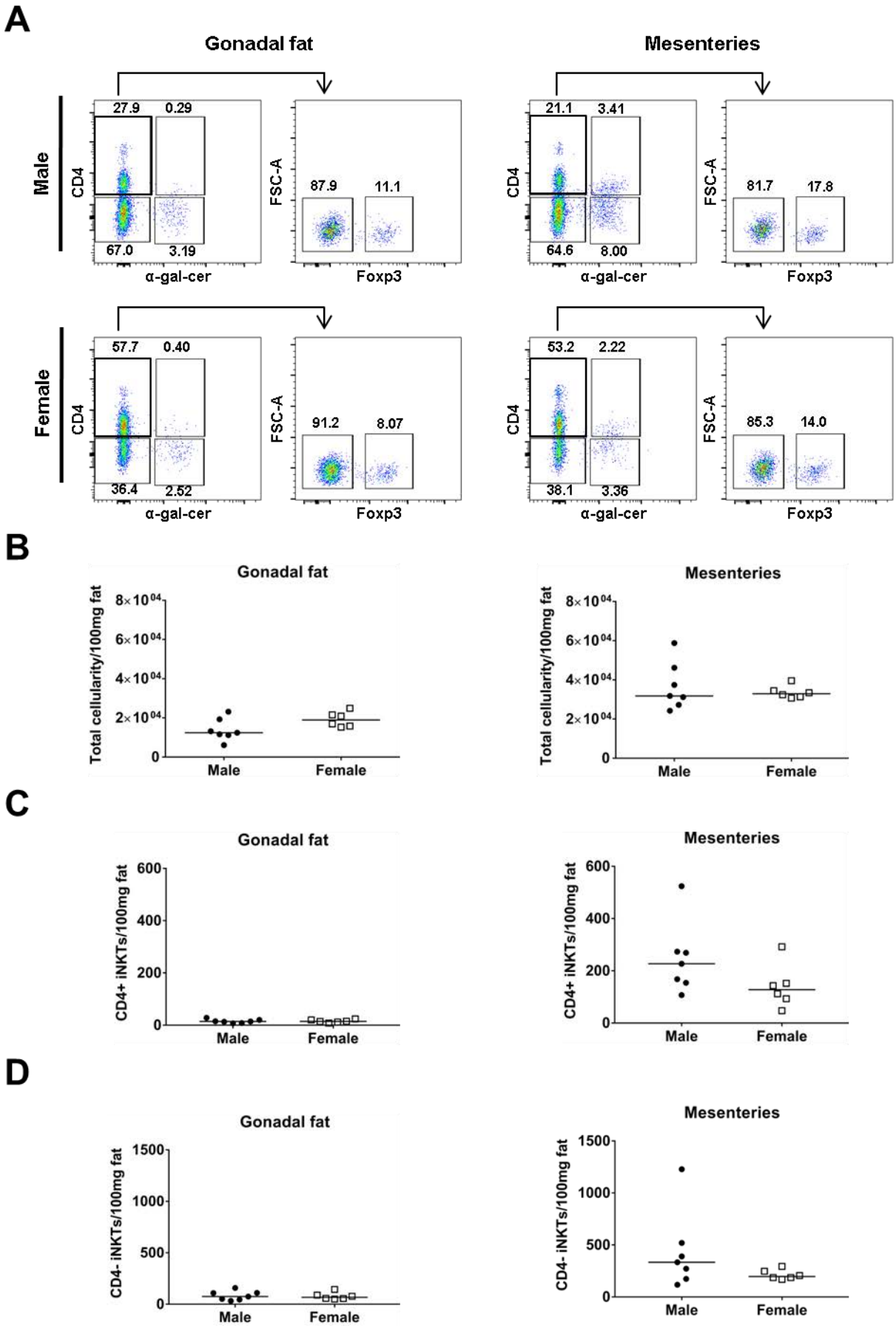
A
Gonadal fat
Mesenteries
Male
Female
CD4
α-gal-cer
FSC-A
Foxp3
27.9
0.29
67.0
3.19
87.9
11.1
21.1
3.41
64.6
8.00
81.7
17.8
57.7
0.40
36.4
2.52
91.2
8.07
53.2
2.22
38.1
3.36
85.3
14.0
B
Gonadal fat
Mesenteries
Total cellularity/100mg fat
8×10^04
6×10^04
4×10^04
2×10^04
0
Male
Female
C
Gonadal fat
Mesenteries
CD4+ iNKTs/100mg fat
600
400
200
0
Male
Female
D
Gonadal fat
Mesenteries
CD4- iNKTs/100mg fat
1500
1000
500
0
Male
Female

Figure 7.6: MLN T cell composition in untreated BALB/c males and females

Cells were isolated from the MLN of adult male and female BALB/c mice, and the T and iNKT cell composition was determined by flow cytometry as described in Materials and Methods. Data for each group was obtained from two technical repeats.

Each data point (n=7, 6 for males and females respectively) represents an individual sample with a line indicating the median value. Statistical significance was determined using a Mann-Whitney two-tailed T test, *p<0.05, **p<0.01, ***p<0.001 and ****p<0.0001.

A) FACS plots showing representative T cell composition in MLN isolated from both male (left) and female (right) animals (pre-gated on live $CD45.2^+$ lymphocytes based on FSC and SSC profile and a viability marker). Numbers indicate percentage of events in each gate.

B) Graph showing absolute number of Total viable cells in MLN from male and female mice (gated on live/$dead^-$ cells).

C) Graph showing absolute number of $CD4^+$ cells in MLN from male and female mice (gated on $CD45.2^+$live/$dead^-$intra$CD3^+CD4^+$α-gal-cer^- cells).

D) Graph showing absolute number of Tregs in MLN from male and female mice (gated on $CD45.2^+$live/$dead^-$intra$CD3^+CD4^+$α-gal-cer^-Foxp3^+ cells).

E) Graph showing absolute number of $CD4^+$ iNKT cells in MLN from male and female mice (gated on $CD45.2^+$live/$dead^-$intra$CD3^+CD4^+$α-gal-cer^+ cells).

F) Graph showing absolute number of $CD4^-$ iNKT cells in MLN from male and female mice (gated on $CD45.2^+$live/$dead^-$intra$CD3^+CD4^-$α-gal-cer^+ cells).

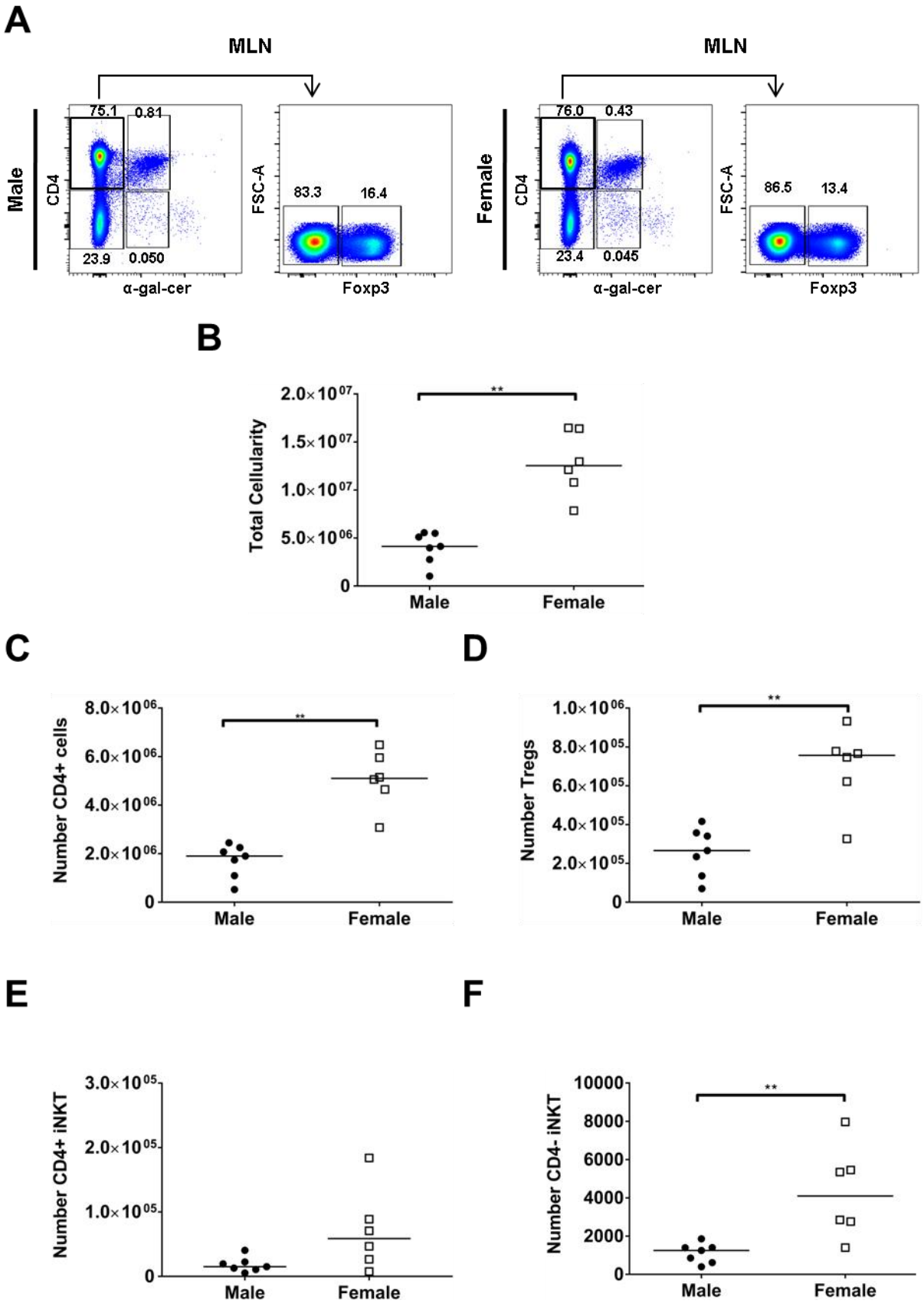
A
MLN
MLN
Male
Female
CD4
α-gal-cer
FSC-A
Foxp3
75.1
0.81
23.9
0.050
83.3
16.4
76.0
0.43
23.4
0.045
86.5
13.4
B
Total Cellularity
2.0×10^07
1.5×10^07
1.0×10^07
5.0×10^06
0
**
Male
Female
C
Number CD4+ cells
8.0×10^06
6.0×10^06
4.0×10^06
2.0×10^06
0
**
Male
Female
D
Number Tregs
1.0×10^06
8.0×10^05
6.0×10^05
4.0×10^05
2.0×10^05
0
**
Male
Female
E
Number CD4+ iNKT
3.0×10^05
2.0×10^05
1.0×10^05
0
Male
Female
F
Number CD4- iNKT
10000
8000
6000
4000
2000
0
**
Male
Female

Figure 7.7: MLN ILC composition in untreated BALB/c males and females

Cells were isolated from the MLN of adult male and female BALB/c mice, and the ILC composition was determined by flow cytometry as described in Materials and Methods. Data for each group was obtained from two technical repeats.

Each data point (n=7, 6 for males and females respectively) represents an individual sample with a line indicating the median value. Statistical significance was determined using a Mann-Whitney two-tailed T test, *p<0.05, **p<0.01, ***p<0.001 and ****p<0.0001.

A) FACS plots showing representative ILC composition in MLN isolated from both male (top) and female (bottom) animals (pre-gated on live CD45.2$^+$ lymphocytes based on FSC and SSC profile and a viability marker). Numbers indicate percentage of events in each gate.

B) Graph showing absolute number of Total ILCs in MLN from male and female mice (gated on CD45.2$^+$live/dead$^-$IL-7Rα$^+$Lin$^-$ cells).

C) Graph showing absolute number of ILC2s in MLN from male and female mice (gated on CD45.2$^+$live/dead$^-$IL-7Rα$^+$Lin$^-$intraCD3$^-$GATA-3$^+$RoRγt$^-$ cells).

D) Graph showing absolute number of ILC3s in MLN from male and female mice (gated on CD45.2$^+$live/dead$^-$IL-7Rα$^+$Lin$^-$intraCD3$^-$RoRγt$^+$ cells).

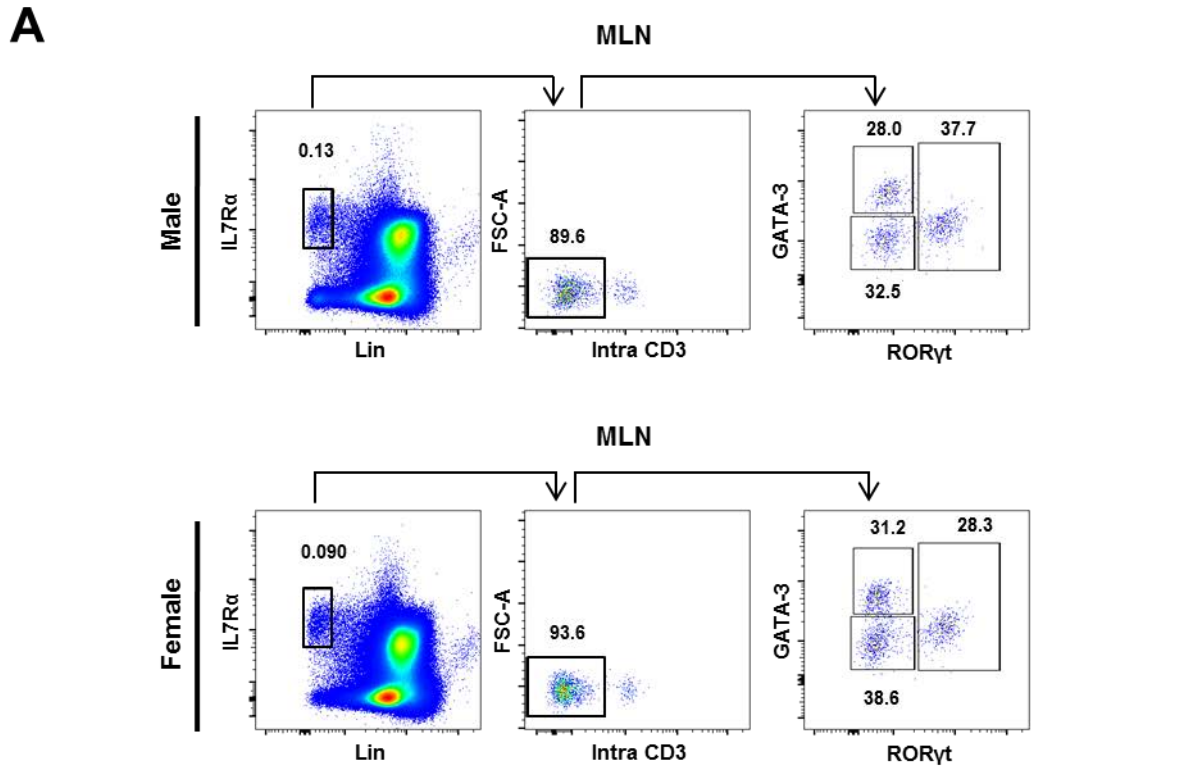
A
MLN
Male
IL7Rα
Lin
0.13
FSC-A
Intra CD3
89.6
GATA-3
RORγt
28.0
37.7
32.5
MLN
Female
IL7Rα
Lin
0.090
FSC-A
Intra CD3
93.6
GATA-3
RORγt
31.2
28.3
38.6

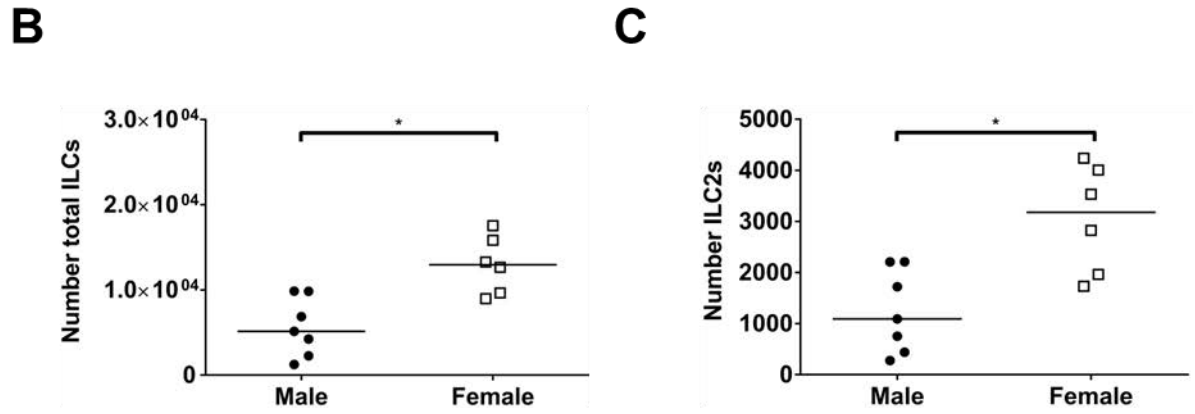
B
Number total ILCs
3.0×10^04
2.0×10^04
1.0×10^04
0
*
Male
Female
C
Number ILC2s
5000
4000
3000
2000
1000
0
*
Male
Female

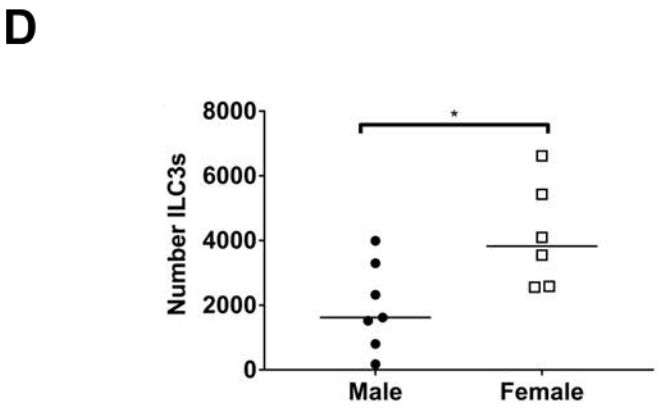
D
Number ILC3s
8000
6000
4000
2000
0
*
Male
Female

Figure 7.8: MLN ILC2 phenotype in untreated BALB/c males and females

Cells were isolated from the MLN of adult male and female BALB/c mice, and the ILC2 phenotype was determined by flow cytometry as described in Materials and Methods. Data for each group was obtained from two technical repeats.

Each data point (n=7, 6 for males and females respectively) represents an individual sample with a line indicating the median value. Statistical significance was determined using a Mann-Whitney two-tailed T test, *p<0.05, **p<0.01, ***p<0.001 and ****p<0.0001.

A) FACS plots showing representative ILC2 staining in MLN isolated from both male (top) and female (bottom) animals (pre-gated on live $CD45.2^+$ lymphocytes based on FSC and SSC profile and a viability marker). Numbers indicate percentage of events in each gate.

B) Histogram showing representative ICOS staining in MLN isolated from female (red lines) or male (blue lines) animals. Vertical dotted black line indicates positive staining. Solid lines indicate ILC2 staining ($CD45.2^+$live/dead$^-$ IL-7Rα^+Lin$^-$intraCD3$^+$ST2$^{+/-}$GATA-3$^+$ cells), dotted lines indicate ICOS FMO control. Numbers indicate the percentage of ICOS$^+$ cells.

C) Histogram showing representative KLRG1 staining in MLN isolated from female (red lines) or male (blue lines) animals. Vertical dotted black line indicates positive staining. Solid lines indicate ILC2 staining ($CD45.2^+$live/dead$^-$IL-7Rα^+Lin$^-$intraCD3$^-$ST2$^+$GATA-3$^+$ cells), dotted lines indicate KLRG1 negative control (gated on $CD45.2^+$live/dead$^-$IL-7Rα^- Lin$^+$intraCD3$^-$ cells). Numbers indicate the percentage of KLRG1$^+$ cells.

D) Graph showing the percentage of ILC2s that are ICOS$^+$ in MLN from male and female mice (gated on $CD45.2^+$live/dead$^-$IL-7Rα^+Lin$^-$intraCD3$^-$ST2$^{+/-}$ GATA-3$^+$ICOS$^+$ cells).

E) Graph showing the expression of ICOS on the surface of ILC2s in MLN from male and female mice (gated on $CD45.2^+$live/dead$^-$IL-7Rα^+Lin$^-$intraCD3$^-$ST2$^{+/-}$ GATA-3$^+$ICOS$^+$ cells).

F) Graph showing the percentage of ILC2s that are KLRG1$^+$in MLN from male and female mice (gated on $CD45.2^+$live/dead$^-$IL-7Rα^+Lin$^-$intraCD3$^-$ST2$^{+/-}$ GATA-3$^+$KLRG1$^+$ cells).

G) Graph showing the expression of KLRG1 on the surface of ILC2s in MLN from male and female mice (gated on $CD45.2^+$live/dead$^-$IL-7Rα^+Lin$^-$intraCD3$^-$ST2$^{+/-}$ GATA-3$^+$KLRG1$^+$ cells). n=4, 4 for males and females respectively.

H) Graph showing the expression of ST2 on the surface of ILC2s in MLN from male and female mice (gated on $CD45.2^+$live/dead$^-$IL-7Rα^+Lin$^-$intraCD3$^-$ST2$^{+/-}$ GATA-3$^+$ cells).

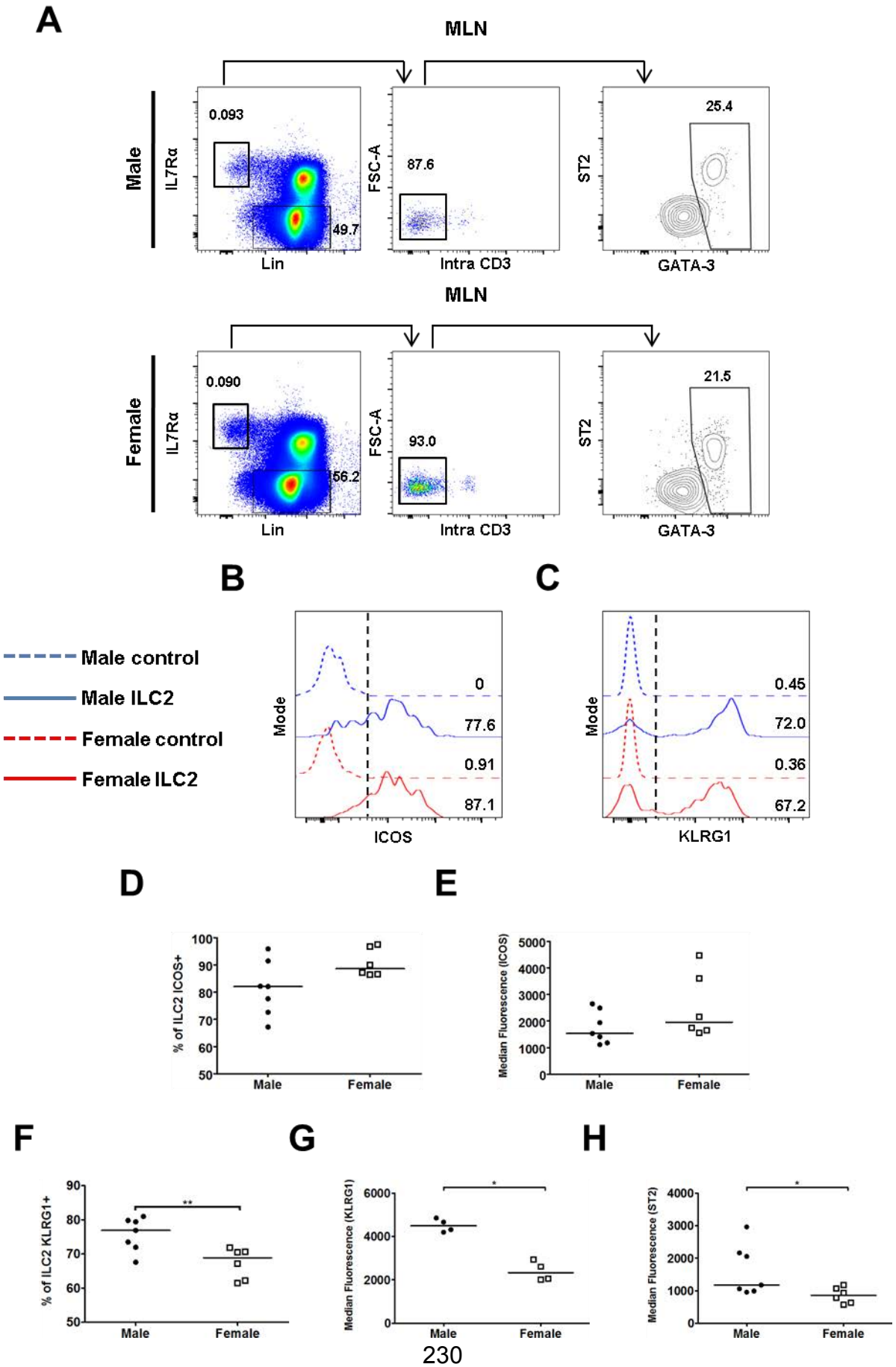
A
MLN
Male
IL7Rα
0.093
49.7
Lin
FSC-A
87.6
Intra CD3
ST2
25.4
GATA-3
MLN
Female
IL7Rα
0.090
56.2
Lin
FSC-A
93.0
Intra CD3
ST2
21.5
GATA-3
B
C
Male control
Male ILC2
Female control
Female ILC2
Mode
0
77.6
0.91
87.1
ICOS
Mode
0.45
72.0
0.36
67.2
KLRG1
D
E
% of ILC2 ICOS+
Male
Female
Median Fluorescence (ICOS)
Male
Female
F
G
H
% of ILC2 KLRG1+
**
Male
Female
Median Fluorescence (KLRG1)
*
Male
Female
Median Fluorescence (ST2)
*
Male
Female

7.3. ILC2 CHEMOKINE RECEPTOR STAINING (SEE CHAPTER 3.3.2)

Figure 7.9: Isotype controls for chemokine receptor staining

Cells were isolated from the ILN, MLN, gonadal fat, mesenteries, lung and SILP of adult male C57BL/6J mice as described in Materials and Methods. Isotype controls for the various chemokine receptors were then assessed by flow cytometry. Data for each group was obtained from two technical repeats.

A) FACS plots showing representative staining of isotype control for CCR8 (pre-gated on live/dead$^-$CD45.2$^+$IL-7Rα$^+$Lin$^-$intraCD3$^-$GATA-3$^+$ cells). Numbers indicate percentage of events in each gate.

B) As in A for CCR9.

C) As in A for CXCR6.

D) As in A for CCRL2.

E) Histogram showing representative staining of isotype control for CCR6 (pre-gated on live/dead$^-$CD45.2$^+$IL-7Rα$^+$Lin$^-$intraCD3$^-$GATA-3$^+$ cells). Vertical dotted black line indicates positive staining. Blue line shows LN control, red line shows adipose tissue control, orange line shows lung control and green line shows SILP control. Numbers indicate percentage of events in each gate.

F) As in E for CCR4.

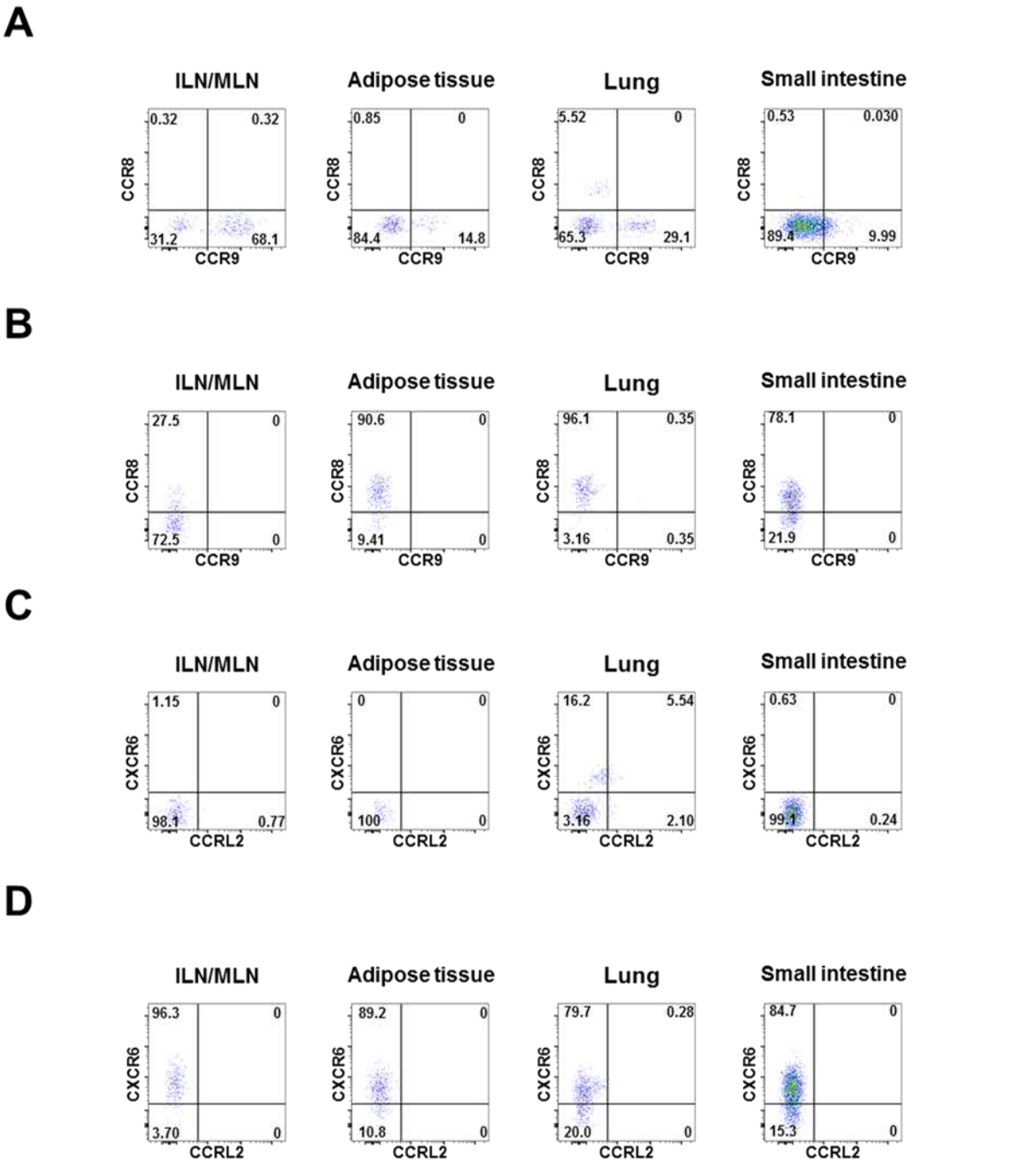
A
ILN/MLN
Adipose tissue
Lung
Small intestine
CCR8
CCR9
0.32
0.32
31.2
68.1
0.85
0
84.4
14.8
5.52
0
65.3
29.1
0.53
0.030
89.4
9.99
B
27.5
0
72.5
0
90.6
0
9.41
0
96.1
0.35
3.16
0.35
78.1
0
21.9
0
C
CXCR6
CCRL2
1.15
0
98.1
0.77
0
0
100
0
16.2
5.54
3.16
2.10
0.63
0
99.1
0.24
D
96.3
0
3.70
0
89.2
0
10.8
0
79.7
0.28
20.0
0
84.7
0
15.3
0
E
Mode
0
0.56
4.78
0
CCR6
F
0
0
0.45
0
CCR4
LN control
Adipose tissue control
Lung control
Small intestine control

7.4. ILC2 CYTOKINE PRODUCTION IN IL-33$^{cit/cit}$ ANIMALS (SEE CHAPTER 4.2)

Figure 7.10: Cytokine production by unstimulated and stimulated ILC2s isolated from WT and IL-33$^{cit/cit}$ animals (median fluorescence)

Cells were isolated from the MLN, gonadal fat and mesenteries of adult male BALB/c and IL-33$^{cit/cit}$ mice (also on BALB/c background) as described in Materials and Methods. The ILC2 cytokine production *ex vivo* was determined by flow cytometry following incubation with PMA, Ionomycin and Brefeldin A (see Materials and Methods for details). Data for each group was obtained from two technical repeats.

Each data point (n=4, 6 for WT and IL-33$^{cit/cit}$ animals respectively) represents an individual sample with a line indicating the median value. Statistical significance was determined using a Mann-Whitney two-tailed T test, *p<0.05, **p<0.01, ***p<0.001 and ****p<0.0001.

A) Graph showing total expression of IL-5 by unstimulated ILC2s in MLN, gonadal fat and mesenteries from WT and IL-33$^{cit/cit}$ mice (media control, gated on CD45.2^{+}live/dead^{-}IL-7Rα^{+}Lin^{-}intraCD3^{-}GATA-3^{+}IL-5^{+}IL-13$^{+/-}$cells).

B) Graph showing expression of IL-13 by unstimulated ILC2s in MLN, gonadal fat and mesenteries from WT and IL-33$^{cit/cit}$ mice (media control, gated on CD45.2^{+}live/dead^{-}IL-7Rα^{+}Lin^{-}intraCD3^{-}GATA-3^{+}IL-5$^{+/-}$IL-13^{+} cells).

C) Graph showing expression of IL-5 by stimulated ILC2s in MLN, gonadal fat and mesenteries from WT and IL-33$^{cit/cit}$ mice (gated on CD45.2^{+}live/dead^{-} IL-7Rα^{+}Lin^{-}intraCD3^{-}GATA-3^{+}IL-5^{+}IL-13$^{+/-}$ cells).

D) Graph showing expression of IL-13 by stimulated ILC2s in MLN, gonadal fat and mesenteries from WT and IL-33$^{cit/cit}$ mice (gated on CD45.2^{+}live/dead^{-} IL-7Rα^{+}Lin^{-}intraCD3^{-}GATA-3^{+}IL-5$^{+/-}$IL-13^{+} cells).

A

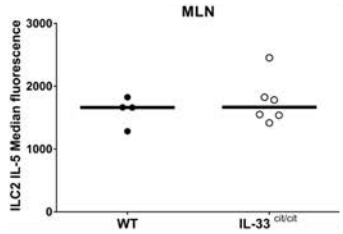
MLN
ILC2 IL-5 Median fluorescence
3000
2000
1000
0
WT
IL-33 cit/cit

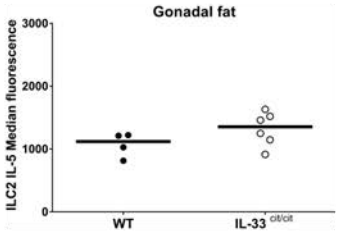
Gonadal fat
ILC2 IL-5 Median fluorescence
3000
2000
1000
0
WT
IL-33 cit/cit

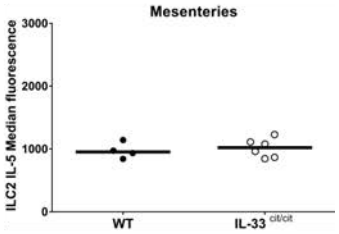
Mesenteries
ILC2 IL-5 Median fluorescence
3000
2000
1000
0
WT
IL-33 cit/cit

B

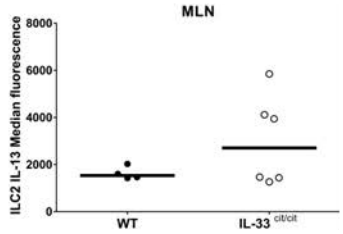
MLN
ILC2 IL-13 Median fluorescence
8000
6000
4000
2000
0
WT
IL-33 cit/cit

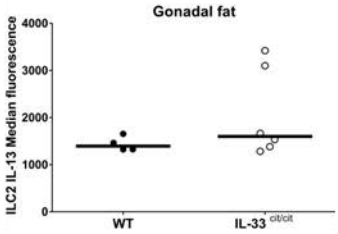
Gonadal fat
ILC2 IL-13 Median fluorescence
4000
3000
2000
1000
0
WT
IL-33 cit/cit

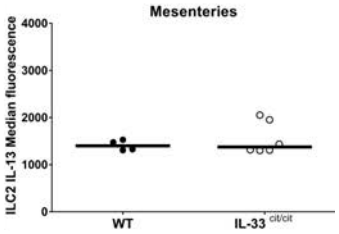
Mesenteries
ILC2 IL-13 Median fluorescence
4000
3000
2000
1000
0
WT
IL-33 cit/cit

C

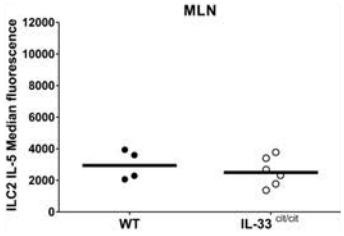
MLN
ILC2 IL-5 Median fluorescence
12000
10000
8000
6000
4000
2000
0
WT
IL-33 cit/cit

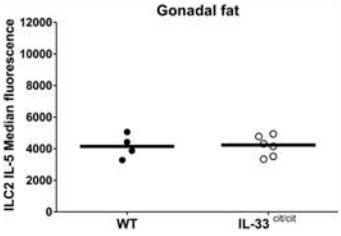
Gonadal fat
ILC2 IL-5 Median fluorescence
12000
10000
8000
6000
4000
2000
0
WT
IL-33 cit/cit

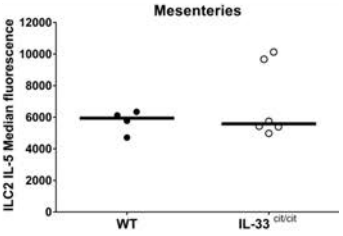
Mesenteries
ILC2 IL-5 Median fluorescence
12000
10000
8000
6000
4000
2000
0
WT
IL-33 cit/cit

D

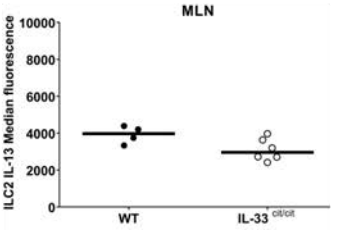
MLN
ILC2 IL-13 Median fluorescence
10000
8000
6000
4000
2000
0
WT
IL-33 cit/cit

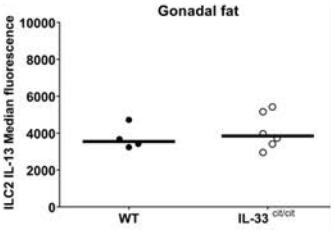
Gonadal fat
ILC2 IL-13 Median fluorescence
10000
8000
6000
4000
2000
0
WT
IL-33 cit/cit

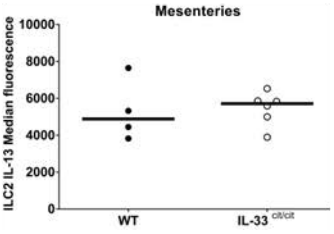
Mesenteries
ILC2 IL-13 Median fluorescence
10000
8000
6000
4000
2000
0
WT
IL-33 cit/cit

7.5. IMMUNE CELL COMPOSITION IN P55/P75$^{-/-}$ ANIMALS (SEE CHAPTER 4.3.1)

Figure 7.11: MLN T cell composition in WT and 55/p75$^{-/-}$ mice

Cells were isolated from the MLN of adult male WT and 55/p75$^{-/-}$ mice (both on C57BL/6J background) as described in Materials and Methods. The T cell composition was determined by flow cytometry, as demonstrated previously. Data for each group was obtained from two technical repeats.

Each data point (n=4, 5 for WT and p55p/75$^{-/-}$ animals respectively) represents an individual sample with a line indicating the median value. Statistical significance was determined using a Mann-Whitney two-tailed T test, *p<0.05, **p<0.01, ***p<0.001 and ****p<0.0001.

A) FACS plots showing representative T cell composition in MLN both WT (left) and p55/p75$^{-/-}$ (right) animals (pre-gated on live CD45.2^{+} lymphocytes based on FSC and SSC profile and a viability marker). Numbers indicate percentage of events in each gate.

B) Graph showing adjusted total cellularity in MLN from WT and p55/p75$^{-/-}$ animals (gated on live/dead^{-} cells).

C) Graph showing adjusted number of CD4^{+} iNKT cells in MLN from WT and p55/p75$^{-/-}$animals (gated on CD45.2^{+}live/dead^{-}intraCD3^{+}CD4^{+}α-gal-cer^{+} cells).

D) Graph showing adjusted number of CD4^{-} iNKT cells in MLN isolated from WT and p55/p75$^{-/-}$ animals (gated on CD45.2^{+}live/dead^{-}intraCD3^{+}CD4^{-}α-gal-cer^{+} cells).

E) Graph showing adjusted number of CD4^{+} cells in MLN isolated from WT and p55/p75$^{-/-}$ animals (gated on CD45.2^{+}live/dead^{-}intraCD3^{+}CD4^{+}α-gal-cer^{-} cells).

F) Graph showing adjusted number of regulatory T cells in MLN isolated from WT and p55/p75$^{-/-}$animals (gated on CD45.2^{+}live/dead^{-}intraCD3^{+}CD4^{+}α-gal-cer^{-} Foxp3^{+} cells).

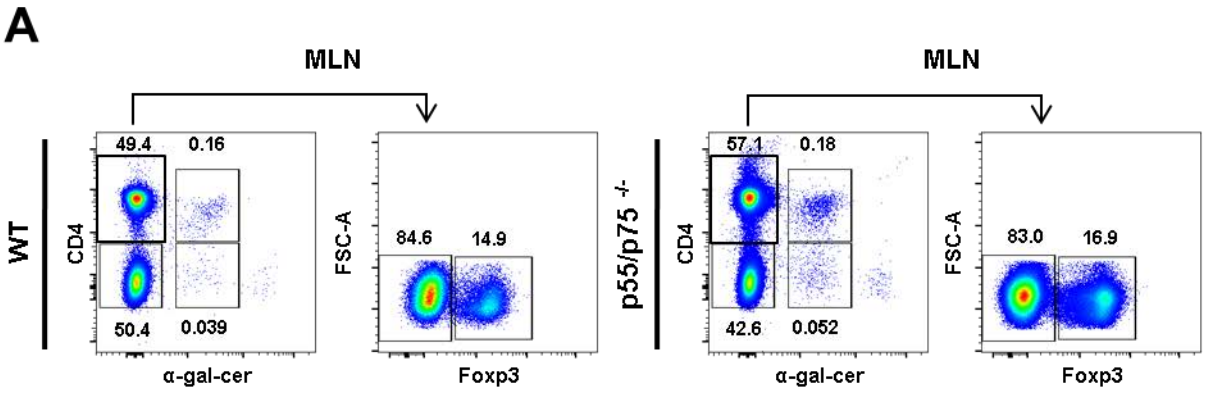
A
MLN
MLN
WT
p55/p75 -/-
CD4
α-gal-cer
FSC-A
Foxp3
49.4
0.16
50.4
0.039
84.6
14.9
57.1
0.18
42.6
0.052
83.0
16.9

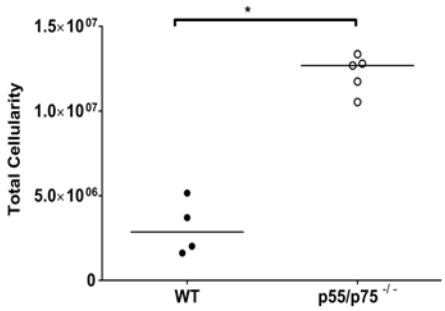
B
Total Cellularity
1.5×10^07
1.0×10^07
5.0×10^06
0
WT
p55/p75 -/-
*

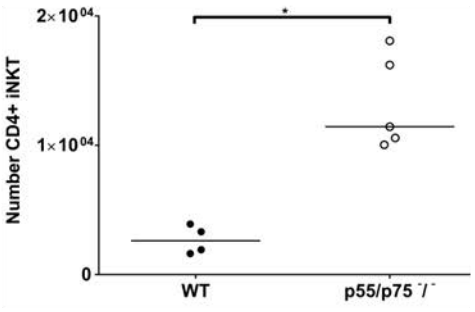
C
Number CD4+ iNKT
2×10^04
1×10^04
0
WT
p55/p75 -/-
*

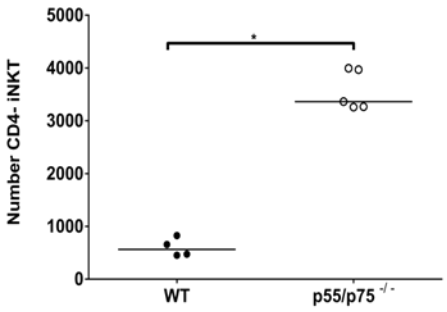
D
Number CD4- iNKT
5000
4000
3000
2000
1000
0
WT
p55/p75 -/-
*

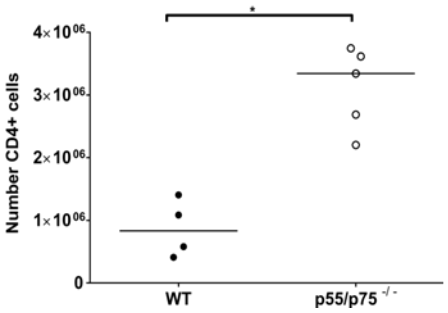
E
Number CD4+ cells
4×10^06
3×10^06
2×10^06
1×10^06
0
WT
p55/p75 -/-
*

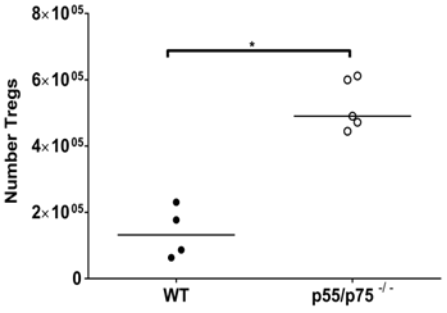
F
Number Tregs
8×10^05
6×10^05
4×10^05
2×10^05
0
WT
p55/p75 -/-
*

Figure 7.12: MLN ILC composition in WT and 55/p75$^{-/-}$ mice

Cells were isolated from the MLN of adult male WT and p55/p75$^{-/-}$ mice (both on C57BL/6J background) as described in Materials and Methods. The ILC cell composition was determined by flow cytometry, as demonstrated previously. Data for each group was obtained from two technical repeats.

Each data point (n=4, 5 for WT and p55p/75$^{-/-}$ animals respectively) represents an individual sample with a line indicating the median value. Statistical significance was determined using a Mann-Whitney two-tailed T test, *p<0.05, **p<0.01, ***p<0.001 and ****p<0.0001.

A) FACS plots showing representative ILC composition in MLN isolated from both WT (top) and p55/p75$^{-/-}$ (bottom) animals (pre-gated on live CD45.2^{+} lymphocytes based on FSC and SSC profile and a viability marker). Numbers indicate percentage of events in each gate.

B) Graph showing absolute number of total ILCs in MLN from WT and p55/p75$^{-/-}$ mice (gated on CD45.2^{+}live/dead^{-}IL-7Rα^{+}Lin^{-} cells).

C) Graph showing absolute number of ILC2s in MLN from WT and p55/p75$^{-/-}$ mice (gated on CD45.2^{+}live/dead^{-}IL-7Rα^{+}Lin^{-}intraCD3^{-}ICOS^{+}CCR6^{-} cells).

D) Graph showing absolute number of LTi in MLN from WT and p55/p75$^{-/-}$ mice (gated on CD45.2^{+}live/dead^{-}IL-7Rα^{+}Lin^{-}intraCD3^{-}ICOS^{-}CCR6^{+} cells).

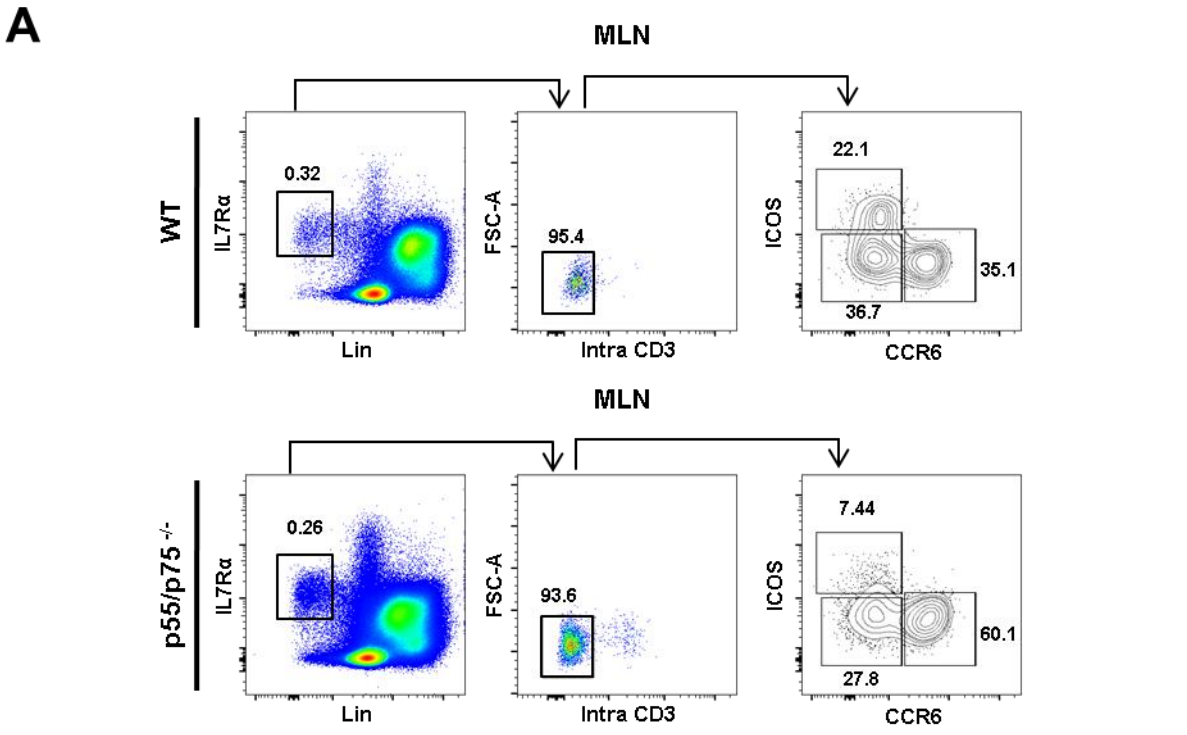
A
MLN
WT
IL7Rα
Lin
0.32
FSC-A
Intra CD3
95.4
ICOS
CCR6
22.1
35.1
36.7
MLN
p55/p75 -/-
IL7Rα
Lin
0.26
FSC-A
Intra CD3
93.6
ICOS
CCR6
7.44
60.1
27.8

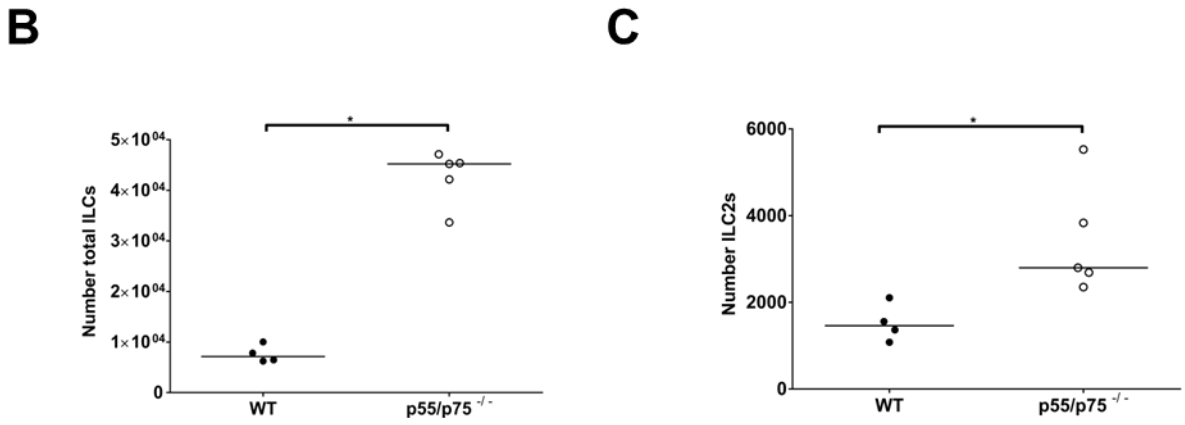
B
Number total ILCs
5×10^04
4×10^04
3×10^04
2×10^04
1×10^04
0
*
WT
p55/p75 -/-
C
Number ILC2s
6000
4000
2000
0
*
WT
p55/p75 -/-

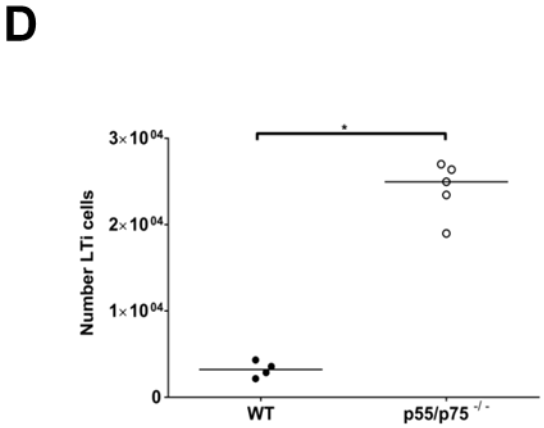
D
Number LTi cells
3×10^04
2×10^04
1×10^04
0
*
WT
p55/p75 -/-

Figure 7.13: MLN ILC2 phenotype in WT and p55/p75$^{-/-}$ mice

Cells were isolated from the MLN of adult male WT and p55/p75$^{-/-}$ mice (both on C57BL/6J background) as described in Materials and Methods. The ILC2 phenotype was determined by flow cytometry as described in the Materials and Methods section. Data for each group was obtained from two technical repeats.

Each data point (n=4, 5 for WT and p55p/75$^{-/-}$ animals respectively) represents an individual sample with a line indicating the median value. Statistical significance was determined using a Mann-Whitney two-tailed T test, *p<0.05, **p<0.01, ***p<0.001 and ****p<0.0001.

A) FACS plots showing representative ILC2 staining in MLN isolated from both WT (top) and p55/p75$^{-/-}$ (bottom) animals (pre-gated on live CD45.2^{+} lymphocytes based on FSC and SSC profile and a viability marker). Numbers indicate percentage of events in each gate.

B) Histogram showing representative KLRG1 staining in MLN isolated from p55/p75$^{-/-}$ (red lines) or WT (blue lines) animals. Vertical dotted black line indicates positive staining. Solid lines show ILC2 staining (CD45.2^{+}live/dead^{-} IL-7Rα^{+}Lin^{-}intraCD3^{+}ST2^{+}ICOS$^{+/-}$ cells), dotted lines show negative control staining (CD45.2^{+}live/dead^{-}IL-7Rα^{-}Lin^{+}intraCD3^{-} cells). Numbers indicate the percentage of KLRG1^{+} cells.

C) Graph showing the percentage of ILC2s that are KLRG1^{+}in MLN from WT and p55/p75$^{-/-}$ mice (gated on CD45.2^{+}live/dead^{-}IL-7Rα^{+}Lin^{-}intraCD3^{+}ST2^{+}ICOS$^{+/-}$ KLRG1^{+} cells).

D) Graph showing the expression of KLRG1on the surface of ILC2s in MLN from WT and p55/p75$^{-/-}$ mice (gated on CD45.2^{+}live/dead^{-}IL-7Rα^{+}Lin^{-} intraCD3^{+}ST2^{+}ICOS$^{+/-}$KLRG1^{+} cells).

E) Graph showing the expression of ST2 on the surface of ILC2s in MLN from WT and p55/p75$^{-/-}$ mice (gated on CD45.2^{+}live/dead^{-}IL-7Rα^{+}Lin^{-} intraCD3^{+}ST2^{+}ICOS$^{+/-}$ cells).

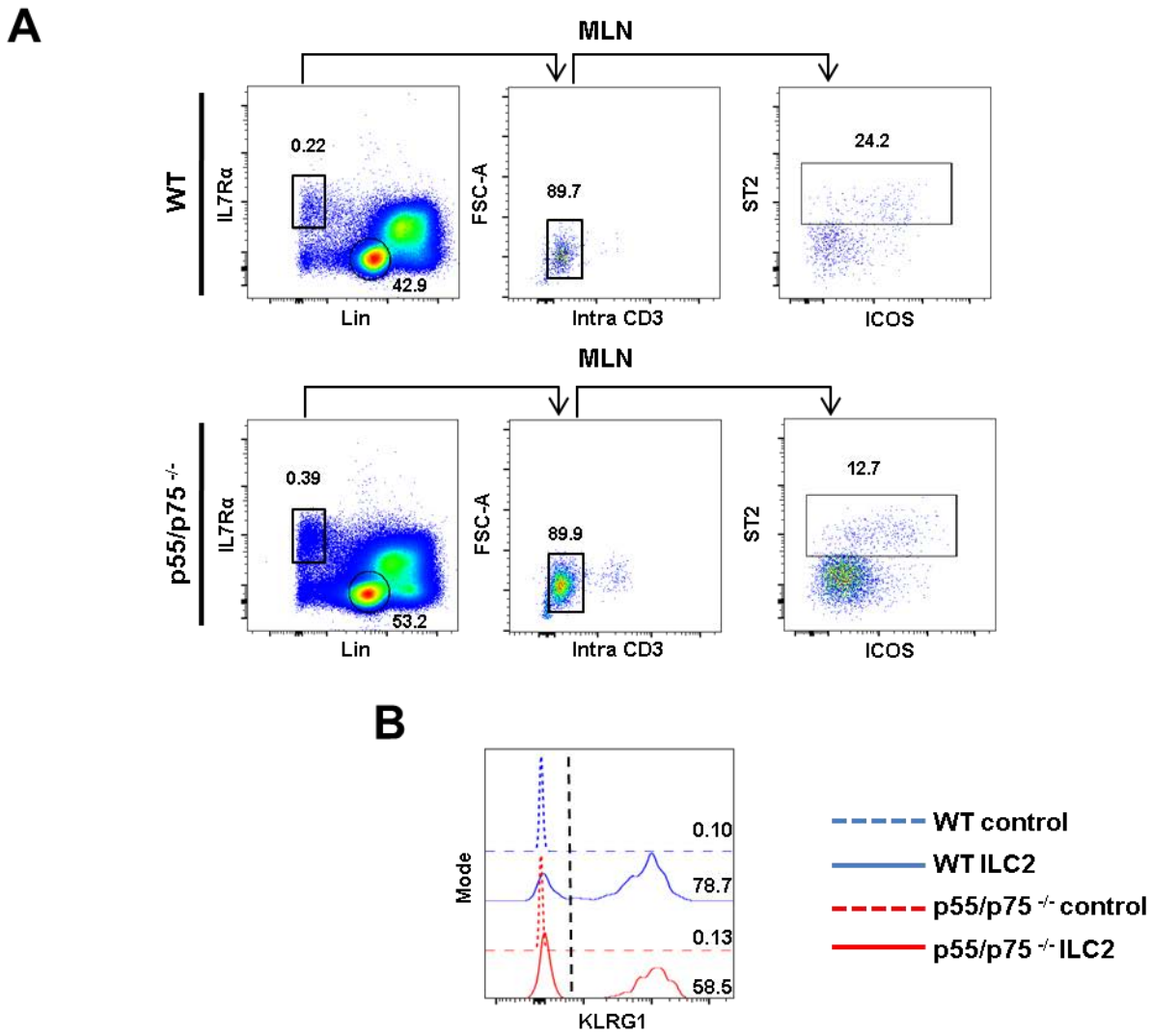
A
MLN
WT
IL7Rα
0.22
42.9
Lin
FSC-A
89.7
Intra CD3
ST2
24.2
ICOS
MLN
p55/p75 -/-
IL7Rα
0.39
53.2
Lin
FSC-A
89.9
Intra CD3
ST2
12.7
ICOS
B
Mode
0.10
78.7
0.13
58.5
KLRG1
WT control
WT ILC2
p55/p75 -/- control
p55/p75 -/- ILC2

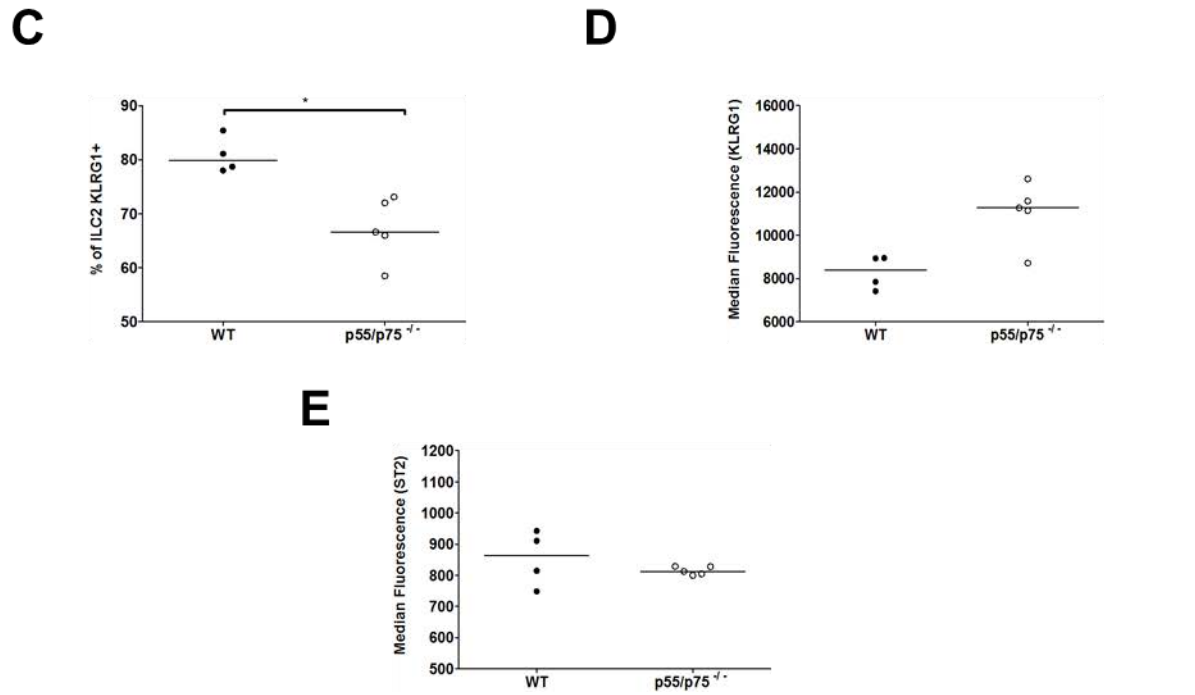
C
% of ILC2 KLRG1+
90
80
70
60
50
*
WT
p55/p75 -/-
D
Median Fluorescence (KLRG1)
16000
14000
12000
10000
8000
6000
WT
p55/p75 -/-
E
Median Fluorescence (ST2)
1200
1100
1000
900
800
700
600
500
WT
p55/p75 -/-

7.6. IMMUNE CELL COMPOSITION IN TNF$^{+/\Delta ARE}$ ANIMALS (SEE CHAPTER 4.3.2)

Figure 7.14: MLN T cell composition in WT and TNF$^{+/\Delta ARE}$ mice

Cells were isolated from the MLN of adult male WT and TNF$^{+/\Delta ARE}$ mice (both on C57BL/6J background) as described in Materials and Methods. The T cell composition was determined by flow cytometry, as demonstrated previously. Data for each group was obtained from four technical repeats.

Each data point (n=7, 6 for WT and TNF$^{+/\Delta ARE}$ animals respectively) represents an individual sample with a line indicating the median value. Statistical significance was determined using a Mann-Whitney two-tailed T test, *p<0.05, **p<0.01, ***p<0.001 and ****p<0.0001.

A) FACS plots showing representative T cell composition in MLN both WT (left) and TNF$^{+/\Delta ARE}$ (right) animals (pre-gated on live CD45.2$^+$ lymphocytes based on FSC and SSC profile and a viability marker). Numbers indicate percentage of events in each gate.

B) Graph showing adjusted total cellularity in MLN from WT and TNF$^{+/\Delta ARE}$ animals (gated on live/dead$^-$ cells).

C) Graph showing adjusted number of CD4$^+$ iNKT cells in MLN from WT and TNF$^{+/\Delta ARE}$ animals (gated on CD45.2$^+$live/dead$^-$intraCD3$^+$CD4$^+$α-gal-cer$^+$ cells).

D) Graph showing adjusted number of CD4$^-$ iNKT cells in MLN isolated from WT and TNF$^{+/\Delta ARE}$ animals (gated on CD45.2$^+$live/dead$^-$intraCD3$^+$CD4$^-$α-gal-cer$^+$ cells).

E) Graph showing adjusted number of CD4$^+$ cells in MLN isolated from WT and TNF$^{+/\Delta ARE}$ animals (gated on CD45.2$^+$live/dead$^-$intraCD3$^+$CD4$^+$α-gal-cer$^-$ cells).

F) Graph showing adjusted number of regulatory T cells in MLN isolated from WT and TNF$^{+/\Delta ARE}$ animals (gated on CD45.2$^+$live/dead$^-$intraCD3$^+$CD4$^+$α-gal-cer$^-$ Foxp3$^+$ cells).

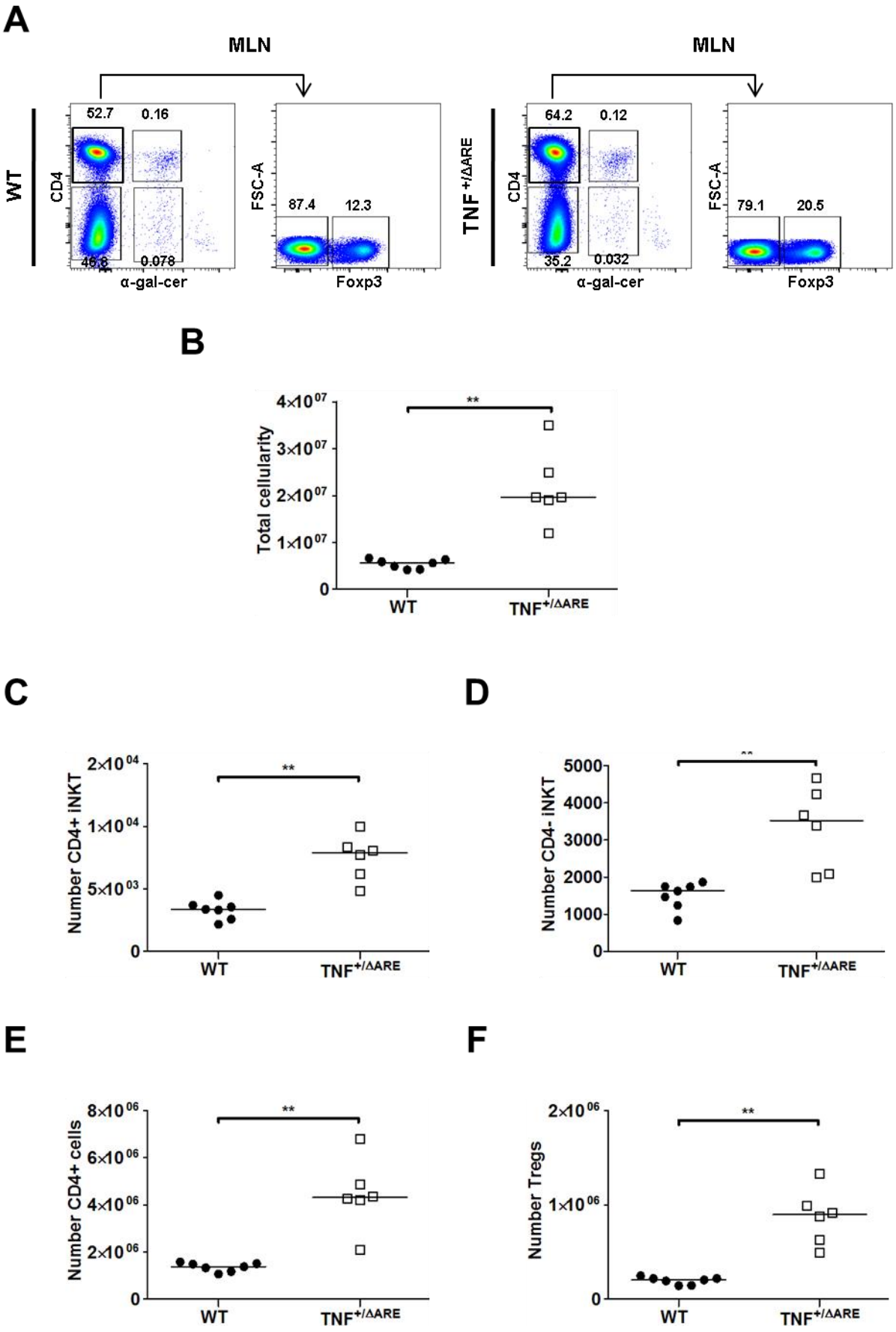
A
MLN
MLN
WT
TNF+/ΔARE
CD4
α-gal-cer
FSC-A
Foxp3
52.7
0.16
46.8
0.078
87.4
12.3
64.2
0.12
35.2
0.032
79.1
20.5
B
Total cellularity
4×10^07
3×10^07
2×10^07
1×10^07
0
**
WT
TNF+/ΔARE
C
Number CD4+ iNKT
2×10^04
1×10^04
5×10^03
0
**
WT
TNF+/ΔARE
D
Number CD4- iNKT
5000
4000
3000
2000
1000
0
**
WT
TNF+/ΔARE
E
Number CD4+ cells
8×10^06
6×10^06
4×10^06
2×10^06
0
**
WT
TNF+/ΔARE
F
Number Tregs
2×10^06
1×10^06
0
**
WT
TNF+/ΔARE

Figure 7.15: MLN ILC composition in WT and TNF$^{+/\Delta ARE}$ mice

Cells were isolated from the MLN of adult male WT and TNF$^{+/\Delta ARE}$ mice (both on C57BL/6J background) as described in Materials and Methods. The ILC cell composition was determined by flow cytometry, as demonstrated previously. Data for each group was obtained from four technical repeats.

Each data point (n=7, 6 for WT and TNF$^{+/\Delta ARE}$ animals respectively) represents an individual sample with a line indicating the median value. Statistical significance was determined using a Mann-Whitney two-tailed T test, *p<0.05, **p<0.01, ***p<0.001 and ****p<0.0001.

A) FACS plots showing representative ILC composition in MLN isolated from both WT (top) and TNF$^{+/\Delta ARE}$ (bottom) animals (pre-gated on live CD45.2^{+} lymphocytes based on FSC and SSC profile and a viability marker). Numbers indicate percentage of events in each gate.

B) Graph showing absolute number of total ILCs in MLN from WT and TNF$^{+/\Delta ARE}$ mice (gated on CD45.2^{+}live/dead^{-}IL-7Rα^{+}Lin^{-} cells).

C) Graph showing absolute number of ILC2s in MLN from WT and TNF$^{+/\Delta ARE}$ mice (gated on CD45.2^{+}live/dead^{-}IL-7Rα^{+}Lin^{-}intraCD3^{-}GATA-3^{+}CCR6^{-} cells).

D) Graph showing absolute number of LTi in MLN from WT and TNF$^{+/\Delta ARE}$ mice (gated on CD45.2^{+}live/dead^{-}IL-7Rα^{+}Lin^{-}intraCD3^{-}GATA-3^{-}CCR6^{+} cells).

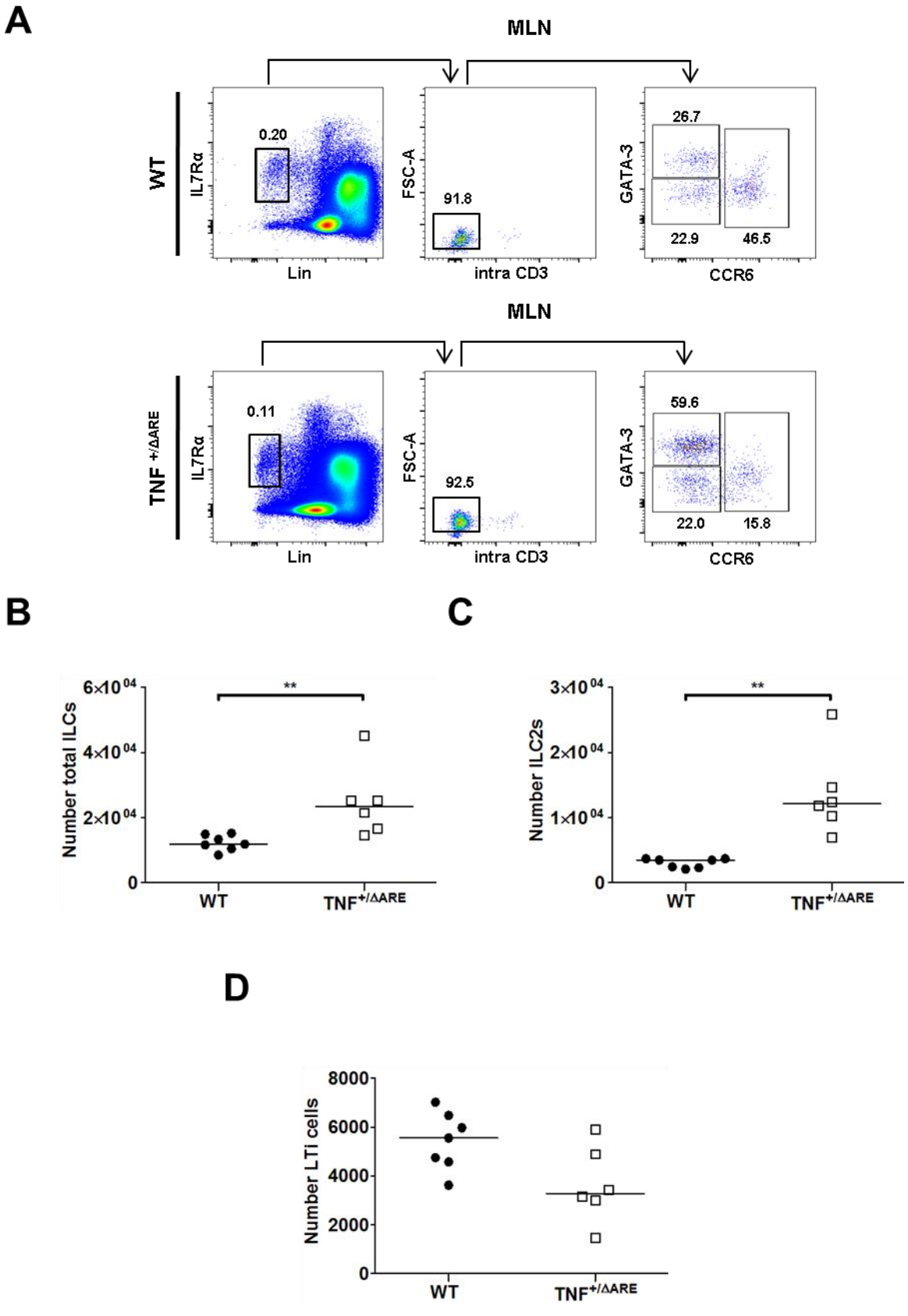
A
MLN
WT
IL7Rα
Lin
0.20
FSC-A
intra CD3
91.8
GATA-3
CCR6
26.7
22.9
46.5
MLN
TNF +/ΔARE
IL7Rα
Lin
0.11
FSC-A
intra CD3
92.5
GATA-3
CCR6
59.6
22.0
15.8
B
Number total ILCs
6×10 04
4×10 04
2×10 04
0
**
WT
TNF+/ΔARE
C
Number ILC2s
3×10 04
2×10 04
1×10 04
0
**
WT
TNF+/ΔARE
D
Number LTi cells
8000
6000
4000
2000
0
WT
TNF+/ΔARE

Figure 7.16: MLN ILC2 phenotype in WT and TNF$^{+/\Delta ARE}$ mice

Cells were isolated from the MLN of adult male WT and TNF$^{+/\Delta ARE}$ mice (both on C57BL/6J background) as described in Materials and Methods. The ILC2 phenotype was determined by flow cytometry as described in the methods section. Data for each group was obtained from four technical repeats.

Each data point (n=9, 6 for WT and TNF$^{+/\Delta ARE}$ animals respectively) represents an individual sample with a line indicating the median value. Statistical significance was determined using a Mann-Whitney two-tailed T test, *p<0.05, **p<0.01, ***p<0.001 and ****p<0.0001.

A) FACS plots showing representative ILC2 staining in MLN isolated from both WT (left) and TNF$^{+/\Delta ARE}$ (right) animals (pre-gated on live CD45.2$^+$ lymphocytes based on FSC and SSC profile and a viability marker). Numbers indicate percentage of events in each gate.

B) Histogram showing representative KLRG1 staining in MLN isolated from TNF$^{+/\Delta ARE}$ (red lines) or WT (blue lines) animals. Vertical dotted black line indicates positive staining. Solid lines show ILC2 staining (CD45.2$^+$live/dead$^-$IL-7Rα$^+$Lin$^-$intraCD3$^-$ST2$^+$ICOS$^{+/-}$ cells), dotted lines show negative control staining (CD45.2$^+$live/dead$^-$IL-7Rα$^-$Lin$^+$intraCD3$^-$ cells). Numbers indicate the percentage of KLRG1$^+$ cells.

C) Graph showing the percentage of ILC2s that are KLRG1$^+$ in MLN from WT and TNF$^{+/\Delta ARE}$ mice (gated on CD45.2$^+$live/dead$^-$IL-7Rα$^+$Lin$^-$intraCD3$^-$ ST2$^+$ICOS$^{+/-}$KLRG1$^+$ cells).

D) Graph showing the expression of KLRG1 on the surface of ILC2s in MLN from WT and TNF$^{+/\Delta ARE}$ mice (gated on CD45.2$^+$live/dead$^-$IL-7Rα$^+$Lin$^-$ intraCD3$^-$ST2$^+$ICOS$^{+/-}$KLRG1$^+$ cells).

E) Graph showing the expression of ST2 on the surface of ILC2s in MLN from WT and TNF$^{+/\Delta ARE}$ mice (gated on CD45.2$^+$live/dead$^-$IL-7Rα$^+$Lin$^-$intraCD3$^-$ ST2$^+$ICOS$^{+/-}$ cells).

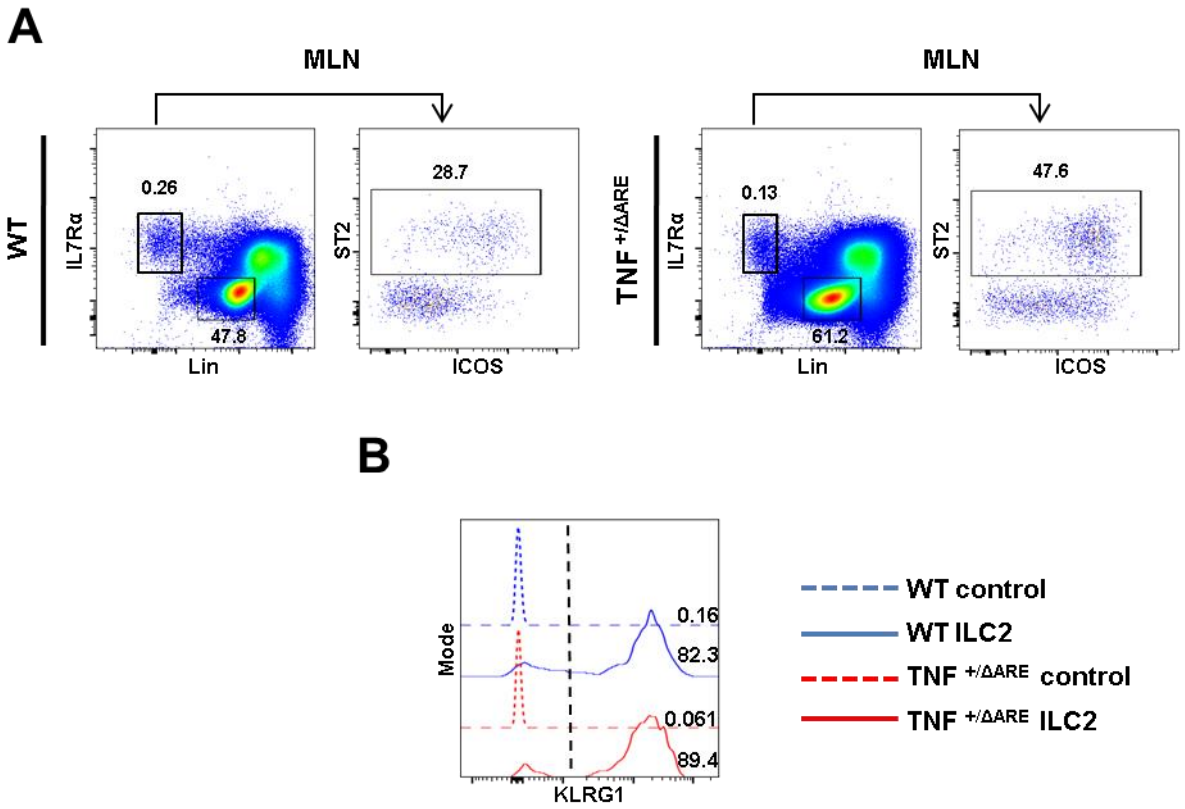
A
MLN
MLN
WT
TNF +/ΔARE
IL7Rα
ST2
0.26
47.8
28.7
0.13
61.2
47.6
Lin
ICOS
B
Mode
0.16
82.3
0.061
89.4
KLRG1
WT control
WT ILC2
TNF +/ΔARE control
TNF +/ΔARE ILC2

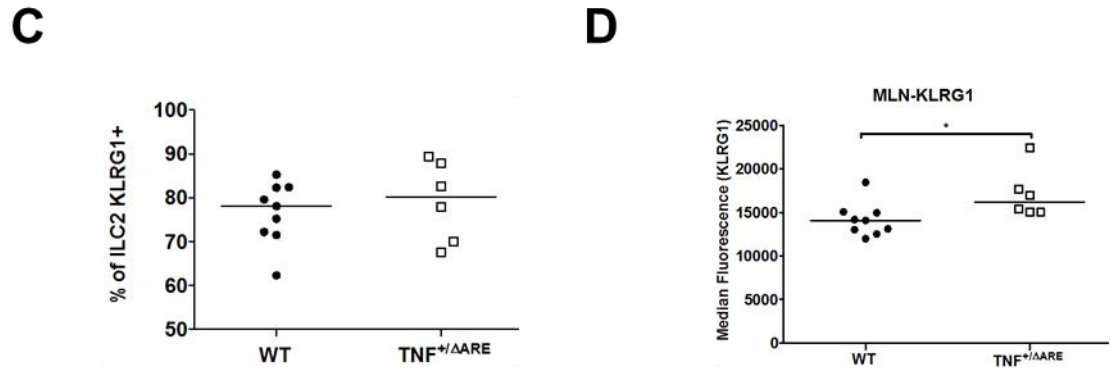
C
% of ILC2 KLRG1+
100
90
80
70
60
50
WT
TNF+/ΔARE
D
MLN-KLRG1
Median Fluorescence (KLRG1)
25000
20000
15000
10000
5000
0
*
WT
TNF+/ΔARE

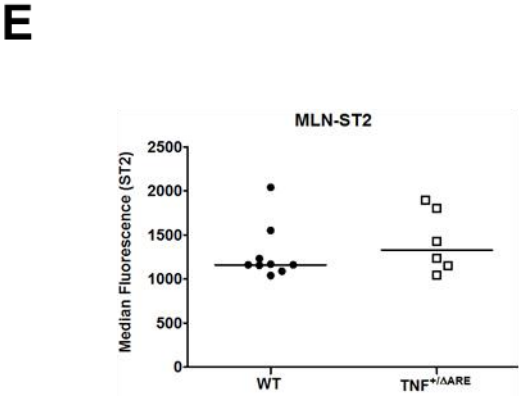
E
MLN-ST2
Median Fluorescence (ST2)
2500
2000
1500
1000
500
0
WT
TNF+/ΔARE

7.7. IMMUNE CELL COMPOSITION OF MLN AT DAY TEN FOLLOWING *H.POLYGYRUS* INFECTION

Figure 7.17: MLN ILC composition at day ten following *H.polygyrus* infection

C57BL/6J males were either infected with *H.polygyrus* larvae (infected), or given PBS as a control, and cells were isolated from MLN ten days post infection (see Materials and Methods). The ILC composition was determined by flow cytometry, as demonstrated previously. Data for each group was obtained from two technical repeats.

Each data point (n=4, 5 for control and infected animals respectively) represents an individual sample with a line indicating the median value. Statistical significance was determined using a Mann-Whitney two-tailed T test, *p<0.05, **p<0.01, ***p<0.001 and ****p<0.0001.

A) FACS plots showing representative ILC composition in MLN from both control (top) and infected (bottom) animals (pre-gated on live CD45.2$^+$ lymphocytes based on FSC and SSC profile and a viability marker). Numbers indicate percentage of events in each gate.

B) Graph showing adjusted number of total ILCs in MLN from control and infected mice (gated on live/dead$^-$CD45.2$^+$IL-7Rα$^+$Lin$^-$ cells).

C) Graph showing adjusted number of ILC2s in MLN from control and infected mice (gated on live/dead$^-$CD45.2$^+$IL-7Rα$^+$Lin$^-$intraCD3$^-$RoRγt$^-$GATA-3$^+$ cells).

D) Graph showing adjusted number of ILC3s in MLN from control and infected mice (gated on live/dead$^-$CD45.2$^+$IL-7Rα$^+$Lin$^-$intraCD3$^-$RoRγt$^+$GATA-3$^-$ cells).

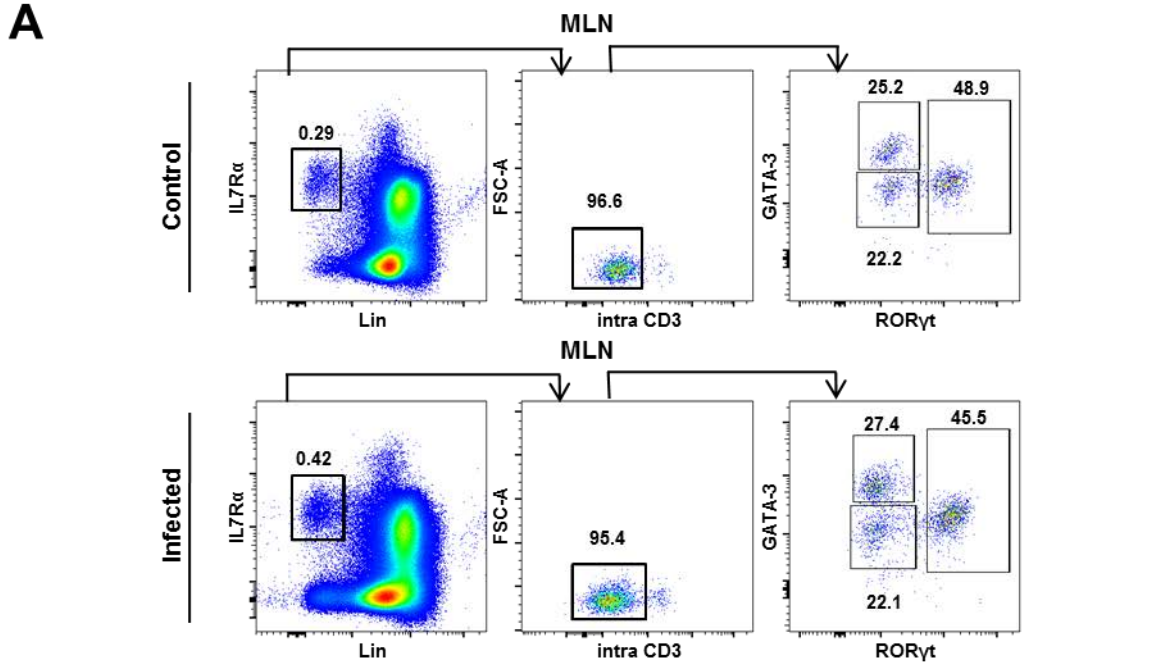
A
MLN
Control
IL7Rα
Lin
0.29
FSC-A
intra CD3
96.6
GATA-3
RORγt
25.2
48.9
22.2
MLN
Infected
IL7Rα
Lin
0.42
FSC-A
intra CD3
95.4
GATA-3
RORγt
27.4
45.5
22.1

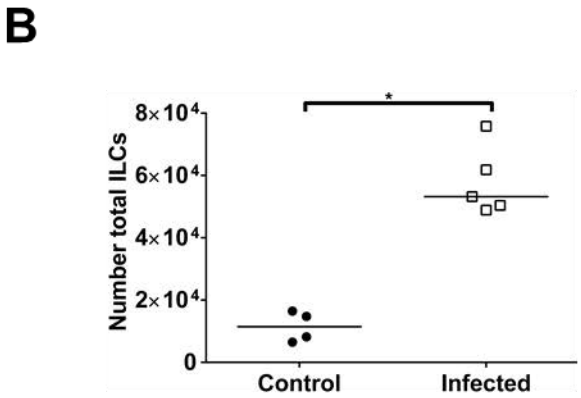
B
Number total ILCs
8×10⁴
6×10⁴
4×10⁴
2×10⁴
0
*
Control
Infected

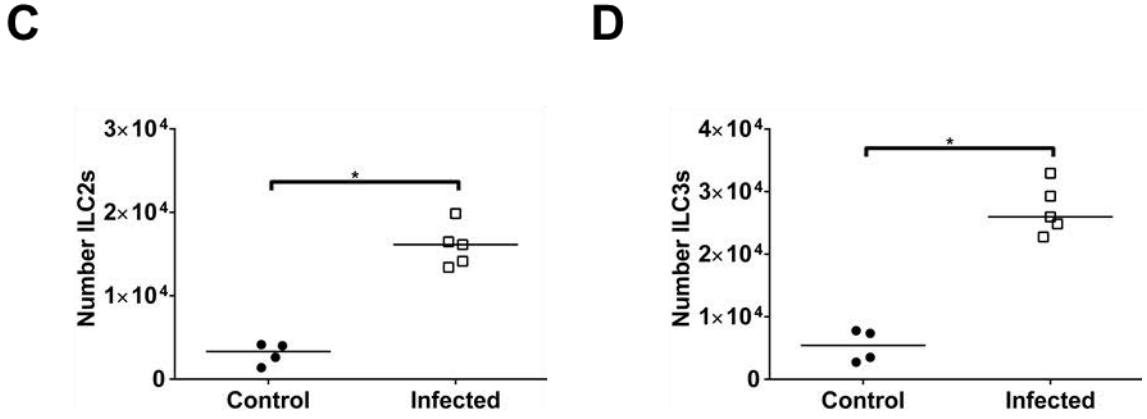
C
Number ILC2s
3×10⁴
2×10⁴
1×10⁴
0
*
Control
Infected
D
Number ILC3s
4×10⁴
3×10⁴
2×10⁴
1×10⁴
0
*
Control
Infected

Figure 7.18: MLN T cell composition at day ten following *H.polygyrus* infection

C57BL/6J males were either infected with *H.polygyrus* larvae (infected), or given PBS as a control, and cells were isolated from MLN ten days post infection (see Materials and Methods). The T cell composition was determined by flow cytometry, as demonstrated previously. Data for each group was obtained from two technical repeats.

Each data point (n=4, 5 for control and infected animals respectively) represents an individual sample with a line indicating the median value. Statistical significance was determined using a Mann-Whitney two-tailed T test, *p<0.05, **p<0.01, ***p<0.001 and ****p<0.0001.

A) FACS plots showing representative T cell composition in MLN from both control (left) and infected (right) animals (pre-gated on live CD45.2$^+$ lymphocytes based on FSC and SSC profile and a viability marker). Numbers indicate percentage of events in each gate.

B) Graph showing adjusted number of CD4$^+$ cells in MLN from control and infected mice (gated on CD45.2$^+$live/dead$^-$intraCD3$^+$CD4$^+$α-gal-cer$^-$ cells).

C) Graph showing adjusted number of regulatory T cells in MLN isolated from control and infected mice (gated on CD45.2$^+$live/dead$^-$ intraCD3$^+$CD4$^+$α-gal-cer$^-$FOXP3$^+$ cells).

D) Graph showing adjusted number of CD4$^+$ iNKT cells in MLN from control and infected mice (gated on CD45.2$^+$live/dead$^-$intraCD3$^+$CD4$^+$α-gal-cer$^+$ cells).

E) Graph showing adjusted number of CD4$^-$ iNKT cells in MLN from control and infected mice (gated on CD45.2$^+$live/dead$^-$intraCD3$^+$CD4$^-$α-gal-cer$^+$ cells).

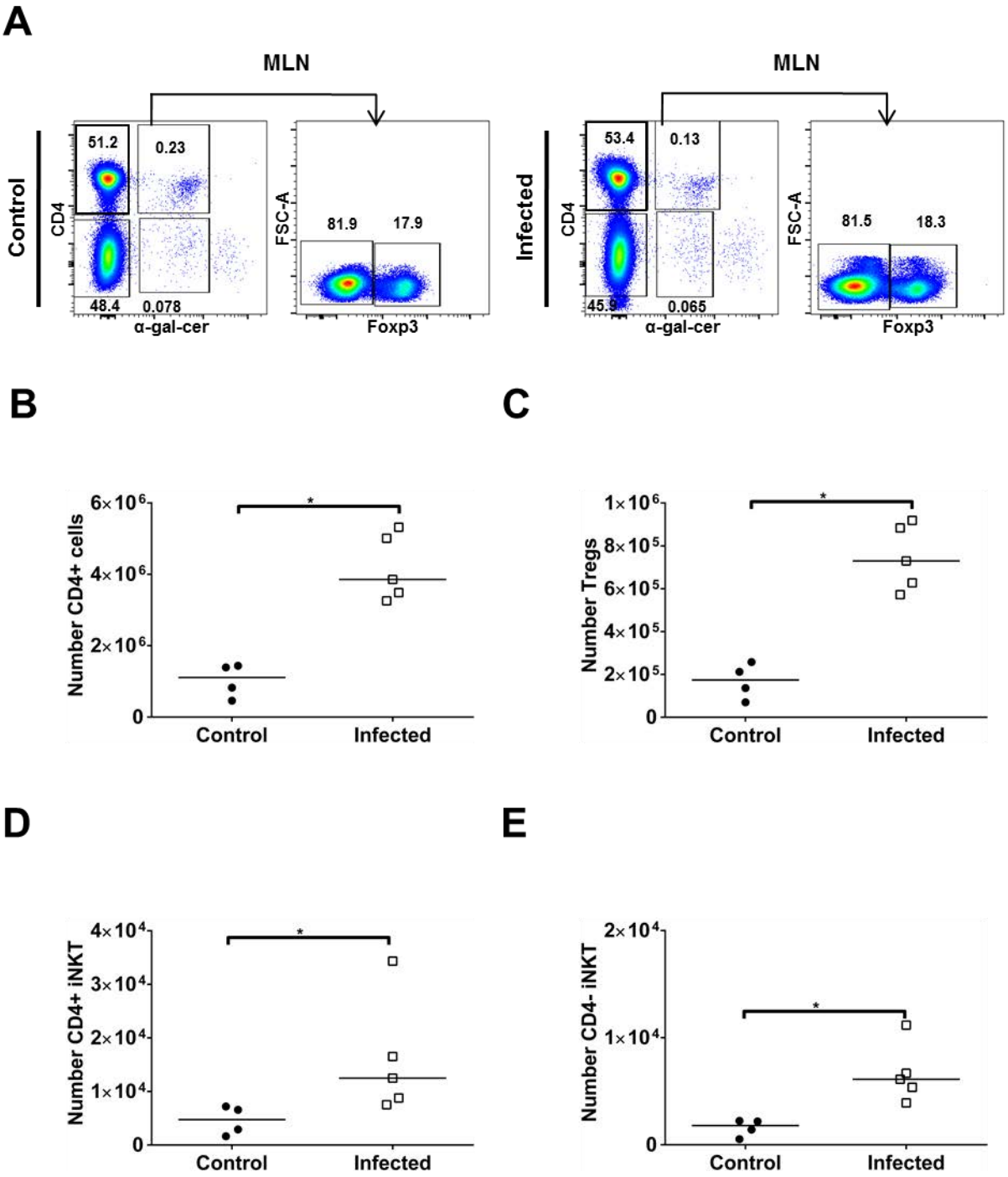
A
MLN
MLN
Control
Infected
CD4
α-gal-cer
FSC-A
Foxp3
51.2
0.23
48.4
0,078
81.9
17.9
53.4
0.13
45.9
0.065
81.5
18.3
B
Number CD4+ cells
6×10^6
4×10^6
2×10^6
0
Control
Infected
*
C
Number Tregs
1×10^6
8×10^5
6×10^5
4×10^5
2×10^5
0
Control
Infected
*
D
Number CD4+ iNKT
4×10^4
3×10^4
2×10^4
1×10^4
0
Control
Infected
*
E
Number CD4- iNKT
2×10^4
1×10^4
0
Control
Infected
*

Figure 7.19: MLN ILC2 phenotype at day ten following *H.polygyrus* infection

C57BL/6J males were either infected with *H.polygyrus* larvae (infected), or given PBS as a control, and cells were isolated from MLN ten days post infection (see Materials and Methods). The ILC2 phenotype was determined by flow cytometry, as demonstrated previously. Data for each group was obtained from two technical repeats.

Each data point (n=4, 5 for control and infected animals respectively) represents an individual sample with a line indicating the median value. Statistical significance was determined using a Mann-Whitney two-tailed T test, *p<0.05, **p<0.01, ***p<0.001 and ****p<0.0001.

A) FACS plots showing representative ILC2 staining in MLN from both control (top) and infected (bottom) animals (pre-gated on live CD45.2$^+$ lymphocytes based on FSC and SSC profile and a viability marker). Numbers indicate percentage of events in each gate.

B) Histogram showing representative ICOS staining in MLN isolated from infected (red line) or control (blue line) animals. Vertical dotted line indicates positive staining. Solid lines show ILC2 staining (CD45.2$^+$live/dead$^-$IL-7Rα$^+$Lin$^-$ intraCD3$^-$ST2$^+$GATA-3$^+$ cells), dotted green line shows ICOS FMO control. Numbers indicate the percentage of ICOS$^+$ cells.

C) Histogram showing representative KLRG1 staining in MLN isolated from infected (red lines) or control (blue lines) animals. Vertical dotted line indicates positive staining. Solid lines show ILC2 staining (CD45.2$^+$live/dead$^-$IL-7Rα$^+$Lin$^-$ intraCD3$^-$ST2$^+$GATA-3$^+$ cells), dotted lines show KLRG1 negative control (gated on CD45.2$^+$live/dead$^-$IL-7Rα$^-$Lin$^+$intraCD3$^-$ cells). Numbers indicate the percentage of KLRG1$^+$ cells.

D) Graph showing percentage of ILC2s expressing ICOS in MLN from control and infected mice (gated on live/dead$^-$CD45.2$^+$IL-7Rα$^+$Lin$^-$intraCD3$^-$ ST2$^+$GATA-3$^+$ICOS$^+$ cells).

E) Graph showing expression of ICOS (median fluorescence) on the surface of ILC2 in MLN from control and infected mice (gated on live/dead$^-$ CD45.2$^+$IL-7Rα$^+$Lin$^-$intraCD3$^-$ST2$^+$GATA-3$^+$ICOS$^+$ cells).

F) Graph showing percentage of ILC2s expressing KLRG1 in MLN from control and infected mice (gated on live/dead$^-$CD45.2$^+$IL-7Rα$^+$Lin$^-$intraCD3$^-$ ST2$^+$GATA-3$^+$KLRG1$^+$ cells).

G) Graph showing expression of KLRG1 (median fluorescence) on the surface of ILC2 in MLN from control and infected mice (gated on live/dead$^-$ CD45.2$^+$IL-7Rα$^+$Lin$^-$intraCD3$^-$ST2$^+$GATA-3$^+$KLRG1$^+$ cells).

H) Graph showing expression of ST2 (median fluorescence) on the surface of ILC2 in MLN from control and infected mice (gated on live/dead$^-$ CD45.2$^+$IL-7Rα$^+$Lin$^-$intraCD3$^-$ST2$^+$GATA-3$^+$cells).

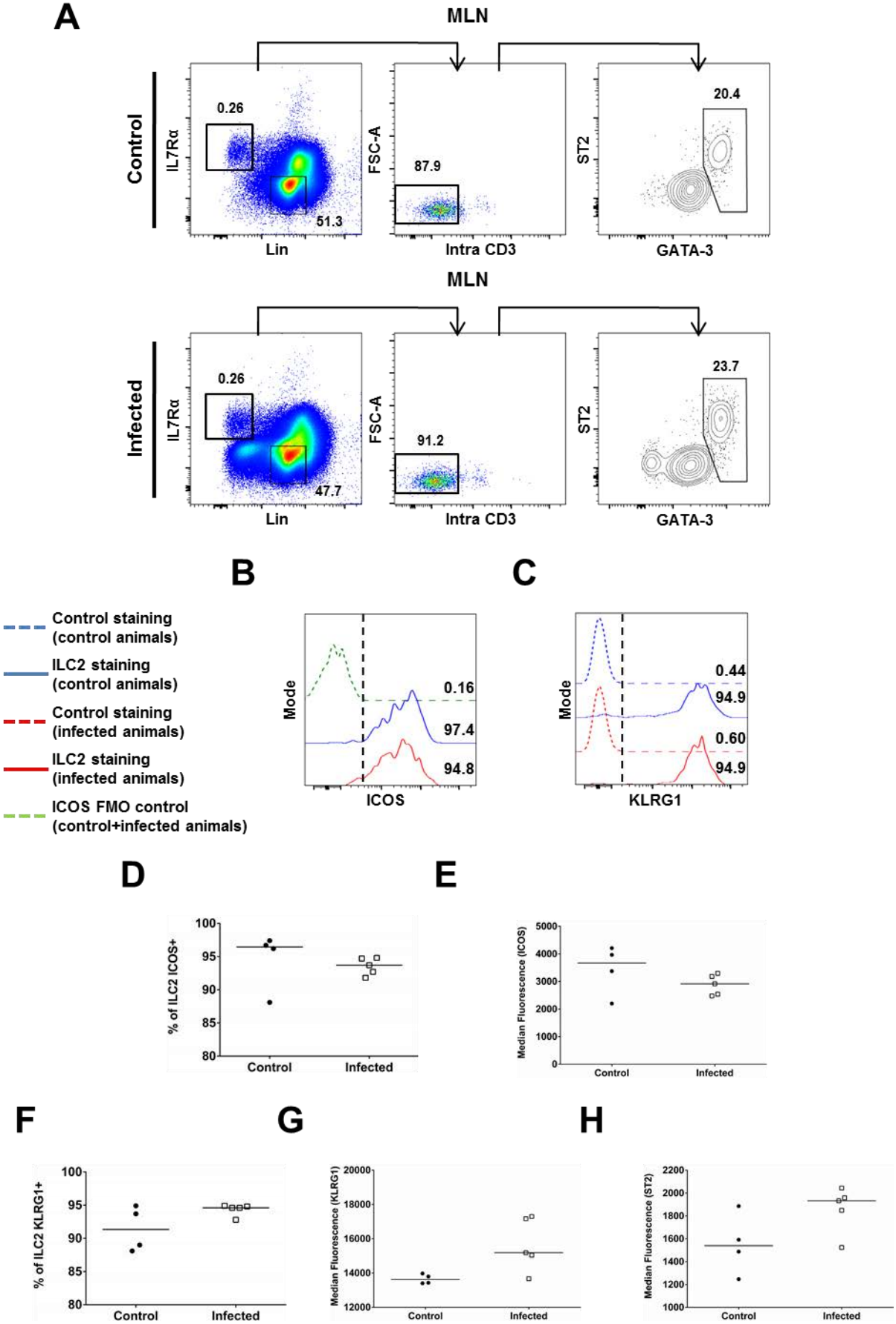
A
MLN
Control
IL7Rα
0.26
51.3
Lin
FSC-A
87.9
Intra CD3
ST2
20.4
GATA-3
MLN
Infected
IL7Rα
0.26
47.7
Lin
FSC-A
91.2
Intra CD3
ST2
23.7
GATA-3
B
C
Control staining (control animals)
ILC2 staining (control animals)
Control staining (infected animals)
ILC2 staining (infected animals)
ICOS FMO control (control+infected animals)
Mode
0.16
97.4
94.8
ICOS
Mode
0.44
94.9
0.60
94.9
KLRG1
D
E
% of ILC2 ICOS+
100
95
90
85
80
Control
Infected
Median Fluorescence (ICOS)
5000
4000
3000
2000
1000
0
Control
Infected
F
G
H
% of ILC2 KLRG1+
100
95
90
85
80
Control
Infected
Median Fluorescence (KLRG1)
20000
18000
16000
14000
12000
Control
Infected
Median Fluorescence (ST2)
2200
2000
1800
1600
1400
1200
1000
Control
Infected

7.8. IMMUNE CELL COMPOSITION OF MLN AT DAY FIVE FOLLOWING *H.POLYGYRUS* INFECTION

Figure 7.20: MLN ILC composition at day five following *H.polygyrus* infection

C57BL/6J males were either infected with *H.polygyrus* larvae (infected), or given PBS as a control, and cells were isolated from MLN five days post infection (see Materials and Methods). The ILC composition was determined by flow cytometry, as demonstrated previously. Data for each group was obtained from three technical repeats.

Each data point (n=7, 7 for control and infected animals respectively) represents an individual sample with a line indicating the median value. Statistical significance was determined using a Mann-Whitney two-tailed T test, *p<0.05, **p<0.01, ***p<0.001 and ****p<0.0001.

A) FACS plots showing representative ILC composition in MLN from both control (top) and infected (bottom) animals (pre-gated on live CD45.2$^+$ lymphocytes based on FSC and SSC profile and a viability marker). Numbers indicate percentage of events in each gate.

B) Graph showing adjusted number of total ILCs in MLN from control and infected mice (gated on live/dead$^-$CD45.2$^+$IL-7Rα$^+$Lin$^-$ cells).

C) Graph showing adjusted number of ILC2s in MLN from control and infected mice (gated on live/dead$^-$CD45.2$^+$IL-7Rα$^+$Lin$^-$intraCD3$^-$RoRγt$^-$GATA-3$^+$ cells).

D) Graph showing adjusted number of ILC3s in MLN from control and infected mice (gated on live/dead$^-$CD45.2$^+$IL-7Rα$^+$Lin$^-$intraCD3$^-$RoRγt$^+$GATA-3$^-$ cells).

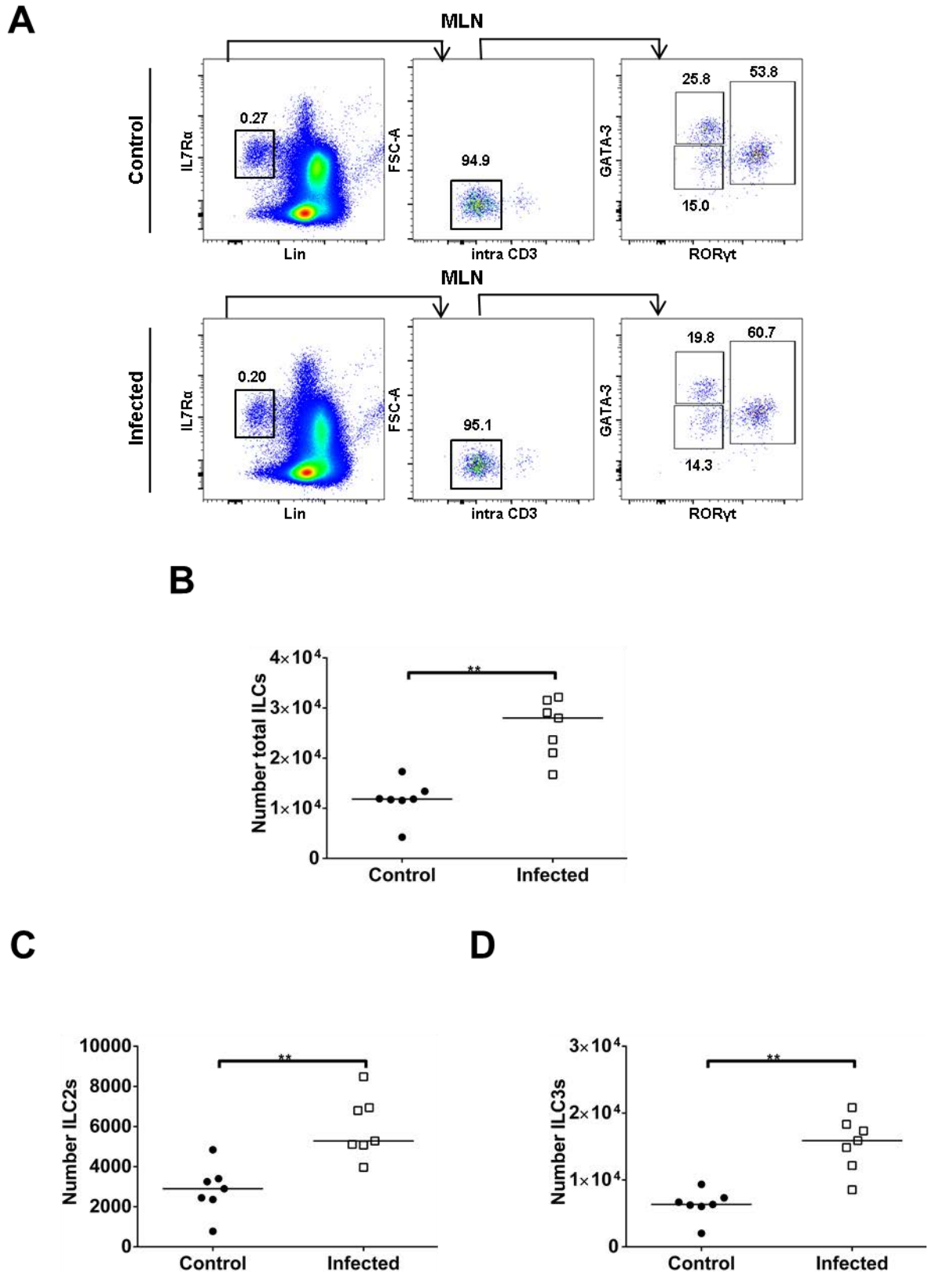
A
MLN
Control
IL7Rα
Lin
0.27
FSC-A
intra CD3
94.9
GATA-3
RORγt
25.8
53.8
15.0
MLN
Infected
IL7Rα
Lin
0.20
FSC-A
intra CD3
95.1
GATA-3
RORγt
19.8
60.7
14.3
B
Number total ILCs
4×10⁴
3×10⁴
2×10⁴
1×10⁴
0
**
Control
Infected
C
Number ILC2s
10000
8000
6000
4000
2000
0
**
Control
Infected
D
Number ILC3s
3×10⁴
2×10⁴
1×10⁴
0
**
Control
Infected

Figure 7.21: MLN T cell composition at day five following *H.polygyrus* infection

C57BL/6J males were either infected with *H.polygyrus* larvae (infected), or given PBS as a control, and cells were isolated from MLN five days post infection (see Materials and Methods). The T cell composition was determined by flow cytometry, as demonstrated previously. Data for each group was obtained from three technical repeats.

Each data point (n=7, 7 for control and infected animals respectively) represents an individual sample with a line indicating the median value. Statistical significance was determined using a Mann-Whitney two-tailed T test, *p<0.05, **p<0.01, ***p<0.001 and ****p<0.0001.

A) FACS plots showing representative T cell composition in MLN from both control (left) and infected (right) animals (pre-gated on live CD45.2$^+$ lymphocytes based on FSC and SSC profile and a viability marker). Numbers indicate percentage of events in each gate.

B) Graph showing adjusted number of CD4$^+$ cells in MLN from control and infected mice (gated on CD45.2$^+$live/dead$^-$intraCD3$^+$CD4$^+$α-gal-cer$^-$ cells).

C) Graph showing adjusted number of regulatory T cells in MLN from control and infected mice (gated on CD45.2$^+$live/dead$^-$intraCD3$^+$CD4$^+$α-gal-cer$^-$FOXP3$^+$ cells).

D) Graph showing adjusted number of CD4$^+$ iNKT cells in MLN from control and infected mice (gated on CD45.2$^+$live/dead$^-$intraCD3$^+$CD4$^+$α-gal-cer$^+$ cells).

E) Graph showing adjusted number of CD4$^-$ iNKT cells in MLN from control and infected mice (gated on CD45.2$^+$live/dead$^-$intraCD3$^+$CD4$^-$α-gal-cer$^+$ cells).

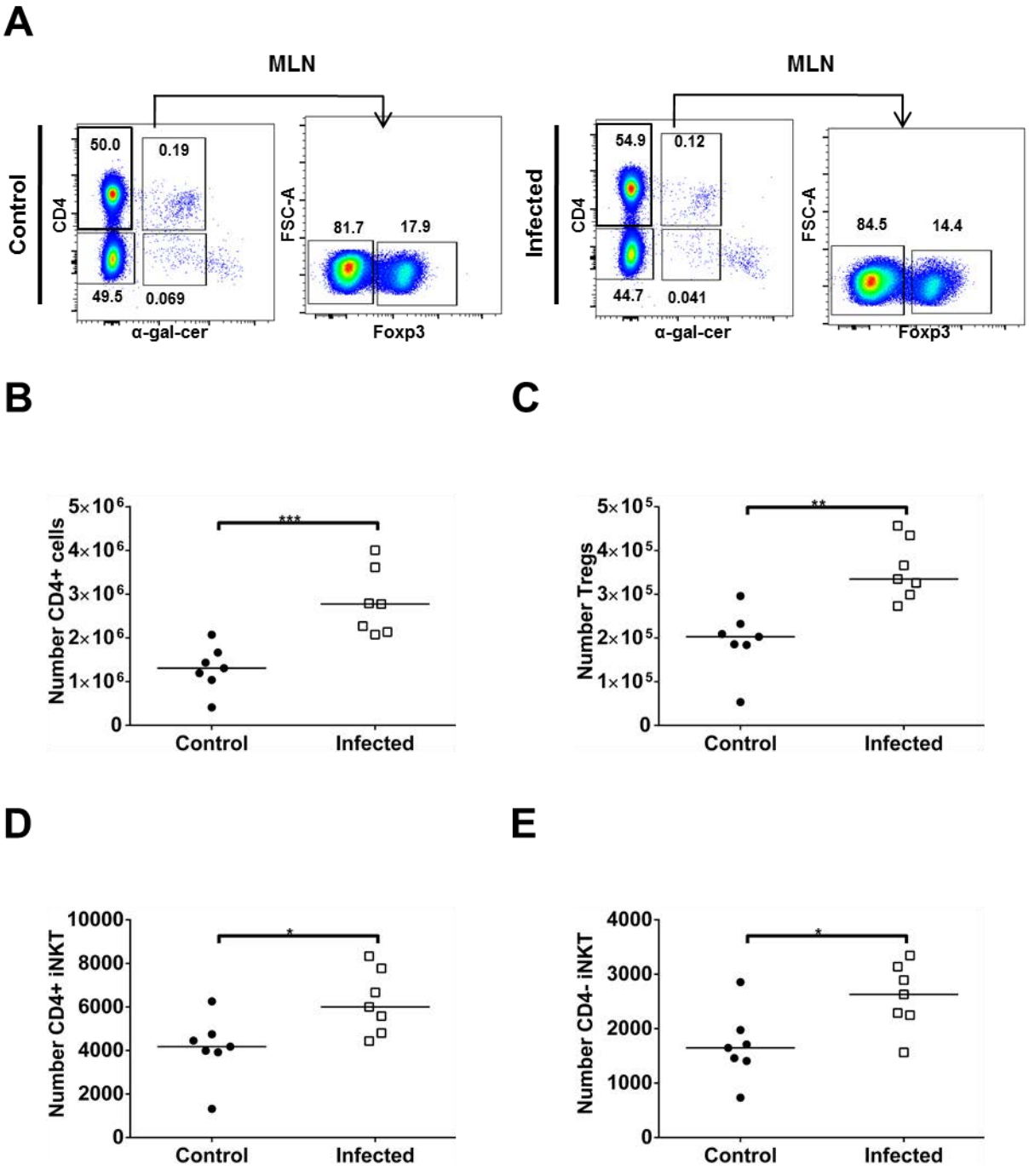
A
MLN
MLN
Control
Infected
CD4
α-gal-cer
FSC-A
Foxp3
50.0
0.19
49.5
0.069
81.7
17.9
54.9
0.12
44.7
0.041
84.5
14.4
B
C
D
E
Number CD4+ cells
Number Tregs
Number CD4+ iNKT
Number CD4- iNKT
Control
Infected
***
**
*
*

Figure 7.22: MLN ILC2 phenotype at day five following *H.polygyrus* infection

C57BL/6J males were either infected with *H.polygyrus* larvae (infected), or given PBS as a control, and cells were isolated from MLN five days post infection (see Materials and Methods). The ILC2 phenotype was determined by flow cytometry, as demonstrated previously. Data for each group was obtained from three technical repeats.

Each data point (n=7, 7 for control and infected animals respectively) represents an individual sample with a line indicating the median value. Statistical significance was determined using a Mann-Whitney two-tailed T test, **p*<0.05, ***p*<0.01, ****p*<0.001 and *****p*<0.0001.

A) FACS plots showing representative ILC2 staining in MLN from both control (top) and infected (bottom) animals (pre-gated on live $CD45.2^+$ lymphocytes based on FSC and SSC profile and a viability marker). Numbers indicate percentage of events in each gate.

B) Histogram showing representative ICOS staining in MLN isolated from infected (red line) or control (blue line) animals. Vertical dotted line indicates positive staining. Solid lines show ILC2 staining ($CD45.2^+$live/dead$^-$IL-7Rα^+Lin$^-$ intraCD3$^-$ST2$^+$GATA-3$^+$ cells), dotted green line shows ICOS FMO control. Numbers indicate the percentage of $ICOS^+$ cells.

C) Histogram showing representative KLRG1 staining in MLN isolated from infected (red lines) or control (blue lines) animals. Vertical dotted line indicates positive staining. Solid lines show ILC2 staining ($CD45.2^+$live/dead$^-$IL-7Rα^+Lin$^-$ intraCD3$^-$ST2$^+$GATA-3$^+$ cells), dotted lines show KLRG1 negative control (gated on$CD45.2^+$live/dead$^-$IL-7Rα^-Lin$^+$intraCD3$^-$ cells). Numbers indicate the percentage of $KLRG1^+$ cells.

D) Graph showing percentage of ILC2s expressing ICOS in MLN from control and infected mice (gated on live/dead$^-$$CD45.2^+$IL-7R$\alpha^+Lin^-$intraCD3$^-$ ST2$^+$GATA-3$^+$$ICOS^+$ cells).

E) Graph showing expression of ICOS (median fluorescence) on the surface of ILC2 in MLN from control and infected mice (gated on live/dead$^-$ $CD45.2^+$IL-7Rα^+Lin$^-$intraCD3$^-$ST2$^+$GATA-3$^+$$ICOS^+$ cells).

F) Graph showing percentage of ILC2s expressing KLRG1 in MLN from control and infected mice (gated on live/dead$^-$$CD45.2^+$IL-7R$\alpha^+Lin^-$intraCD3$^-$ ST2$^+$GATA-3$^+$$KLRG1^+$ cells).

G) Graph showing expression of KLRG1 (median fluorescence) on the surface of ILC2 in MLN from control and infected mice (gated on live/dead$^-$ $CD45.2^+$IL-7Rα^+Lin$^-$intraCD3$^-$ST2$^+$GATA-3$^+$$KLRG1^+$ cells).

H) Graph showing expression of ST2 (median fluorescence) on the surface of ILC2 in MLN from infected and control mice (gated on live/dead$^-$ $CD45.2^+$IL-7Rα^+Lin$^-$intraCD3$^-$ST2$^+$GATA-3$^+$cells).

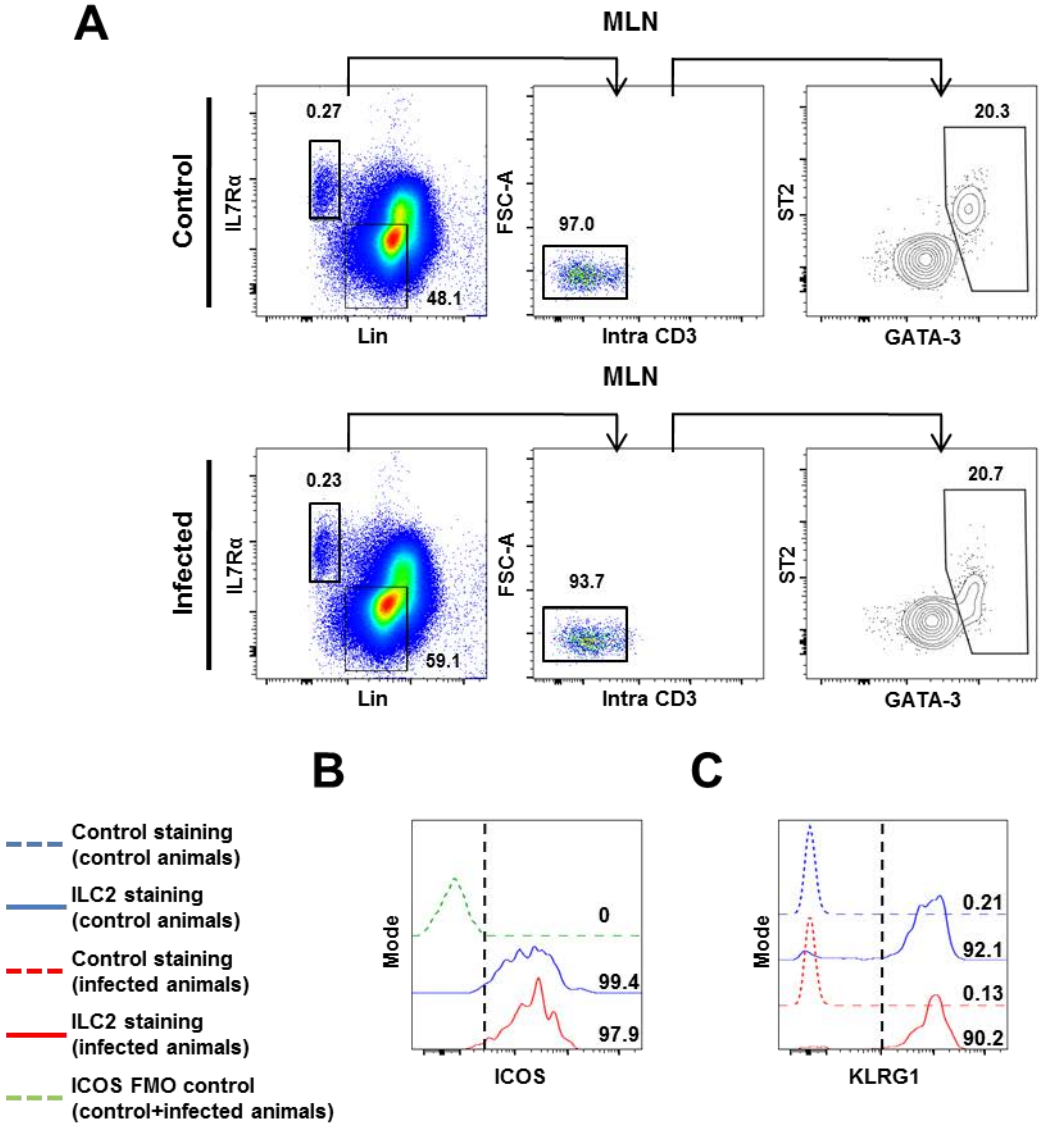
A
MLN
Control
IL7Rα
0.27
48.1
Lin
FSC-A
97.0
Intra CD3
ST2
20.3
GATA-3
MLN
Infected
IL7Rα
0.23
59.1
Lin
FSC-A
93.7
Intra CD3
ST2
20.7
GATA-3

B
C
Control staining (control animals)
ILC2 staining (control animals)
Control staining (infected animals)
ILC2 staining (infected animals)
ICOS FMO control (control+infected animals)
Mode
0
99.4
97.9
ICOS
Mode
0.21
92.1
0.13
90.2
KLRG1

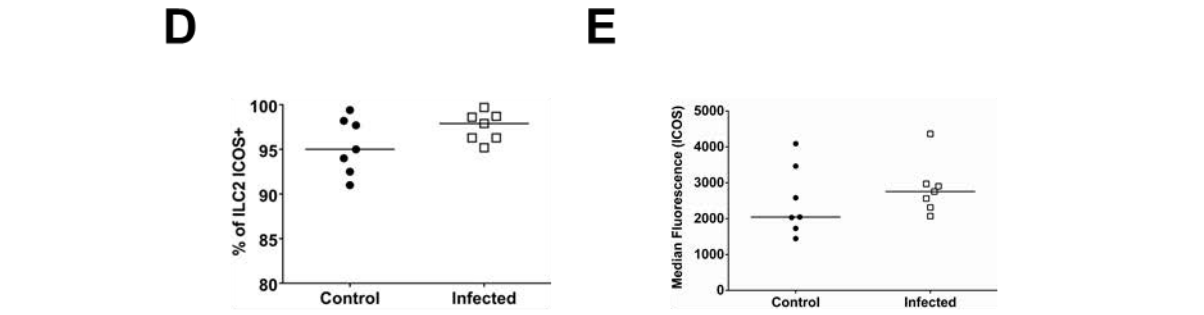
D
E
% of ILC2 ICOS+
100
95
90
85
80
Control
Infected
Median Fluorescence (ICOS)
5000
4000
3000
2000
1000
0
Control
Infected

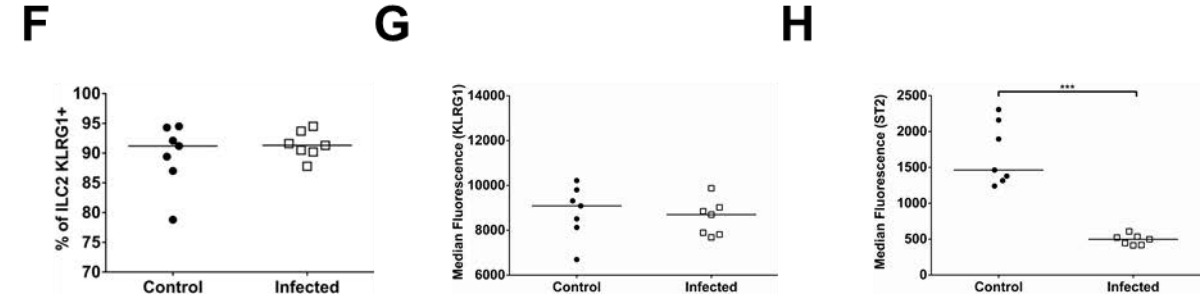
F
G
H
% of ILC2 KLRG1+
100
95
90
85
80
75
70
Control
Infected
Median Fluorescence (KLRG1)
14000
12000
10000
8000
6000
Control
Infected
Median Fluorescence (ST2)
***
2500
2000
1500
1000
500
0
Control
Infected

7.9. ILC2 PHENOTYPE AT DAY FIVE FOLLOWING H.POLYGYRUS INFECTION

Figure 7.23: Adipose tissue chemokine receptor isotype staining and expression at day five following *H.polygyrus* infection

C57BL/6J males were either infected with *H.polygyrus* larvae, or given PBS as a control, and cells were isolated from the gonadal fat and mesenteries five days post infection (see Materials and Methods). The ILC2 proliferation was measured by flow cytometry and quantified in different chemokine receptor profiles. Data for each group was obtained from two technical repeats.

Each data point (n=5, 6 for control and infected animals respectively) represents an individual sample with a line indicating the median value. Statistical significance was determined using a Mann-Whitney two-tailed T test, *p<0.05, **p<0.01, ***p<0.001 and ****p<0.0001.

A) Flow cytometry analysis showing representative isotype staining for CCR8 in both ATs and MLN (pre-gated on CD45.2$^+$live/dead$^-$IL-7Rα$^+$Lin$^-$GATA-3$^+$ cells). Numbers indicate percentage of events in each gate.

B) Flow cytometry analysis showing representative isotype staining for CCR9 in both ATs and MLN (pre-gated on CD45.2$^+$live/dead$^-$IL-7Rα$^+$Lin$^-$GATA-3$^+$ cells). Numbers indicate percentage of events in each gate.

C) Graph showing ILC2s expression (median fluorescence) of CCR8 in gonadal fat and mesenteries from control and infected mice (gated on CD45.2$^+$live/dead$^-$IL-7Rα$^+$Lin$^-$intraCD3$^-$GATA-3$^+$CCR8$^+$ cells).

D) Graph showing ILC2s expression (median fluorescence) of CCR9 in gonadal fat and mesenteries from control and infected mice (gated on CD45.2$^+$live/dead$^-$IL-7Rα$^+$Lin$^-$intraCD3$^-$GATA-3$^+$CCR9$^+$cells).

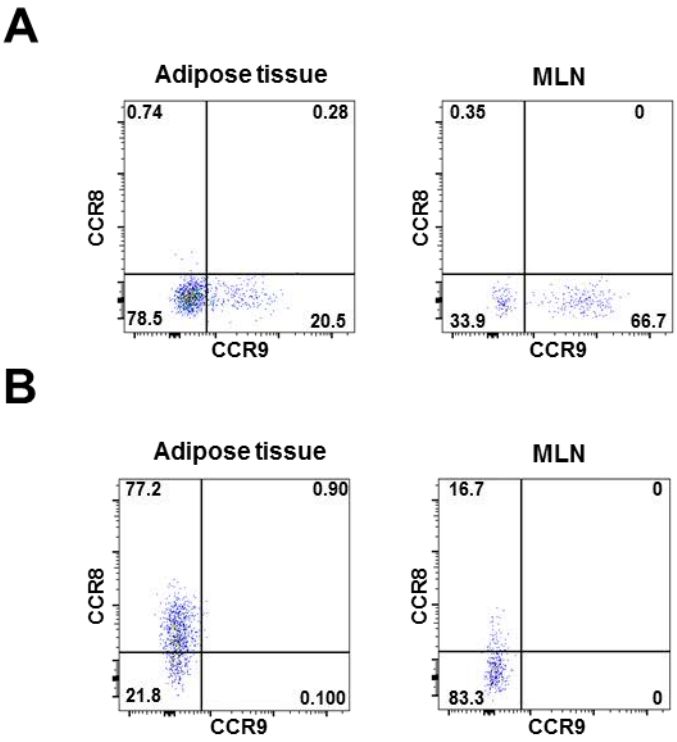
A
Adipose tissue
MLN
0.74
0.28
78.5
20.5
0.35
0
33.9
66.7
CCR8
CCR9
B
Adipose tissue
MLN
77.2
0.90
21.8
0.100
16.7
0
83.3
0
CCR8
CCR9

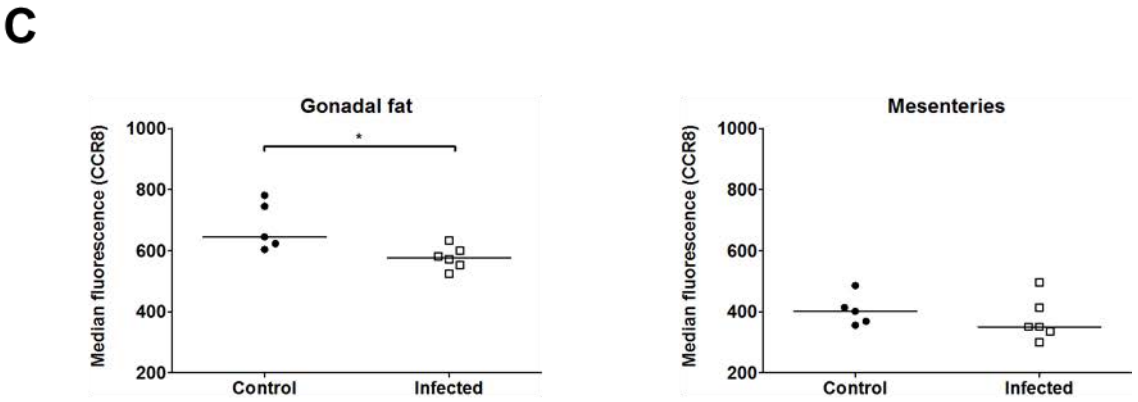
C
Gonadal fat
Mesenteries
Median fluorescence (CCR8)
1000
800
600
400
200
*
Control
Infected

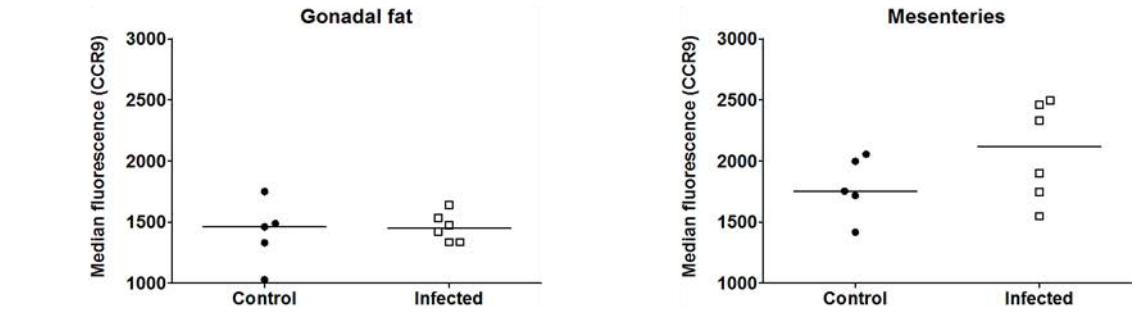
D
Gonadal fat
Mesenteries
Median fluorescence (CCR9)
3000
2500
2000
1500
1000
Control
Infected

Figure 7.24: MLN ILC2 chemokine receptor expression at day five following *H.polygyrus* infection

C57BL/6J males were either infected with *H.polygyrus* larvae, or given PBS as a control, and cells were isolated from the MLN five days post infection (see Materials and Methods). The ILC2 chemokine receptor expression was determined by flow cytometry, as demonstrated previously. Data for each group was obtained from two technical repeats.

Each data point (n=5, 6 for control and infected animals respectively) represents an individual sample with a line indicating the median value. Statistical significance was determined using a Mann-Whitney two-tailed T test, *p<0.05, **p<0.01, ***p<0.001 and ****p<0.0001.

A) FACS plots showing representative ILC2 chemokine receptor staining in MLN from both control (left) and infected (right) animals (gated on CD45.2$^+$live/dead$^-$IL-7Rα$^+$Lin$^-$ cells). Numbers indicate percentage of events in each gate.

B) Graph showing percentage of CCR8$^+$CCR9$^-$ ILC2s in MLN from control and infected mice (gated on CD45.2$^+$live/dead$^-$IL-7Rα$^+$Lin$^-$intraCD3$^-$ GATA-3$^+$CCR8$^+$CCR9$^-$ cells).

C) Graph showing percentage of CCR8$^-$CCR9$^+$ ILC2s in MLN from control and infected mice (gated on CD45.2$^+$live/dead$^-$IL-7Rα$^+$Lin$^-$intraCD3$^-$GATA-3$^+$CCR8$^-$ CCR9$^+$ cells).

D) Graph showing percentage of CCR8$^+$CCR9$^+$ ILC2s in MLN from control and infected mice (gated on CD45.2$^+$live/dead$^-$IL-7Rα$^+$Lin$^-$intraCD3$^-$ GATA-3$^+$CCR8$^+$CCR9$^+$ cells).

E) Graph showing ILC2 expression (median fluorescence) of CCR8 in MLN from control and infected mice (gated on CD45.2$^+$live/dead$^-$IL-7Rα$^+$Lin$^-$intraCD3$^-$ GATA-3$^+$CCR8$^+$ cells).

F) Graph showing ILC2 expression (median fluorescence) of CCR9 in MLN from control and infected mice (gated on CD45.2$^+$live/dead$^-$IL-7Rα$^+$Lin$^-$intraCD3$^-$ GATA-3$^+$CCR9$^+$ cells).

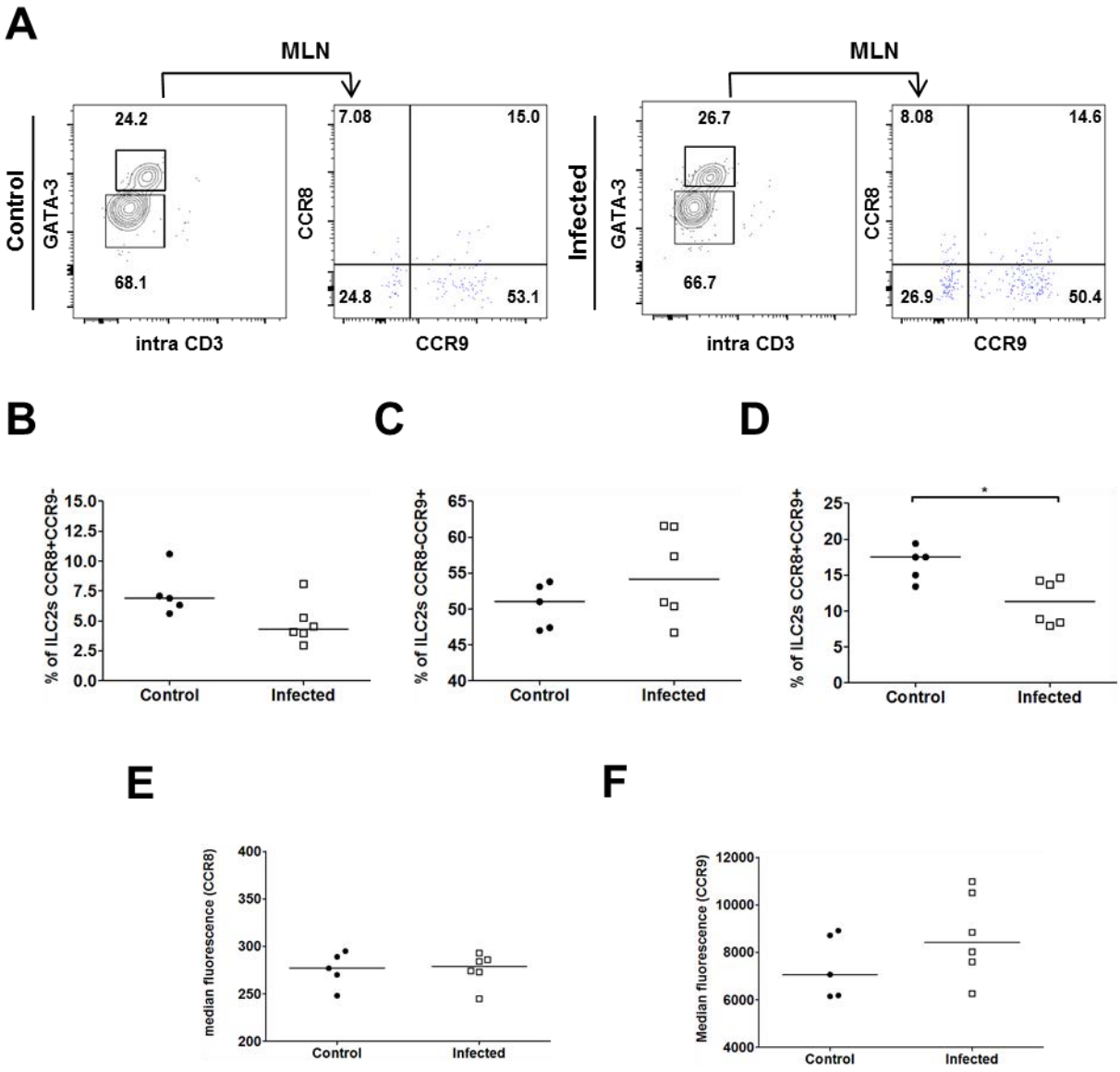
A
MLN
Control
GATA-3
24.2
68.1
intra CD3
CCR8
7.08
15.0
24.8
53.1
CCR9
MLN
Infected
GATA-3
26.7
66.7
intra CD3
CCR8
8.08
14.6
26.9
50.4
CCR9
B
% of ILC2s CCR8+CCR9-
Control
Infected
C
% of ILC2s CCR8-CCR9+
Control
Infected
D
% of ILC2s CCR8+CCR9+
*
Control
Infected
E
median fluorescence (CCR8)
Control
Infected
F
Median fluorescence (CCR9)
Control
Infected

Figure 7.25: MLN ILC2 proliferation following *H.polygyrus* infection

C57BL/6J males were either infected with *H.polygyrus* larvae, or given PBS as a control, and cells were isolated from the MLN five days post infection (see Materials and Methods for details). The ILC2 proliferation was measured by flow cytometry and quantified in different chemokine receptor profiles. Data for each group was obtained from two technical repeats.

Each data point (n=5, 6 for control and infected animals respectively) represents an individual sample with a line indicating the median value. Statistical significance was determined using a Mann-Whitney two-tailed T test, *p<0.05, **p<0.01, ***p<0.001 and ****p<0.0001.

A) Flow cytometry analysis showing representative ILC2 Ki-67 staining in different ILC2 chemokine receptor subsets in MLN from both control (left) and infected (right) animals (gated on CD45.2$^+$live/dead$^-$IL-7Rα$^+$Lin$^-$GATA-3$^+$ cells). Numbers indicate percentage of events in each gate. Dotted horizontal black line indicates positive events.

B) Graph showing percentage of Ki-67$^+$ ILC2s in MLN from control and infected mice (gated on CD45.2$^+$live/dead$^-$IL-7Rα$^+$Lin$^-$intraCD3$^-$GATA-3$^+$ cells).

C) Graph showing percentage of CCR8$^+$CCR9$^-$ ILC2s which are Ki-67$^+$ in MLN from control and infected mice (gated on CD45.2$^+$live/dead$^-$IL-7Rα$^+$Lin$^-$ intraCD3$^-$GATA-3$^+$CCR8$^+$CCR9$^-$ cells).

D) Graph showing percentage of CCR8$^-$CCR9$^+$ ILC2s which are Ki-67$^+$ in MLN from control and infected mice (gated on CD45.2$^+$live/dead$^-$IL-7Rα$^+$Lin$^-$ intraCD3$^-$GATA-3$^+$CCR8$^-$CCR9$^+$ cells).

E) Graph showing percentage of CCR8$^+$CCR9$^+$ ILC2s which are Ki-67$^+$ in MLN from control and infected mice (gated on CD45.2$^+$live/dead$^-$IL-7Rα$^+$Lin$^-$ intraCD3$^-$GATA-3$^+$CCR8$^+$CCR9$^+$ cells).

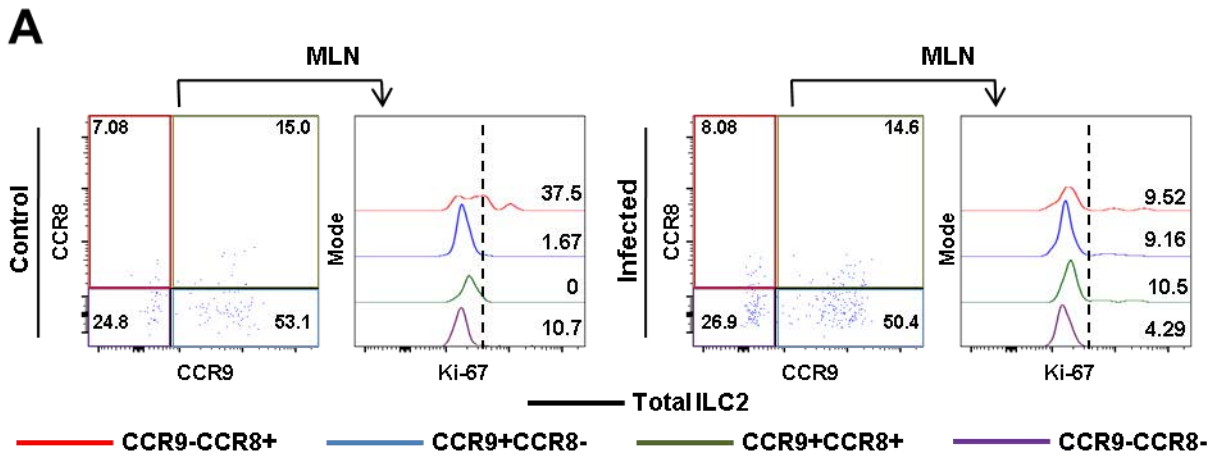
A
MLN
MLN
Control
Infected
CCR8
CCR9
Mode
Ki-67
7.08
15.0
24.8
53.1
37.5
1.67
0
10.7
8.08
14.6
26.9
50.4
9.52
9.16
10.5
4.29
Total ILC2
CCR9-CCR8+
CCR9+CCR8-
CCR9+CCR8+
CCR9-CCR8-

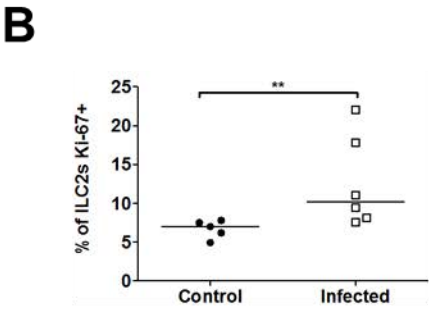
B
% of ILC2s Ki-67+
**
Control
Infected

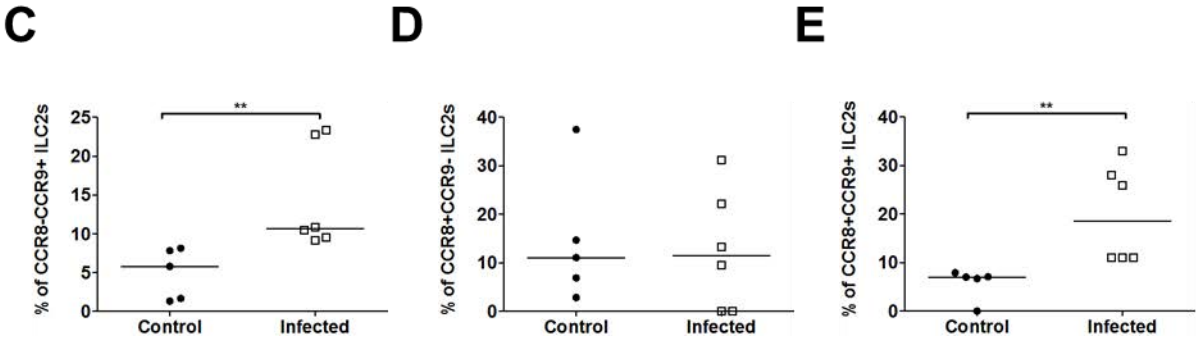
C
D
E
% of CCR8-CCR9+ ILC2s
% of CCR8+CCR9- ILC2s
% of CCR8+CCR9+ ILC2s
**
Control
Infected

Figure 7.26: Comparison of ILC2 and T cell proliferation following *H.polygyrus* infection

C57BL/6J males were either infected with *H.polygyrus* larvae, or given PBS as a control, and cells were isolated from the MLN, gonadal fat and mesenteries five days post infection (see Materials and Methods for details). The ILC2 and T cell proliferation was measured by flow cytometry. Data for each group was obtained from two technical repeats.

Each data point (n=5, 6 for control and infected animals respectively) represents an individual sample with a line indicating the median value. Statistical significance was determined using a Mann-Whitney two-tailed T test, *p<0.05, **p<0.01, ***p<0.001 and ****p<0.0001.

A) Histograms showing representative Ki-67 staining in ILC2s (left) or IL-7Rα$^+$CD3$^+$ cells (right) from infected (red line) or control (blue line) animals. Samples isolated from MLN (top), gonadal fat (bottom left) and mesenteries (bottom right). Dotted green line shows Ki-67 FMO control.

B) Graph showing percentage of ILC2s which are Ki-67$^+$ in MLN, gonadal fat and mesenteries from control and infected mice (gated on CD45.2$^+$live/dead$^-$IL-7Rα$^+$Lin$^-$intraCD3$^-$GATA-3$^+$Ki-67$^+$ cells).

C) Graph showing percentage of T cells which are Ki-67$^+$ in MLN, gonadal fat and mesenteries from control and infected mice (gated on CD45.2$^+$live/dead$^-$IL-7Rα$^+$Lin$^+$intraCD3$^+$Ki-67$^+$ cells).

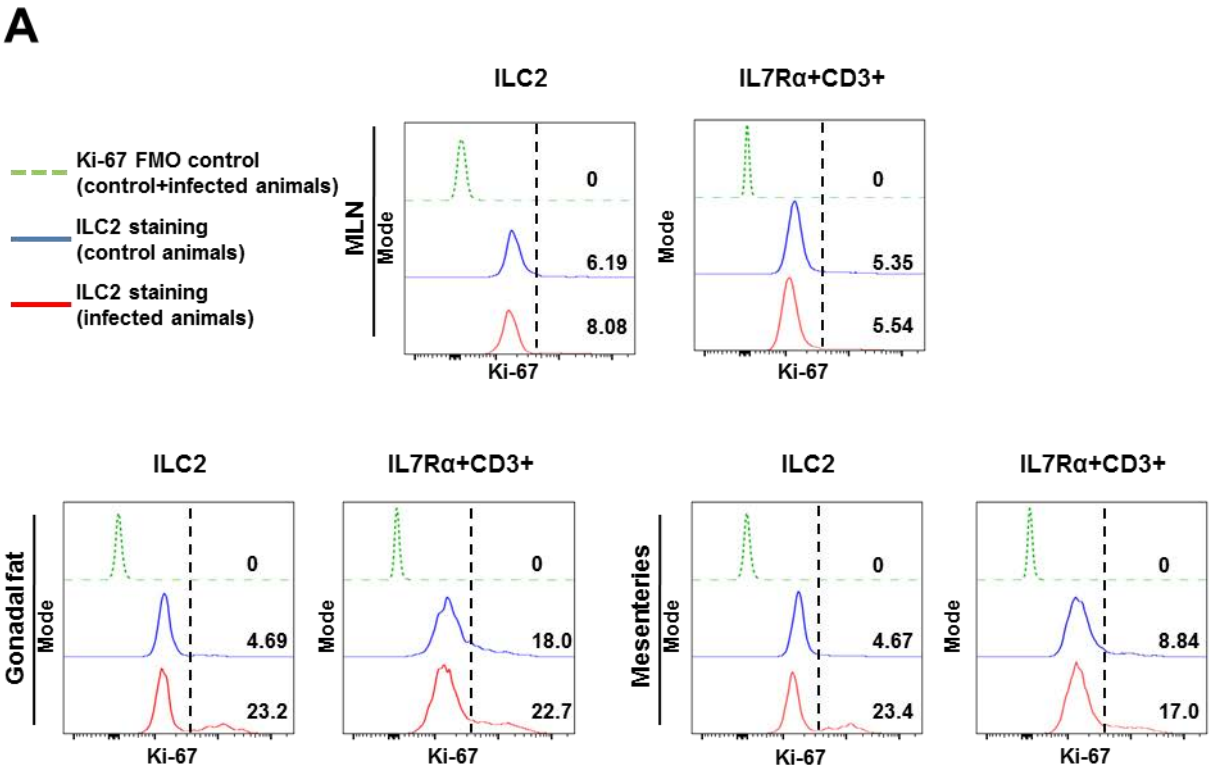
A
ILC2
IL7Rα+CD3+
Ki-67 FMO control
(control+infected animals)
ILC2 staining
(control animals)
ILC2 staining
(infected animals)
MLN
Mode
0
6.19
8.08
5.35
5.54
Ki-67
Gonadal fat
4.69
23.2
18.0
22.7
Mesenteries
4.67
23.4
8.84
17.0

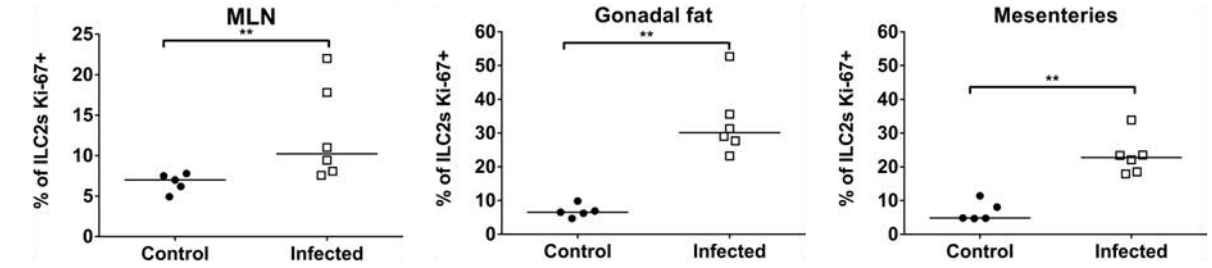
B
MLN
Gonadal fat
Mesenteries
% of ILC2s Ki-67+
**
Control
Infected

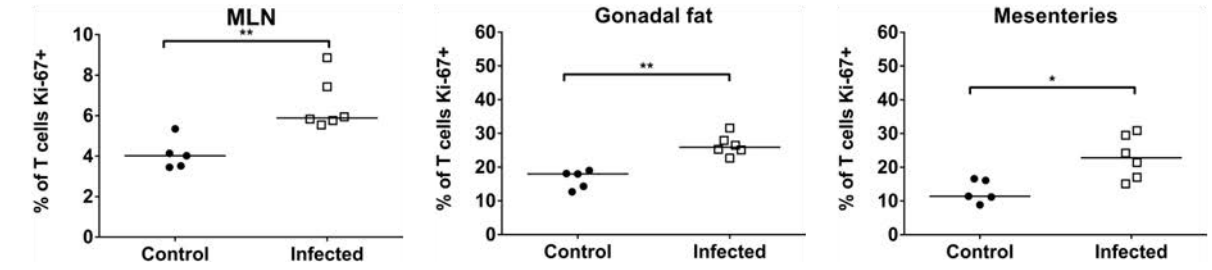
C
MLN
Gonadal fat
Mesenteries
% of T cells Ki-67+
**
*
Control
Infected

8. LIST OF REFERENCES

ACTON, S. E., ASTARITA, J. L., MALHOTRA, D., LUKACS-KORNEK, V., FRANZ, B., HESS, P. R., JAKUS, Z., KULIGOWSKI, M., FLETCHER, A. L., ELPEK, K. G., BELLEMARE-PELLETIER, A., SCEATS, L., REYNOSO, E. D., GONZALEZ, S. F., GRAHAM, D. B., CHANG, J., PETERS, A., WOODRUFF, M., KIM, Y. A., SWAT, W., MORITA, T., KUCHROO, V., CARROLL, M. C., KAHN, M. L., WUCHERPFENNIG, K. W. & TURLEY, S. J. 2012. Podoplanin-rich stromal networks induce dendritic cell motility via activation of the C-type lectin receptor CLEC-2. *Immunity,* 37**,** 276-89.

ALEXOPOULOU, L., PASPARAKIS, M. & KOLLIAS, G. 1997. A murine transmembrane tumor necrosis factor (TNF) transgene induces arthritis by cooperative p55/p75 TNF receptor signaling. *Eur J Immunol,* 27**,** 2588-92.

ANNUNZIATO, F., COSMI, L., LIOTTA, F., LAZZERI, E., MANETTI, R., VANINI, V., ROMAGNANI, P., MAGGI, E. & ROMAGNANI, S. 2002. Phenotype, localization, and mechanism of suppression of CD4(+)CD25(+) human thymocytes. *J Exp Med,* 196**,** 379-87.

ANSEL, K. M., HARRIS, R. B. & CYSTER, J. G. 2002. CXCL13 is required for B1 cell homing, natural antibody production, and body cavity immunity. *Immunity,* 16**,** 67-76.

ARNOLD, A. P., REUE, K., EGHBALI, M., VILAIN, E., CHEN, X., GHAHRAMANI, N., ITOH, Y., LI, J., LINK, J. C., NGUN, T. & WILLIAMS-BURRIS, S. M. 2016. The importance of having two X chromosomes. *Philos Trans R Soc Lond B Biol Sci,* 371**,** 20150113.

ARTIS, D. & SPITS, H. 2015. The biology of innate lymphoid cells. *Nature,* 517**,** 293-301.

AZEEZ, O. I., MEINTJES, R. & CHAMUNORWA, J. P. 2014. Fat body, fat pad and adipose tissues in invertebrates and vertebrates: the nexus. *Lipids Health Dis,* 13**,** 71.

BAI, Z., CAI, L., UMEMOTO, E., TAKEDA, A., TOHYA, K., KOMAI, Y., VEERAVEEDU, P. T., HATA, E., SUGIURA, Y., KUBO, A., SUEMATSU, M., HAYASAKA, H., OKUDAIRA, S., AOKI, J., TANAKA, T., ALBERS, H. M., OVAA, H. & MIYASAKA, M. 2013. Constitutive lymphocyte transmigration across the basal lamina of high endothelial venules is regulated by the autotaxin/lysophosphatidic acid axis. *J Immunol,* 190**,** 2036-48.

BAJENOFF, M. 2012. Stromal cells control soluble material and cellular transport in lymph nodes. *Front Immunol,* 3**,** 304.

BAJENOFF, M., EGEN, J. G., KOO, L. Y., LAUGIER, J. P., BRAU, F., GLAICHENHAUS, N. & GERMAIN, R. N. 2006. Stromal cell networks regulate lymphocyte entry, migration, and territoriality in lymph nodes. *Immunity,* 25**,** 989-1001.

BAL, S. M., BERNINK, J. H., NAGASAWA, M., GROOT, J., SHIKHAGAIE, M. M., GOLEBSKI, K., VAN DRUNEN, C. M., LUTTER, R., JONKERS, R. E.,

HOMBRINK, P., BRUCHARD, M., VILLAUDY, J., MUNNEKE, J. M., FOKKENS, W., ERJEFALT, J. S., SPITS, H. & ROS, X. R. 2016. IL-1beta, IL-4 and IL-12 control the fate of group 2 innate lymphoid cells in human airway inflammation in the lungs. *Nat Immunol,* 17**,** 636-45.

BAPAT, S. P., MYOUNG SUH, J., FANG, S., LIU, S., ZHANG, Y., CHENG, A., ZHOU, C., LIANG, Y., LEBLANC, M., LIDDLE, C., ATKINS, A. R., YU, R. T., DOWNES, M., EVANS, R. M. & ZHENG, Y. 2015. Depletion of fat-resident Treg cells prevents age-associated insulin resistance. *Nature,* 528**,** 137-41.

BARLOW, J. L., PEEL, S., FOX, J., PANOVA, V., HARDMAN, C. S., CAMELO, A., BUCKS, C., WU, X., KANE, C. M., NEILL, D. R., FLYNN, R. J., SAYERS, I., HALL, I. P. & MCKENZIE, A. N. 2013. IL-33 is more potent than IL-25 in provoking IL-13-producing nuocytes (type 2 innate lymphoid cells) and airway contraction. *J Allergy Clin Immunol,* 132**,** 933-41.

BARNIG, C., CERNADAS, M., DUTILE, S., LIU, X., PERRELLA, M. A., KAZANI, S., WECHSLER, M. E., ISRAEL, E. & LEVY, B. D. 2013. Lipoxin A4 regulates natural killer cell and type 2 innate lymphoid cell activation in asthma. *Sci Transl Med,* 5**,** 174ra26.

BARSHESHET, Y., WILDBAUM, G., LEVY, E., VITENSHTEIN, A., AKINSEYE, C., GRIGGS, J., LIRA, S. A. & KARIN, N. 2017. CCR8+FOXp3+ Treg cells as master drivers of immune regulation. *Proc Natl Acad Sci U S A,* 114**,** 6086-6091.

BENEZECH, C., LUU, N. T., WALKER, J. A., KRUGLOV, A. A., LOO, Y., NAKAMURA, K., ZHANG, Y., NAYAR, S., JONES, L. H., FLORES-LANGARICA, A., MCINTOSH, A., MARSHALL, J., BARONE, F., BESRA, G., MILES, K., ALLEN, J. E., GRAY, M., KOLLIAS, G., CUNNINGHAM, A. F., WITHERS, D. R., TOELLNER, K. M., JONES, N. D., VELDHOEN, M., NEDOSPASOV, S. A., MCKENZIE, A. N. J. & CAAMANO, J. H. 2015. Inflammation-induced formation of fat-associated lymphoid clusters. *Nat Immunol,* 16**,** 819-828.

BENEZECH, C., MADER, E., DESANTI, G., KHAN, M., NAKAMURA, K., WHITE, A., WARE, C. F., ANDERSON, G. & CAAMANO, J. H. 2012. Lymphotoxin-beta receptor signaling through NF-kappaB2-RelB pathway reprograms adipocyte precursors as lymph node stromal cells. *Immunity,* 37**,** 721-34.

BENEZECH, C., WHITE, A., MADER, E., SERRE, K., PARNELL, S., PFEFFER, K., WARE, C. F., ANDERSON, G. & CAAMANO, J. H. 2010. Ontogeny of stromal organizer cells during lymph node development. *J Immunol,* 184**,** 4521-30.

BERNINK, J. H., KRABBENDAM, L., GERMAR, K., DE JONG, E., GRONKE, K., KOFOED-NIELSEN, M., MUNNEKE, J. M., HAZENBERG, M. D., VILLAUDY, J., BUSKENS, C. J., BEMELMAN, W. A., DIEFENBACH, A., BLOM, B. & SPITS, H. 2015. Interleukin-12 and -23 Control Plasticity of CD127(+) Group 1 and Group 3 Innate Lymphoid Cells in the Intestinal Lamina Propria. *Immunity,* 43**,** 146-60.

BERNINK, J. H., PETERS, C. P., MUNNEKE, M., TE VELDE, A. A., MEIJER, S. L., WEIJER, K., HREGGVIDSDOTTIR, H. S., HEINSBROEK, S. E., LEGRAND,

N., BUSKENS, C. J., BEMELMAN, W. A., MJOSBERG, J. M. & SPITS, H. 2013. Human type 1 innate lymphoid cells accumulate in inflamed mucosal tissues. *Nat Immunol,* 14**,** 221-9.

BIANCHI, M. E. 2007. DAMPs, PAMPs and alarmins: all we need to know about danger. *J Leukoc Biol,* 81**,** 1-5.

BJORNDAL, B., BURRI, L., STAALESEN, V., SKORVE, J. & BERGE, R. K. 2011. Different adipose depots: their role in the development of metabolic syndrome and mitochondrial response to hypolipidemic agents. *J Obes,* 2011**,** 490650.

BLUM, K. S. & PABST, R. 2006. Keystones in lymph node development. *J Anat,* 209**,** 585-95.

BOEHM, T., IWANAMI, N. & HESS, I. 2012. Evolution of the immune system in the lower vertebrates. *Annu Rev Genomics Hum Genet,* 13**,** 127-49.

BONECCHI, R., BIANCHI, G., BORDIGNON, P. P., D'AMBROSIO, D., LANG, R., BORSATTI, A., SOZZANI, S., ALLAVENA, P., GRAY, P. A., MANTOVANI, A. & SINIGAGLIA, F. 1998. Differential expression of chemokine receptors and chemotactic responsiveness of type 1 T helper cells (Th1s) and Th2s. *J Exp Med,* 187**,** 129-34.

BOOS, M. D., YOKOTA, Y., EBERL, G. & KEE, B. L. 2007. Mature natural killer cell and lymphoid tissue-inducing cell development requires Id2-mediated suppression of E protein activity. *J Exp Med,* 204**,** 1119-30.

BOULENOUAR, S., MICHELET, X., DUQUETTE, D., ALVAREZ, D., HOGAN, A. E., DOLD, C., O'CONNOR, D., STUTTE, S., TAVAKKOLI, A., WINTERS, D., EXLEY, M. A., O'SHEA, D., BRENNER, M. B., VON ANDRIAN, U. & LYNCH, L. 2017. Adipose Type One Innate Lymphoid Cells Regulate Macrophage Homeostasis through Targeted Cytotoxicity. *Immunity,* 46**,** 273-286.

BRENDOLAN, A. & CAAMANO, J. H. 2012. Mesenchymal cell differentiation during lymph node organogenesis. *Front Immunol,* 3**,** 381.

BRENNER, D., BLASER, H. & MAK, T. W. 2015. Regulation of tumour necrosis factor signalling: live or let die. *Nat Rev Immunol,* 15**,** 362-74.

BRESTOFF, J. R., KIM, B. S., SAENZ, S. A., STINE, R. R., MONTICELLI, L. A., SONNENBERG, G. F., THOME, J. J., FARBER, D. L., LUTFY, K., SEALE, P. & ARTIS, D. 2015. Group 2 innate lymphoid cells promote beiging of white adipose tissue and limit obesity. *Nature,* 519**,** 242-6.

BROMLEY, S. K., MEMPEL, T. R. & LUSTER, A. D. 2008. Orchestrating the orchestrators: chemokines in control of T cell traffic. *Nat Immunol,* 9**,** 970-80.

BRUDER-NASCIMENTO, T., EKELEDO, O. J., ANDERSON, R., LE, H. B. & BELIN DE CHANTEMELE, E. J. 2017. Long Term High Fat Diet Treatment: An Appropriate Approach to Study the Sex-Specificity of the Autonomic and Cardiovascular Responses to Obesity in Mice. *Front Physiol,* 8**,** 32.

BRUNO, S. & DARZYNKIEWICZ, Z. 1992. Cell cycle dependent expression and stability of the nuclear protein detected by Ki-67 antibody in HL-60 cells. *Cell Prolif,* 25**,** 31-40.

BUSCHER, K., WANG, H., ZHANG, X., STRIEWSKI, P., WIRTH, B., SAGGU, G., LUTKE-ENKING, S., MAYADAS, T. N., LEY, K., SOROKIN, L. & SONG, J. 2016. Protection from septic peritonitis by rapid neutrophil recruitment through omental high endothelial venules. *Nat Commun,* 7**,** 10828.

CALIFANO, D., CHO, J. J., UDDIN, M. N., LORENTSEN, K. J., YANG, Q., BHANDOOLA, A., LI, H. & AVRAM, D. 2015. Transcription Factor Bcl11b Controls Identity and Function of Mature Type 2 Innate Lymphoid Cells. *Immunity,* 43**,** 354-68.

CAMBERIS, M., LE GROS, G. & URBAN, J., JR. 2003. Animal model of Nippostrongylus brasiliensis and Heligmosomoides polygyrus. *Curr Protoc Immunol,* Chapter 19**,** Unit 19 12.

CARNAUD, C., LEE, D., DONNARS, O., PARK, S. H., BEAVIS, A., KOEZUKA, Y. & BENDELAC, A. 1999. Cutting edge: Cross-talk between cells of the innate immune system: NKT cells rapidly activate NK cells. *J Immunol,* 163**,** 4647-50.

CASERTA, F., TCHKONIA, T., CIVELEK, V. N., PRENTKI, M., BROWN, N. F., MCGARRY, J. D., FORSE, R. A., CORKEY, B. E., HAMILTON, J. A. & KIRKLAND, J. L. 2001. Fat depot origin affects fatty acid handling in cultured rat and human preadipocytes. *Am J Physiol Endocrinol Metab,* 280**,** E238-47.

CAWTHORN, W. P., HEYD, F., HEGYI, K. & SETHI, J. K. 2007. Tumour necrosis factor-alpha inhibits adipogenesis via a beta-catenin/TCF4(TCF7L2)-dependent pathway. *Cell Death Differ,* 14**,** 1361-73.

CHAE, G. N. & KWAK, S. J. 2003. NF-kappaB is involved in the TNF-alpha induced inhibition of the differentiation of 3T3-L1 cells by reducing PPARgamma expression. *Exp Mol Med,* 35**,** 431-7.

CHANG, J. E. & TURLEY, S. J. 2015. Stromal infrastructure of the lymph node and coordination of immunity. *Trends Immunol,* 36**,** 30-9.

CHANG, Y. J., KIM, H. Y., ALBACKER, L. A., BAUMGARTH, N., MCKENZIE, A. N., SMITH, D. E., DEKRUYFF, R. H. & UMETSU, D. T. 2011. Innate lymphoid cells mediate influenza-induced airway hyper-reactivity independently of adaptive immunity. *Nat Immunol,* 12**,** 631-8.

CHEA, S., POSSOT, C., PERCHET, T., PETIT, M., CUMANO, A. & GOLUB, R. 2015. CXCR6 Expression Is Important for Retention and Circulation of ILC Precursors. *Mediators Inflamm,* 2015**,** 368427.

CHEN, X., OPPENHEIM, J. J. & HOWARD, O. M. 2005. BALB/c mice have more CD4+CD25+ T regulatory cells and show greater susceptibility to suppression of their CD4+CD25- responder T cells than C57BL/6 mice. *J Leukoc Biol,* 78**,** 114-21.

CHERRIER, M., SAWA, S. & EBERL, G. 2012. Notch, Id2, and RORgammat sequentially orchestrate the fetal development of lymphoid tissue inducer cells. *J Exp Med,* 209**,** 729-40.

CHO, K. W., ZAMARRON, B. F., MUIR, L. A., SINGER, K., PORSCHE, C. E., DELPROPOSTO, J. B., GELETKA, L., MEYER, K. A., O'ROURKE, R. W. & LUMENG, C. N. 2016. Adipose Tissue Dendritic Cells Are Independent

Contributors to Obesity-Induced Inflammation and Insulin Resistance. *J Immunol,* 197**,** 3650-3661.

CHUSYD, D. E., WANG, D., HUFFMAN, D. M. & NAGY, T. R. 2016. Relationships between Rodent White Adipose Fat Pads and Human White Adipose Fat Depots. *Front Nutr,* 3**,** 10.

CIPOLLETTA, D., KOLODIN, D., BENOIST, C. & MATHIS, D. 2011. Tissular T(regs): a unique population of adipose-tissue-resident Foxp3+CD4+ T cells that impacts organismal metabolism. *Semin Immunol,* 23**,** 431-7.

COHEN, P., LEVY, J. D., ZHANG, Y., FRONTINI, A., KOLODIN, D. P., SVENSSON, K. J., LO, J. C., ZENG, X., YE, L., KHANDEKAR, M. J., WU, J., GUNAWARDANA, S. C., BANKS, A. S., CAMPOREZ, J. P., JURCZAK, M. J., KAJIMURA, S., PISTON, D. W., MATHIS, D., CINTI, S., SHULMAN, G. I., SEALE, P. & SPIEGELMAN, B. M. 2014. Ablation of PRDM16 and beige adipose causes metabolic dysfunction and a subcutaneous to visceral fat switch. *Cell,* 156**,** 304-16.

COLANTONIO, L., IELLEM, A., SINIGAGLIA, F. & D'AMBROSIO, D. 2002. Skin-homing CLA+ T cells and regulatory CD25+ T cells represent major subsets of human peripheral blood memory T cells migrating in response to CCL1/I-309. *Eur J Immunol,* 32**,** 3506-14.

CONSTANTINIDES, M. G., MCDONALD, B. D., VERHOEF, P. A. & BENDELAC, A. 2014. A committed precursor to innate lymphoid cells. *Nature,* 508**,** 397-401.

COPPACK, S. W. 2007. Pro-inflammatory cytokines and adipose tissue. *Proceedings of the Nutrition Society,* 60**,** 349-356.

CRANE, J. D., PALANIVEL, R., MOTTILLO, E. P., BUJAK, A. L., WANG, H., FORD, R. J., COLLINS, A., BLUMER, R. M., FULLERTON, M. D., YABUT, J. M., KIM, J. J., GHIA, J. E., HAMZA, S. M., MORRISON, K. M., SCHERTZER, J. D., DYCK, J. R., KHAN, W. I. & STEINBERG, G. R. 2015. Inhibiting peripheral serotonin synthesis reduces obesity and metabolic dysfunction by promoting brown adipose tissue thermogenesis. *Nat Med,* 21**,** 166-72.

CRUZ-MIGONI, S. & CAAMANO, J. 2016. Fat-Associated Lymphoid Clusters in Inflammation and Immunity. *Front Immunol,* 7**,** 612.

CUPEDO, T., VONDENHOFF, M. F., HEEREGRAVE, E. J., DE WEERD, A. E., JANSEN, W., JACKSON, D. G., KRAAL, G. & MEBIUS, R. E. 2004. Presumptive lymph node organizers are differentially represented in developing mesenteric and peripheral nodes. *J Immunol,* 173**,** 2968-75.

CYSTER, J. G. 1999. Chemokines and cell migration in secondary lymphoid organs. *Science,* 286**,** 2098-102.

CZECH, M. P. 2017. Insulin action and resistance in obesity and type 2 diabetes. *Nat Med,* 23**,** 804-814.

DARZYNKIEWICZ, Z., ZHAO, H., ZHANG, S., LEE, M. Y., LEE, E. Y. & ZHANG, Z. 2015. Initiation and termination of DNA replication during S phase in relation to cyclins D1, E and A, p21WAF1, Cdt1 and the p12 subunit of DNA polymerase delta revealed in individual cells by cytometry. *Oncotarget,* 6**,** 11735-50.

DE HENAU, O., DEGROOT, G. N., IMBAULT, V., ROBERT, V., DE POORTER, C., MCHEIK, S., GALES, C., PARMENTIER, M. & SPRINGAEL, J. Y. 2016. Signaling Properties of Chemerin Receptors CMKLR1, GPR1 and CCRL2. *PLoS One,* 11**,** e0164179.

DE VOOGHT, V., VANOIRBEEK, J. A., LUYTS, K., HAENEN, S., NEMERY, B. & HOET, P. H. 2010. Choice of mouse strain influences the outcome in a mouse model of chemical-induced asthma. *PLoS One,* 5**,** e12581.

DEMERATH, E. W., SUN, S. S., ROGERS, N., LEE, M., REED, D., CHOH, A. C., COUCH, W., CZERWINSKI, S. A., CHUMLEA, W. C., SIERVOGEL, R. M. & TOWNE, B. 2007. Anatomical patterning of visceral adipose tissue: race, sex, and age variation. *Obesity (Silver Spring),* 15**,** 2984-93.

DI SANTO, J. P. 2014. Staying innate: transcription factor maintenance of innate lymphoid cell identity. *Immunol Rev,* 261**,** 169-76.

DIEFENBACH, A. 2015. Profiling the diversity of innate lymphoid cells. *Nat Immunol,* 16**,** 222-4.

DIEU-NOSJEAN, M. C., GOC, J., GIRALDO, N. A., SAUTES-FRIDMAN, C. & FRIDMAN, W. H. 2014. Tertiary lymphoid structures in cancer and beyond. *Trends Immunol,* 35**,** 571-80.

DOHERTY, T. A., KHORRAM, N., LUND, S., MEHTA, A. K., CROFT, M. & BROIDE, D. H. 2013. Lung type 2 innate lymphoid cells express cysteinyl leukotriene receptor 1, which regulates TH2 cytokine production. *J Allergy Clin Immunol,* 132**,** 205-13.

DONG, C., JUEDES, A. E., TEMANN, U. A., SHRESTA, S., ALLISON, J. P., RUDDLE, N. H. & FLAVELL, R. A. 2001. ICOS co-stimulatory receptor is essential for T-cell activation and function. *Nature,* 409**,** 97-101.

DONNINELLI, G., DEL CORNO, M., PIERDOMINICI, M., SCAZZOCCHIO, B., VARI, R., VARANO, B., PACELLA, I., PICONESE, S., BARNABA, V., D'ARCHIVIO, M., MASELLA, R., CONTI, L. & GESSANI, S. 2017. Distinct Blood and Visceral Adipose Tissue Regulatory T Cell and Innate Lymphocyte Profiles Characterize Obesity and Colorectal Cancer. *Front Immunol,* 8**,** 643.

DUMOUTIER, L., DE HEUSCH, M., ORABONA, C., SATOH-TAKAYAMA, N., EBERL, G., SIRARD, J. C., DI SANTO, J. P. & RENAULD, J. C. 2011. IL-22 is produced by gammaC-independent CD25+ CCR6+ innate murine spleen cells upon inflammatory stimuli and contributes to LPS-induced lethality. *Eur J Immunol,* 41**,** 1075-85.

EBERL, G., DI SANTO, J. P. & VIVIER, E. 2015. The brave new world of innate lymphoid cells. *Nat Immunol,* 16**,** 1-5.

EBERL, G., MARMON, S., SUNSHINE, M. J., RENNERT, P. D., CHOI, Y. & LITTMAN, D. R. 2004. An essential function for the nuclear receptor RORgamma(t) in the generation of fetal lymphoid tissue inducer cells. *Nat Immunol,* 5**,** 64-73.

EDENS, N. K., FRIED, S. K., KRAL, J. G., HIRSCH, J. & LEIBEL, R. L. 1993. In vitro lipid synthesis in human adipose tissue from three abdominal sites. *Am J Physiol,* 265**,** E374-9.

ELEWA, Y. H., ICHII, O. & KON, Y. 2016. Comparative analysis of mediastinal fat-associated lymphoid cluster development and lung cellular infiltration in murine autoimmune disease models and the corresponding normal control strains. *Immunology,* 147**,** 30-40.

ELEWA, Y. H. A., ICHII, O. & KON, Y. 2017. Sex-related differences in autoimmune-induced lung lesions in MRL/MpJ-fas(lpr) mice are mediated by the development of mediastinal fat-associated lymphoid clusters. *Autoimmunity,* 50**,** 306-316.

ESSER-VON BIEREN, J., MOSCONI, I., GUIET, R., PIERSGILLI, A., VOLPE, B., CHEN, F., GAUSE, W. C., SEITZ, A., VERBEEK, J. S. & HARRIS, N. L. 2013. Antibodies trap tissue migrating helminth larvae and prevent tissue damage by driving IL-4Ralpha-independent alternative differentiation of macrophages. *PLoS Pathog,* 9**,** e1003771.

FEUERER, M., HERRERO, L., CIPOLLETTA, D., NAAZ, A., WONG, J., NAYER, A., LEE, J., GOLDFINE, A. B., BENOIST, C., SHOELSON, S. & MATHIS, D. 2009. Lean, but not obese, fat is enriched for a unique population of regulatory T cells that affect metabolic parameters. *Nat Med,* 15**,** 930-9.

FILBEY, K. J., GRAINGER, J. R., SMITH, K. A., BOON, L., VAN ROOIJEN, N., HARCUS, Y., JENKINS, S., HEWITSON, J. P. & MAIZELS, R. M. 2014. Innate and adaptive type 2 immune cell responses in genetically controlled resistance to intestinal helminth infection. *Immunol Cell Biol,* 92**,** 436-48.

FINKELMAN, F. D., MADDEN, K. B., CHEEVER, A. W., KATONA, I. M., MORRIS, S. C., GATELY, M. K., HUBBARD, B. R., GAUSE, W. C. & URBAN, J. F., JR. 1994. Effects of interleukin 12 on immune responses and host protection in mice infected with intestinal nematode parasites. *J Exp Med,* 179**,** 1563-72.

FINLAY, C. M., STEFANSKA, A. M., WALSH, K. P., KELLY, P. J., BOON, L., LAVELLE, E. C., WALSH, P. T. & MILLS, K. H. 2016. Helminth Products Protect against Autoimmunity via Innate Type 2 Cytokines IL-5 and IL-33, Which Promote Eosinophilia. *J Immunol,* 196**,** 703-14.

FINNEY, C. A., TAYLOR, M. D., WILSON, M. S. & MAIZELS, R. M. 2007. Expansion and activation of CD4(+)CD25(+) regulatory T cells in Heligmosomoides polygyrus infection. *Eur J Immunol,* 37**,** 1874-86.

FISCHER, K., RUIZ, H. H., JHUN, K., FINAN, B., OBERLIN, D. J., VAN DER HEIDE, V., KALINOVICH, A. V., PETROVIC, N., WOLF, Y., CLEMMENSEN, C., SHIN, A. C., DIVANOVIC, S., BROMBACHER, F., GLASMACHER, E., KEIPERT, S., JASTROCH, M., NAGLER, J., SCHRAMM, K. W., MEDRIKOVA, D., COLLDEN, G., WOODS, S. C., HERZIG, S., HOMANN, D., JUNG, S., NEDERGAARD, J., CANNON, B., TSCHOP, M. H., MULLER, T. D. & BUETTNER, C. 2017. Alternatively activated macrophages do not synthesize catecholamines or contribute to adipose tissue adaptive thermogenesis. *Nat Med,* 23**,** 623-630.

FLETCHER, A. L., LUKACS-KORNEK, V., REYNOSO, E. D., PINNER, S. E., BELLEMARE-PELLETIER, A., CURRY, M. S., COLLIER, A. R., BOYD, R. L. & TURLEY, S. J. 2010. Lymph node fibroblastic reticular cells directly present peripheral tissue antigen under steady-state and inflammatory conditions. *J Exp Med,* 207**,** 689-97.

FLETCHER, A. L., MALHOTRA, D., ACTON, S. E., LUKACS-KORNEK, V., BELLEMARE-PELLETIER, A., CURRY, M., ARMANT, M. & TURLEY, S. J. 2011. Reproducible isolation of lymph node stromal cells reveals site-dependent differences in fibroblastic reticular cells. *Front Immunol,* 2**,** 35.

FORSTER, R., MATTIS, A. E., KREMMER, E., WOLF, E., BREM, G. & LIPP, M. 1996. A putative chemokine receptor, BLR1, directs B cell migration to defined lymphoid organs and specific anatomic compartments of the spleen. *Cell,* 87**,** 1037-47.

FORSTER, R., SCHUBEL, A., BREITFELD, D., KREMMER, E., RENNER-MULLER, I., WOLF, E. & LIPP, M. 1999. CCR7 coordinates the primary immune response by establishing functional microenvironments in secondary lymphoid organs. *Cell,* 99**,** 23-33.

FORT, M. M., CHEUNG, J., YEN, D., LI, J., ZURAWSKI, S. M., LO, S., MENON, S., CLIFFORD, T., HUNTE, B., LESLEY, R., MUCHAMUEL, T., HURST, S. D., ZURAWSKI, G., LEACH, M. W., GORMAN, D. M. & RENNICK, D. M. 2001. IL-25 induces IL-4, IL-5, and IL-13 and Th2-associated pathologies in vivo. *Immunity,* 15**,** 985-95.

FOX, C. J., HAMMERMAN, P. S. & THOMPSON, C. B. 2005. Fuel feeds function: energy metabolism and the T-cell response. *Nat Rev Immunol,* 5**,** 844-52.

FRIED, S. K., LEIBEL, R. L., EDENS, N. K. & KRAL, J. G. 1993. Lipolysis in intraabdominal adipose tissues of obese women and men. *Obes Res,* 1**,** 443-8.

FUJII, S., SHIMIZU, K., SMITH, C., BONIFAZ, L. & STEINMAN, R. M. 2003. Activation of natural killer T cells by alpha-galactosylceramide rapidly induces the full maturation of dendritic cells in vivo and thereby acts as an adjuvant for combined CD4 and CD8 T cell immunity to a coadministered protein. *J Exp Med,* 198**,** 267-79.

GASTEIGER, G., FAN, X., DIKIY, S., LEE, S. Y. & RUDENSKY, A. Y. 2015. Tissue residency of innate lymphoid cells in lymphoid and nonlymphoid organs. *Science,* 350**,** 981-5.

GEER, E. B. & SHEN, W. 2009. Gender differences in insulin resistance, body composition, and energy balance. *Gend Med,* 6 Suppl 1**,** 60-75.

GERNER, M. Y., KASTENMULLER, W., IFRIM, I., KABAT, J. & GERMAIN, R. N. 2012. Histo-cytometry: a method for highly multiplex quantitative tissue imaging analysis applied to dendritic cell subset microanatomy in lymph nodes. *Immunity,* 37**,** 364-76.

GOMBERT, M., DIEU-NOSJEAN, M. C., WINTERBERG, F., BUNEMANN, E., KUBITZA, R. C., DA CUNHA, L., HAAHTELA, A., LEHTIMAKI, S., MULLER,

A., RIEKER, J., MELLER, S., PIVARCSI, A., KORECK, A., FRIDMAN, W. H., ZENTGRAF, H. W., PAVENSTADT, H., AMARA, A., CAUX, C., KEMENY, L., ALENIUS, H., LAUERMA, A., RUZICKA, T., ZLOTNIK, A. & HOMEY, B. 2005. CCL1-CCR8 interactions: an axis mediating the recruitment of T cells and Langerhans-type dendritic cells to sites of atopic skin inflammation. *J Immunol,* 174**,** 5082-91.

GRIESENAUER, B. & PACZESNY, S. 2017. The ST2/IL-33 Axis in Immune Cells during Inflammatory Diseases. *Front Immunol,* 8**,** 475.

GRIFFITH, J. W., SOKOL, C. L. & LUSTER, A. D. 2014. Chemokines and chemokine receptors: positioning cells for host defense and immunity. *Annu Rev Immunol,* 32**,** 659-702.

GRUNDEMANN, C., BAUER, M., SCHWEIER, O., VON OPPEN, N., LASSING, U., SAUDAN, P., BECKER, K. F., KARP, K., HANKE, T., BACHMANN, M. F. & PIRCHER, H. 2006. Cutting edge: Identification of E-cadherin as a ligand for the murine killer cell lectin-like receptor G1. *Journal of Immunology,* 176**,** 1311-1315.

GUIGAS, B. & MOLOFSKY, A. B. 2015. A worm of one's own: how helminths modulate host adipose tissue function and metabolism. *Trends Parasitol,* 31**,** 435-41.

GUNN, M. D., NGO, V. N., ANSEL, K. M., EKLAND, E. H., CYSTER, J. G. & WILLIAMS, L. T. 1998. A B-cell-homing chemokine made in lymphoid follicles activates Burkitt's lymphoma receptor-1. *Nature,* 391**,** 799-803.

HALIM, T. Y., HWANG, Y. Y., SCANLON, S. T., ZAGHOUANI, H., GARBI, N., FALLON, P. G. & MCKENZIE, A. N. 2016. Group 2 innate lymphoid cells license dendritic cells to potentiate memory TH2 cell responses. *Nat Immunol,* 17**,** 57-64.

HALVERSON, R., TORRES, R. M. & PELANDA, R. 2004. Receptor editing is the main mechanism of B cell tolerance toward membrane antigens. *Nat Immunol,* 5**,** 645-50.

HAMS, E., LOCKSLEY, R. M., MCKENZIE, A. N. & FALLON, P. G. 2013. Cutting edge: IL-25 elicits innate lymphoid type 2 and type II NKT cells that regulate obesity in mice. *J Immunol,* 191**,** 5349-53.

HAN, M., RAJPUT, C., HONG, J. Y., LEI, J., HINDE, J. L., WU, Q., BENTLEY, J. K. & HERSHENSON, M. B. 2017. The Innate Cytokines IL-25, IL-33, and TSLP Cooperate in the Induction of Type 2 Innate Lymphoid Cell Expansion and Mucous Metaplasia in Rhinovirus-Infected Immature Mice. *J Immunol,* 199**,** 1308-1318.

HANABUCHI, S., ITO, T., PARK, W. R., WATANABE, N., SHAW, J. L., ROMAN, E., ARIMA, K., WANG, Y. H., VOO, K. S., CAO, W. & LIU, Y. J. 2010. Thymic stromal lymphopoietin-activated plasmacytoid dendritic cells induce the generation of FOXP3+ regulatory T cells in human thymus. *J Immunol,* 184**,** 2999-3007.

HARDMAN, C. S., PANOVA, V. & MCKENZIE, A. N. 2013. IL-33 citrine reporter mice reveal the temporal and spatial expression of IL-33 during allergic lung inflammation. *Eur J Immunol,* 43**,** 488-98.

HASHIGUCHI, M., KASHIWAKURA, Y., KOJIMA, H., KOBAYASHI, A., KANNO, Y. & KOBATA, T. 2015. IL-33 activates eosinophils of visceral adipose tissue both directly and via innate lymphoid cells. *Eur J Immunol,* 45**,** 876-85.

HASHIMOTO, K., UCHIKAWA, R., TEGOSHI, T., TAKEDA, K., YAMADA, M. & ARIZONO, N. 2009. Depleted intestinal goblet cells and severe pathological changes in SCID mice infected with Heligmosomoides polygyrus. *Parasite Immunol,* 31**,** 457-65.

HENSON, S. M. & AKBAR, A. N. 2009. KLRG1--more than a marker for T cell senescence. *Age* 31**,** 285-91.

HENSON, S. M., FRANZESE, O., MACAULAY, R., LIBRI, V., AZEVEDO, R. I., KIANI-ALIKHAN, S., PLUNKETT, F. J., MASTERS, J. E., JACKSON, S., GRIFFITHS, S. J., PIRCHER, H. P., SOARES, M. V. & AKBAR, A. N. 2009. KLRG1 signaling induces defective Akt (ser473) phosphorylation and proliferative dysfunction of highly differentiated CD8+ T cells. *Blood,* 113**,** 6619-28.

HEPWORTH, M. R., DANILOWICZ-LUEBERT, E., RAUSCH, S., METZ, M., KLOTZ, C., MAURER, M. & HARTMANN, S. 2012. Mast cells orchestrate type 2 immunity to helminths through regulation of tissue-derived cytokines. *Proc Natl Acad Sci U S A,* 109**,** 6644-9.

HIMMS-HAGEN, J. 1990. Brown adipose tissue thermogenesis: interdisciplinary studies. *FASEB J,* 4**,** 2890-8.

HOTAMISLIGIL, G. S. 2006. Inflammation and metabolic disorders. *Nature,* 444**,** 860-7.

HOTAMISLIGIL, G. S. 2010. Endoplasmic reticulum stress and the inflammatory basis of metabolic disease. *Cell,* 140**,** 900-17.

HOTAMISLIGIL, G. S., SHARGILL, N. S. & SPIEGELMAN, B. M. 1993. Adipose expression of tumor necrosis factor-alpha: direct role in obesity-linked insulin resistance. *Science,* 259**,** 87-91.

HOTEZ, P. J., BRINDLEY, P. J., BETHONY, J. M., KING, C. H., PEARCE, E. J. & JACOBSON, J. 2008. Helminth infections: the great neglected tropical diseases. *J Clin Invest,* 118**,** 1311-21.

HOYLER, T., KLOSE, C. S., SOUABNI, A., TURQUETI-NEVES, A., PFEIFER, D., RAWLINS, E. L., VOEHRINGER, D., BUSSLINGER, M. & DIEFENBACH, A. 2012. The transcription factor GATA-3 controls cell fate and maintenance of type 2 innate lymphoid cells. *Immunity,* 37**,** 634-48.

HUANG, H. Y. & LUTHER, S. A. 2012. Expression and function of interleukin-7 in secondary and tertiary lymphoid organs. *Semin Immunol,* 24**,** 175-89.

HUANG, Y., GUO, L., QIU, J., CHEN, X., HU-LI, J., SIEBENLIST, U., WILLIAMSON, P. R., URBAN, J. F., JR. & PAUL, W. E. 2015. IL-25-responsive, lineage-

negative KLRG1(hi) cells are multipotential 'inflammatory' type 2 innate lymphoid cells. *Nat Immunol,* 16**,** 161-9.

HUNTINGTON, N. D., TABARIAS, H., FAIRFAX, K., BRADY, J., HAYAKAWA, Y., DEGLI-ESPOSTI, M. A., SMYTH, M. J., TARLINTON, D. M. & NUTT, S. L. 2007. NK cell maturation and peripheral homeostasis is associated with KLRG1 up-regulation. *Journal of Immunology,* 178**,** 4764-4770.

HUSSAARTS, L., GARCIA-TARDON, N., VAN BEEK, L., HEEMSKERK, M. M., HAEBERLEIN, S., VAN DER ZON, G. C., OZIR-FAZALALIKHAN, A., BERBEE, J. F., WILLEMS VAN DIJK, K., VAN HARMELEN, V., YAZDANBAKHSH, M. & GUIGAS, B. 2015. Chronic helminth infection and helminth-derived egg antigens promote adipose tissue M2 macrophages and improve insulin sensitivity in obese mice. *FASEB J,* 29**,** 3027-39.

HUTLOFF, A., DITTRICH, A. M., BEIER, K. C., ELJASCHEWITSCH, B., KRAFT, R., ANAGNOSTOPOULOS, I. & KROCZEK, R. A. 1999. ICOS is an inducible T-cell co-stimulator structurally and functionally related to CD28. *Nature,* 397**,** 263-6.

IANNUZZI, M. C., RYBICKI, B. A. & TEIRSTEIN, A. S. 2007. Sarcoidosis. *N Engl J Med,* 357**,** 2153-65.

INNGJERDINGEN, M., DAMAJ, B. & MAGHAZACHI, A. A. 2000. Human NK cells express CC chemokine receptors 4 and 8 and respond to thymus and activation-regulated chemokine, macrophage-derived chemokine, and I-309. *J Immunol,* 164**,** 4048-54.

ISLAM, S. A., CHANG, D. S., COLVIN, R. A., BYRNE, M. H., MCCULLY, M. L., MOSER, B., LIRA, S. A., CHARO, I. F. & LUSTER, A. D. 2011. Mouse CCL8, a CCR8 agonist, promotes atopic dermatitis by recruiting IL-5+ T(H)2 cells. *Nat Immunol,* 12**,** 167-77.

JACKSON-JONES, L. H., DUNCAN, S. M., MAGALHAES, M. S., CAMPBELL, S. M., MAIZELS, R. M., MCSORLEY, H. J., ALLEN, J. E. & BENEZECH, C. 2016. Fat-associated lymphoid clusters control local IgM secretion during pleural infection and lung inflammation. *Nat Commun,* 7**,** 12651.

JACKSON, J. A., TURNER, J. D., RENTOUL, L., FAULKNER, H., BEHNKE, J. M., HOYLE, M., GRENCIS, R. K., ELSE, K. J., KAMGNO, J., BOUSSINESQ, M. & BRADLEY, J. E. 2004. T helper cell type 2 responsiveness predicts future susceptibility to gastrointestinal nematodes in humans. *J Infect Dis,* 190**,** 1804-11.

JANEWAY, C. 2005. *Immunobiology : the immune system in health and disease,* New York ; London, Garland Science.

JOVICIC, N., JEFTIC, I., JOVANOVIC, I., RADOSAVLJEVIC, G., ARSENIJEVIC, N., LUKIC, M. L. & PEJNOVIC, N. 2015. Differential Immunometabolic Phenotype in Th1 and Th2 Dominant Mouse Strains in Response to High-Fat Feeding. *PLoS One,* 10**,** e0134089.

JUELKE, K. & ROMAGNANI, C. 2016. Differentiation of human innate lymphoid cells (ILCs). *Curr Opin Immunol,* 38**,** 75-85.

JUKES, J. P., WOOD, K. J. & JONES, N. D. 2012. Bystander activation of iNKT cells occurs during conventional T-cell alloresponses. *Am J Transplant,* 12**,** 590-9.

JUNG, C., HUGOT, J. P. & BARREAU, F. 2010. Peyer's Patches: The Immune Sensors of the Intestine. *Int J Inflam,* 2010**,** 823710.

KAKKAR, R. & LEE, R. T. 2008. The IL-33/ST2 pathway: therapeutic target and novel biomarker. *Nat Rev Drug Discov,* 7**,** 827-40.

KALDJIAN, E. P., GRETZ, J. E., ANDERSON, A. O., SHI, Y. & SHAW, S. 2001. Spatial and molecular organization of lymph node T cell cortex: a labyrinthine cavity bounded by an epithelium-like monolayer of fibroblastic reticular cells anchored to basement membrane-like extracellular matrix. *Int Immunol,* 13**,** 1243-53.

KAMACHI, F., ISSHIKI, T., HARADA, N., AKIBA, H. & MIYAKE, S. 2015. ICOS promotes group 2 innate lymphoid cell activation in lungs. *Biochem Biophys Res Commun,* 463**,** 739-45.

KANG, Y. E., KIM, J. M., JOUNG, K. H., LEE, J. H., YOU, B. R., CHOI, M. J., RYU, M. J., KO, Y. B., LEE, M. A., LEE, J., KU, B. J., SHONG, M., LEE, K. H. & KIM, H. J. 2016. The Roles of Adipokines, Proinflammatory Cytokines, and Adipose Tissue Macrophages in Obesity-Associated Insulin Resistance in Modest Obesity and Early Metabolic Dysfunction. *PLoS One,* 11**,** e0154003.

KARP, N. A., MASON, J., BEAUDET, A. L., BENJAMINI, Y., BOWER, L., BRAUN, R. E., BROWN, S. D. M., CHESLER, E. J., DICKINSON, M. E., FLENNIKEN, A. M., FUCHS, H., ANGELIS, M. H., GAO, X., GUO, S., GREENAWAY, S., HELLER, R., HERAULT, Y., JUSTICE, M. J., KURBATOVA, N., LELLIOTT, C. J., LLOYD, K. C. K., MALLON, A. M., MANK, J. E., MASUYA, H., MCKERLIE, C., MEEHAN, T. F., MOTT, R. F., MURRAY, S. A., PARKINSON, H., RAMIREZ-SOLIS, R., SANTOS, L., SEAVITT, J. R., SMEDLEY, D., SORG, T., SPEAK, A. O., STEEL, K. P., SVENSON, K. L., INTERNATIONAL MOUSE PHENOTYPING, C., WAKANA, S., WEST, D., WELLS, S., WESTERBERG, H., YAACOBY, S. & WHITE, J. K. 2017. Prevalence of sexual dimorphism in mammalian phenotypic traits. *Nat Commun,* 8**,** 15475.

KATAKAI, T., HARA, T., LEE, J. H., GONDA, H., SUGAI, M. & SHIMIZU, A. 2004. A novel reticular stromal structure in lymph node cortex: an immuno-platform for interactions among dendritic cells, T cells and B cells. *Int Immunol,* 16**,** 1133-42.

KATAKAI, T., SUTO, H., SUGAI, M., GONDA, H., TOGAWA, A., SUEMATSU, S., EBISUNO, Y., KATAGIRI, K., KINASHI, T. & SHIMIZU, A. 2008. Organizer-like reticular stromal cell layer common to adult secondary lymphoid organs. *J Immunol,* 181**,** 6189-200.

KIM, D., MEBIUS, R. E., MACMICKING, J. D., JUNG, S., CUPEDO, T., CASTELLANOS, Y., RHO, J., WONG, B. R., JOSIEN, R., KIM, N., RENNERT, P. D. & CHOI, Y. 2000. Regulation of peripheral lymph node genesis by the tumor necrosis factor family member TRANCE. *J Exp Med,* 192**,** 1467-78.

KIM, M. H., TAPAROWSKY, E. J. & KIM, C. H. 2015a. Retinoic Acid Differentially Regulates the Migration of Innate Lymphoid Cell Subsets to the Gut. *Immunity,* 43**,** 107-19.

KIM, M. S., YAN, J., WU, W., ZHANG, G., ZHANG, Y. & CAI, D. 2015b. Rapid linkage of innate immunological signals to adaptive immunity by the brain-fat axis. *Nat Immunol,* 16**,** 525-33.

KINTSCHER, U., HARTGE, M., HESS, K., FORYST-LUDWIG, A., CLEMENZ, M., WABITSCH, M., FISCHER-POSOVSZKY, P., BARTH, T. F., DRAGUN, D., SKURK, T., HAUNER, H., BLUHER, M., UNGER, T., WOLF, A. M., KNIPPSCHILD, U., HOMBACH, V. & MARX, N. 2008. T-lymphocyte infiltration in visceral adipose tissue: a primary event in adipose tissue inflammation and the development of obesity-mediated insulin resistance. *Arterioscler Thromb Vasc Biol,* 28**,** 1304-10.

KIRKLAND, J. L., HOLLENBERG, C. H. & GILLON, W. S. 1990. Age, anatomic site, and the replication and differentiation of adipocyte precursors. *Am J Physiol,* 258**,** C206-10.

KLEIN, S. L. & FLANAGAN, K. L. 2016. Sex differences in immune responses. *Nat Rev Immunol,* 16**,** 626-38.

KLOSE, C. S. & ARTIS, D. 2016. Innate lymphoid cells as regulators of immunity, inflammation and tissue homeostasis. *Nat Immunol,* 17**,** 765-74.

KLOSE, C. S. N., FLACH, M., MOHLE, L., ROGELL, L., HOYLER, T., EBERT, K., FABIUNKE, C., PFEIFER, D., SEXL, V., FONSECA-PEREIRA, D., DOMINGUES, R. G., VEIGA-FERNANDES, H., ARNOLD, S. J., BUSSLINGER, M., DUNAY, I. R., TANRIVER, Y. & DIEFENBACH, A. 2014. Differentiation of type 1 ILCs from a common progenitor to all helper-like innate lymphoid cell lineages. *Cell,* 157**,** 340-356.

KOLODIN, D., VAN PANHUYS, N., LI, C., MAGNUSON, A. M., CIPOLLETTA, D., MILLER, C. M., WAGERS, A., GERMAIN, R. N., BENOIST, C. & MATHIS, D. 2015. Antigen- and cytokine-driven accumulation of regulatory T cells in visceral adipose tissue of lean mice. *Cell Metab,* 21**,** 543-57.

KOSTER, A., STENHOLM, S., ALLEY, D. E., KIM, L. J., SIMONSICK, E. M., KANAYA, A. M., VISSER, M., HOUSTON, D. K., NICKLAS, B. J., TYLAVSKY, F. A., SATTERFIELD, S., GOODPASTER, B. H., FERRUCCI, L., HARRIS, T. B. & HEALTH, A. B. C. S. 2010. Body fat distribution and inflammation among obese older adults with and without metabolic syndrome. *Obesity (Silver Spring),* 18**,** 2354-61.

KOYASU, S. & MORO, K. 2013. Th2-type innate immune responses mediated by natural helper cells. *Ann N Y Acad Sci,* 1283**,** 43-9.

KUMAMOTO, Y., CAMPOREZ, J. P., JURCZAK, M. J., SHANABROUGH, M., HORVATH, T., SHULMAN, G. I. & IWASAKI, A. 2016. CD301b(+) Mononuclear Phagocytes Maintain Positive Energy Balance through Secretion of Resistin-like Molecule Alpha. *Immunity,* 45**,** 583-96.

KUMAR, V., SCANDELLA, E., DANUSER, R., ONDER, L., NITSCHKE, M., FUKUI, Y., HALIN, C., LUDEWIG, B. & STEIN, J. V. 2010. Global lymphoid tissue remodeling during a viral infection is orchestrated by a B cell-lymphotoxin-dependent pathway. *Blood,* 115**,** 4725-33.

KWON, H., LAURENT, S., TANG, Y., ZONG, H., VEMULAPALLI, P. & PESSIN, J. E. 2014. Adipocyte-specific IKKbeta signaling suppresses adipose tissue inflammation through an IL-13-dependent paracrine feedback pathway. *Cell Rep,* 9**,** 1574-83.

LAFFONT, S., BLANQUART, E., SAVIGNAC, M., CENAC, C., LAVERNY, G., METZGER, D., GIRARD, J. P., BELZ, G. T., PELLETIER, L., SEILLET, C. & GUERY, J. C. 2017. Androgen signaling negatively controls group 2 innate lymphoid cells. *J Exp Med,* 214**,** 1581-1592.

LAMPS, L. W. 2015. Hepatic Granulomas: A Review With Emphasis on Infectious Causes. *Arch Pathol Lab Med,* 139**,** 867-75.

LEE, J., HO, W. H., MARUOKA, M., CORPUZ, R. T., BALDWIN, D. T., FOSTER, J. S., GODDARD, A. D., YANSURA, D. G., VANDLEN, R. L., WOOD, W. I. & GURNEY, A. L. 2001. IL-17E, a novel proinflammatory ligand for the IL-17 receptor homolog IL-17Rh1. *J Biol Chem,* 276**,** 1660-4.

LEE, M. J., WU, Y. & FRIED, S. K. 2013. Adipose tissue heterogeneity: implication of depot differences in adipose tissue for obesity complications. *Mol Aspects Med,* 34**,** 1-11.

LEE, M. W., ODEGAARD, J. I., MUKUNDAN, L., QIU, Y., MOLOFSKY, A. B., NUSSBAUM, J. C., YUN, K., LOCKSLEY, R. M. & CHAWLA, A. 2015a. Activated type 2 innate lymphoid cells regulate beige fat biogenesis. *Cell,* 160**,** 74-87.

LEE, Y. J., WANG, H., STARRETT, G. J., PHUONG, V., JAMESON, S. C. & HOGQUIST, K. A. 2015b. Tissue-Specific Distribution of iNKT Cells Impacts Their Cytokine Response. *Immunity,* 43**,** 566-78.

LEFF, T. & GRANNEMAN, J. G. 2010. *Adipose tissue in health and disease,* Weinheim, Wiley-Blackwell.

LI, W., GERMAIN, R. N. & GERNER, M. Y. 2017. Multiplex, quantitative cellular analysis in large tissue volumes with clearing-enhanced 3D microscopy (Ce3D). *Proc Natl Acad Sci U S A,* 114**,** E7321-E7330.

LIDELL, M. E., BETZ, M. J. & ENERBACK, S. 2014. Brown adipose tissue and its therapeutic potential. *J Intern Med,* 276**,** 364-77.

LIM, A. I., MENEGATTI, S., BUSTAMANTE, J., LE BOURHIS, L., ALLEZ, M., ROGGE, L., CASANOVA, J. L., YSSEL, H. & DI SANTO, J. P. 2016. IL-12 drives functional plasticity of human group 2 innate lymphoid cells. *J Exp Med,* 213**,** 569-83.

LIM, A. I., VERRIER, T., VOSSHENRICH, C. A. & DI SANTO, J. P. 2017. Developmental options and functional plasticity of innate lymphoid cells. *Curr Opin Immunol,* 44**,** 61-68.

LIM, S., HONEK, J., XUE, Y., SEKI, T., CAO, Z., ANDERSSON, P., YANG, X., HOSAKA, K. & CAO, Y. 2012. Cold-induced activation of brown adipose tissue and adipose angiogenesis in mice. *Nat Protoc,* 7**,** 606-15.

LINK, A., VOGT, T. K., FAVRE, S., BRITSCHGI, M. R., ACHA-ORBEA, H., HINZ, B., CYSTER, J. G. & LUTHER, S. A. 2007. Fibroblastic reticular cells in lymph nodes regulate the homeostasis of naive T cells. *Nat Immunol,* 8**,** 1255-65.

LOCKSLEY, R. M., KILLEEN, N. & LENARDO, M. J. 2001. The TNF and TNF receptor superfamilies: integrating mammalian biology. *Cell,* 104**,** 487-501.

LOHNING, M., STROEHMANN, A., COYLE, A. J., GROGAN, J. L., LIN, S., GUTIERREZ-RAMOS, J. C., LEVINSON, D., RADBRUCH, A. & KAMRADT, T. 1998. T1/ST2 is preferentially expressed on murine Th2 cells, independent of interleukin 4, interleukin 5, and interleukin 10, and important for Th2 effector function. *Proc Natl Acad Sci U S A,* 95**,** 6930-5.

LUCI, C., REYNDERS, A., IVANOV, II, COGNET, C., CHICHE, L., CHASSON, L., HARDWIGSEN, J., ANGUIANO, E., BANCHEREAU, J., CHAUSSABEL, D., DALOD, M., LITTMAN, D. R., VIVIER, E. & TOMASELLO, E. 2009. Influence of the transcription factor ROR gamma t on the development of NKp46+ cell populations in gut and skin. *Nat Immunol,* 10**,** 75-82.

LUMENG, C. N., BODZIN, J. L. & SALTIEL, A. R. 2007. Obesity induces a phenotypic switch in adipose tissue macrophage polarization. *J Clin Invest,* 117**,** 175-84.

LUND, S. J., PORTILLO, A., CAVAGNERO, K., BAUM, R. E., NAJI, L. H., BADRANI, J. H., MEHTA, A., CROFT, M., BROIDE, D. H. & DOHERTY, T. A. 2017. Leukotriene C4 Potentiates IL-33-Induced Group 2 Innate Lymphoid Cell Activation and Lung Inflammation. *J Immunol,* 199**,** 1096-1104.

LYNCH, L. 2014. Adipose invariant natural killer T cells. *Immunology,* 142**,** 337-46.

LYNCH, L., HOGAN, A. E., DUQUETTE, D., LESTER, C., BANKS, A., LECLAIR, K., COHEN, D. E., GHOSH, A., LU, B., CORRIGAN, M., STEVANOVIC, D., MARATOS-FLIER, E., DRUCKER, D. J., O'SHEA, D. & BRENNER, M. 2016. iNKT Cells Induce FGF21 for Thermogenesis and Are Required for Maximal Weight Loss in GLP1 Therapy. *Cell Metab,* 24**,** 510-9.

LYNCH, L., MICHELET, X., ZHANG, S., BRENNAN, P. J., MOSEMAN, A., LESTER, C., BESRA, G., VOMHOF-DEKREY, E. E., TIGHE, M., KOAY, H. F., GODFREY, D. I., LEADBETTER, E. A., SANT'ANGELO, D. B., VON ANDRIAN, U. & BRENNER, M. B. 2015. Regulatory iNKT cells lack expression of the transcription factor PLZF and control the homeostasis of T(reg) cells and macrophages in adipose tissue. *Nat Immunol,* 16**,** 85-95.

LYNCH, L., NOWAK, M., VARGHESE, B., CLARK, J., HOGAN, A. E., TOXAVIDIS, V., BALK, S. P., O'SHEA, D., O'FARRELLY, C. & EXLEY, M. A. 2012. Adipose tissue invariant NKT cells protect against diet-induced obesity and metabolic disorder through regulatory cytokine production. *Immunity,* 37**,** 574-87.

LYNCH, L., O'SHEA, D., WINTER, D. C., GEOGHEGAN, J., DOHERTY, D. G. & O'FARRELLY, C. 2009. Invariant NKT cells and CD1d(+) cells amass in human omentum and are depleted in patients with cancer and obesity. *Eur J Immunol,* 39**,** 1893-901.

MAAZI, H., BANIE, H., ALEMAN MUENCH, G. R., PATEL, N., WANG, B., SANKARANARAYANAN, I., BHARGAVA, V., SATO, T., LEWIS, G., CESARONI, M., KARRAS, J., DAS, A., SOROOSH, P. & AKBARI, O. 2017. Activated plasmacytoid dendritic cells regulate type 2 innate lymphoid cell-mediated airway hyperreactivity. *J Allergy Clin Immunol*.

MAAZI, H., PATEL, N., SANKARANARAYANAN, I., SUZUKI, Y., RIGAS, D., SOROOSH, P., FREEMAN, G. J., SHARPE, A. H. & AKBARI, O. 2015. ICOS:ICOS-ligand interaction is required for type 2 innate lymphoid cell function, homeostasis, and induction of airway hyperreactivity. *Immunity,* 42**,** 538-51.

MACKLEY, E. C., HOUSTON, S., MARRIOTT, C. L., HALFORD, E. E., LUCAS, B., CEROVIC, V., FILBEY, K. J., MAIZELS, R. M., HEPWORTH, M. R., SONNENBERG, G. F., MILLING, S. & WITHERS, D. R. 2015. CCR7-dependent trafficking of RORgamma(+) ILCs creates a unique microenvironment within mucosal draining lymph nodes. *Nat Commun,* 6**,** 5862.

MACOTELA, Y., BOUCHER, J., TRAN, T. T. & KAHN, C. R. 2009. Sex and depot differences in adipocyte insulin sensitivity and glucose metabolism. *Diabetes,* 58**,** 803-12.

MAIZELS, R. M., HEWITSON, J. P., MURRAY, J., HARCUS, Y. M., DAYER, B., FILBEY, K. J., GRAINGER, J. R., MCSORLEY, H. J., REYNOLDS, L. A. & SMITH, K. A. 2012. Immune modulation and modulators in Heligmosomoides polygyrus infection. *Exp Parasitol,* 132**,** 76-89.

MALHOTRA, D., FLETCHER, A. L. & TURLEY, S. J. 2013. Stromal and hematopoietic cells in secondary lymphoid organs: partners in immunity. *Immunol Rev,* 251**,** 160-76.

MAN, K., KUTYAVIN, V. I. & CHAWLA, A. 2017. Tissue Immunometabolism: Development, Physiology, and Pathobiology. *Cell Metab,* 25**,** 11-26.

MARKLE, J. G. & FISH, E. N. 2014. SeXX matters in immunity. *Trends Immunol,* 35**,** 97-104.

MARTIN, C. E., SPASOVA, D. S., FRIMPONG-BOATENG, K., KIM, H. O., LEE, M., KIM, K. S. & SURH, C. D. 2017. Interleukin-7 Availability Is Maintained by a Hematopoietic Cytokine Sink Comprising Innate Lymphoid Cells and T Cells. *Immunity,* 47**,** 171-182 e4.

MARTINEZ-GONZALEZ, I., MATHA, L., STEER, C. A., GHAEDI, M., POON, G. F. & TAKEI, F. 2016. Allergen-Experienced Group 2 Innate Lymphoid Cells Acquire Memory-like Properties and Enhance Allergic Lung Inflammation. *Immunity,* 45**,** 198-208.

MARTINEZ-GONZALEZ, I., MATHA, L., STEER, C. A. & TAKEI, F. 2017. Immunological Memory of Group 2 Innate Lymphoid Cells. *Trends Immunol,* 38**,** 423-431.

MASHIKO, S., MEHTA, H., BISSONNETTE, R. & SARFATI, M. 2017. Increased frequencies of basophils, type 2 innate lymphoid cells and Th2 cells in skin of patients with atopic dermatitis but not psoriasis. *J Dermatol Sci*.

MATSUDA, J. L., MALLEVAEY, T., SCOTT-BROWNE, J. & GAPIN, L. 2008. CD1d-restricted iNKT cells, the 'Swiss-Army knife' of the immune system. *Curr Opin Immunol,* 20**,** 358-68.

MCLAUGHLIN, T., LIU, L. F., LAMENDOLA, C., SHEN, L., MORTON, J., RIVAS, H., WINER, D., TOLENTINO, L., CHOI, O., ZHANG, H., HUI YEN CHNG, M. & ENGLEMAN, E. 2014. T-cell profile in adipose tissue is associated with insulin resistance and systemic inflammation in humans. *Arterioscler Thromb Vasc Biol,* 34**,** 2637-43.

MEBIUS, R. E. 2003. Organogenesis of lymphoid tissues. *Nat Rev Immunol,* 3**,** 292-303.

MEBIUS, R. E. & KRAAL, G. 2005. Structure and function of the spleen. *Nat Rev Immunol,* 5**,** 606-16.

MEZA-PEREZ, S. & RANDALL, T. D. 2017. Immunological Functions of the Omentum. *Trends Immunol,* 38**,** 526-536.

MILLER, A. M., ASQUITH, D. L., HUEBER, A. J., ANDERSON, L. A., HOLMES, W. M., MCKENZIE, A. N., XU, D., SATTAR, N., MCINNES, I. B. & LIEW, F. Y. 2010. Interleukin-33 induces protective effects in adipose tissue inflammation during obesity in mice. *Circ Res,* 107**,** 650-8.

MILLER, M. D., HATA, S., DE WAAL MALEFYT, R. & KRANGEL, M. S. 1989. A novel polypeptide secreted by activated human T lymphocytes. *J Immunol,* 143**,** 2907-16.

MILNER, J. J. & BECK, M. A. 2012. The impact of obesity on the immune response to infection. *Proc Nutr Soc,* 71**,** 298-306.

MIONNET, C., SANOS, S. L., MONDOR, I., JORQUERA, A., LAUGIER, J. P., GERMAIN, R. N. & BAJENOFF, M. 2011. High endothelial venules as traffic control points maintaining lymphocyte population homeostasis in lymph nodes. *Blood,* 118**,** 6115-22.

MJOSBERG, J. M., TRIFARI, S., CRELLIN, N. K., PETERS, C. P., VAN DRUNEN, C. M., PIET, B., FOKKENS, W. J., CUPEDO, T. & SPITS, H. 2011. Human IL-25- and IL-33-responsive type 2 innate lymphoid cells are defined by expression of CRTH2 and CD161. *Nat Immunol,* 12**,** 1055-62.

MOLOFSKY, A. B., NUSSBAUM, J. C., LIANG, H. E., VAN DYKEN, S. J., CHENG, L. E., MOHAPATRA, A., CHAWLA, A. & LOCKSLEY, R. M. 2013. Innate lymphoid type 2 cells sustain visceral adipose tissue eosinophils and alternatively activated macrophages. *J Exp Med,* 210**,** 535-49.

MOLOFSKY, A. B., SAVAGE, A. K. & LOCKSLEY, R. M. 2015a. Interleukin-33 in Tissue Homeostasis, Injury, and Inflammation. *Immunity,* 42**,** 1005-19.

MOLOFSKY, A. B., VAN GOOL, F., LIANG, H. E., VAN DYKEN, S. J., NUSSBAUM, J. C., LEE, J., BLUESTONE, J. A. & LOCKSLEY, R. M. 2015b. Interleukin-33 and Interferon-gamma Counter-Regulate Group 2 Innate Lymphoid Cell Activation during Immune Perturbation. *Immunity,* 43**,** 161-74.

MONROY, F. G. & ENRIQUEZ, F. J. 1992. Heligmosomoides polygyrus: a model for chronic gastrointestinal helminthiasis. *Parasitol Today,* 8**,** 49-54.

MONTICELLI, L. A., SONNENBERG, G. F., ABT, M. C., ALENGHAT, T., ZIEGLER, C. G., DOERING, T. A., ANGELOSANTO, J. M., LAIDLAW, B. J., YANG, C. Y., SATHALIYAWALA, T., KUBOTA, M., TURNER, D., DIAMOND, J. M., GOLDRATH, A. W., FARBER, D. L., COLLMAN, R. G., WHERRY, E. J. & ARTIS, D. 2011. Innate lymphoid cells promote lung-tissue homeostasis after infection with influenza virus. *Nat Immunol,* 12**,** 1045-54.

MORA, J. R., BONO, M. R., MANJUNATH, N., WENINGER, W., CAVANAGH, L. L., ROSEMBLATT, M. & VON ANDRIAN, U. H. 2003. Selective imprinting of gut-homing T cells by Peyer's patch dendritic cells. *Nature,* 424**,** 88-93.

MORIMOTO, M., SAITO, C., MUTO, C., AKAMATSU, Y., CHIBA, T., ABE, T., AZUMA, N. & SUTO, Y. 2015. Impairment of host resistance to helminthes with age in murine small intestine. *Parasite Immunol,* 37**,** 171-9.

MORO, K., EALEY, K. N., KABATA, H. & KOYASU, S. 2015. Isolation and analysis of group 2 innate lymphoid cells in mice. *Nat Protoc,* 10**,** 792-806.

MORO, K., KABATA, H., TANABE, M., KOGA, S., TAKENO, N., MOCHIZUKI, M., FUKUNAGA, K., ASANO, K., BETSUYAKU, T. & KOYASU, S. 2016. Interferon and IL-27 antagonize the function of group 2 innate lymphoid cells and type 2 innate immune responses. *Nat Immunol,* 17**,** 76-86.

MORO, K., YAMADA, T., TANABE, M., TAKEUCHI, T., IKAWA, T., KAWAMOTO, H., FURUSAWA, J., OHTANI, M., FUJII, H. & KOYASU, S. 2010. Innate production of T(H)2 cytokines by adipose tissue-associated c-Kit(+)Sca-1(+) lymphoid cells. *Nature,* 463**,** 540-4.

MOYRON-QUIROZ, J. E., RANGEL-MORENO, J., KUSSER, K., HARTSON, L., SPRAGUE, F., GOODRICH, S., WOODLAND, D. L., LUND, F. E. & RANDALL, T. D. 2004. Role of inducible bronchus associated lymphoid tissue (iBALT) in respiratory immunity. *Nat Med,* 10**,** 927-34.

NAIR, M. G. & HERBERT, D. R. 2016. Immune polarization by hookworms: taking cues from T helper type 2, type 2 innate lymphoid cells and alternatively activated macrophages. *Immunology,* 148**,** 115-24.

NEILL, D. R. & MCKENZIE, A. N. 2011. Nuocytes and beyond: new insights into helminth expulsion. *Trends Parasitol,* 27**,** 214-21.

NEILL, D. R., WONG, S. H., BELLOSI, A., FLYNN, R. J., DALY, M., LANGFORD, T. K., BUCKS, C., KANE, C. M., FALLON, P. G., PANNELL, R., JOLIN, H. E. & MCKENZIE, A. N. 2010. Nuocytes represent a new innate effector leukocyte that mediates type-2 immunity. *Nature,* 464**,** 1367-70.

NGO, V. N., TANG, H. L. & CYSTER, J. G. 1998. Epstein-Barr virus-induced molecule 1 ligand chemokine is expressed by dendritic cells in lymphoid

tissues and strongly attracts naive T cells and activated B cells. *J Exp Med,* 188**,** 181-91.

NISHIMURA, S., MANABE, I., NAGASAKI, M., ETO, K., YAMASHITA, H., OHSUGI, M., OTSU, M., HARA, K., UEKI, K., SUGIURA, S., YOSHIMURA, K., KADOWAKI, T. & NAGAI, R. 2009. CD8+ effector T cells contribute to macrophage recruitment and adipose tissue inflammation in obesity. *Nat Med,* 15**,** 914-20.

NISHIMURA, S., MANABE, I., TAKAKI, S., NAGASAKI, M., OTSU, M., YAMASHITA, H., SUGITA, J., YOSHIMURA, K., ETO, K., KOMURO, I., KADOWAKI, T. & NAGAI, R. 2013. Adipose Natural Regulatory B Cells Negatively Control Adipose Tissue Inflammation. *Cell Metab*.

O'NEILL, L. A. & PEARCE, E. J. 2016. Immunometabolism governs dendritic cell and macrophage function. *J Exp Med,* 213**,** 15-23.

O'SULLIVAN, T. E., RAPP, M., FAN, X., WEIZMAN, O. E., BHARDWAJ, P., ADAMS, N. M., WALZER, T., DANNENBERG, A. J. & SUN, J. C. 2016. Adipose-Resident Group 1 Innate Lymphoid Cells Promote Obesity-Associated Insulin Resistance. *Immunity,* 45**,** 428-41.

ODEGAARD, J. I., RICARDO-GONZALEZ, R. R., RED EAGLE, A., VATS, D., MOREL, C. R., GOFORTH, M. H., SUBRAMANIAN, V., MUKUNDAN, L., FERRANTE, A. W. & CHAWLA, A. 2008. Alternative M2 activation of Kupffer cells by PPARdelta ameliorates obesity-induced insulin resistance. *Cell Metab,* 7**,** 496-507.

OHNE, Y., SILVER, J. S., THOMPSON-SNIPES, L., COLLET, M. A., BLANCK, J. P., CANTAREL, B. L., COPENHAVER, A. M., HUMBLES, A. A. & LIU, Y. J. 2016. IL-1 is a critical regulator of group 2 innate lymphoid cell function and plasticity. *Nat Immunol,* 17**,** 646-55.

OKWAN-DUODU, D., UMPIERREZ, G. E., BRAWLEY, O. W. & DIAZ, R. 2013. Obesity-driven inflammation and cancer risk: role of myeloid derived suppressor cells and alternately activated macrophages. *Am J Cancer Res,* 3**,** 21-33.

OLIPHANT, C. J., HWANG, Y. Y., WALKER, J. A., SALIMI, M., WONG, S. H., BREWER, J. M., ENGLEZAKIS, A., BARLOW, J. L., HAMS, E., SCANLON, S. T., OGG, G. S., FALLON, P. G. & MCKENZIE, A. N. 2014. MHCII-mediated dialog between group 2 innate lymphoid cells and CD4(+) T cells potentiates type 2 immunity and promotes parasitic helminth expulsion. *Immunity,* 41**,** 283-95.

ONDER, L., DANUSER, R., SCANDELLA, E., FIRNER, S., CHAI, Q., HEHLGANS, T., STEIN, J. V. & LUDEWIG, B. 2013. Endothelial cell-specific lymphotoxin-beta receptor signaling is critical for lymph node and high endothelial venule formation. *J Exp Med,* 210**,** 465-73.

ONDER, L., MORBE, U., PIKOR, N., NOVKOVIC, M., CHENG, H. W., HEHLGANS, T., PFEFFER, K., BECHER, B., WAISMAN, A., RULICKE, T., GOMMERMAN, J., MUELLER, C. G., SAWA, S., SCANDELLA, E. & LUDEWIG, B. 2017.

Lymphatic Endothelial Cells Control Initiation of Lymph Node Organogenesis. *Immunity,* 47**,** 80-92 e4.

OUCHI, N., PARKER, J. L., LUGUS, J. J. & WALSH, K. 2011. Adipokines in inflammation and metabolic disease. *Nat Rev Immunol,* 11**,** 85-97.

PACLIK, D., STEHLE, C., LAHMANN, A., HUTLOFF, A. & ROMAGNANI, C. 2015. ICOS regulates the pool of group 2 innate lymphoid cells under homeostatic and inflammatory conditions in mice. *Eur J Immunol,* 45**,** 2766-72.

PAL, D., DASGUPTA, S., KUNDU, R., MAITRA, S., DAS, G., MUKHOPADHYAY, S., RAY, S., MAJUMDAR, S. S. & BHATTACHARYA, S. 2012. Fetuin-A acts as an endogenous ligand of TLR4 to promote lipid-induced insulin resistance. *Nat Med,* 18**,** 1279-85.

PAPADAKIS, K. A., LANDERS, C., PREHN, J., KOUROUMALIS, E. A., MORENO, S. T., GUTIERREZ-RAMOS, J. C., HODGE, M. R. & TARGAN, S. R. 2003. CC chemokine receptor 9 expression defines a subset of peripheral blood lymphocytes with mucosal T cell phenotype and Th1 or T-regulatory 1 cytokine profile. *J Immunol,* 171**,** 159-65.

PEARCE, E. L. & PEARCE, E. J. 2013. Metabolic pathways in immune cell activation and quiescence. *Immunity,* 38**,** 633-43.

PELLY, V. S., KANNAN, Y., COOMES, S. M., ENTWISTLE, L. J., RUCKERL, D., SEDDON, B., MACDONALD, A. S., MCKENZIE, A. & WILSON, M. S. 2016. IL-4-producing ILC2s are required for the differentiation of TH2 cells following Heligmosomoides polygyrus infection. *Mucosal Immunol,* 9**,** 1407-1417.

PESCHON, J. J., TORRANCE, D. S., STOCKING, K. L., GLACCUM, M. B., OTTEN, C., WILLIS, C. R., CHARRIER, K., MORRISSEY, P. J., WARE, C. B. & MOHLER, K. M. 1998. TNF receptor-deficient mice reveal divergent roles for p55 and p75 in several models of inflammation. *J Immunol,* 160**,** 943-52.

PETROVIC, N., WALDEN, T. B., SHABALINA, I. G., TIMMONS, J. A., CANNON, B. & NEDERGAARD, J. 2010. Chronic peroxisome proliferator-activated receptor gamma (PPARgamma) activation of epididymally derived white adipocyte cultures reveals a population of thermogenically competent, UCP1-containing adipocytes molecularly distinct from classic brown adipocytes. *J Biol Chem,* 285**,** 7153-64.

PISHDADIAN, A., VARASTEH, A. R. & SANKIAN, M. 2012. Type 2 innate lymphoid cells: friends or foes-role in airway allergic inflammation and asthma. *J Allergy (Cairo),* 2012**,** 130937.

POND, C. M. 2002. Adipose tissue, the immune system and exercise fatigue: how activated lymphocytes compete for lipids. *Biochem Soc Trans,* 30**,** 270-5.

POSSOT, C., SCHMUTZ, S., CHEA, S., BOUCONTET, L., LOUISE, A., CUMANO, A. & GOLUB, R. 2011. Notch signaling is necessary for adult, but not fetal, development of RORgammat(+) innate lymphoid cells. *Nat Immunol,* 12**,** 949-58.

PRADHAN, A. D., MANSON, J. E., RIFAI, N., BURING, J. E. & RIDKER, P. M. 2001. C-reactive protein, interleukin 6, and risk of developing type 2 diabetes mellitus. *JAMA,* 286**,** 327-34.

PRICE, A. E., LIANG, H. E., SULLIVAN, B. M., REINHARDT, R. L., EISLEY, C. J., ERLE, D. J. & LOCKSLEY, R. M. 2010. Systemically dispersed innate IL-13-expressing cells in type 2 immunity. *Proc Natl Acad Sci U S A,* 107**,** 11489-94.

PRUNET-MARCASSUS, B., COUSIN, B., CATON, D., ANDRE, M., PENICAUD, L. & CASTEILLA, L. 2006. From heterogeneity to plasticity in adipose tissues: site-specific differences. *Exp Cell Res,* 312**,** 727-36.

QIU, Y., NGUYEN, K. D., ODEGAARD, J. I., CUI, X., TIAN, X., LOCKSLEY, R. M., PALMITER, R. D. & CHAWLA, A. 2014. Eosinophils and type 2 cytokine signaling in macrophages orchestrate development of functional beige fat. *Cell,* 157**,** 1292-308.

QURESHI, O. S., ZHENG, Y., NAKAMURA, K., ATTRIDGE, K., MANZOTTI, C., SCHMIDT, E. M., BAKER, J., JEFFERY, L. E., KAUR, S., BRIGGS, Z., HOU, T. Z., FUTTER, C. E., ANDERSON, G., WALKER, L. S. & SANSOM, D. M. 2011. Trans-endocytosis of CD80 and CD86: a molecular basis for the cell-extrinsic function of CTLA-4. *Science,* 332**,** 600-3.

RAMANAN, D., BOWCUTT, R., LEE, S. C., TANG, M. S., KURTZ, Z. D., DING, Y., HONDA, K., GAUSE, W. C., BLASER, M. J., BONNEAU, R. A., LIM, Y. A., LOKE, P. & CADWELL, K. 2016. Helminth infection promotes colonization resistance via type 2 immunity. *Science,* 352**,** 608-12.

RANDOLPH, G. J. 2016. CCR7: Unifying Disparate Journeys to the Lymph Node. *J Immunol,* 196**,** 3-4.

RANDOLPH, G. J., ANGELI, V. & SWARTZ, M. A. 2005. Dendritic-cell trafficking to lymph nodes through lymphatic vessels. *Nat Rev Immunol,* 5**,** 617-28.

RANGEL-MORENO, J., MOYRON-QUIROZ, J. E., CARRAGHER, D. M., KUSSER, K., HARTSON, L., MOQUIN, A. & RANDALL, T. D. 2009. Omental milky spots develop in the absence of lymphoid tissue-inducer cells and support B and T cell responses to peritoneal antigens. *Immunity,* 30**,** 731-43.

RAO, R. R., LONG, J. Z., WHITE, J. P., SVENSSON, K. J., LOU, J., LOKURKAR, I., JEDRYCHOWSKI, M. P., RUAS, J. L., WRANN, C. D., LO, J. C., CAMERA, D. M., LACHEY, J., GYGI, S., SEEHRA, J., HAWLEY, J. A. & SPIEGELMAN, B. M. 2014. Meteorin-like is a hormone that regulates immune-adipose interactions to increase beige fat thermogenesis. *Cell,* 157**,** 1279-91.

RAUBER, S., LUBER, M., WEBER, S., MAUL, L., SOARE, A., WOHLFAHRT, T., LIN, N. Y., DIETEL, K., BOZEC, A., HERRMANN, M., KAPLAN, M. H., WEIGMANN, B., ZAISS, M. M., FEARON, U., VEALE, D. J., CANETE, J. D., DISTLER, O., RIVELLESE, F., PITZALIS, C., NEURATH, M. F., MCKENZIE, A. N. J., WIRTZ, S., SCHETT, G., DISTLER, J. H. W. & RAMMING, A. 2017. Resolution of inflammation by interleukin-9-producing type 2 innate lymphoid cells. *Nat Med,* 23**,** 938-944.

RAUSCH, S., HUEHN, J., KIRCHHOFF, D., RZEPECKA, J., SCHNOELLER, C., PILLAI, S., LODDENKEMPER, C., SCHEFFOLD, A., HAMANN, A., LUCIUS, R. & HARTMANN, S. 2008. Functional analysis of effector and regulatory T cells in a parasitic nematode infection. *Infect Immun,* 76**,** 1908-19.

RAZZOLI, M., FRONTINI, A., GURNEY, A., MONDINI, E., CUBUK, C., KATZ, L. S., CERO, C., BOLAN, P. J., DOPAZO, J., VIDAL-PUIG, A., CINTI, S. & BARTOLOMUCCI, A. 2016. Stress-induced activation of brown adipose tissue prevents obesity in conditions of low adaptive thermogenesis. *Mol Metab,* 5**,** 19-33.

REDDY, S. T. 2017. Immunology: The patterns of T-cell target recognition. *Nature,* 547**,** 36-38.

REYNOLDS, L. A., FILBEY, K. J. & MAIZELS, R. M. 2012. Immunity to the model intestinal helminth parasite Heligmosomoides polygyrus. *Semin Immunopathol,* 34**,** 829-46.

RIGAS, D., LEWIS, G., ARON, J. L., WANG, B., BANIE, H., SANKARANARAYANAN, I., GALLE-TREGER, L., MAAZI, H., LO, R., FREEMAN, G. J., SHARPE, A. H., SOROOSH, P. & AKBARI, O. 2017. Type 2 innate lymphoid cell suppression by regulatory T cells attenuates airway hyperreactivity and requires inducible T-cell costimulator-inducible T-cell costimulator ligand interaction. *J Allergy Clin Immunol,* 139**,** 1468-1477 e2.

ROBBINS, S. H., NGUYEN, K. B., TAKAHASHI, N., MIKAYAMA, T., BIRON, C. A. & BROSSAY, L. 2002. Cutting edge: inhibitory functions of the killer cell lectin-like receptor G1 molecule during the activation of mouse NK cells. *J Immunol,* 168**,** 2585-9.

ROBINETTE, M. L., FUCHS, A., CORTEZ, V. S., LEE, J. S., WANG, Y., DURUM, S. K., GILFILLAN, S., COLONNA, M. & IMMUNOLOGICAL GENOME, C. 2015. Transcriptional programs define molecular characteristics of innate lymphoid cell classes and subsets. *Nat Immunol,* 16**,** 306-17.

ROEDIGER, B., KYLE, R., TAY, S. S., MITCHELL, A. J., BOLTON, H. A., GUY, T. V., TAN, S. Y., FORBES-BLOM, E., TONG, P. L., KOLLER, Y., SHKLOVSKAYA, E., IWASHIMA, M., MCCOY, K. D., LE GROS, G., FAZEKAS DE ST GROTH, B. & WENINGER, W. 2015. IL-2 is a critical regulator of group 2 innate lymphoid cell function during pulmonary inflammation. *J Allergy Clin Immunol,* 136**,** 1653-63 e1-7.

ROEDIGER, B., KYLE, R., YIP, K. H., SUMARIA, N., GUY, T. V., KIM, B. S., MITCHELL, A. J., TAY, S. S., JAIN, R., FORBES-BLOM, E., CHEN, X., TONG, P. L., BOLTON, H. A., ARTIS, D., PAUL, W. E., FAZEKAS DE ST GROTH, B., GRIMBALDESTON, M. A., LE GROS, G. & WENINGER, W. 2013. Cutaneous immunosurveillance and regulation of inflammation by group 2 innate lymphoid cells. *Nat Immunol,* 14**,** 564-73.

ROOZENDAAL, R., MEMPEL, T. R., PITCHER, L. A., GONZALEZ, S. F., VERSCHOOR, A., MEBIUS, R. E., VON ANDRIAN, U. H. & CARROLL, M. C. 2009. Conduits mediate transport of low-molecular-weight antigen to lymph node follicles. *Immunity,* 30**,** 264-76.

RUBTSOV, Y. P., RASMUSSEN, J. P., CHI, E. Y., FONTENOT, J., CASTELLI, L., YE, X., TREUTING, P., SIEWE, L., ROERS, A., HENDERSON, W. R., JR., MULLER, W. & RUDENSKY, A. Y. 2008. Regulatory T cell-derived interleukin-10 limits inflammation at environmental interfaces. *Immunity,* 28**,** 546-58.

SAITO, M., OKAMATSU-OGURA, Y., MATSUSHITA, M., WATANABE, K., YONESHIRO, T., NIO-KOBAYASHI, J., IWANAGA, T., MIYAGAWA, M., KAMEYA, T., NAKADA, K., KAWAI, Y. & TSUJISAKI, M. 2009. High incidence of metabolically active brown adipose tissue in healthy adult humans: effects of cold exposure and adiposity. *Diabetes,* 58**,** 1526-31.

SALIMI, M., BARLOW, J. L., SAUNDERS, S. P., XUE, L., GUTOWSKA-OWSIAK, D., WANG, X., HUANG, L. C., JOHNSON, D., SCANLON, S. T., MCKENZIE, A. N., FALLON, P. G. & OGG, G. S. 2013. A role for IL-25 and IL-33-driven type-2 innate lymphoid cells in atopic dermatitis. *J Exp Med,* 210**,** 2939-50.

SANDEL, P. C. & MONROE, J. G. 1999. Negative selection of immature B cells by receptor editing or deletion is determined by site of antigen encounter. *Immunity,* 10**,** 289-99.

SATOH-TAKAYAMA, N., LESJEAN-POTTIER, S., VIEIRA, P., SAWA, S., EBERL, G., VOSSHENRICH, C. A. & DI SANTO, J. P. 2010. IL-7 and IL-15 independently program the differentiation of intestinal CD3-NKp46+ cell subsets from Id2-dependent precursors. *J Exp Med,* 207**,** 273-80.

SATOH-TAKAYAMA, N., SERAFINI, N., VERRIER, T., REKIKI, A., RENAULD, J. C., FRANKEL, G. & DI SANTO, J. P. 2014. The chemokine receptor CXCR6 controls the functional topography of interleukin-22 producing intestinal innate lymphoid cells. *Immunity,* 41**,** 776-88.

SATOH, M., ANDOH, Y., CLINGAN, C. S., OGURA, H., FUJII, S., ESHIMA, K., NAKAYAMA, T., TANIGUCHI, M., HIRATA, N., ISHIMORI, N., TSUTSUI, H., ONOE, K. & IWABUCHI, K. 2012. Type II NKT cells stimulate diet-induced obesity by mediating adipose tissue inflammation, steatohepatitis and insulin resistance. *PLoS One,* 7**,** e30568.

SAUNDERS, S. P., MORAN, T., FLOUDAS, A., WURLOD, F., KASZLIKOWSKA, A., SALIMI, M., QUINN, E. M., OLIPHANT, C. J., NUNEZ, G., MCMANUS, R., HAMS, E., IRVINE, A. D., MCKENZIE, A. N., OGG, G. S. & FALLON, P. G. 2016. Spontaneous atopic dermatitis is mediated by innate immunity, with the secondary lung inflammation of the atopic march requiring adaptive immunity. *J Allergy Clin Immunol,* 137**,** 482-91.

SCANDELLA, E., BOLINGER, B., LATTMANN, E., MILLER, S., FAVRE, S., LITTMAN, D. R., FINKE, D., LUTHER, S. A., JUNT, T. & LUDEWIG, B. 2008. Restoration of lymphoid organ integrity through the interaction of lymphoid tissue-inducer cells with stroma of the T cell zone. *Nat Immunol,* 9**,** 667-75.

SCHAERLI, P., EBERT, L., WILLIMANN, K., BLASER, A., ROOS, R. S., LOETSCHER, P. & MOSER, B. 2004. A skin-selective homing mechanism for human immune surveillance T cells. *J Exp Med,* 199**,** 1265-75.

SCHIPPER, H. S., RAKHSHANDEHROO, M., VAN DE GRAAF, S. F., VENKEN, K., KOPPEN, A., STIENSTRA, R., PROP, S., MEERDING, J., HAMERS, N.,

BESRA, G., BOON, L., NIEUWENHUIS, E. E., ELEWAUT, D., PRAKKEN, B., KERSTEN, S., BOES, M. & KALKHOVEN, E. 2012. Natural killer T cells in adipose tissue prevent insulin resistance. *J Clin Invest,* 122**,** 3343-54.

SCHMITZ, J., OWYANG, A., OLDHAM, E., SONG, Y., MURPHY, E., MCCLANAHAN, T. K., ZURAWSKI, G., MOSHREFI, M., QIN, J., LI, X., GORMAN, D. M., BAZAN, J. F. & KASTELEIN, R. A. 2005. IL-33, an interleukin-1-like cytokine that signals via the IL-1 receptor-related protein ST2 and induces T helper type 2-associated cytokines. *Immunity,* 23**,** 479-90.

SCHULTE, S., SUKHOVA, G. K. & LIBBY, P. 2008. Genetically programmed biases in Th1 and Th2 immune responses modulate atherogenesis. *Am J Pathol,* 172**,** 1500-8.

SCHUTYSER, E., STRUYF, S. & VAN DAMME, J. 2003. The CC chemokine CCL20 and its receptor CCR6. *Cytokine Growth Factor Rev,* 14**,** 409-26.

SCHWARTZKOPFF, S., GRUNDEMANN, C., SCHWEIER, O., ROSSHART, S., KARJALAINEN, K. E., BECKER, K. F. & PIRCHER, H. 2007. Tumor-associated E-cadherin mutations affect binding to the killer cell lectin-like receptor G1 in humans. *J Immunol,* 179**,** 1022-9.

SEALE, P., BJORK, B., YANG, W., KAJIMURA, S., CHIN, S., KUANG, S., SCIME, A., DEVARAKONDA, S., CONROE, H. M., ERDJUMENT-BROMAGE, H., TEMPST, P., RUDNICKI, M. A., BEIER, D. R. & SPIEGELMAN, B. M. 2008. PRDM16 controls a brown fat/skeletal muscle switch. *Nature,* 454**,** 961-7.

SERAFINI, N., VOSSHENRICH, C. A. & DI SANTO, J. P. 2015. Transcriptional regulation of innate lymphoid cell fate. *Nat Rev Immunol,* 15**,** 415-28.

SEVERINO, P., PALOMINO, D. T., ALVARENGA, H., ALMEIDA, C. B., PASQUALIM, D. C., CURY, A., SALVALAGGIO, P. R., DE VASCONCELOS MACEDO, A. L., ANDRADE, M. C., ALOIA, T., BROMBERG, S., RIZZO, L. V., ROCHA, F. A. & MARTI, L. C. 2017. Human Lymph Node-Derived Fibroblastic and Double-Negative Reticular Cells Alter Their Chemokines and Cytokines Expression Profile Following Inflammatory Stimuli. *Front Immunol,* 8**,** 141.

SHAN, B., WANG, X., WU, Y., XU, C., XIA, Z., DAI, J., SHAO, M., ZHAO, F., HE, S., YANG, L., ZHANG, M., NAN, F., LI, J., LIU, J., LIU, J., JIA, W., QIU, Y., SONG, B., HAN, J. J., RUI, L., DUAN, S. Z. & LIU, Y. 2017. The metabolic ER stress sensor IRE1alpha suppresses alternative activation of macrophages and impairs energy expenditure in obesity. *Nat Immunol,* 18**,** 519-529.

SHARP, L. Z., SHINODA, K., OHNO, H., SCHEEL, D. W., TOMODA, E., RUIZ, L., HU, H., WANG, L., PAVLOVA, Z., GILSANZ, V. & KAJIMURA, S. 2012. Human BAT possesses molecular signatures that resemble beige/brite cells. *PLoS One,* 7**,** e49452.

SHEVACH, E. M. 2009. Mechanisms of foxp3+ T regulatory cell-mediated suppression. *Immunity,* 30**,** 636-45.

SHIMOKAWA, C., KANAYA, T., HACHISUKA, M., ISHIWATA, K., HISAEDA, H., KURASHIMA, Y., KIYONO, H., YOSHIMOTO, T., KAISHO, T. & OHNO, H.

2017. Mast Cells Are Crucial for Induction of Group 2 Innate Lymphoid Cells and Clearance of Helminth Infections. *Immunity,* 46**,** 863-874 e4.

SHIMOTSUMA, M., SHIELDS, J. W., SIMPSON-MORGAN, M. W., SAKUYAMA, A., SHIRASU, M., HAGIWARA, A. & TAKAHASHI, T. 1993. Morpho-physiological function and role of omental milky spots as omentum-associated lymphoid tissue (OALT) in the peritoneal cavity. *Lymphology,* 26**,** 90-101.

SHINODA, K., LUIJTEN, I. H., HASEGAWA, Y., HONG, H., SONNE, S. B., KIM, M., XUE, R., CHONDRONIKOLA, M., CYPESS, A. M., TSENG, Y. H., NEDERGAARD, J., SIDOSSIS, L. S. & KAJIMURA, S. 2015. Genetic and functional characterization of clonally derived adult human brown adipocytes. *Nat Med,* 21**,** 389-94.

SILVER, J. S., KEARLEY, J., COPENHAVER, A. M., SANDEN, C., MORI, M., YU, L., PRITCHARD, G. H., BERLIN, A. A., HUNTER, C. A., BOWLER, R., ERJEFALT, J. S., KOLBECK, R. & HUMBLES, A. A. 2016. Inflammatory triggers associated with exacerbations of COPD orchestrate plasticity of group 2 innate lymphoid cells in the lungs. *Nat Immunol,* 17**,** 626-35.

SMITHGALL, M. D., COMEAU, M. R., YOON, B. R., KAUFMAN, D., ARMITAGE, R. & SMITH, D. E. 2008. IL-33 amplifies both Th1- and Th2-type responses through its activity on human basophils, allergen-reactive Th2 cells, iNKT and NK cells. *Int Immunol,* 20**,** 1019-30.

SOUMELIS, V., RECHE, P. A., KANZLER, H., YUAN, W., EDWARD, G., HOMEY, B., GILLIET, M., HO, S., ANTONENKO, S., LAUERMA, A., SMITH, K., GORMAN, D., ZURAWSKI, S., ABRAMS, J., MENON, S., MCCLANAHAN, T., DE WAAL-MALEFYT RD, R., BAZAN, F., KASTELEIN, R. A. & LIU, Y. J. 2002. Human epithelial cells trigger dendritic cell mediated allergic inflammation by producing TSLP. *Nat Immunol,* 3**,** 673-80.

SPITS, H., ARTIS, D., COLONNA, M., DIEFENBACH, A., DI SANTO, J. P., EBERL, G., KOYASU, S., LOCKSLEY, R. M., MCKENZIE, A. N., MEBIUS, R. E., POWRIE, F. & VIVIER, E. 2013. Innate lymphoid cells--a proposal for uniform nomenclature. *Nat Rev Immunol,* 13**,** 145-9.

SPITS, H. & CUPEDO, T. 2012. Innate lymphoid cells: emerging insights in development, lineage relationships, and function. *Annu Rev Immunol,* 30**,** 647-75.

SPOONER, C. J., LESCH, J., YAN, D., KHAN, A. A., ABBAS, A., RAMIREZ-CARROZZI, V., ZHOU, M., SORIANO, R., EASTHAM-ANDERSON, J., DIEHL, L., LEE, W. P., MODRUSAN, Z., PAPPU, R., XU, M., DEVOSS, J. & SINGH, H. 2013. Specification of type 2 innate lymphocytes by the transcriptional determinant Gfi1. *Nat Immunol,* 14**,** 1229-36.

STRISSEL, K. J., DENIS, G. V. & NIKOLAJCZYK, B. S. 2014. Immune regulators of inflammation in obesity-associated type 2 diabetes and coronary artery disease. *Curr Opin Endocrinol Diabetes Obes,* 21**,** 330-8.

SUAREZ-ZAMORANO, N., FABBIANO, S., CHEVALIER, C., STOJANOVIC, O., COLIN, D. J., STEVANOVIC, A., VEYRAT-DUREBEX, C., TARALLO, V., RIGO, D., GERMAIN, S., ILIEVSKA, M., MONTET, X., SEIMBILLE, Y.,

HAPFELMEIER, S. & TRAJKOVSKI, M. 2015. Microbiota depletion promotes browning of white adipose tissue and reduces obesity. *Nat Med,* 21**,** 1497-1501.

TAKAI, T. 2012. TSLP expression: cellular sources, triggers, and regulatory mechanisms. *Allergol Int,* 61**,** 3-17.

TAKATORI, H., KANNO, Y., WATFORD, W. T., TATO, C. M., WEISS, G., IVANOV, II, LITTMAN, D. R. & O'SHEA, J. J. 2009. Lymphoid tissue inducer-like cells are an innate source of IL-17 and IL-22. *J Exp Med,* 206**,** 35-41.

TAKAYAMA, T., KAMADA, N., CHINEN, H., OKAMOTO, S., KITAZUME, M. T., CHANG, J., MATUZAKI, Y., SUZUKI, S., SUGITA, A., KOGANEI, K., HISAMATSU, T., KANAI, T. & HIBI, T. 2010. Imbalance of NKp44(+)NKp46(-) and NKp44(-)NKp46(+) natural killer cells in the intestinal mucosa of patients with Crohn's disease. *Gastroenterology,* 139**,** 882-92, 892 e1-3.

TCHKONIA, T., GIORGADZE, N., PIRTSKHALAVA, T., THOMOU, T., DEPONTE, M., KOO, A., FORSE, R. A., CHINNAPPAN, D., MARTIN-RUIZ, C., VON ZGLINICKI, T. & KIRKLAND, J. L. 2006. Fat depot-specific characteristics are retained in strains derived from single human preadipocytes. *Diabetes,* 55**,** 2571-8.

TCHKONIA, T., THOMOU, T., ZHU, Y., KARAGIANNIDES, I., POTHOULAKIS, C., JENSEN, M. D. & KIRKLAND, J. L. 2013. Mechanisms and metabolic implications of regional differences among fat depots. *Cell Metab,* 17**,** 644-656.

TERZIROLI BERETTA-PICCOLI, B., MAINETTI, C., PEETERS, M. A. & LAFFITTE, E. 2018. Cutaneous Granulomatosis: a Comprehensive Review. *Clin Rev Allergy Immunol,* 54**,** 131-146.

TESSMER, M. S., FUGERE, C., STEVENAERT, F., NAIDENKO, O. V., CHONG, H. J., LECLERCQ, G. & BROSSAY, L. 2007. KLRG1 binds cadherins and preferentially associates with SHIP-1. *Int Immunol,* 19**,** 391-400.

THAISS, C. A., LEVY, M., ITAV, S. & ELINAV, E. 2016. Integration of Innate Immune Signaling. *Trends Immunol,* 37**,** 84-101.

THOMAS, S. Y., HOU, R., BOYSON, J. E., MEANS, T. K., HESS, C., OLSON, D. P., STROMINGER, J. L., BRENNER, M. B., GUMPERZ, J. E., WILSON, S. B. & LUSTER, A. D. 2003. CD1d-restricted NKT cells express a chemokine receptor profile indicative of Th1-type inflammatory homing cells. *J Immunol,* 171**,** 2571-80.

TOMURA, M. & KABASHIMA, K. 2013. Analysis of cell movement between skin and other anatomical sites in vivo using photoconvertible fluorescent protein "Kaede"-transgenic mice. *Methods Mol Biol,* 961**,** 279-86.

TURNER, J. D., FAULKNER, H., KAMGNO, J., CORMONT, F., VAN SNICK, J., ELSE, K. J., GRENCIS, R. K., BEHNKE, J. M., BOUSSINESQ, M. & BRADLEY, J. E. 2003. Th2 cytokines are associated with reduced worm burdens in a human intestinal helminth infection. *J Infect Dis,* 188**,** 1768-75.

UHM, M. & SALTIEL, A. R. 2015. White, brown, and beige; type 2 immunity gets hot. *Immunity,* 42**,** 15-7.

URBAN, J. F., JR., KATONA, I. M. & FINKELMAN, F. D. 1991. Heligmosomoides polygyrus: CD4+ but not CD8+ T cells regulate the IgE response and protective immunity in mice. *Exp Parasitol,* 73**,** 500-11.

URBAN, J. F., JR., MALISZEWSKI, C. R., MADDEN, K. B., KATONA, I. M. & FINKELMAN, F. D. 1995. IL-4 treatment can cure established gastrointestinal nematode infections in immunocompetent and immunodeficient mice. *J Immunol,* 154**,** 4675-84.

URBAN, J. F., JR., NOBEN-TRAUTH, N., DONALDSON, D. D., MADDEN, K. B., MORRIS, S. C., COLLINS, M. & FINKELMAN, F. D. 1998. IL-13, IL-4Ralpha, and Stat6 are required for the expulsion of the gastrointestinal nematode parasite Nippostrongylus brasiliensis. *Immunity,* 8**,** 255-64.

V. RECKLINGHAUSEN, F. 1863. Ueber Eiter- und Bindegewebskörperchen. *Archiv für pathologische Anatomie und Physiologie und für klinische Medicin,* 28**,** 157-197.

VAN DE PAVERT, S. A. & MEBIUS, R. E. 2010. New insights into the development of lymphoid tissues. *Nat Rev Immunol,* 10**,** 664-74.

VAN DE PAVERT, S. A., OLIVIER, B. J., GOVERSE, G., VONDENHOFF, M. F., GREUTER, M., BEKE, P., KUSSER, K., HOPKEN, U. E., LIPP, M., NIEDERREITHER, K., BLOMHOFF, R., SITNIK, K., AGACE, W. W., RANDALL, T. D., DE JONGE, W. J. & MEBIUS, R. E. 2009. Chemokine CXCL13 is essential for lymph node initiation and is induced by retinoic acid and neuronal stimulation. *Nat Immunol,* 10**,** 1193-9.

VAN DYKEN, S. J., NUSSBAUM, J. C., LEE, J., MOLOFSKY, A. B., LIANG, H. E., POLLACK, J. L., GATE, R. E., HALIBURTON, G. E., YE, C. J., MARSON, A., ERLE, D. J. & LOCKSLEY, R. M. 2016. A tissue checkpoint regulates type 2 immunity. *Nat Immunol,* 17**,** 1381-1387.

VAN ZANDT, P. D., CYPESS, R. H. & ZIDIAN, J. L. 1973. Development of age and sex resistance to Nematospiroides dubius in the mouse following single and multiple infections. *J Parasitol,* 59**,** 977-9.

VASANTHAKUMAR, A., MORO, K., XIN, A., LIAO, Y., GLOURY, R., KAWAMOTO, S., FAGARASAN, S., MIELKE, L. A., AFSHAR-STERLE, S., MASTERS, S. L., NAKAE, S., SAITO, H., WENTWORTH, J. M., LI, P., LIAO, W., LEONARD, W. J., SMYTH, G. K., SHI, W., NUTT, S. L., KOYASU, S. & KALLIES, A. 2015. The transcriptional regulators IRF4, BATF and IL-33 orchestrate development and maintenance of adipose tissue-resident regulatory T cells. *Nat Immunol,* 16**,** 276-85.

VELY, F., BARLOGIS, V., VALLENTIN, B., NEVEN, B., PIPEROGLOU, C., EBBO, M., PERCHET, T., PETIT, M., YESSAAD, N., TOUZOT, F., BRUNEAU, J., MAHLAOUI, N., ZUCCHINI, N., FARNARIER, C., MICHEL, G., MOSHOUS, D., BLANCHE, S., DUJARDIN, A., SPITS, H., DISTLER, J. H., RAMMING, A., PICARD, C., GOLUB, R., FISCHER, A. & VIVIER, E. 2016. Evidence of innate lymphoid cell redundancy in humans. *Nat Immunol,* 17**,** 1291-1299.

VENKEN, K., SEEUWS, S., ZABEAU, L., JACQUES, P., DECRUY, T., COUDENYS, J., VERHEUGEN, E., WINDELS, F., CATTEEUW, D., DRENNAN, M., VAN CALENBERGH, S., LAMBRECHT, B. N., YOSHIMURA, A., TAVERNIER, J. & ELEWAUT, D. 2014. A bidirectional crosstalk between iNKT cells and adipocytes mediated by leptin modulates susceptibility for T cell mediated hepatitis. *J Hepatol,* 60**,** 175-82.

VIRTANEN, K. A., LIDELL, M. E., ORAVA, J., HEGLIND, M., WESTERGREN, R., NIEMI, T., TAITTONEN, M., LAINE, J., SAVISTO, N. J., ENERBACK, S. & NUUTILA, P. 2009. Functional brown adipose tissue in healthy adults. *N Engl J Med,* 360**,** 1518-25.

VOEHRINGER, D., BLASER, C., BRAWAND, P., RAULET, D. H., HANKE, T. & PIRCHER, H. 2001. Viral infections induce abundant numbers of senescent CD8 T cells. *J Immunol,* 167**,** 4838-43.

VOEHRINGER, D., REESE, T. A., HUANG, X., SHINKAI, K. & LOCKSLEY, R. M. 2006. Type 2 immunity is controlled by IL-4/IL-13 expression in hematopoietic non-eosinophil cells of the innate immune system. *J Exp Med,* 203**,** 1435-46.

VOM STEEG, L. G., VERMILLION, M. S., HALL, O. J., ALAM, O., MCFARLAND, R., CHEN, H., ZIRKIN, B. & KLEIN, S. L. 2016. Age and testosterone mediate influenza pathogenesis in male mice. *Am J Physiol Lung Cell Mol Physiol,* 311**,** L1234-L1244.

VONARBOURG, C. & DIEFENBACH, A. 2012. Multifaceted roles of interleukin-7 signaling for the development and function of innate lymphoid cells. *Semin Immunol,* 24**,** 165-74.

VONARBOURG, C., MORTHA, A., BUI, V. L., HERNANDEZ, P. P., KISS, E. A., HOYLER, T., FLACH, M., BENGSCH, B., THIMME, R., HOLSCHER, C., HONIG, M., PANNICKE, U., SCHWARZ, K., WARE, C. F., FINKE, D. & DIEFENBACH, A. 2010. Regulated expression of nuclear receptor RORgammat confers distinct functional fates to NK cell receptor-expressing RORgammat(+) innate lymphocytes. *Immunity,* 33**,** 736-51.

VONDENHOFF, M. F., GREUTER, M., GOVERSE, G., ELEWAUT, D., DEWINT, P., WARE, C. F., HOORWEG, K., KRAAL, G. & MEBIUS, R. E. 2009. LTbetaR signaling induces cytokine expression and up-regulates lymphangiogenic factors in lymph node anlagen. *J Immunol,* 182**,** 5439-45.

WAHID, F. N. & BEHNKE, J. M. 1993. Immunological relationships during primary infection with Heligmosomoides polygyrus (Nematospiroides dubius): parasite specific IgG1 antibody responses and primary response phenotype. *Parasite Immunol,* 15**,** 401-13.

WALKER, J. A. & MCKENZIE, A. N. 2013. Development and function of group 2 innate lymphoid cells. *Curr Opin Immunol,* 25**,** 148-55.

WANG, X., CHO, B., SUZUKI, K., XU, Y., GREEN, J. A., AN, J. & CYSTER, J. G. 2011. Follicular dendritic cells help establish follicle identity and promote B cell retention in germinal centers. *J Exp Med,* 208**,** 2497-510.

WATANABE, H., NUMATA, K., ITO, T., TAKAGI, K. & MATSUKAWA, A. 2004. Innate immune response in Th1- and Th2-dominant mouse strains. *Shock,* 22**,** 460-6.

WEISBERG, S. P., MCCANN, D., DESAI, M., ROSENBAUM, M., LEIBEL, R. L. & FERRANTE, A. W., JR. 2003. Obesity is associated with macrophage accumulation in adipose tissue. *J Clin Invest,* 112**,** 1796-808.

WENTWORTH, J. M., NASELLI, G., BROWN, W. A., DOYLE, L., PHIPSON, B., SMYTH, G. K., WABITSCH, M., O'BRIEN, P. E. & HARRISON, L. C. 2010. Pro-inflammatory CD11c+CD206+ adipose tissue macrophages are associated with insulin resistance in human obesity. *Diabetes,* 59**,** 1648-56.

WHITE, A., CARRAGHER, D., PARNELL, S., MSAKI, A., PERKINS, N., LANE, P., JENKINSON, E., ANDERSON, G. & CAAMANO, J. H. 2007. Lymphotoxin a-dependent and -independent signals regulate stromal organizer cell homeostasis during lymph node organogenesis. *Blood,* 110**,** 1950-9.

WILLARD-MACK, C. L. 2006. Normal structure, function, and histology of lymph nodes. *Toxicol Pathol,* 34**,** 409-24.

WINER, D. A., WINER, S., SHEN, L., WADIA, P. P., YANTHA, J., PALTSER, G., TSUI, H., WU, P., DAVIDSON, M. G., ALONSO, M. N., LEONG, H. X., GLASSFORD, A., CAIMOL, M., KENKEL, J. A., TEDDER, T. F., MCLAUGHLIN, T., MIKLOS, D. B., DOSCH, H. M. & ENGLEMAN, E. G. 2011. B cells promote insulin resistance through modulation of T cells and production of pathogenic IgG antibodies. *Nat Med,* 17**,** 610-7.

WINER, S., CHAN, Y., PALTSER, G., TRUONG, D., TSUI, H., BAHRAMI, J., DORFMAN, R., WANG, Y., ZIELENSKI, J., MASTRONARDI, F., MAEZAWA, Y., DRUCKER, D. J., ENGLEMAN, E., WINER, D. & DOSCH, H. M. 2009. Normalization of obesity-associated insulin resistance through immunotherapy. *Nat Med,* 15**,** 921-9.

WITHERS, D. R., GASPAL, F. M., MACKLEY, E. C., MARRIOTT, C. L., ROSS, E. A., DESANTI, G. E., ROBERTS, N. A., WHITE, A. J., FLORES-LANGARICA, A., MCCONNELL, F. M., ANDERSON, G. & LANE, P. J. 2012. Cutting edge: lymphoid tissue inducer cells maintain memory CD4 T cells within secondary lymphoid tissue. *J Immunol,* 189**,** 2094-8.

WOJNO, E. D., MONTICELLI, L. A., TRAN, S. V., ALENGHAT, T., OSBORNE, L. C., THOME, J. J., WILLIS, C., BUDELSKY, A., FARBER, D. L. & ARTIS, D. 2015. The prostaglandin D(2) receptor CRTH2 regulates accumulation of group 2 innate lymphoid cells in the inflamed lung. *Mucosal Immunol,* 8**,** 1313-23.

WOOD, I. S., WANG, B. & TRAYHURN, P. 2009. IL-33, a recently identified interleukin-1 gene family member, is expressed in human adipocytes. *Biochem Biophys Res Commun,* 384**,** 105-9.

WU, D., MOLOFSKY, A. B., LIANG, H. E., RICARDO-GONZALEZ, R. R., JOUIHAN, H. A., BANDO, J. K., CHAWLA, A. & LOCKSLEY, R. M. 2011. Eosinophils sustain adipose alternatively activated macrophages associated with glucose homeostasis. *Science,* 332**,** 243-7.

WU, H., GHOSH, S., PERRARD, X. D., FENG, L., GARCIA, G. E., PERRARD, J. L., SWEENEY, J. F., PETERSON, L. E., CHAN, L., SMITH, C. W. & BALLANTYNE, C. M. 2007. T-cell accumulation and regulated on activation, normal T cell expressed and secreted upregulation in adipose tissue in obesity. *Circulation,* 115**,** 1029-38.

WU, J., BOSTROM, P., SPARKS, L. M., YE, L., CHOI, J. H., GIANG, A. H., KHANDEKAR, M., VIRTANEN, K. A., NUUTILA, P., SCHAART, G., HUANG, K., TU, H., VAN MARKEN LICHTENBELT, W. D., HOEKS, J., ENERBACK, S., SCHRAUWEN, P. & SPIEGELMAN, B. M. 2012. Beige adipocytes are a distinct type of thermogenic fat cell in mouse and human. *Cell,* 150**,** 366-76.

XU, T., STEWART, K. M., WANG, X., LIU, K., XIE, M., KYU RYU, J., LI, K., MA, T., WANG, H., NI, L., ZHU, S., CAO, N., ZHU, D., ZHANG, Y., AKASSOGLOU, K., DONG, C., DRIGGERS, E. M. & DING, S. 2017. Metabolic control of TH17 and induced Treg cell balance by an epigenetic mechanism. *Nature,* 548**,** 228-233.

XU, W. & DI SANTO, J. P. 2013. Taming the beast within: regulation of innate lymphoid cell homeostasis and function. *J Immunol,* 191**,** 4489-96.

XUE, B., RIM, J. S., HOGAN, J. C., COULTER, A. A., KOZA, R. A. & KOZAK, L. P. 2007. Genetic variability affects the development of brown adipocytes in white fat but not in interscapular brown fat. *J Lipid Res,* 48**,** 41-51.

XUE, L., SALIMI, M., PANSE, I., MJOSBERG, J. M., MCKENZIE, A. N., SPITS, H., KLENERMAN, P. & OGG, G. 2014. Prostaglandin D2 activates group 2 innate lymphoid cells through chemoattractant receptor-homologous molecule expressed on TH2 cells. *J Allergy Clin Immunol,* 133**,** 1184-94.

XUE, R., LYNES, M. D., DREYFUSS, J. M., SHAMSI, F., SCHULZ, T. J., ZHANG, H., HUANG, T. L., TOWNSEND, K. L., LI, Y., TAKAHASHI, H., WEINER, L. S., WHITE, A. P., LYNES, M. S., RUBIN, L. L., GOODYEAR, L. J., CYPESS, A. M. & TSENG, Y. H. 2015. Clonal analyses and gene profiling identify genetic biomarkers of the thermogenic potential of human brown and white preadipocytes. *Nat Med,* 21**,** 760-8.

YANG, Z., GRINCHUK, V., SMITH, A., QIN, B., BOHL, J. A., SUN, R., NOTARI, L., ZHANG, Z., SESAKI, H., URBAN, J. F., JR., SHEA-DONOHUE, T. & ZHAO, A. 2013. Parasitic nematode-induced modulation of body weight and associated metabolic dysfunction in mouse models of obesity. *Infect Immun,* 81**,** 1905-14.

YEOH, B. S. & VIJAY-KUMAR, M. 2015. Debugging the host browns the fat. *Nat Med,* 21**,** 1390-1.

YING, S., O'CONNOR, B., RATOFF, J., MENG, Q., FANG, C., COUSINS, D., ZHANG, G., GU, S., GAO, Z., SHAMJI, B., EDWARDS, M. J., LEE, T. H. & CORRIGAN, C. J. 2008. Expression and cellular provenance of thymic stromal lymphopoietin and chemokines in patients with severe asthma and chronic obstructive pulmonary disease. *J Immunol,* 181**,** 2790-8.

YING, S., O'CONNOR, B., RATOFF, J., MENG, Q., MALLETT, K., COUSINS, D., ROBINSON, D., ZHANG, G. Z., ZHAO, J. S., LEE, T. H. & CORRIGAN, C.

2005. Thymic stromal lymphopoietin expression is increased in asthmatic airways and correlates with expression of TH2-attracting chemokines and disease severity. *Journal of Immunology,* 174**,** 8183-8190.

YOKOTA, Y., MANSOURI, A., MORI, S., SUGAWARA, S., ADACHI, S., NISHIKAWA, S. & GRUSS, P. 1999. Development of peripheral lymphoid organs and natural killer cells depends on the helix-loop-helix inhibitor Id2. *Nature,* 397**,** 702-6.

YOSHIDA, H., NAITO, A., INOUE, J., SATOH, M., SANTEE-COOPER, S. M., WARE, C. F., TOGAWA, A., NISHIKAWA, S. & NISHIKAWA, S. 2002. Different cytokines induce surface lymphotoxin-alphabeta on IL-7 receptor-alpha cells that differentially engender lymph nodes and Peyer's patches. *Immunity,* 17**,** 823-33.

YOSHIMURA, T. & OPPENHEIM, J. J. 2011. Chemokine-like receptor 1 (CMKLR1) and chemokine (C-C motif) receptor-like 2 (CCRL2); two multifunctional receptors with unusual properties. *Exp Cell Res,* 317**,** 674-84.

YOUNG, S. G. & ZECHNER, R. 2013. Biochemistry and pathophysiology of intravascular and intracellular lipolysis. *Genes Dev,* 27**,** 459-84.

YU, X., WANG, Y., DENG, M., LI, Y., RUHN, K. A., ZHANG, C. C. & HOOPER, L. V. 2014. The basic leucine zipper transcription factor NFIL3 directs the development of a common innate lymphoid cell precursor. *Elife,* 3.

ZENG, W., PIRZGALSKA, R. M., PEREIRA, M. M., KUBASOVA, N., BARATEIRO, A., SEIXAS, E., LU, Y. H., KOZLOVA, A., VOSS, H., MARTINS, G. G., FRIEDMAN, J. M. & DOMINGOS, A. I. 2015. Sympathetic neuro-adipose connections mediate leptin-driven lipolysis. *Cell,* 163**,** 84-94.

ZHANG, K., XU, X., PASHA, M. A., SIEBEL, C. W., COSTELLO, A., HACZKU, A., MACNAMARA, K., LIANG, T., ZHU, J., BHANDOOLA, A., MAILLARD, I. & YANG, Q. 2017. Cutting Edge: Notch Signaling Promotes the Plasticity of Group-2 Innate Lymphoid Cells. *J Immunol,* 198**,** 1798-1803.

ZINGONI, A., SOTO, H., HEDRICK, J. A., STOPPACCIARO, A., STORLAZZI, C. T., SINIGAGLIA, F., D'AMBROSIO, D., O'GARRA, A., ROBINSON, D., ROCCHI, M., SANTONI, A., ZLOTNIK, A. & NAPOLITANO, M. 1998. The chemokine receptor CCR8 is preferentially expressed in Th2 but not Th1 cells. *J Immunol,* 161**,** 547-51.